

**Extrapolating from Experimental to Human  
Studies via the *in vitro* Paradigm**

**Edward Llewellyn Bowen**

PhD

**University of York**

**Biology**

**September 2015**

## Thesis Abstract

Despite being the “gold standard” for toxicity testing, rat *in vivo* studies are estimated to be only 37-50% accurate at predicting xenobiotic toxicity in humans. If validated, *in vitro* systems could be incorporated into toxicity testing, allowing direct comparisons to be made between humans and rats and facilitating a reduction of *in vivo* testing. In this project, a normal rat urothelial (NRU) cell culture system was developed and optimised for comparison against an established normal human urothelial (NHU) cell culture system. NRU cells had a reduced lifespan in culture compared to NHU cells, leading to an investigation of the pathways regulating cellular proliferation. The PI3K/Akt pathway was found to be active in proliferating NRU cells, whereas the EGFR/MAPK and  $\beta$ -catenin pathways were confirmed to regulate NHU cell proliferation. Inhibition of the PI3K/Akt pathway enabled NRU cells to be subcultured to passage 2, most probably by enabling EGFR/MAPK and  $\beta$ -catenin pathway activation, although this requires experimental confirmation. To further increase cell lifespan, the proto-oncogene BMI1 was overexpressed in NRU and NHU cells, with the effects on lifespan and differentiation compared against both human telomerase reverse transcriptase (hTERT) overexpressing and control (empty vector) cells. NRU cell lifespan was not increased by BMI1 or hTERT overexpression. BMI1 overexpression increased NHU cell lifespan in culture, comparable with hTERT overexpression, but further work is required to determine the extent of the effects on lifespan and phenotype beyond passage 12. Finally, the metabolic competence of urothelial cells was explored, with a focus on the cytochrome P450 2B (CYP2B) family of metabolic enzymes. Xenobiotic induction of CYP2B expression by rat urothelium was demonstrated *in vivo* but not in NRU and NHU cells. Xenobiotic-induced CYP2B protein expression was achieved in a rat *ex vivo* organ culture model. Together these results identify a previously unknown metabolic capability of urothelial cells that can be modelled *ex vivo*, and demonstrate fundamental differences in rat and human urothelial cell physiology that support the validation of human tissue-specific *in vitro* models for assessment of xenobiotic toxicity.

# Contents

<b>Thesis Abstract</b> .....	<b>2</b>
<b>Contents</b> .....	<b>3</b>
<b>Figures</b> .....	<b>8</b>
<b>Tables</b> .....	<b>21</b>
<b>Acknowledgements</b> .....	<b>22</b>
<b>Authors Declaration</b> .....	<b>23</b>
<b>Chapter 1 - Introduction</b> .....	<b>24</b>
<b>1.1 The <i>in vitro</i> paradigm</b> .....	<b>25</b>
<b>1.2 Predicting human toxicity</b> .....	<b>26</b>
<b>1.3 <i>In vitro</i> toxicology studies</b> .....	<b>29</b>
<b>1.4 Aims:</b> .....	<b>31</b>
1.4.1 Objectives.....	31
<b>Chapter 2 - Materials and Methods</b> .....	<b>32</b>
<b>2.1 General</b> .....	<b>33</b>
<b>2.2 Commercial Suppliers</b> .....	<b>33</b>
<b>2.3 General laboratory equipment</b> .....	<b>33</b>
<b>2.4 Stock Solutions</b> .....	<b>33</b>
<b>2.5 Cell and Tissue Culture</b> .....	<b>34</b>
2.5.1 General.....	34
2.5.2 Primary Normal Urothelial Cell Culture .....	34
2.5.3 Assays.....	38
2.5.4 Population doubling curves .....	39
2.5.5 NHU cell differentiation .....	39
2.5.6 Retropack™ PT67 Packaging Cell Line .....	40
2.5.7 Cryo-preservation and thawing .....	40
2.5.8 Testing cell lines for Mycoplasma .....	41
<b>2.6 Molecular Biology</b> .....	<b>42</b>
2.6.1 General.....	42
2.6.2 Glass and Plasticware.....	42
2.6.3 Analysis of Gene Expression .....	42
2.6.4 Plasmids .....	46
2.6.5 Molecular cloning and retroviral plasmid generation .....	49

2.6.6 Amplification of plasmid DNA.....	51
<b>2.7 Protein Analysis.....</b>	<b>52</b>
2.7.1 Antibodies .....	52
2.7.1 Immunofluorescence labelling.....	54
2.7.2 Immunolabelling of tissue sections.....	55
2.7.3 Image capture and analysis.....	59
2.7.4 Western Blotting .....	60
<b>2.8 Statistical analysis .....</b>	<b>63</b>
<b>Chapter 3 - Optimisation of a normal rat urothelial cell culture system.....</b>	<b>64</b>
<b>3.1 Chapter Introduction .....</b>	<b>65</b>
3.1.1 The Bladder .....	65
3.1.2 The Urothelium .....	65
3.1.3 Urothelial cell culture models.....	70
<b>3.2 Chapter Aim .....</b>	<b>74</b>
3.2.1 Objectives.....	74
<b>3.3 Experimental approach.....</b>	<b>75</b>
3.3.1 Cell isolation protocol .....	75
3.3.2 Adapting the NRU cell isolation protocol.....	77
3.3.3 Optimising NRU cell culture conditions .....	77
3.3.4 Summary of experimental approach .....	78
3.3.5 Cell lines .....	79
<b>3.4 Results .....</b>	<b>80</b>
3.4.1 Initial comparisons of rat and human urothelium in situ .....	80
3.4.2 NRU cell culture using protocols established for NHU cells. ....	80
3.4.3 Optimisation of the NRU cell isolation protocol.....	83
3.4.4 The effect of fetal bovine serum on primary NRU cell cultures .....	87
3.4.5 NRU cell seeding density.....	95
3.4.6 Optimising surface substrate for NRU cell growth .....	96
<b>3.5 Conclusions and Discussion .....</b>	<b>101</b>
<b>3.6 Key findings.....</b>	<b>102</b>
<b>Chapter 4 - The regulation of Normal Rat Urothelial (NRU) and Normal Human Urothelial (NHU) cell proliferation <i>in vitro</i> .....</b>	<b>103</b>
<b>4.1 Chapter Introduction .....</b>	<b>105</b>
<b>4.2 Chapter Aim .....</b>	<b>107</b>

4.2.1 – Objectives.....	107
<b>4.3 Experimental Approach .....</b>	<b>108</b>
4.3.1 - Proliferation pathways.....	108
4.3.2 Extracellular calcium .....	108
4.3.3 - Cell lines .....	111
<b>4.4. Results – NHU cells .....</b>	<b>112</b>
4.4.1 – Growth Kinetics.....	112
4.4.2 – Proliferation pathways.....	114
4.4.3 – Pharmacological interrogation of proliferation pathways.....	117
4.4.4 – Conclusions .....	118
<b>4.5 Results – NRU cells .....</b>	<b>119</b>
4.5.1 – Growth Kinetics.....	119
4.5.2 –Ki67 expression .....	121
4.5.3 – Phospho-ERK, $\beta$ -catenin and phospho-Akt expression.....	121
4.5.4 – Removal of exogenous EGF.....	128
4.5.5 – PI3K/Akt pathway inhibition .....	129
4.5.6 – Physiological (2mM) extracellular calcium .....	133
4.5.7 – Reduced extracellular calcium .....	136
<b>4.6 Results summary .....</b>	<b>140</b>
<b>4.7 Conclusions and Discussion.....</b>	<b>142</b>
<b>4.8 Key findings.....</b>	<b>143</b>
<b>Chapter 5 - Overexpression of BMI1 in NRU and NHU cells .....</b>	<b>144</b>
<b>5.1 Chapter Introduction .....</b>	<b>145</b>
5.1.1 Immortalised cell lines .....	145
5.1.2 <i>In vitro</i> immortalisation .....	146
5.1.3 Immortalisation of urothelial cell culture models .....	147
5.1.4 Overexpression of BMI1.....	148
<b>5.2 Aim .....</b>	<b>151</b>
5.2.1 Objectives.....	151
<b>5.3 Experimental approach.....</b>	<b>152</b>
5.3.1 Development of a BMI1 overexpressing retroviral cell line .....	152
5.3.2 Effect of BMI1 or hTERT overexpression on NRU cell growth and lifespan in culture .....	152

5.3.3 Effect of BMI1 and hTERT overexpression on NHU cell growth, lifespan and ability to form a functional barrier in culture .....	153
5.3.4 Cell lines .....	153
<b>5.4 Results .....</b>	<b>154</b>
5.4.1 Development of a BMI1 overexpressing pLXSN retrovirus.....	154
5.4.2 Overexpression of BMI1 and hTERT in NRU cells.....	159
5.4.3 The effect of overexpressing BMI1 and hTERT on NHU cell growth.....	163
5.4.4 Generation of a functional barrier <i>in vitro</i> .....	168
<b>5.5 Conclusions and Discussion .....</b>	<b>173</b>
<b>5.6 Key Findings .....</b>	<b>174</b>
<b>Chapter 6 - Induction of Urothelial Cytochrome P450 2B expression <i>in vivo</i> and <i>in vitro</i>.....</b>	<b>175</b>
<b>6.1 Chapter Introduction .....</b>	<b>176</b>
6.1.1 Cellular Metabolism .....	176
6.1.2 Xenobiotic metabolism in humans and rats .....	176
6.1.3 Cytochrome P450 enzymes.....	178
6.1.4 CYPs and the bladder .....	179
6.1.5 Modelling CYPs <i>in vitro</i> .....	181
<b>6.2 Aim .....</b>	<b>183</b>
6.2.1 Objectives.....	183
<b>6.2 Experimental approach.....</b>	<b>184</b>
6.2.1 CYP2B induction <i>in vivo</i> .....	184
6.2.2 CYP2B induction <i>in vitro</i> .....	184
6.2.3 CYP2B induction in <i>ex vivo</i> organ culture models.....	184
6.2.4 Cell lines .....	185
<b>6.3 Results .....</b>	<b>186</b>
6.3.1 CYP2B expression in rat urothelium .....	186
6.3.2 CYP2B homologue expression in rat urothelial cells.....	193
6.3.4 Rat <i>In vivo</i> case study – chemical induction of CYP2B .....	196
6.3.4 Investigation of urothelial CYP2B expression <i>in vitro</i> .....	200
<b>6.4 Conclusions and Discussion .....</b>	<b>208</b>
<b>6.5 Key findings.....</b>	<b>208</b>
<b>Chapter 7 Discussion.....</b>	<b>209</b>
<b>7.1 Development of a NRU cell culture system .....</b>	<b>211</b>

<b>7.2 Regulation of urothelial growth pathways.....</b>	<b>214</b>
<b>7.3 Immortalisation of normal urothelial cells.....</b>	<b>219</b>
<b>7.4 Xenobiotic induction of CYP2B enzymes in urothelial cells .....</b>	<b>221</b>
<b>7.5 Practical difficulties experienced during the project.....</b>	<b>222</b>
<b>7.5 Limitations and future work.....</b>	<b>223</b>
<b>Chapter 8 Appendices .....</b>	<b>226</b>
<b>Appendices 1 – Materials and Method.....</b>	<b>226</b>
Appendix 1.1 – Tissue harvesting and <i>in vivo</i> experimentation locations.....	226
Appendix 1.2 – List of Suppliers .....	227
Appendix 1.3 Online resources .....	228
Appendix 1.4 – Solutions .....	229
Appendix 1.6 Primers.....	233
Appendix 1.7 – Aseptic removal of rat bladder tissue.....	235
<b>Appendices 2 – Results.....</b>	<b>238</b>
Appendices 2.1 Antibody specificity .....	238
Appendices 2.2 Primer T <sub>m</sub> optimisation (examples).....	244
<b>Appendix 2.3 – BMI1 protein coding sequence.....</b>	<b>246</b>
<b>Appendix 2.4 - CYP2B negative (no primary antibody) controls.....</b>	<b>247</b>
<b>Abbreviations .....</b>	<b>250</b>
<b>Bibliography .....</b>	<b>252</b>

## Figures

Figure 1.1 – The in vitro paradigm is a potential system for improving the extrapolation of data from rats in vivo to humans in vivo. Schematic of the in vitro paradigm illustrating how rat and human in vitro models can be combined with rats in vivo to predict results in humans in vivo. ....	25
Figure 1.2 – The pharmaceutical compound development pipeline. Details of the use of in vitro models in target discovery, validation and optimisation (Blue) and in vivo models in preclinical and clinical toxicology testing (red). The approximate time periods, costs and number of compounds at each stage of development as of 2000 in the US are indicated (adapted from DiMasi et al., 2003)...	28
Figure 2.1 - Schematic representation of pGEM <sup>®</sup> T easy vector adapted from the Promega pGEM <sup>®</sup> T and pGEM <sup>®</sup> T easy vector technical manual showing the T7 and SP6 promoter regions. ....	47
Figure 2.2 - schematic representation of pLXSN vector used for gene overexpression adapted from the Clontech pLXSN technical manual. The four restriction enzyme digestion sites within the multiple cloning region are labelled. ....	48
Figure 3.1 – PPAR $\gamma$ activation of urothelial differentiation-associated gene expression. Cartoon depicting activation of PPAR $\gamma$ binding through the binding of a PPAR $\gamma$ ligand, initiating heterodimerization with RXR. The PPAR $\gamma$ -RXR transcription factor then binds to peroxisome proliferator response elements (PPRE), resulting in secondary transcription factor expression. These transcription factors subsequently activate differentiation-associated genes.....	68
Figure 3.2 - The isolation of normal human urothelial (NHU) cells. An annotated cartoon detailing the various stems of the NHU cell isolation protocol including the initial EDTA “stripping” phase, urothelial cell sheet removal and finally the collagenase IV disaggregation of NHU cells prior to cell seeding. ....	76
Figure 3.3 – The NRU cell isolation protocol. A cartoon illustrating the various processes involved in urothelial cell isolation and culture. The stages (numbered in red) correspond to those in Table 3.2. ....	78
Figure 3.4 – Differences in the tissue thickness and number of proliferative cells in the native urothelium of humans and rats. Immunolabelling of the urothelial cell marker cytokeratin 7 (CK7) (top & middle) and the cell proliferation marker Ki67 (bottom) in rat (left) and human (right) bladders. Superficial, intermediate and basal cell zones are labelled. Scale bars = 50 $\mu$ m. Results have been repeated in multiple individual rat bladders (n=<5). ....	81
Figure 3.5 – NRU cells were not cleanly isolated by the NHU cell isolation protocol. Phase contrast images of NRU-HS cells after isolation using the NHU cell (EDTA/Collagenase) isolation protocol (Section 3.3.1), prior to being seeded. Scale bar = 250 $\mu$ m. ....	82

Figure 3.6 – NRU cells isolated with the NHU cell isolation protocol had limited growth in culture. Growth curve were generated (Section 2.5.3.1) for NRU-HS cell growth over 9 days cultured in KSFMc after isolation using the NHU cell isolation protocol (Section 3). Data points represent mean  $\pm$  SD. (n=3, R006a, R006b, R006c) ..... 82

Figure 3.7 – EDTA/Collagenase and Dispase/trypsin isolation protocols enabled near-complete isolation of urothelial cells. Urothelial cell marker cytokeratin 7 (CK7) immunolabelling in native rat bladders (A&B) and in rat bladders after urothelial cell isolation using the EDTA protocol (Section 3.3.1; C, E & G) and Dispase/trypsin protocol (Section 3.3.2; D, F & H). Labelled cells were specifically identified and imaged. Scale bar = 50 $\mu$ m. (n=3, R008, R009, R0010). ..... 84

Figure 3.8 – Complete removal of the urothelium was achieved by stripping human bladder tissue using the EDTA/Collagenase protocol. Labelling of the urothelial cell marker cytokeratin 7 (CK7) in native human ureter (left) and human bladder tissue after urothelial cell isolation (right) using the EDTA/collagenase protocol (Section 3.3.1). Scale bar = 50 $\mu$ m. .... 85

Figure 3.9 – Clean isolation of NRU cells was achieved using the dispase/trypsin but not the EDTA/collagenase protocols. Phase contrast images showing primary NRU-HS cells in suspension after isolation with the EDTA/collagenase (Section 3.3.1; left) and Dispase/trypsin (Section 3.3.2; right) protocols on a haemocytometer. Scale bar = 250 $\mu$ m. (n=3, R008, R009, R0010). ..... 85

Figure 3.10 – Primary NRU cells formed more colonies after dispase/trypsin isolation compared to EDTA/collagenase isolation. Colony formation assay (Section 2.5.3.2) of NRU-HS (adult) cells isolated using both the EDTA/collagenase (Section 3.3.1) and dispase/trypsin (Section 3.3.2) protocols as indicated and cultured on N<sub>2</sub> plasma treated tissue culture plastic. Cells from 2.5 bladders were pooled per well and cultured for 5 days in KSFMc +5%FBS. Data points represent the mean  $\pm$  Range (n=2, R009, R0013). ..... 86

Figure 3.11 – NRU-HS cells grew in presence but not in the absence of serum. Representative phase contrast images of NRU-HS cell growth in culture over 7 days in KSFMc medium  $\pm$  5%Fetal Bovine Serum (FBS) (n=3 NRU cell lines, R009, R013, R015). Scale bar = 50  $\mu$ m. .... 88

Figure 3.12 – One NRU-SD cell line grew equally in both serum-free and serum-supplemented medium. Representative phase contrast images of NRU-SD cell growth in culture over 7 days in KSFMc medium  $\pm$  5%Fetal Bovine Serum (FBS) (n=1 NRU cell line, R007). Scale bar = 50 $\mu$ m. .... 89

Figure 3.13 – NRU-W cells grew in the absence but not in the presence of serum. Representative phase contrast images of NRU-W cell growth in culture over 7 days in KSFMc medium  $\pm$  5%Fetal Bovine Serum (FBS) n=3 NRU cell lines, R008, R010, R012). Scale bar = 50 $\mu$ m. .... 90

Figure 3.14 – NHU cells grew normally in serum-free medium but had reduced growth and an altered morphology in serum-supplemented medium. Representative phase contrast images of NHU cell

growth in culture over 7 days in KSFMc medium ± 5%FBS (n=3 NHU cell lines, Y984, Y1052, Y1183).  
Scale bar = 50µm..... 91

Figure 3.15 – NRU-W cells grew in the absence of serum whereas NRU-HS cells required serum to grow. Growth curves were generated (Section 2.5.3.1) for NRU-W (R008, R010, R012) & NRU-HS (R009, R013, R015) cell cultured over 7 days in KSFMc ± 5% FBS. Data points represent mean percentage reduction in alamarBlue<sup>®</sup> ±SD (n=3)..... 93

Figure 3.16 – NHU cells show standard expansion and plateau phases of growth when cultured in KSFMc medium. Growth curves were generated (Section 2.5.3.1) for three subcultured (P2) NHU cell lines cultured over 7 days in KSFMc medium. Data points represent mean percentage reduction in alamarBlue<sup>®</sup> ±SD (n=3, Y984, Y1052, Y1183)..... 93

Figure 3.17 – NRU-W cells had significantly greater growth in serum-free medium compared to serum-supplemented medium. Graphs show percentage of alamarBlue<sup>®</sup> reduction (Section 2.5.3.1) by NRU-W cell cultures on days 6 (left) and 10 (right) of maintenance in KSFMc medium. Data points represent mean ±SD (n=3). Student T-Test (paired, 2-tailed) was conducted, \* p <0.05. .... 94

Figure 3.18 – NRU-HS cells had significantly increased growth in serum-supplemented medium compared to serum-free medium. Graphs show the percentage of alamarBlue<sup>®</sup> reduction (Section 2.5.3.1) by NRU-HS cell cultures on days 6 (left) and 10 (right) of maintenance in KSFMc medium. Data points represent mean ±SD (n=3). Student T-Test (paired, 2-tailed) was conducted, \* p <0.05. .... 94

Figure 3.19 –  $1 \times 10^4$  cells/cm<sup>2</sup> was the optimal seeding density for NRU-HS cells. NRU-HS cells were seeded at  $1 \times 10^3$ ,  $1 \times 10^4$  and  $1 \times 10^5$  cells per cm<sup>2</sup>, cultured in KSFMc +5% FBS for 5 days before a colony formation assay (Section 2.5.3.2) was performed. Data points represent mean ±SD (n=3, R022, R023, R024). Student T Test (paired, 2-tailed) was conducted, \* = p <0.05. .... 95

Figure 3.20 – NRU-HS cells grew best in the presence of serum and on N<sub>2</sub>-plasma treated tissue culture plastic. Colony formation assays (Section 2.5.3.2) were conducted to examine NRU-HS (P0) cell growth on collagen I and N<sub>2</sub> plasma-treated tissue culture plastic in KSFMc ± 5%FBS. Cells were cultured for 5 days on 6 well plates. Data points represent the mean number of colonies ±SD (n=3, R016, R017, R020). Student T Tests (Paired, 2-tailed) were conducted, \* = p <0.05, \*\* = p <0.01. .... 96

Figure 3.21 - NRU-HS cells were successfully subcultured after dispase/trypsin isolation but not after EDTA/collagenase isolation. NRU- HS cells growth after EDTA/Collagenase and Dispase/trypsin isolation. On day 8 cells were passaged (Section 2.5.2.4) and split 1:3 before being reseeded at a density of  $1 \times 10^4$  cells/cm<sup>2</sup>. Growth curves were generated for these cells (see ..... 98

Figure 3.22 – EDTA/collagenase isolated cells did not grow after being passaged. Growth curves were generated (Section 2.5.3.1) for three NRU-HS cell lines isolated using the EDTA/collagenase protocol

(Section 3.3.1) in primary culture (day 1-7) and after subcultured (day 9-13). Data points represent mean percentage reduction in alamarBlue<sup>®</sup> ±SD (n=3, R025, R027, R028)..... 99

Figure 3.23 – Dispase/trypsin isolated cells were capable of growth after being passaged. Growth curves were generated (Section 2.5.3.1) for three NRU-HS cell lines isolated using the dispase/trypsin protocol (Section 3.3.2) in primary culture (day 1-7) and after subcultured (Day 9-13). Data points represent mean percentage reduction in alamarBlue<sup>®</sup> ±SD (n=3, R025, R027, R028). ..... 100

Figure 4.1 - Summary of the EGF/MAPK, Wnt/ $\beta$ -catenin and PI3K/Akt pathways. Release of  $\beta$ -catenin (left) from the GSK3 $\beta$  destruction complex enables  $\beta$ -catenin to translocate to either the cell nucleus where it regulates gene expression to promote cell proliferation and survival or, under conditions of high calcium, be incorporated into adherens junctions at the cell membrane. Activation of EGFR (centre) by EGF activates the MAPK pathway to regulate gene expression to promote cell proliferation, survival and migration while inhibiting apoptosis. Activation of the PI3K/Akt pathway (right), for instance by IGFR activation can activate the mTOR pathway through TCS complex inhibition, inhibits apoptosis through inhibition of Bad and while regulating gene expression to promote cell growth and inhibit apoptosis. .... 110

Figure 4.2 – NHU cell growth was inhibited by EGFR/MAPK inhibition but GSK3 $\beta$  inhibition and PI3K/Akt activation had no effect on growth. A cell biomass assay (Section 2.5.3.1) was conducted on NHU cells cultured in KSFMc medium ± the agonists/inhibitors indicated. Cell culture medium was changed on the days indicated. Data points represent combined means ±SD. (n=3, Y1430, Y1437, Y1461) ..... 113

Figure 4.3 - NHU cell growth was significantly inhibited by EGFR inhibition on Days 5, 7 and 9. Statistical analysis was conducted on Growth curves presented in Figure 4.2 comparing treatment versus control (n=3; Y1430, Y1437, Y1461). An ANOVA test was conducted followed by a Tukey's post hoc test (\* = p <0.05, \*\* = p <0.01, \*\*\* = p<0.001; n=3). ..... 113

Figure 4.4 – In undifferentiated NHU cells, Active $\beta$ -catenin and phospho-ERK expression is nuclear and phospho-Akt is not expressed. Representative immunofluorescence labelling of Ki67, Active $\beta$ -catenin, phospho-ERK and phospho-Akt in NHU cells cultured in KSFMc (0.09mM Ca<sup>2+</sup>) medium. Scale bar = 50 $\mu$ m (n=3; Y1430, Y1437, Y1461). ..... 115

Figure 4.5 – In differentiated (ABS/Ca<sup>2+</sup>), Active $\beta$ -catenin is both nucleus and membrane localise and a switch in phospho-ERK and Phospho-Akt expression has occurred compared to undifferentiated NHU cells (Figure 4.6). Representative immunofluorescence labelling of Ki67, Active $\beta$ -catenin, phospho-ERK and phospho-Akt in differentiated NHU cells cultured in KSFMc (2mM Ca<sup>2+</sup>) medium supplemented with 5% ABS. Scale bar = 50 $\mu$ m (n=3; Y1430, Y1437, Y1461). ..... 116

Figure 4.6 – EGFR/MAPK inhibition significantly reduced expression of proliferation marker Ki67 and proliferation pathway markers Active  $\beta$ -catenin, phospho-ERK and phospho-Akt compared to control cells. Inhibition of GSK3 $\beta$  and activation of the PI3K/Akt pathway (IGF1) did not affect proliferation

marker Ki67 expression. Quantification of fluorescence intensity of Ki67, Nuclear active  $\beta$  catenin, phospho-Akt and phospho-ERK labelling in NHU cells cultured for 5 days in KSFMc medium (control) with the agonists/inhibitors indicated. (n=3 cell lines; Y1430, Y1437, Y1461). Error bars = SD. An ANOVA test was conducted with a Tukeys post hoc test (\*=p<0.05, \*\*=p<0.01, \*\*\*=p<0.1 compared to control) ..... 118

Figure 4.7 – EGFR/MAPK inhibition reduced NRU cells growth over 9 days of culture. Cell biomass assay (Section 2.5.3.1) for NRU cells cultured in KSFMc medium  $\pm$  the agonists/antagonists indicated. Cell culture medium was changed on the days indicated. Data points represent combined means  $\pm$ SD. (n=3; R037, R038, R039)..... 120

Figure 4.8 – Quantification of NRU cell growth curves presented in Figure 4.7. Results represent combined means  $\pm$ SD (n=3; R037, R038, R039). An ANOVA test was conducted with a Tukeys post hoc test (\*=p<0.05, \*\*=p<0.01 compared to control). ..... 120

Figure 4.9 – Ki67 expression appears increased in NRU cells after 5 days of PI3K/Akt expression. Representative images of Ki67 labelling in NRU cells cultured for 5 days in KSFMc with the agonists/antagonists indicated (n=3; R040, R041, R042). Scale bar = 50 $\mu$ m. .... 123

Figure 4.10 – Phospho-ERK was not expressed in control, EGFR/MAPK inhibited,  $\beta$ -catenin pathway activated or PI3K/Akt pathway activated NRU cells. Representative images of Phospho-ERK labelling in NRU cells cultured for 5 days in KSFMc with the agonists/antagonists indicated (n=3; R040, R041, R042). Scale bar = 50 $\mu$ m..... 124

Figure 4.11 - Active  $\beta$ -catenin labelling was clearly nuclear in control and MAPK inhibited cells, nuclear/perinuclear in GSK3 $\beta$ -inhibited cells and clearly membrane-localised in PI3K/Akt pathway activated NRU cells. Cells were cultured for 5 days in KSFMc with the agonists/antagonists indicated (n=3; R040, R041, R042). Scale bar = 50 $\mu$ m. .... 125

Figure 4.12 – Phospho-Akt expression was present in control and in proliferation pathway activated/inhibited NRU cells. Representative images of phospho-Akt (S47333) labelling in NRU cells cultured for 5 days in KSFMc with the agonists/antagonists indicated (n=3; R040, R041, R042). Scale bar = 50 $\mu$ m. .... 126

Figure 4.13 – Ki67 and phospho-Akt expression were significantly increased by IGF1 stimulation but Ki67 was reduced by EGFR/MAPK inhibition. Mean fluorescence intensity of Ki67, Active  $\beta$ -catenin and phospho-Akt labelling (arbitrary values) for three separate NRU cell lines. Results represent combined means from three separate cell lines  $\pm$ SD. Quantification was conducted using TissueGnostics TissueQuest software (Section 2.7.3). (\*\*=p<0.01, using a 2-way ANOVA test with a Tukeys post hoc test of comparison). ..... 127

Figure 4.14 – Removal of EGF had no effect on NRU cells growth in two cell lines (R050 & R051). NRU cell biomass assays (Section 2.5.3.1) for two NRU cell lines (R050 and R051) cultured in KSFMc

medium and KSFMc medium without exogenous EGF. Cell culture medium was changed on days 1, 3, 5 and 7. Data points represent experimental means  $\pm$ SD..... 128

Figure 4.15 – NRU cells grew being passaged twice when the PI3K/Akt pathway was inhibited whereas NRU cells cultured in KSFMc alone died after passage. 2 Phase contrast images showing NRU cells after passage 2 having been cultured in KSFMc alone or in the presence of the PI3K/Akt inhibitor LY294002. Cells were monitored over 9 days in culture (n=3; R048, R052, R055) Scale bar = 50 $\mu$ m. .... 130

Figure 4.16 – Phospho-Akt was inhibited in NRU cells by the PI3K/Akt inhibitor LY294002. Representative Immunofluorescence labelling of Ki67, active  $\beta$  catenin and phospho-Akt (red) in NRU and NHU cells cultured in KSFMc with DMSO (0.01%), LY294002 or LY294002 + SB415286. Nuclei were labelled with Hoechst 33248 (blue). (n=2; R048 & R055). Scale bar = 50 $\mu$ m. .... 131

Figure 4.17– Differentiation-associated markers ZO-1 and Claudin 4 were expressed in control and PI3K/Akt inhibited NRU cells. Representative immunofluorescence labelling of Claudin 4 and ZO-1 in NRU cells after 5 days of treatment with LY294002 and LY294002 + SB415286. Nuclei were labelled with Hoechst 33258 (blue). (n=2; R048 & R055). Scale bar = 50 $\mu$ m. .... 132

Figure 4.18 – No difference was seen in the expression of differentiation-associated markers ZO-1 and Claudin 4 in control and PI3K/Akt inhibited NRU cells. Mean fluorescence intensity of Claudin 4 and ZO-1 labelling (arbitrary values) for two separate NRU cell lines after treatment with LY294002 with and without SB415286. Results represent mean values  $\pm$ SD. .... 132

Figure 4.19 – NRU cells cultured in high extracellular calcium (2 mM) showed the same growth kinetics as those seen in low (0.09 mM Ca<sup>2+</sup>) up to 5 days in culture. NRU cell biomass assay (Section 2.5.3.1) for cells cultured in KSFMc medium (2mM Ca<sup>2+</sup>)  $\pm$  the agonists/antagonists indicated. Cell culture medium was changed on the days indicated. Data points represent combined means  $\pm$ SD (n=3; R046, R047, R049)..... 134

Figure 4.20 – EGFR/MAPK inhibitors significantly reduced NRU cell growth over 9 days of culture whereas all cells cultured in KSFMc (2 mM Ca<sup>+</sup>) had reduced growth at day 9 compared to cells cultured in KSFMc medium (0.09 mM Ca<sup>2+</sup>). Results represent combined means  $\pm$ SD (n=3; R046, R047, R049). (\*=p<0.05, \*\*=p<0.01 using a 2-way ANOVA with a Tukeys post hoc test of comparison). .... 134

Figure 4.21 – ZO-1 and Claudin 4 were both expressed in NRU cells cultured in KSFMc medium with 0.09 mM and 2 mM extracellular calcium ion concentrations. Representative immunofluorescence labelling of ZO-1, and claudin 4 in NRU (P0) cells. Cells were cultured for 5 days in low and physiological (2mM) calcium concentrations before being fixed and labelled. Cell nuclei were labelled with Hoechst 33258 (n=3; R046, R047, R049). Scale bar = 50 $\mu$ m. .... 135

Figure 4.22 – Uroplakin 3a (UP3a) was not expressed by NRU cells but aquaporin 3 (AQP3) was expressed by NRU cells cultured in 0.09 and 2 mM calcium ion concentrations. No visible difference was visible in AQP3 expression between cells cultured in different calcium ion concentrations. Representative immunofluorescence labelling of the differentiation-associated markers uroplakin 3a (UP3a), and aquaporin 3 (AQP3) in NRU (P0) cells. Cells were cultured for 5 days in low and physiological (2mM) calcium concentrations before being fixed and labelled. Cell nuclei were labelled with Hoechst 33258 (n=3; R046, R047, R049). Scale bar = 50µm. .... 135

Figure 4.23 – NRU cell density was visibly reduced at 0.015 mM calcium ion concentrations compared to cells cultured on 0.09 mM Ca<sup>2+</sup>. Phase contrast images of NRU cells cultured in KSFMc medium containing 0.09, 0.06, 0.03 and 0.015mM calcium as indicated on day 5 of culture. Scale bar = 50µm. .... 136

Figure 4.24 - Extracellular calcium ion concentration of 0.015 and 0.03 mM reduced NRU cell growth in culture. NRU cell growth assay (Section 2.5.3.1) in KSFMc medium containing 0.09, 0.06, 0.03 and 0.015mM calcium as indicated. Growth curves were measured using the alamarBlue assay. Data points represent combined means ±SD, (n=3; R052, R055, R056)..... 137

Figure 4.25 – Extracellular calcium ion concentrations of 0.015 and 0.03 mM significantly reduced NRU cell growth after 5 and 7 days of culture, respectively. Growth curves (Section 2.5.3.1) of NRU cells cultured in KSFMc containing 0.015, 0.03, 0.06 and 0.09mM Ca<sup>2+</sup> ions. Results represent combined means ±SD, (n=3; R052, R055, R056). (\*=p<0.05, \*\*=p<0.01, using a 2-way ANOVA with a Tukeys post hoc test of comparison). .... 137

Figure 4.26 – Phospho-Akt expression appeared to decrease when the extracellular calcium concentration was decreased however the Ki67 expression was unaffected at calcium concentrations of 0.06 and 0.03 mM. Representative immunofluorescence images of Ki67 and phospho-Akt labelling in NRU cells cultured in 0.09, 0.06, 0.03 and 0.015mM Ca<sup>2+</sup> KSFMc for 5 days (n=3; R052, R055, R056). Scale bar = 50µm. .... 138

Figure 4.27– Summary of the effects on activating/inhibiting the EGFR/MAPK,..... 140

Figure 4.28 – Summary of the effects of modulating the extracellular calcium ion concentration on NRU cell proliferation and growth pathways..... 141

Figure 5.1 – BMI1 increases cell self-renewal, proliferation and stemness while decreasing apoptosis and senescence. Cartoon illustrating some of the molecular actions of BMI1 associated with stemness and immortalisation. BMI1 activates transcription factors KLF4, SOX2 and GATA3 as well as the telomerase reverse transcriptase (TERT) to promote self-renewal and stemness. BMI1 activation of the NF-κB and P16<sup>INK4a</sup> pathways result in increased cell proliferation while inhibition of P21 inhibits apoptosis. Downstream inhibition of E-cadherin enables epithelial mesenchymal transition (EMT) and cell invasion (adapted from Siddique & Saleem, 2012). .... 149

Figure 5.2 – BMI1 transcripts are expressed by P0, proliferating and differentiated NHU cells. Next generation sequencing (Section 2.6.3.9) data showing mean reads per kilobase per million mapped reads (RPKM) for BMI1 transcript expression in freshly isolated (P0), proliferating (pro) and differentiated (dif) NHU cells (n=3 individual donors). ..... 154

Figure 5.3 – Successful ligation of BMI1 into pGEM T and subsequent transfection of E.Coli, as confirmed by antibiotic selection. Ampicillin-selection of XL1-Blue competent E. coli were transformed with pGEM T easy BMI1, pGEM T easy insert DNA (+ control) and negative (untransformed) controls after 24 hours of culture at 37°C (Section 2.6.5). ..... 156

Figure 5.4 – BMI1 was accurately amplified from NHU cell RNA with only two, non-amino acid altering mutations. BMI1 was sequenced (Section 2.6.5.5) after amplification from NHU RNA. Restriction sites are coloured in yellow, the Kozak sequence in green and alternate exons colours in black and grey. Two bases that were changed from the Reference sequence are highlighted in red. .... 156

Figure 5.5 - BMI1 was successfully cut from the pGEMT BMI1 vector. Gel electrophoresis (section 2.6.5.3) of pGEM T BMI1 isolated from transformed XL1-Blue competent E. coli (1), after single BamH1 restriction enzyme digestion (2) and after a double restriction enzyme digestion with BamH1 and Hpa1 (3). The ladder indicates the size of the product in base pairs. .... 157

Figure 5.6 - BMI1 was successfully ligated into pLXSN vector and used to transfect bacteria. Colony RT-PCR (Section 2.6.3.8) amplifying BMI1 (221bp) from 8 bacterial colonies after transfection with pLXSN BMI1. Base pair ladder indicates the size of the product in base pairs. .... 157

Figure 5.7 – Packaging cells were successfully transfected with pLXSN BMI1, pLXSN hTERT and pLXSN Empty vectors. Phase contrast images of PT67 packaging cells transfected with pLXSN empty, pLXSN hTERT & pLXSN BMI1 on days 3 and 5 of G418 selection showing complete death of untransfected cells. Scale bar = 50 µm. .... 158

Figure 5.8 – NRU cells were successfully transfected with pLXSN Empty vector, pLXSN hTERT, pLXSN BMI1 vectors. Phase contrast images of transduced and untransduced NRU cells cultured in KSFMc medium (0.06mM Ca<sup>2+</sup>) during the first 7 days after subculture (P1) under G418 selection. Scale bar = 50 µm. .... 160

Figure 5.9 – BMI1 and hTERT were both expressed by NRU cells overexpressing BMI1. RT-PCR (section 2.6.3.8) showing BMI1 expression in NRU cells (P1) transduced with pLXSN BMI1 (B), pLXSN empty vector (E) and pLXSN hTERT (H). GAPDH was included as a loading control. .... 161

Figure 5.10 – hTERT and BMI1 overexpressing cells did not survive after passage 2. Phase contrast images of transduced NRU cells cultured in KSFMc medium (0.06 mM Ca<sup>2+</sup>) on days 3, 5 and 7 after second subculture (P2). Cells remained under G418 selection pressure. Scale bar = 50 µm. .... 161

Figure 5.11 – BMI1 and hTERT overexpressing NRU cells grew at passage 1 equivalent to control cells. AlamarBlue assay (Section 2.5.3.1) generated growth curves for control, pLXSN BMI1 and pLXSN hTERT transfected NRU cells (P1) cultured in KSFMc medium (0.06 mM Ca<sup>2+</sup>) containing G418 selection. Error bars represent ±SD (n=3, R041, R042, R046)..... 162

Figure 5.12 – BMI1 and hTERT overexpressing NRU cells failed to grow at passage 2. AlamarBlue assay (Section 2.5.3.1) generated growth curves for control, pLXSN BMI1 and pLXSN hTERT transfected NRU cells (P2) cultured in KSFMc medium (0.06 mM Ca<sup>2+</sup>) containing G418 selection. Error bars represent ±SD (n=3, R041, R042, R046). ..... 162

Figure 5.13 – BMI1 and hTERT overexpression increased NHU cell lifespan in culture compared to control cells. NHU cell population doubling curves (Section 2.5.4) were generated for two cell lines transduced with pLXSN BMI1, pLXSN hTERT and pLXSN empty vector. Numbers indicate the passage number of the cell line at each time point (n=2, Y1533 and Y1570)..... 164

Figure 5.14 – BMI1 and hTERT overexpressing NHU cells maintained a normal morphology in culture up to passage 9 whereas control (Empty vector) NHU cells became more rounded and were less densely packed in culture. Representative phase contrast images of NHU cells transduced with pLXSN BMI1, pLXSN hTERT and pLXSN empty vector at passages 6-9. (n=1, Y1533). Scale bar = 50 µm. .... 165

Figure 5.15 – BMI1 expression was maintained in NHU cells over multiple passages. RT-PCR (section 2.6.3.8) results showing BMI1 and hTERT expression in BMI1 overexpressing NHU cells at passages 2-12 (Y1533). Water was used as a negative (no-template) control, RNA from BMI1 or hTERT-overexpressing PT67 was used as positive controls; GAPDH was used as a loading control. .... 167

Figure 5.16 - BMI1 and hTERT were both expressed by hTERT overexpressing NHU cells over several passages. RT-PCR (Section 2.6.3.8) results showing BMI1 and hTERT expression in hTERT overexpressing NHU cells at passages 2-12 (Y1533). Water was used as a negative control, BMI1 or hTERT overexpressing PT67 cDNA as positive controls and GAPDH as a loading control. (n=2, Y1533, Y1570) ..... 167

Figure 5.17 – BMI1 and hTERT were not expressed by Empty vector (control) NHU cells. RT-PCR (section 2.6.3.8) results showing BMI1 and hTERT expression in pLXSN Empty vector transduced NHU cells at passages 2-8 (Y1533). Water was used as a negative control, BMI1 or hTERT overexpressing PT67 cDNA as positive controls and GAPDH as a loading control. (n=2, Y1533, Y1570)..... 168

Figure 5.18 – Functional TEER barriers (>1000 kOhm.cm<sup>2</sup>) were generated by control, BMI1 and hTERT overexpressing NHU cells at passage 3. TEER measurements (Section 2.5.5.2) for two NHU cell lines (P3) transfected with pLXSN BMI1, pLXSN hTERT or pLXSN empty vector. Error bars represent ±SD for three replicate cultures. .... 169

Figure 5.19 - Functional TEER barriers (>1000 kOhm.cm<sup>2</sup>) were generated by control, BMI1 and hTERT overexpressing NHU cells at passage 6. TEER measurements (Section 2.5.5.2) for two NHU cell lines (P6) transfected with pLXSN BMI1, pLXSN hTERT or pLXSN empty vector. Error bars represent ±SD for three replicate cultures. .... 171

Figure 5.20 – BMI1 overexpressing NHU cells generated a functional TEER barrier (>1000 kOhm.cm<sup>2</sup>) at passage 10 unlike hTERT overexpressing NHU cells. TEER measurements (Section 2.5.5.2) for two NHU cell lines (P6) transfected with pLXSN BMI1, pLXSN hTERT or pLXSN empty vector. Error bars represent ±SD for three replicate cultures. .... 172

Figure 6.1 – Illustration of Phase I and Phase II xenobiotic metabolic reactions. Phase I metabolism, predominantly conducted by CYPs, involving oxidation of electrophilic xenobiotics or reduction of nucleophilic xenobiotics. Phase II conjugation reactions then take place to add glutathione groups (SG) sulfate groups (SO<sub>3</sub>H), acetyl groups (Ac) and glucuronide groups (GI) to the phase I metabolite, rendering the compound inactive. Phase II metabolites are then further metabolised or immediately removed from the body. .... 177

Figure 6.2 – percentage of total CYP metabolism of pharmaceutical agents by the individual CYP enzymes. The 8 CYP enzymes responsible for pharmaceutical agent metabolism and the percentage of pharmaceutical agents they metabolise are depicted (adapted from Wrighton and Stevens, 1992). .... 179

Figure 6.3 - Phenobarbital induces nuclear translation of CAR where it heterodimerises with RXR to bind to the PBREM, facilitating CYP2B gene expression. Phenobarbital also induces PXR to bind to either PBREM or XREM, also facilitating CYP2B gene expression. .... 180

Figure 6.4 – CYP2B1/2 expression was induced in rat bladders after 3 days of phenobarbital treatment in vivo. CYP2B1/2 was immunolabelled (Section 2.7.2) in control and phenobarbital-treated rat urothelium after 3 days of treatment. Scale bars = 50 µm (n=3 individual rats)..... 187

Figure 6.5 - CYP2B1/2 expression was induced in rat bladders after 7 days of phenobarbital treatment in vivo. CYP2B1/2 was immunolabelled (Section 2.7.2) in control and phenobarbital-treated rat urothelium after 7 days of treatment. Scale bars = 50 µm (n=3 individual rats)..... 188

Figure 6.6 – CYP2B1/2 expression was induced in rat bladders after 14 days of phenobarbital treatment in vivo. CYP2B1/2 was immunolabelled (Section 2.7.2) in control and phenobarbital-treated rat urothelium after 14 days of treatment. Scale bars = 50 µm (n=3 individual rats)..... 189

Figure 6.7 – CYP2B1/2 was expressed by hepatocytes in close proximity to blood vessels in phenobarbital-treated by not control rat livers after 7 days of treatment in vivo. CYP2B1/2 was immunolabelled (Section 2.7.2) in control and phenobarbital-treated rat liver sections after 7 days of dietary administration. Sections are shown at multiple magnifications to illustrate the specific

labelling pattern around blood vessels (indicated by arrows) in phenobarbital-treated animals. Scale bars = 200  $\mu$ m (n = 3 individual rats)..... 190

Figure 6.8 - CYP2B1/2 expression was significantly increased in phenobarbital-treated rat urothelium compared to controls. Computational quantification (Section 2.7.3) of urothelial CYP2B1/2 immunolabelling in control and phenobarbital-treated rats after 3 (D3), 7 (D7) and 14 (D14) days dietary administration was conducted. Mean DAB intensity in >1000 urothelial cells from three rat bladders per treatment/time group were generated using TissueGnostics software after CYP2B immunolabelling. Error bars  $\pm$  SD (n=3). (\* = p <0.05, \*\* = p <0.01, \*\*\* = p<0.001, using a 2-way ANOVA with a Tukeys post hoc test of comparison)..... 191

Figure 6.9 – CYP2B enzymes were expressed in rat urothelial cells after 7 days of dietary phenobarbital treatment. RT-PCR of CYP2B expression in rat urothelial cDNA after 7 days of treatment with a vehicle control or phenobarbital. Krt7 was included as a control urothelial cell marker, smooth muscle actin (SMA) as a marker of stromal cell contamination and GAPDH as a loading control. Positive (+) and negative (-) primer controls were rat liver cDNA (CYP2B & GAPDH), normal rat urothelial cell cDNA (Krt7) and rat genomic DNA (SMA). Negative (no template) control substituted water for cDNA. Reverse transcriptase negative (RT-) samples were also included alongside reverse transcriptase positive (RT+) samples as controls for genomic DNA contamination. .... 192

Figure 6.10 – The specific CYP2B enzyme expressed in rat urothelial cells was not able to be confirmed by RT-PCR. RT-PCR (30 cycles) was conducted on control or 7-day phenobarbital-treated rat urothelial cDNA. Specific primers were designed to amplify each of the 6 CYP2B enzymes found in rat. GAPDH was included as a loading control. Positive (+) control cDNA and negative (-) no template (water) controls were included for each primer set. Rat liver cDNA was used as a control for CYP2B1/2, CYP2B3, CYP2B12, CYP2B15 and for GAPDH primers. Rat skin cDNA was used as positive control for CYP2B21 primers. .... 194

Figure 6.11 – 5 of the 6 CYP2B genes expressed in rats were expressed by rat urothelial cells in response to phenobarbital. Aligned sequencing of cloned CYP2B RT-PCR product from 1 control and 5 phenobarbital-treated urothelial samples using generic CYP2B primers. Individual CYP2B enzymes were identified from small base pair variations within the amplified region. These differences are shaded to indicate specificity of CYP2B product, as indicated by colour in the table. Primer regions are shaded in yellow at either end of the sequence. .... 195

Figure 6.12 – Hepatic CYP content was increased in a dose dependant manner in response to the Syngenta compound. Mean total hepatic Cytochrome P450 content in control and dosed male (Blue) and female (red) rats after 28 days of treatment. Error bars represent  $\pm$ SD (n=5). .... 197

Figure 6.13 – Hepatic CYP2B enzyme expression was increased in response to the Syngenta compound in a dose dependant manner. Hepatic 7-pentoxoresorufin O-depentylase (CYP2B marker)

activity in control and dosed male (blue) and female (red) rats after 28 days of treatment. Error bars represent  $\pm$ SD (n=5). ..... 197

Figure 6.14 – CYP2B expression was induced in rat hepatocytes after 28 days of treatment with the Syngenta compound. Immunohistochemistry labelling of CYP2B1/2 was conducted in liver sections from control rats and rats treated with a developmental compound after 28 days of treatment. Scale bars = 200  $\mu$ m. Arrows indicate the location of blood vessels. Results were replicated in three individual animals per group (n=3). ..... 198

Figure 6.15 – CYP2B1/2 expression was induced by the Syngenta compound in vivo after dietary administration for 28 days. Immunohistochemistry labelling of CYP2B1/2 was conducted on control (left) and Syngenta compound-treated (right) rat urothelium after 28 days of treatment. Arrows indicate examples of strong superficial cell labelling. Scale bars = 50  $\mu$ m. (n=4). ..... 199

Figure 6.16 – Phenobarbital had no visible effect on NRU cells in culture after 72 hours of treatment. Phase contrast images showing primary (P0) and subcultured (P1) NRU cells after 72 hours in control medium (KSFMc) with 500  $\mu$ M phenobarbital. Scale bar = 50  $\mu$ m (n=2; R051, R053). ..... 200

Figure 6.17 – CYP2B enzyme induction did not occur in NRU cells in response to phenobarbital. RT-PCR results showing CYP2B expression in primary and subcultured (P1) NRU cells after 72 hours treatment with 500  $\mu$ M phenobarbital (Pheno). Rat liver cDNA was used as positive control, water as a negative control and GAPDH as a loading control (n=2 cell lines; R051 & R053). ..... 201

Figure 6.18 - Confirmation of urothelial cell layer maintenance in control and phenobarbital-treated rat organ cultures. Immunolabelling of the basal cell marker cytokeratin 5 (CK5), the whole urothelial cell marker cytokeratin 7 (CK7), the proliferation marker Ki67 and the superficial cell maker uroplakin 3a (UPK3A) in native rat bladder and in control and phenobarbital-treated (500  $\mu$ M) rat organ cultures (OC) after 72 hours of culture. Scale bar = 50  $\mu$ m. .... 203

Figure 6.19 – CYP2B enzyme induction occurred in rat organ cultures after 72 hours of treatment with phenobarbital. Immunolabelling of CYP2B1/2 was conducted in control and phenobarbital-treated (500  $\mu$ M) rat organ cultures generated from two independent Wistar rat bladders after 72 hours treatment. Scale bar = 50  $\mu$ m (n=2 individual rat bladders). ..... 204

Figure 6.20 – CYP2B enzyme expression was not induced in rat organ cultures in response to 72 hours of phenobarbital treatment. RT-PCR results showing CYP2B expression in isolated urothelial cells from organ cultures after 72 hours treatment with phenobarbital at concentrations of 250 and 500  $\mu$ M. Rat liver cDNA was used as positive control, water as a negative control and GAPDH as a loading control (n=1 NRU cell line). ..... 204

Figure 6.21 – Differentiated NHU cells were not visible affected by treatment with phenobarbital over 72 hours. Phase contrast images showing differentiated (ABS/Ca<sup>2+</sup>) NHU cells after 24 and 72 hours in 500  $\mu$ M phenobarbital. Scale bar = 50  $\mu$ m. .... 205

Figure 6.22 – CYP2B6 and associated CYP3A4 enzyme transcript induction did not occur in NHU cells in response to 72 hours of phenobarbital treatment. RT-PCR results for CYP2B6 and CYP3A4 expression in human urothelial cells after 72 hours of treatment. Human genomic DNA was included as a positive template control (+). GAPDH was included as a loading control. .... 207

Figure 6.23 – CYP2B6 and associated CYP3A4 enzyme protein induction did not occur in NHU cells in response to 72 hours of phenobarbital treatment. Western blot analysis of CYP2B6 and CYP3A4 expression in control and phenobarbital-treated, differentiated (ABS/Ca<sup>2+</sup>) NHU cell microsomes. Differentiated NHU cells were cultured for 72 hours in differentiation medium (KSFMc containing 5%ABS and 2mM Ca<sup>2+</sup>) ± 500µM phenobarbital. Human liver microsomes were included as positive controls, with rat liver microsomes as negative controls for CYP2B6. Cytochrome P450 reductase (CPR) was included as a loading control..... 207

Figure 7.1 – inhibitory crosstalk can occur between the EGFR/MAPK and the PI3K/Akt pathways but has yet to be investigated in urothelial cells. In conditions of physiological (2 mM) extracellular Ca<sup>2+</sup> ions, β-catenin is sequestered to the cell membrane and does not participate in regulation of gene expression, stimulating proliferation. EGF-stimulated ERK activation results in a decrease in the tyrosine phosphorylation of Gab1 and a decreased association with the PI3K, resulting in reduced activation (Yu et al, 2002). This is possibly achieved through the regulation of SHP2 (not shown), although this has not been confirmed. Akt has been shown to antagonises Raf activity by direct phosphorylation of Ser 259. This modification creates a binding site for 14-3-3 protein (not shown), which is a known negative regulator of Raf (Zimmerman and Moelling, 1999). Under conditions of physiological extracellular calcium ion concentrations, β-catenin is sequestered to cell membranes and form adherens junctions with E-cadherin (Georgopoulous et al., 2014). .... 218

## Tables

Table 2.2.1 - Agonists/Antagonists.....	37
Table 2.2 Plasmids.....	46
Table 2.3 Agarose gel preparations (w/v) .....	50
Table 2.4 Primary Antibodies .....	53
Table 2.5 - Secondary antibodies .....	53
Table 3.1 – Details of NRU Isolation Protocols in the Literature.....	73
Table 3.2 – The main stages of NRU cell isolation and culture with potential variables .....	78
Table 3.3 – NRU cell lines .....	79
Table 3.4 - NHU cell lines.....	79
Table 4.1 Pharmaceutical agonists/antagonists.....	109
Table 4.2 NHU Cells .....	111
Table 4.3 NRU Cells .....	111
Table 5.1 NRU Cells .....	153
Table 5.2 NHU Cells .....	153
Table 6.1 NRU Cells .....	185
Table 6.2 NHU Cells .....	185

## **Acknowledgements**

Firstly I must thank my supervisors at the University of York, Prof. Jenny Southgate and Dr. Simon Baker, for their advice, guidance and patience over the course of this project. Additionally, I would like to thank all members of the JBU, past and present, for their support and friendship and in particular the PhD students who I have worked with over the past 4 years.

I would also like to thank Syngenta for supporting this project and my industrial supervisors Mr Paul Rawlinson, Dr. Pratibha Mistry and Dr. Jayne Wright for everything they have contributed during our collaboration.

The rat tissue used in this project was donated by the Food and Environment Research Agency (FERA), the research group of Prof. Joanna Neill at the University of Manchester, Covance, Dr. Khawar Abbas at the University of Leeds, Syngenta and the technical staff in the BSF at the University of York. Without these contributions, this project could not have been conducted and as such I would like to acknowledge and thank them for their kindness and generosity.

Finally, I would like to thank my family and friends for all of their support and help. In York, special mention must go to all associated with the Phoenix and the York bar billiards society. Most importantly, I want to thank my parents and brother who have supported me tirelessly through all levels of education. I am forever grateful for all that they have done.

## **Authors Declaration**

The candidate confirms that the work submitted in this thesis is his own and that it has only been submitted to this institution. Appropriate credit has been given where reference has been made to the work of others. Data produced by Syngenta (Chapter 6, Figures 6.11-6.12) have been included with their full knowledge and permission.

## Chapter 1 - Introduction

<b>1.1 The <i>in vitro</i> paradigm.....</b>	<b>25</b>
<b>1.2 Predicting human toxicity .....</b>	<b>26</b>
<b>1.3 <i>In vitro</i> toxicology studies .....</b>	<b>29</b>
<b>1.4 Aims:.....</b>	<b>31</b>
1.4.1 Objectives.....	31

## 1.1 The *in vitro* paradigm

The *in vitro* paradigm describes a system that allows for the extrapolation of clinically relevant data from *in vivo* animal models to humans using cell culture systems. *In vitro* models have the potential to act a conduit between species, ensuring that results seen in animals *in vivo* accurately predict the effects in man (Blaauboer and Andersen, 2007).

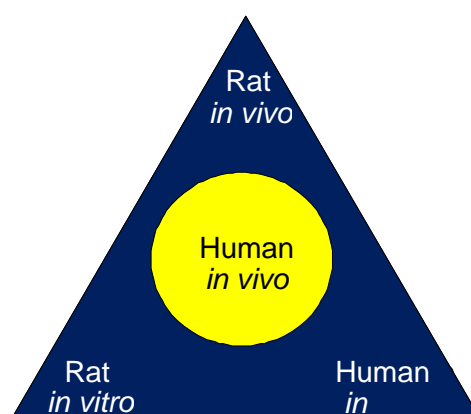


**Figure 1.1 – The *in vitro* paradigm is a potential system for improving the extrapolation of data from rats *in vivo* to humans *in vivo*.** Schematic of the *in vitro* paradigm illustrating how rat and human *in vitro* models can be combined with rats *in vivo* to predict results in humans *in vivo*.

Through the use of *in vitro* models, interspecies variations in physiology can be detected and accounted for when extrapolating results to humans. The establishment of robust methods to propagate and differentiate human cells in culture has significantly increased the potential of human cell culture models and, in addition to bridging the gap between *in vivo* animal models and humans, *in vitro* models may also have the ability to replace animals in a number of circumstances (Andersen and Krewski, 2009; McKim, 2010; Perel et al., 2007). *In vitro* models have the additional advantage of having lower ethical and financial costs when compared to experiments *in vivo* (reviewed by Andersen and Krewski, 2009). The full potential of *in vitro* systems, however, has yet to be realised and it is only with further development and validation that the use of *in vitro* models can be fully exploited.

The development of comparable *in vitro* cell culture systems in different species has allowed for side-by-side experimentation and assessment. By developing comparable rat and human *in vitro* cell culture systems, the relevance of results generated by rat *in vivo* studies to humans can be determined. Any differences in cellular physiology between rats and humans are revealed by such comparisons, allowing for more informed extrapolations of results to be made between the species (reviewed by Krewski et al., 2011).

## 1.2 Predicting human toxicity

Toxicology studies aim to identify whether a chemical entity will have toxic effects on humans after administration or exposure (Wexler, 2009). By understanding the risk posed to humans by novel chemical entities, they can be removed from development or appropriate levels of control put in place to avoid toxic exposure. Current toxicity studies rely heavily on *in vivo* assays in multiple species to understand a chemical's toxicity, with the findings being extrapolated from mammalian *in vivo* models to humans (reviewed by Blaauboer and Andersen, 2007)

Approximately 80% of animals used in toxicology studies are rodents with rats being the most commonly used species (reviewed by Guarino, 2009). Regulatory agencies normally require compounds to be subsequently tested in an additional non-rodent species in order to satisfy chemical/pharmaceutical safety licensing criteria. In 2008 a review of toxicity studies found that xenogeneic *in vivo* models were on average 37-50% reliable at predicting the effects of novel chemical entities on humans (reviewed by Perel et al., 2007). It attributed the number of novel chemical entities failing during clinical trials (post mammalian *in vivo* testing) to the low predictive accuracy in translating results between animals *in vivo* and humans.

Although animals such as rodents have for many years been the "gold standard" model for toxicological research, it has become apparent that the genetic, molecular and physiological differences that exist between animals and humans can inhibit

results from accurately being extrapolated between species (Rosenkranz and Cunningham, 2005). In response to xenobiotic or physical insults, different species are capable of responding in different ways. To quote the title of one review on the effect of species variations in toxicology, “A mouse is not a rat is not a man” (reviewed by Cunningham, 2002). There is an ever-increasing body of literature that demonstrates that species differences can significantly inhibit accurate extrapolation between rodents and humans.

There are a number of reported cases in which normal rat physiology has led to inaccurate predictions of human toxicity. One example that demonstrates this is in relation to kidney and bladder cancer. Rat hepatocytes synthesize alpha-2U globulin, a protein that binds to a number of xenobiotic compounds in blood before being filtered by the kidneys. Bound alpha-2U globulin accumulates in rat kidneys, leading to nephropathy and tumours. One of the compounds that alpha-2U globulin is known to bind to in rats is the artificial sweetener saccharin. The conjugate formed is filtered by the kidneys and stored in the bladder where it forms silicate crystals. These crystals mechanically damage the lining of the bladder and can lead to pathologies including cancer. Results produced in rats *in vivo* showing saccharin was carcinogenic were responsible for the compound being banned by a number of countries in the 1970s and 1980s (Priebe and Kauffman, 1980). As humans do not synthesize alpha-2U globulin this mechanism of carcinogenesis is not relevant to humans and in 1999, a review by the International Agency for Research on Cancer conclusively showed that saccharin could not be considered a human carcinogen (IARC, 1999; Takayama et al., 1998; Whysner and Williams, 1996).

Alternatively, examples exist in which pharmaceutical compounds believed to be safe based on animal *in vivo* data were toxic when given to human patients at concentrations significantly lower than the No Observable Adverse Effect Level (NOAEL). In 2006, an experimental immunoregulatory agent (the monoclonal antibody TGN1412), which had passed pre-clinical testing in both rodents and non-human primates, caused multi-organ failure when given to healthy clinical trial

volunteers at a dose 500 times lower than the NOAEL. The symptoms observed in the trial volunteers are thought to be as a result of CD4<sup>+</sup> effector memory T-cell activation by TGN1412. Variations in CD4<sup>+</sup> effector memory T-cells between the test species and humans (in particular the lack of CD28 expression), is thought to be responsible for the failure to predict this compounds toxicity in humans (Suntharalingam et al., 2006; Stebbings et al., 2007; Eastwood et al., 2010).

These examples, while rare, are by no means unprecedented and highlight the necessity for alternative, more relevant, model systems to be developed to replace or validate results generated by *in vivo* studies. Additionally, models that can be used to understand the mechanisms of toxicity enable species variations in physiology to be accounted for when extrapolating between rats and humans. From an industry perspective, methods that can accurately detect toxicity at an earlier stage of the chemical development pipeline are beneficial as they increase efficiency and reduce costs.

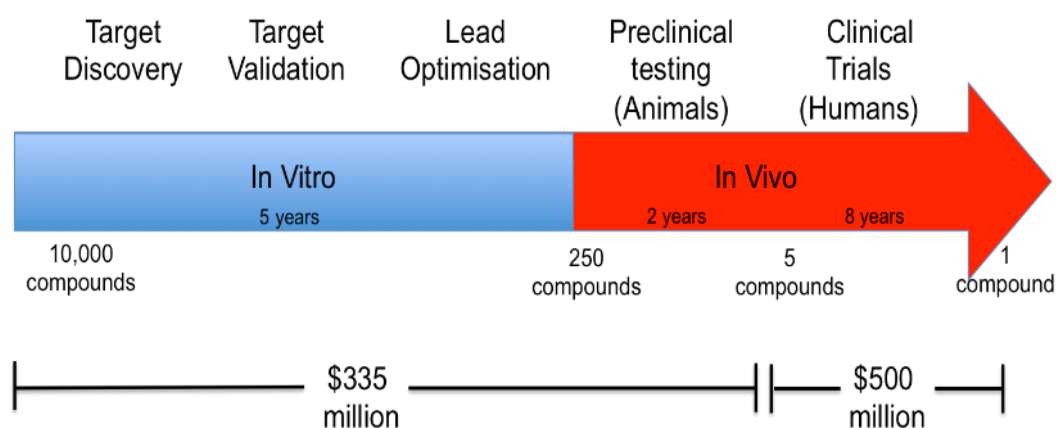


**Figure 1.2 – The pharmaceutical compound development pipeline.** Details of the use of *in vitro* models in target discovery, validation and optimisation (Blue) and *in vivo* models in preclinical and clinical toxicology testing (red). The approximate time periods, costs and number of compounds at each stage of development as of 2000 in the US are indicated (adapted from DiMasi et al., 2003).

### 1.3 *In vitro* toxicology studies

Currently *in vitro* models are used to a limited extent in early toxicity studies to identify whether xenobiotics affect a small number of specific targets, such as the human Ether-a-go-go Related Gene (hERG) channel. These targets are studied due to the consequences of inhibiting their normal function, for example blockade of the hERG channels causes long Q-T (LQT) syndrome or torsade de pointes, which can lead to acute heart failure and death (Witchel and Hancox, 2000; Netzer et al., 2001).

The use of *in vitro* models in toxicology has been strongly advocated as a means to improve the predictive accuracy of toxicity studies (Andersen, 2003; Andersen and Krewski, 2009; Andersen and Krewski, 2010; Krewski et al., 2011). The need to supplement and/or replace animal *in vivo* testing with more human-relevant models has driven advancements in human *in vitro* systems, as well as tissue engineering research, but as of yet their use has not been widely adopted (reviewed by Pampaloni et al., 2007; McKim, 2010; Parasuraman, 2011; Thomas et al., 2012; Soldatow et al., 2013). *In vitro* systems offer the advantage of providing moderately high-throughput screening systems at a significantly reduced cost when compared to *in vivo* studies. They also offer the ability to understanding cellular mechanisms of toxicity (Burden et al., 2015; Krewski et al., 2011). The current disadvantages with *in vitro* systems, however, include a lack of consistency in generating cell lines, a difficulty in producing cell lines with a high capacity for expansion and developing cell lines that retain their normal characteristics *in vitro* (Hartung and Daston, 2009). These factors have led to a lack of confidence in the predictive accuracy and reproducibility of results obtained from *in vitro* models. In order to validate existing human *in vitro* models and establish credible *in vitro* systems to support and replace *in vivo* models in toxicity studies, comparative rodent and human *in vitro* systems need to be developed and assessed. By having the ability to conduct side-by-side comparisons of xenobiotic toxicity in rats and humans *in vitro*, interspecies differences in responses to xenobiotics can be determined, increasing the predictive accuracy of toxicity studies (van Ravenzwaay and Leibold, 2004; Roesems et al.,

1997; Louisse et al., 2010; reviewed by Andersen and Krewski, 2009; reviewed by Hartung and Daston, 2009).

In this study, bladder-derived epithelial (urothelial) cell lines will be developed, optimised and analysed as potential models for use in toxicity testing. *In vitro* systems enable the analysis of organ-specific toxicity, and having validated models of the organs systems at risk of insult from toxic xenobiotics would be of value. As described in Chapter 3, the urothelium can be exposed to high levels of xenobiotics secreted in urine and, as such, the use of *in vitro* models of the urothelium in toxicity testing would allow for the risks of xenobiotic-induced urothelial toxicity to be established.

## 1.4 Aims:

To conduct a comparison of normal rat and human urothelial cell culture systems as a means of validating a normal urothelial *in vitro* system for use in toxicity studies. Species variations in normal urothelial cell physiology will be explored, attempts made to immortalise normal urothelial cells and novel metabolic capabilities of urothelial cells investigated both *in vivo* and *in vitro*.

### 1.4.1 Objectives

1. Develop a normal rat urothelial cell culture system that has congruence to an already established normal human urothelial cell culture system
2. Investigate the signal transduction pathways regulating NRU cell proliferation
3. Immortalise NRU and NHU cells through the overexpression of BMI1 and hTERT
4. Investigate the induction of Cytochrome P450 2B expression in normal rat urothelial cells *in vivo* and *in vitro*

## Chapter 2 - Materials and Methods

<b>2. Materials and Methods</b> .....	<b>32</b>
<b>2.1 General</b> .....	<b>33</b>
<b>2.2 Commercial Suppliers</b> .....	<b>33</b>
<b>2.3 General laboratory equipment</b> .....	<b>33</b>
<b>2.4 Stock Solutions</b> .....	<b>33</b>
<b>2.5 Cell and Tissue Culture</b> .....	<b>34</b>
2.5.1 General.....	34
2.5.2 Primary Normal Urothelial Cell Culture .....	34
2.5.3 Assays.....	38
2.5.4 Population doubling curves .....	39
2.5.5 NHU cell differentiation .....	39
2.5.6 Retropack™ PT67 Packaging Cell Line .....	40
2.5.7 Cryo-preservation and thawing .....	40
2.5.8 Testing cell lines for Mycoplasma .....	41
<b>2.6 Molecular Biology</b> .....	<b>42</b>
2.6.1 General.....	42
2.6.2 Glass and Plasticware.....	42
2.6.3 Analysis of Gene Expression .....	42
2.6.4 Plasmids .....	46
2.6.5 Molecular cloning and retroviral plasmid generation .....	49
2.6.6 Amplification of plasmid DNA.....	51
<b>2.7 Protein Analysis</b> .....	<b>52</b>
2.7.1 Antibodies .....	52
2.7.1 Immunofluorescence labelling.....	54
2.7.2 Immunolabelling of tissue sections.....	55
2.7.3 Image capture and analysis.....	59
2.7.4 Western Blotting .....	60

## 2.1 General

All experimental work within this thesis was conducted within the Jack Birch Unit for Molecular Carcinogenesis or the central Technology Facility in the Department of Biology at the University of York, with the exception of tissue harvesting and *in vivo* studies which were conducted at several locations listed in Appendix 1.1.

## 2.2 Commercial Suppliers

Details of all commercial suppliers and manufacturers can be found in Appendix 1.2. The supplier or manufacturer is indicated in the text.

## 2.3 General laboratory equipment

All metal dissection instruments, Pasteur glass pipettes (SLS) and pipette tips (Starlab) were autoclaved in a Harvard/LTE Series 100 autoclave at 121°C (1 bar) for 20 minutes and air dried at 80 °C. Sterile, single use plasticware was purchased from Sterlin (SLS) with the exception of RNase/DNase-free pipette tips which were from StarStedt, RNase-free tubes (Ambion) and serological pipettes (StarStedt).

## 2.4 Stock Solutions

Unless otherwise indicated stock solutions were prepared with ultra-pure water from a Purelab Ultra Genetic (Elga) ultraviolet purification unit. Heat-stable solutions were autoclaved at 121 °C (1 bar) for 20 minutes and cooled to ambient temperature before use. Solutions that were unable to be autoclaved were filter-sterilised using an Acrodisc low-protein binding Tuffryn® HT syringe filter (pore size 0.2 µm; Sigma Aldrich) if intended for cell culture use.

## 2.5 Cell and Tissue Culture

### 2.5.1 General

Aseptic technique was employed when isolating and culturing cells. Routine cell culture procedures were conducted within a recycling laminar flow class II safety cabinet (Medical Air Technology) and work involving retroviruses was conducted in an externally ducted (Envair) cabinet. All cabinets were disinfected using 70 % ethanol (Sigma) before each use and were cleaned once per week using Mikrozid® AF disinfectant (SLS). All waste medium from cells was aspirated into Virkon® (10 % w/v) traps and left for at least 30 minutes before disposal. Medium from cells exposed to retrovirus was left for 24 hours in Virkon® (10 % w/v) prior to disposal. All reagents were obtained from Sigma Aldrich, unless otherwise indicated, and were of tissue culture grade. Cells were incubated in Heracell 240 incubator (Thermo Scientific) at 37 °C in a humidified atmosphere of 5 % CO<sub>2</sub> (urothelial cells) or 10 % CO<sub>2</sub> (PT67 cells) in air. Cells were counted as single cell suspensions using an improved Neubauer haemocytometer (VWR) and a phase contrast microscope (EVOS™). All centrifugation was carried out in a bench top centrifuge (Sigma Aldrich) at 400 g for 5 minutes, unless otherwise stated.

### 2.5.2 Primary Normal Urothelial Cell Culture

#### 2.5.2.1 Rat Tissue Specimens

Surplus rat bladders were donated by the Food and Environment Research Agency (FERA), Sand Hutton, York, and research groups at the University of Manchester, the University of Leeds and the University of York. A small number of rats were also purchased for the specific purpose of harvesting bladder tissue. Ethical approval was obtained from the Department of Biology Ethics committee at the University of York to use both surplus tissue and to purchase animals as a source of bladder tissue.

Rats were killed using an approved schedule one procedure. Whole rat bladders were aseptically dissected from the animals at time of death (appendix 1.7) and placed into 25 mL polystyrene Universal tubes containing 10 mL of sterile transport medium (Southgate et al., 1994) (Hanks balanced salt solution (HBSS) (Gibco) containing 20 kallikrein-inhibiting units/mL of Aprotinin (Trasyol; Bayer), 10 mM HEPES pH 7.6 (Gibco) for a maximum of 4 hours. Samples were kept, where possible, at 4 °C until processing. Rat bladders from the same source were given an arbitrary record number (R-number) and the origin, age, strain and sex of the animals were recorded as well as details on whether tissue was fixed in 10 % (v/v) formalin for histology. Details of the R-numbers used can be found in the experimental approach section of each chapter.

#### **2.5.2.2 Human tissue Specimens**

Human bladder, ureter and renal pelvis specimens were obtained by surgeons at York District Hospital, St. James's University Hospital in Leeds, Leeds General Infirmary in Leeds and Pinderfields Hospital, Mid Yorkshire Hospitals NHS Trust in Wakefield. Tissue biopsies were taken with fully informed consent from patients with no history of urothelial neoplasia and with the permission of an NHS Research Ethics Committee. Biopsies were collected in sterile 25 mL polystyrene Universal tubes containing 15 mL of sterile transport medium. Samples were stored at 4 °C until processed. Upon processing each sample was given a sequential record number (Y-number) and details of the patient's age, gender and operation were recorded. Details of the Y number used can be found in the experimental approach section of each chapter.

#### **2.5.2.3 Isolation of Primary Urothelial cells**

The protocol for isolating urothelium from human tissue samples was performed as described in Southgate et al. (1994; 2002). Normal human tissue specimens were placed in a Petri-dish (Thermo Fisher) and dissected to remove excess fat and expose the urothelium using scissors and forceps. Tissue was incubated at 37 °C for

4 hours in 5 mL of EDTA stripper medium (Appendix 1.4.2) before urothelial sheets were physically removed using forceps. These sheets were collected via centrifugation and resuspended in Collagenase IV (400 U) solution (Appendix 1.4.2). The solution was incubated for 20 minutes at 37 °C before the cells were collected again via centrifugation and resuspended in Keratinocyte Serum Free Medium complete with 5 ng/mL epidermal growth factor (rhEGF; Life Technologies), 50 µg/mL bovine pituitary extract (BPE; Life Technologies) and 30 ng/mL cholera toxin (Sigma Aldrich) (KSFMc). Cells were counted and then seeded into N<sub>2</sub> plasma treated tissue culture flasks, petri dishes or plates (Starstedt). The normal rat urothelial cell isolation protocol was based upon the above method for NHU cell isolation, but optimised as described in Chapter 3.

#### **2.5.2.4 Subculture of Rat and Human urothelial cell lines**

NRU cells were passaged when cell colonies appeared to reach a maximum size and density. NHU cells were subcultured when approximately 90 % confluent. Cells were incubated in 0.1 % (w/v) Ethylenediaminetetra-acetic acid disodium salt (EDTA) solution (Appendix 1.4.2) for 5 minutes at 37 °C to chelate calcium and initiate cell dissociation. Cells were then incubated in 0.5 mL of Hank's balanced salt solution (HBSS; Life Technologies) containing 0.25 % (w/v) trypsin and 0.02 % (w/v) EDTA for 1-2 minutes at 37 °C. Cells dissociation was enhanced by physically tapping the flask/dish/plate several times. Upon dissociation cells were resuspended in 5 of KSFMc containing 2 mg of Soya bean trypsin inhibitor (Sigma Aldrich) and collected by centrifugation. NRU cells seeding densities and subculture are optimised in Chapter 3. NHU cells were reseeded at a ratio of 1:3 and used for experiments between passage 0-7 (P0-P7).

#### **2.5.2.5 Differentiation of normal human urothelial cells**

NHU cells were cultured until 80 % confluent in KSFMc. At 80-90 % confluent the medium was supplemented with 5 % of batch tested adult bovine serum (ABS; Harlan Sera-lab). Cells were cultured in KSFMc +5 % ABS until confluent at which

point the extracellular calcium concentration was increased to 2 mM using CaCl<sub>2</sub>. Once the calcium ion concentration was increased, cells were used for experiments after 5 days. For experimental controls, the same Y-number NHU cells were cultured in KSFMc and harvested at the same time point.

### 2.5.2.6 Pharmacological Agonists & Antagonists

The agonists and antagonists used in this study are listed in Table 2.1 along with their working concentrations. Compounds were reconstituted under aseptic conditions in sterile Elga H<sub>2</sub>O or tissue culture grade dimethyl sulfoxide (DMSO; Sigma) according to manufactures instructions and frozen (-20 °C) in single use aliquots. All compounds were titrated before use to determine effective concentrations and stock concentrations were calculated to ensure that DMSO concentrations did not exceed 0.1 % total volume.

**Table 2.2.1 - Agonists/Antagonists**

Compound	Target	Supplier	**Published IC <sub>50</sub>	Vehicle (0.1 %)
PD153035 (PD)	EGFR	Calbiochem	25 pM	DMSO
UO126	MEK1/2 inhibitor	Calbiochem	72/58 nM	DMSO
SB415286 (SB)	GSK3 $\beta$	<b>Sigma Aldrich</b>	2.9 $\mu$ M	DMSO
IGF1	IGFR	Sigma Aldrich	n/a	PBS
LY294002 (LY)	PI3K	Calbiochem	1.4 $\mu$ M	DMSO

## 2.5.3 Assays

### 2.5.3.1 Cell biomass assay

The alamarBlue® assay was used to assess urothelial cell growth over 10 daytime courses. Urothelial cells were cultured in either 96 or 12 well plates. AlamarBlue® reagent (Serotec) was diluted 1:10 in culture medium and added to cells (200 µL per well on a 96 well plate, 1.5 mL per well on a 12 well plate) for 4 hours in a humidified incubator at 37 °C (5 % CO<sub>2</sub>). 96 well plates could be immediately analysed on a MultiSkan Ascent 96/384 Plate Reader (Thermo Scientific) at wavelengths of 570 and 630 nm. Medium from 12 well plates was carefully removed and pipetted into a 96 well plate before being analysed. A no cell control was always included.

The percentage reduction in alamarBlue® was calculated using the following equation provided by the manufacturers:

$$\left[ \frac{(34798 \times \text{NRU cells @ 570 nm}) - (80586 \times \text{NRU cells @ 630 nm})}{(155677 \times \text{no cells @ 630 nm}) - (5494 \times \text{no cells @ 570 nm})} \times 100 \right]$$

34798 - molar extinction coefficient of oxidized alamarBlue (Blue) at 600nm

80586 - molar extinction coefficient (E) of oxidized alamarBlue (Blue) at 570nm

155677 - molar extinction coefficient of reduced alamarBlue (Red) at 570nm

5494 - molar extinction coefficient of reduced alamarBlue (Red) at 600nm

After analysing the reduction, diluted alamarBlue® reagent was removed from cells and replaced with fresh KSFMc medium and the cell cultures maintained.

### 2.5.3.2 Colony formation assay

NRU cells were isolated using either the EDTA/collagenase IV or Dispase II isolation protocols and seeded at a range of densities onto N<sub>2</sub> plasma treated tissue culture plastic 6 well plates (StarStedt) or 6 well plates (StarStedt) coated with 5 µg/cm<sup>2</sup> Collagen I (from rat tail; Sigma Aldrich) in sterile PBS for 2 hours immediately prior to seeding. Cell medium was changed after 24 hours and then every 2-3 days. After 5 days of culture, urothelial cells were fixed using methanol:

acetone (1:1; v/v) for 30 seconds at ambient temperature before being stained with 0.1 % crystal violet (sigma Aldrich) in 75 % ethanol (v/v) for 5 minutes. Plates were rinsed for 5 minutes under running tap water and air-dried inverted at ambient temperature. Colonies were imaged using an Odyssey infrared imaging system (LiCor) and analysed using ImageJ software.

### 2.5.4 Population doubling curves

Population doubling (PD) values were calculated for NHU cells when passaged according to the following formula:

$$PD = \sum \frac{\log \left( \frac{Ch_n}{Cp_n} \right)}{\log 2}$$

**Ch** is the number of cells harvested after passage, **Cp** is the number of cells seeded and **n** is the passage number.

### 2.5.5 NHU cell differentiation

#### 2.5.5.1 Differentiation

A method of inducing NHU cell differentiation and the subsequent formation of a “biomimetic urothelium” has previously been established (Cross et al. 2005). Briefly, 80 % confluent NHU cells were cultured for 5 days in KSFMc medium supplemented with 5 % adult bovine serum (ABS) (v/v). Cells were passaged, left for 24 hours and the extracellular calcium ion concentration increased to 2 mM through the addition of CaCl<sub>2</sub> (Sigma Aldrich) in PBS. Cells were maintained for up to 10 days after the increase in calcium concentration.

#### 2.5.5.2 Transepithelial electrical resistance (TEER)

To generate a “biomimetic urothelium” that generated a TEER, NHU cells were seeded onto Snapwell™ membranes after 5 days culture in KSFMc + 5 % ABS at a density of 5 × 10<sup>5</sup> cells per Snapwell™ in a volume of 500 μL. 4 mL of medium was

placed in the outer chamber and at 24 hours all medium replaced with KSFMc (2 mM Ca<sup>2+</sup>) + 5 % ABS (v/v). Medium was changed every 2-3 days.

TEER was measured, as an indicator of barrier function and differentiation capability, using an EVOM™ Epithelial Voltohmmeter (World Precision Instruments) after sterilisation in Cidex Plus reagent (World Precision Instruments) and having been rinsed twice in sterile KSFMc medium + 5 % ABS (v/v).

### **2.5.6 Retropack™ PT67 Packaging Cell Line**

The PT67 packaging cell line is a NIH3T3 fibroblast derived cell line purchased from Clontech. This cell line has been genetically engineered to produce retroviral genes gag, pol and env, enabling it to produce a replication-defective retrovirus with a broad (amphotropic) mammalian host range once transfected with a retroviral vector such as pLXSN. PT67 cells were cultured in Dulbecco's Modified Eagle's Medium (DMEM; Life Technologies) supplemented with 10 % (v/v) fetal bovine serum (FBS; Harlan Sera-Lab) and were passaged using the same protocol as for urothelial cells (2.6.2.4). Before being transfected with a retroviral vector, PT67 cells underwent Hypoxanthine Aminopterin Thymidine (HAT; Life Technologies) medium selection as recommended by the supplier. PT67 cells were cultured for 5 days in DMEM/10 % FBS with 100nm aminopterin followed by 5 days in DMEM/10 % FBS-HAT medium (30nm hypoxanthine, 1 M aminopterin, 20 mM thymidine). Finally cells were cultured for 5 days in DMEM/10 % FBS-HT (30 mM hypoxanthine, 20 mM thymidine) and immediately cryo-preserved.

### **2.5.7 Cryo-preservation and thawing**

Cells were harvested using EDTA/trypsin in versene as during passaging. Cells were centrifuged and resuspended in cell medium (KSFMc for urothelial cells, DMEM/10 %FBS for PT67 cells) containing 10 % (v/v) FBS and 10 % dimethyl sulfoxide (DMSO). Approximately 1x10<sup>6</sup> cells were aliquoted into polypropylene

cryovials (Greiner) and placed into a “Mr Frosty” (Nalgene; Thermo Scientific) containing 250 mL of isopropanol (SLS) that had been kept at 4 °C for >2 hours. The “Mr Frosty” was placed into a -80 °C freezer for 12-16 hours before the cryovials were transferred into Statebourne storage dewers containing liquid nitrogen (-196 °C).

To thaw cells, Cryovials were removed from liquid nitrogen and rapidly warmed to 37 °C. 5 mL of appropriate medium was added and cells centrifuged before being resuspended in medium and seeded as required.

### **2.5.8 Testing cell lines for Mycoplasma**

All cell lines were tested for Mycoplasma by looking for the presence of extra-nuclear staining with the DNA intercalator Hoechst 33258 (Sigma Aldrich). Cells were seeded at a density of  $1 \times 10^4$  cells per well onto autoclaved 12 well glass slides (Hendley-Essex) in sterile Hereaus boxes (Sartorius). Cells were allowed to attach for 4 hours before the chambers of the Hereaus box were flooded with 5 mL of the appropriate medium. Cells were cultured until 50-60 % confluent before being fixed for 30 seconds in methanol: acetone (1:1; Sigma Aldrich), air-dried and stored at -20 °C. To stain cells with Hoechst 33258, slides were defrosted to room temperature and incubated for 5 minutes in 0.1 µg/mL Hoechst 33258 in PBS in the dark. Cells were rinsed twice in PBS, air-dried and mounted in antifade. Slides were examined using an Olympus Bx60 microscope using the appropriate epifluorescence filter set.

## 2.6 Molecular Biology

### 2.6.1 General

Microbiology work was conducted according to the University of York guidelines for Good Microbiological Practise. Aseptic technique was used at all times and all benches were cleaned before and after use with 2 % (w/v) Virkon® and 70 % ethanol (Sigma). All waste solutions were treated in 2 % (w/v) Virkon® for 24 hours before disposal. Glass and plasticware used was submerged in 2 % Virkon® for 24 hours before being either autoclaved and disposed of or washed for reuse.

### 2.6.2 Glass and Plasticware

5 and 10 mL liquid cultures were incubated in 25 mL polystyrene Universal tubes. 500 mL glass Buchner flasks were used for overnight incubation of liquid cultures. Luria-Broth Agar was poured into 9 cm UV-irradiated Petri dishes (Thermo Fisher) and allowed to set at room temperature. Single use inoculating loops (Thermo Fisher) and a 100 % ethanol (Sigma Aldrich) sterilised glass L-shaped spreader was used for plating bacteria.

### 2.6.3 Analysis of Gene Expression

#### 2.6.3.1 General

RNase Zap® was used to treat all surfaces and pipettes before working with RNA. All glass and plasticware was incubated overnight at ambient temperature in 0.1 % diethyl pyrocarbonate (DEPC; Sigma Aldrich) to inactivate any RNase's present. DEPC was inactivated by autoclaving in a Harvard/LTE Series 100 autoclave at 121°C (1 bar) for 20 minutes and air dried at 80 °C. Only DNase and RNase free pipette tips (Axygen; Thermo Fisher) and nuclease-free microcentrifuge tubes (Ambion; Thermo Fischer) were used. All water was incubated in DEPC overnight at room temperature and autoclaved prior to use.

### 2.6.3.2 RNA extraction

RNA was extracted from cultured cells and tissue samples using TRIzol™ reagent (Life Technologies). For cultured cells, medium was removed and the cells rinsed twice in 8 mL's of PBS. 1 mL of TRIzol™ was added and the flask left for 5 minutes on a rotary shaker. A cell scraper (StarStedt) was used to remove all of the cells from the tissue culture plastic and they were collected in the TRIzol™ reagent into 1.5 mL microcentrifuge tubes. At this point samples were able to be stored at -80 °C and defrosted on ice when required. Samples were left at ambient temperature for 5 minutes before 0.2 mL of chloroform (BDH) was added and the tubes vortexed for 15 seconds. Samples were incubated for 5 minutes at ambient temperature and centrifuged (12,000 g) for 15 minutes at 4 °C in a Hettich Mikro-200R. The upper aqueous (clear) phase was carefully removed into a fresh 1.5 mL microcentrifuge tube, 0.5 mL of isopropanol added and the sample mixed by inverting 5 times. The samples were incubated at ambient temperature for 10 minutes before being centrifuge (12,000 g) for 20 minutes at 4 °C. The supernatant was removed and the RNA pellet resuspended in 0.5 mL of 75 % (v/v) ethanol. The pellet was recovered by centrifuging (7,500 g) for 5 minutes at 4 °C, resuspended a second time in 75 % (v/v) ethanol before being collected for a final time by centrifuging (7,500 g) for 5 minutes at 4 °C. The pellet was air-dried and resuspended in 30 µL of DEPC-treated H<sub>2</sub>O.

### 2.6.3.3 DNase treatment

RNA samples were treated using a DNase I, RNase-free kit (Thermo Scientific) according to the manufacturer's instructions. Briefly, to a 30 µL RNA sample, 3.7 µL of 10 x reaction buffer with MgCl<sub>2</sub> and 3.7 µL of DNase I, RNase-free were added and incubated for 30 minutes at 37 °C. 3.7 µL of 50 nM ethylenediaminetetraacetic acid (EDTA) were added, the solution mixed by pipetting and heated to 65 °C for 10 minutes.

#### 2.6.3.4 RNA quantification

The quantification and quality of isolated RNA was assessed after DNase treatment using a Nanodrop™ UV/visible spectrophotometer (Shamadzu).

#### 2.6.3.5 Removing RNA contamination

If RNA was found to be contaminated (e.g. with ethanol or salt), as indicated by low spectrophotometer 260:230 nm ratio values, it was cleaned by alcohol and salt precipitation. 3 M sodium acetate (1:9) and 100 % ethanol (2.5 x volume) were added, the sample vortexed and then left at -80 °C overnight (16 hours). Samples were centrifuged (12,000 g) for 30 minutes at 4 °C in a Hettich Mikro-200R, the pellets resuspended in 500 µL of 70 % (v/v) ethanol and collected again by centrifugation (7,500 g) for 5 minutes at 4 °C. Pellets were air-dried and resuspended in 30 µL of DEPC-treated H<sub>2</sub>O.

#### 2.6.3.6 cDNA Synthesis

cDNA was generated from 1 µg of total RNA using 50 ng of random hexamer primers and the Superscript™ first-strand cDNA synthesis kit (Invitrogen). RNA and random hexamer primers were added together and the total volume made up to 12 µl with DEPC-treated water. The sample was heated to 65 °C for 10 minutes before being left on ice for 2 minutes. 7 µL of a “master mix” containing 2 µL of reverse transcriptase buffer, 2 µL of 25 mM MgCl<sub>2</sub>, 2 µL of 0.1 mM dithiothreitol (DTT) and 1 µL of 10 µM dinucleotide triphosphate (dNTP) mix was added to each sample and incubated at ambient temperature for 2 minutes. 1 unit of Superscript™ II reverse transcriptase enzyme was added and samples incubated for 10 minutes at 25 °C and 50 minutes at 42 °C. The reaction was inactivated by heating to 70 °C for 15 minutes. cDNA was stored at -20 °C. For each RNA sample a negative control reaction was conducted in which Superscript™ II reverse transcriptase enzyme was not included (RT negative).

### 2.6.3.7 PCR Primer design and optimisation

The messenger RNA (mRNA) coding sequences for the gene of interest were accessed from the Ensembl database. If multiple protein-coding transcript variants exist for the gene of interest, or if the primers were being designed to amplify multiple genes with high sequence homologies, sequences were aligned using Kalign (EMBL library). Primers were designed using Primer-Blast (NCBI) to be 17-23 base pairs (bp) in length and have a melting temperature ( $T_m$ ) of between 55 and 65 °C. GC content was restricted to 40-60 %. Where possible primers were designed to amplify a region within a single exon. Primers were ordered from Eurofins and upon arrival reconstituted to a concentration of 100 mM in DEPC-treated H<sub>2</sub>O before being stored at -20 °C. Primer stocks were diluted 1:10 (10 mM) prior to use. Primer sequences can be found in appendix 1.6.

The optimal  $T_m$  and primer binding efficiency were established by gradient RT-PCR (appendix 2.2). RT-PCR reactions were set up as described in section 2.6.3.8. with either genomic DNA (non-exon spanning primers) or control cDNA (exon-spanning primers) used in place of sample cDNA. 8 identical samples were subjected to the standard RT-PCR conditions but at a range of temperatures between 55 and 65 °C. The efficiency of the PCR reactions at the range of temperatures was assessed by agarose gel electrophoresis (section 2.6.5.2 and 2.6.5.3). The  $T_m$  in which the strongest band at the correct molecular weight was produced and in which no additional bands occurred was chosen for RT-PCR.

### 2.6.3.8 RT-PCR

Standard RT-PCR was conducted using GoTaq® G2 Flexi DNA Polymerase (Promega) according to the manufactures instructions. Briefly, a master mix was created containing 4 µl of 5X Green GoTaq® Flexi Buffer, 2 µl of 25 mM MgCl<sub>2</sub>, 2 µl of 10 mM forward primer, 2 µL of 10 mM reverse primer, 0.4 µl of dNTP mix (25 mM of aDTP, dCTP, dGTP, dTTP; Promega), 8.5 µl of DEPC-treated H<sub>2</sub>O and 0.1 µl of GoTaq® G2 Flexi DNA Polymerase (Promega). 19 µL of master mix was added to 1 µl of sample cDNA in a thin-walled 8-well strip PCR tube (Axygen; Thermo

Fisher). The RT-PCR reaction was conducted in a Bio-Rad T100™ thermocycler. Samples were heated to 95 °C for 3 minutes initially to activate the enzyme before completing 30 cycles of 95 °C for 30 seconds, the annealing temperature ( $T_m$ ) for 1 minute and 72 °C for 1 minute. After 30 cycles samples a final elongation step of 72 °C for 5 minutes was conducted before samples were cooled to and kept at 4 °C. Assessment of RT-PCR products was by gel electrophoresis (see sections 2.7.4.2 and 2.7.4.3).

### 2.6.3.9 Next generation sequencing

Next generation sequencing data was accessed from the JBU next generation sequencing archive. This data was generated from samples of freshly isolated (P0), proliferating (Pro) and differentiated (ABS/ $Ca^{2+}$ ) NHU cells from three individual donors. Samples were analysed on a Illumina Hiseq2000 and results normalised before being uploaded onto the database.

### 2.6.4 Plasmids

Details of the two plasmids used within this project are listed in **Error! Reference source not found..2** and diagrams can be found in **Error! Reference source not found.2.1** and 2.1.

**Table 2.2 Plasmids**

Vector name	Supplier	Size (Kb)	Promoter	Use
pGEM T easy Vector	Promega	3.015	T7 & SP6	Cloning PCR products
pLXSN	Clontech	5.874	SV40	Gene overexpression

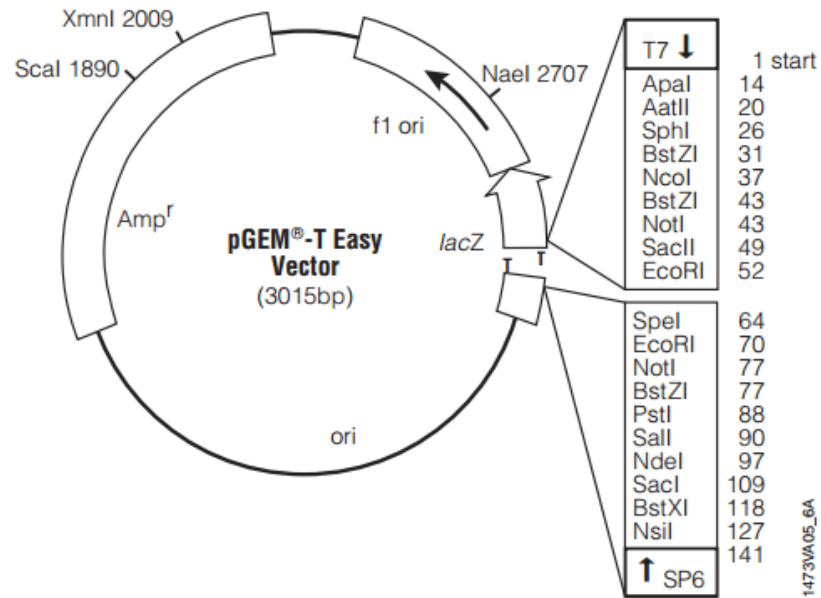
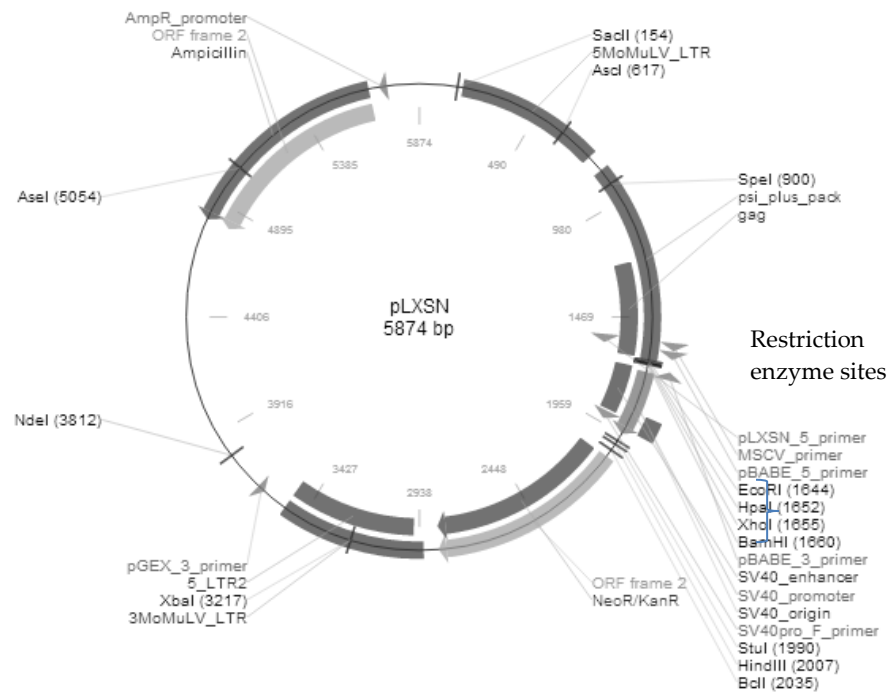


Figure 2.1 - Schematic representation of pGEM<sup>®</sup>T easy vector adapted from the Promega pGEM<sup>®</sup>T and pGEM<sup>®</sup>T easy vector technical manual showing the T7 and SP6 promoter regions.



**Figure 2.2 - schematic representation of pLXSN vector used for gene overexpression adapted from the Clontech pLXSN technical manual. The four restriction enzyme digestion sites within the multiple cloning region are labelled.**

## 2.6.5 Molecular cloning and retroviral plasmid generation

### 2.6.5.1 Restriction enzyme digest

Restriction digest enzymes were chosen based upon sites that existed in pLXSN retroviral plasmid. BamH1 and Hpa1 sites were incorporated onto the end of primers designed to amplify the target gene cDNA. Once ligated into pGEM<sup>®</sup>T easy vector, restriction digest was carried out. 2-3 µg of plasmid DNA were digested with 5 units of a single restriction enzyme (New England Biolabs) in the appropriate buffer at a temperature of 37 °C for 3 hours. The DNA was recovered using a PCR purification kit (Quiagen) and the process repeated using a second restriction enzyme. The order in which the two enzymes (BamH1 and Hpa1) were used varied with no difference noted in the efficiency.

### 2.6.5.2 Agarose gel preparation

A plastic gel mould was cleaned with distilled H<sub>2</sub>O, the ends sealed with autoclave tape and plastic gel combs inserted into the designated positions. High purity agarose (Life Technologies) was mixed with TBE buffer (Appendix 1.4.4) and microwaved for 2-5 minutes until all of the agarose had dissolved. The amount of agarose used was dependent on the size of the product expected (**Error! Reference source not found.**). SYBR<sup>®</sup>Safe DNA gel stain (Invitrogen) was added according to the manufactures instructions (1:1000), the solution mixed by swirling and poured into the mould. The gel was then left to set at room temperature for 20-30 minutes. The combs and autoclave tape were removed and the gel mould carefully placed into a Horizon<sup>®</sup> 58 electrophoresis gel tank (Gibco<sup>®</sup>; Life Technologies). The tank was the filled with enough TBE buffer to completely cover the gel by 5 mM.

Table 2.3 Agarose gel preparations (w/v)

Percentage agarose gel	Agarose (mg) per 200 mL TBE	PCR product length (bp)
1.5 %	3 mg	>1500
2 %	4 mg	500 - 1500
2.5 %	5 mg	<500
4 %	8 mg	*Separating 2 bands within 50 bp of each other

\* When separating two bands, temperature and electrophoresis times were optimised for each individual product

### 2.6.5.3 Agarose gel electrophoresis

DNA samples from restriction digests and mini/maxi preps were diluted in 6x loading buffer (Blue: orange loading dye; Promega) and 18  $\mu$ L were loaded into wells of an agarose gel. 6  $\mu$ L of Hyperladder IV (DNA < 1000 bp; Bioline) or 4  $\mu$ L of GeneRuler (DNA < 10,000; Thermo Fisher) were added to a separate well and a voltage of 100 V passed across the gel for 30-60 minutes. In the case of separating two bands of similar lengths (<50 bp), a 4 % gel would be made and run on ice at 40 V overnight. Gels were visualised using a Gene Genius bio-imaging system and Genesnap 7.07 software (Syngene).

### 2.6.5.4 Ligation

The amount of vector and insert DNA used in a reaction were calculated using the following formula:

$$\frac{\text{Mass (ng) of Vector} \times \text{Length (kb) of insert}}{\text{Length (kb) of Vector}} \times 3 = \text{Mass (ng) of insert}$$

50 ng of cut vector was ligated as standard. The solution also contained the insert DNA, 2  $\mu$ L of 10x ligation buffer (50 mM Tris-HCL [pH 7.8], 10 mM MgCl<sub>2</sub>, 20 mM dithiothreitol, 10 mM ATP, 50 mg/mL of bovine serum albumin; Promega), 1  $\mu$ L (200 units) of T4 DNA ligase (Promega). dH<sub>2</sub>O was added to make a final volume of

20  $\mu$ l. The reaction was incubated for 3 hours prior to bacterial transformation (section 2.6.6.1).

### **2.6.5.5 Sequencing**

Sequencing was conducted by the Technology Facility (Genomics) in the department of biology, University of York. 300 ng of plasmid template and specific primers (Appendix 1.6) were sent for analysis on an Applied Biosystems 3130XL genetic analyser. Results were analysed using Chromas (v2.4.3; Technelysium Pty Ltd). Alignment was conducted using Kalign (EMBL library).

## **2.6.6 Amplification of plasmid DNA**

### **2.6.6.1 Transformation of competent E-coli**

A 50  $\mu$ L aliquot of XL1-Blue Subcloning-Grade Competent cells (Agilent) were transformed using 5  $\mu$ L of ligated plasmid DNA. The plasmid and cells were gently mixed together by pipetting and incubated on ice for 30 minutes. The cells were then heat shocked at 42 °C for 45 seconds before being returned to ice for 2 minutes. 250  $\mu$ L of S.O.C medium (Life Technologies) was added to the cells and the culture incubated on an orbital shaker at 225 rpm for 1 hour at 37 °C. Various volumes (50-200  $\mu$ L) of the cell suspension was spread onto a LB Agar (Appendix 2.4.4) plate containing 100  $\mu$ g/mL ampicillin and incubated overnight, inverted, at 37 °C. 5 mL of LB containing 100  $\mu$ g/mL ampicillin was then inoculated with a single colony, picked using a sterile pipet tip, and incubated for 4 hours at 37 °C on an orbital shaker (225 rpm). This culture was then used to inoculate 50 mL LB broth which was incubated overnight at 37 °C on an orbital shaker (225 rpm).

### **2.6.6.2 Plasmid purification**

Plasmid purification was conducted using Midi Endotoxin-free plasmid extraction Kits™ (Quaigen) according to the instructions. Overnight 50  $\mu$ L cultures of transformed bacteria were collected by centrifugation (4000 g for 15 minutes) and

the pellet resuspended in 4 mL of P1 buffer. 4 mL of P2 buffer was added and the solution inverted several times before being incubated at ambient temperature for 5 minutes. 4 mL of N3 buffer (chilled to 4 °C) was added and the solution inverted several times until mixed thoroughly.

### **2.6.6.3 Bacterial Glycerol stocks**

750 µL of overnight LB cell suspensions were aliquoted into a 1.5 mL cryovial® with 250 µL of sterile 80 % (v/v) glycerol. The solution was mixed and then stored at -80 °C. To recover bacteria a glycerol stock was removed from -80 °C and a sterile inoculation loop used to streak colonies on a LB agar plate (Appendix 2.4.4) (100 µg/mL ampicillin) which was then incubated, inverted, overnight at 37 °C.

## **2.7 Protein Analysis**

### **2.7.1 Antibodies**

The primary antibodies in this work are listed in Table 2.4 with details of the concentrations that they were used at. Working antibody concentrations were optimised for each technique using known positive controls and positive and negative controls were included in each experiment conducted (Appendix 2.1). Antibody diluents were specific for each technique. Primary antibodies were aliquoted and stored according to the manufactures instructions. Fluorochrome-conjugated or biotin-conjugated secondary antibodies are listed in Table 2.5 with details of working concentrations. Antibodies were titrated prior to use and stored, according to the manufactures advice, in the dark at 4 °C.

Table 2.4 Primary Antibodies

Antigen	Clone	Host	Supplier	Use	Molecular weight of antigen
<b>Cytokeratin 7</b>	LP1K	Mouse	CRUK	IHC 1:1000 IF 1:1000	56 kDa
<b>Cytokeratin 5</b>		Sheep	The Binding Site	IHC 1:250 IF 1:100	
<b>Ki67</b>	MM1	Mouse	Novocastra	IHC 1:100 IF 1:400	
<b>Active <math>\beta</math>-catenin</b>	8.00E+07	Mouse	Millipore	IHC 1:300 IF 1:500 WB 5:3000	92 kDa
<b>Phospho-Akt (S473)</b>	D9E	Rabbit	Cell Signalling	IF 1:100 WB 1:1000	60 kDa
<b>Phospho-MAPK (P42/44)</b>	D13.14.4E	Rabbit	Cell Signalling	IF 1:100 WB 1:1000	42/44 kDa
<b>Claudin 4</b>	3E2C1	Mouse	Zymed	IF 1:250	22 kDa
<b>ZO-1</b>	ZO1	Rabbit	Zymed	IF 1:800	68 kDa
<b>Uroplakin 3a</b>	AU1	Mouse	Progen	IHC 1:200 IF 1:25	
<b>CYP2B1/2</b>	2S3	Rabbit	Kind gift from Dr R Edwards	IHC 1:2000 WB 1:1000	42 kDa
<b>CYP2B6</b>	1.6.94	Rabbit	Kind gift from Dr R Edwards	WB 1:1000	42 kDa

Table 2.5 - Secondary antibodies

Antigen	Conjugate	Host	Supplier	Application
<b>Mouse IgG</b>	Alexa 488	Goat	Molecular Probes	Immunofluorescence
<b>Mouse IgG</b>	Alexa 594	Goat	Molecular Probes	Immunofluorescence
<b>Rabbit IgG</b>	Alexa 488	Goat	Molecular Probes	Immunofluorescence
<b>Rabbit IgG</b>	Alexa 594	Goat	Molecular Probes	Immunofluorescence
<b>Goat IgG</b>	Alexa 488	Donkey	Molecular Probes	Immunofluorescence
<b>Goat IgG</b>	Alexa 594	Donkey	Molecular Probes	Immunofluorescence
<b>Mouse IgG</b>	Alexa 680	Goat	Life Technologies	Western Blotting
<b>Rabbit IgG</b>	Alexa 800	Goat	Life Technologies	Western Blotting
<b>Mouse IgG</b>	Biotin	Rabbit	Dako	Immunohistochemistry
<b>Rabbit IgG</b>	Biotin	Goat	Dako	Immunohistochemistry
<b>Goat IgG</b>	Biotin	Rabbit	Dako	Immunohistochemistry

## 2.7.1 Immunofluorescence labelling

Specific antibody labelling of NHU cells was used to quantify protein expression within cells and assess distribution throughout cells. A target-protein specific primary antibody is used to label the target within cells before a fluorophore-conjugated secondary antibody was used to bind specifically to the primary antibody. The fluorophore was then excited by an appropriate wavelength of light and visualised and quantified.

### 2.7.1.1 Slide preparation

Teflon<sup>®</sup> coated 12-well multisport slide (CA Hendley) were cleaned with 70 % (v/v) ethanol and sterilised by autoclaving, after which aseptic technique was observed. Slides were placed into Hereaus boxes using forceps and 50  $\mu$ L of cells suspension at a density of  $5 \times 10^4$  cells/mL seeded directly onto each well. Slides were incubated for 4 hours at 37 °C to allow cell adhesion before slides were flooded with 5 mL of cell culture medium. At the time points indicated in the results, cell culture medium was removed and cells fixed.

### 2.7.1.2 Fixation

Cells were fixed with either methanol: acetone (50:50) or with 10 % (v/v) formalin (appendix 1.4.3) depending on the target protein and/or primary antibody being used. For methanol: acetone fixation, cells were incubated for 30 seconds at ambient temperature in 5 mL methanol: acetone before being air-dried and stored at -20 °C. For formalin fixation, cells were incubated for 30 minutes in 10 % (v/v) formalin in PBS and then rinsed twice for 5 minutes in PBS. Cells were permeabilised with 0.5 % (v/v) Triton-X in PBS for 1 hour before being rinsed for 5 minutes in PBS. Cells were stored in PBS at 4 °C for no more than 48 hours. Before labelling slides were removed from PBS but the cells were not allowed to dry.

### **2.7.1.3 Immunofluorescence labelling of cells**

A liquid blocker super pap pen (Daido Sangyo) was used to draw around wells before labelling. 50  $\mu$ L of primary antibodies, diluted in TBS (appendix 2.4.4) with 0.1 % (v/v) BSA (Pierce) and 0.1 %  $\text{NaN}_3$  (w/v; Sigma Aldrich), was added to each well of the slide and incubated at 4 °C overnight (approximately 16 hours). A negative TBS only well was always included. After incubation, slides were rinsed 3 times for 5 minutes in TBS at ambient temperature on an orbital shaker. 50  $\mu$ L of the appropriate Alexa 488 or Alexa 594 secondary antibody diluted in TBS was then placed on each well and the slides incubated at ambient temperature for one hour in the dark. Slides were rinsed a further 3 times for 5 minutes in TBS on an orbital shaker before being stained with Hoechst 33258 (0.1  $\mu$ g/mL in TBS). Slides were rinsed a final time for 5 minutes in TBS on an orbital shaker before being air-dried, mounted in DABCO/glycerol antifade (Appendix 1.4.3) and a coverslip secured using nail varnish.

### **2.7.1.4 Imaging immunofluorescence labelled cells**

Cells were imaged using either the x20, x40 and x60 oil immersion objectives on a Olympus BX60 microscope under epifluorescent illumination or using the fluorescence imaging function of a Axio Scan.Z1 slide scanner (Zeiss). The Olympus BX60 microscope was equipped with excitation and emission filters for bisnizimide, FITC and Texas Red and an Olympus DP50 digital camera for imaging. Images were assessed in Image-Pro® Plus software (MediaCybernetics). AxioScan.Z1 images were recorded and analysed in Zen (2011) Blue edition software (Zeiss).

## **2.7.2 Immunolabelling of tissue sections**

### **2.7.2.1 Tissue fixation, embedding and sectioning**

Rat and human tissue was fixed in 10 % (v/v) formalin for 24 hours (less than 1  $\text{cm}^2$ ) or 48 hours (1-2  $\text{cm}^2$ ) dependant on size. If tissue was larger than 2  $\text{cm}^2$  in size it was

dissected into an appropriate number of pieces, which were embedded separately. Formalin was removed and replaced with 70 % (v/v) ethanol for at least 24 hours before embedding. For long-term storage before embedding, 70 % (v/v) ethanol was replaced like for like at 24 hours and samples stored at ambient temperature. Tissue was placed into labelled cassettes and then either a short dehydration protocol used for small (less than 1 cm<sup>2</sup>) bladder tissue or a longer dehydration protocol used for larger (1-2 cm<sup>2</sup>) bladder samples and denser tissue types including liver and kidney. The short protocol involved 3 x 10 minute washes in 100 % ethanol followed by 2 x 10 minute washes in 100 % propan-2ol (Thermo Fisher) and 4 x 10 minute washes in 100 % xylene (Fisher Scientific). Cassettes were then immersed in molten paraffin wax (Thermo Scientific) at 60°C which was changed every 15 minutes for an hour. The longer dehydration protocol involved a 2 hour incubation in 90 % (v/v) ethanol followed by a 2 hour incubation in 100 % ethanol and a 2 hour incubation in xylene. Samples were then left overnight (approximately 16 hours) in paraffin wax at 65 °C which was followed by 3 x 30 minute incubations in fresh paraffin wax. After both dehydration protocols, tissue sections were orientated appropriately and embedded in fresh paraffin wax which was chilled on a cold plate set at -12 °C at left for at least 12 hours before sectioning. To generate sections, blocks were chilled on the cold plate set at -12 °C for at least half an hour before 5 µm sections were cut on a microtome (Leica RM 2135). Individual sections were floated in a water bath set at 40 °C and collected onto Superfrost® Plus glass slides (Thermo Fisher). Slides were air dried and baked at 50 °C on a hot plate for 30 minutes. Immediately prior to use slides were dewaxed and rehydrated by 4 x 1 minute incubations in xylene, 3 x 1 minute incubations in 100 % ethanol and 1 x 1 minute incubation in 70 % (v/v) ethanol before being left in distilled water for one minute.

### **2.7.2.2 Endogenous peroxidase inactivation and antigen retrieval**

Endogenous peroxidases are present in a number of cells (e.g. red blood cells) and could interfere with the labelling process. To inhibit endogenous peroxidase activity slides were incubated at ambient temperature in 3 % (v/v) H<sub>2</sub>O<sub>2</sub> (Thermo Fisher) for 10 minutes and rinsed in distilled water for 10 minutes.

To prevent formalin cross-linking from masking antigens one of four antigen retrieval protocols was used after peroxidase inhibition. These protocols were:

i. Citric acid

Slides were immersed and weighted down in 10 mM citric acid (pH 6.0; Thermo Fisher) and microwaved at 900 W for 13 minutes. Following microwaving slides were chilled on ice and rinsed in distilled water.

ii. Trypsin

Slides were incubated at 37 °C in 100 mL 0.1 % (w/v) trypsin from porcine pancreas (Sigma Aldrich) in 0.1 % (v/v) CaCl<sub>2</sub> solution at pH 7.8 for 10 minutes and then rinsed in distilled water.

iii. Trypsin and citric acid

Slides were incubated for 1 minute at 37 °C in 100 mL 0.1 % (w/v) trypsin from porcine pancreas in 0.1 % (v/v) CaCl<sub>2</sub> solution at pH 7.8 before being transferred into 10 mM citric acid (pH 6.0) and microwaved at 900 W for 13 minutes. Slides were subsequently chilled on ice and rinsed in distilled water.

iv. EDTA

Slides were immersed and weighted down in 1 mM EDTA solution (pH 8.0) and microwaved at 900 Watts for 13 minutes before being chilled on ice and rinsed in distilled water.

Each antibody was tested with each of the antigen retrieval protocols at a range of concentrations and with a concentration and protocol chosen that produced clear labelling with minimal background.

### 2.7.2.3 Immunoperoxidase labelling

Slides were immersed in TBS (Appendix 1.4.3) and placed into Shandon Sequenzas (Thermo Fisher) on cover plates. Each slide was blocked for 10 minutes with 100  $\mu$ L Avidin (Vector Laboratories), washed twice with TBS, and blocked for 10 minutes with 100  $\mu$ L Biotin (Vector Laboratories). Slides were washed twice in TBS, incubated for 5 minutes in 100  $\mu$ L of 10 % (v/v) serum (Dako) from the secondary antibody host animal followed by overnight (approximately 16 hour) incubation in an appropriate concentration (Table 2.4) of the primary antibody at 4 °C. The primary antibody was removed by washing slides twice in TBS. Slides were then incubated at ambient temperature for half an hour in an appropriate concentration (Table 2.5) of an appropriate biotinylated secondary antibody. The secondary antibody was removed by washing twice in TBS and 100  $\mu$ L of streptavidin-Horseradish peroxidase (HRP) (Vector Laboratories), prepared 30 minutes prior to use according to the manufactures instructions, was added to each slide and incubated at ambient temperature for 30 minutes. Slides were washed twice in TBS and 200  $\mu$ L SigmaFAST diaminobenzidine (DAB) (Sigma Aldrich), prepared in dH<sub>2</sub>O according to the manufactures instructions, added to each slide for 10 minutes. Slides were rinsed in dH<sub>2</sub>O, counterstained for 30 seconds in Mayers Haematoxylin (appendix 2.34.3) and dehydrated through 1 x 1 minute 75 % (v/v) ethanol incubation, 3 x 1 minute 100 % ethanol incubations and 2 x 1 minute 100 % Xylene incubations. Slides were left air dry and mounted under a coverslip in DPX mounting fluid (CellPath).

### 2.7.2.4 Immunoperoxidase labelling using the catalysed signal amplification kit

An catalysed signal amplification (CSA) kit was purchased from Dako and used according to the manufacturer's instructions. Briefly, after antigen retrieval (Section 2.7.2.2), slides were placed into sequenzas and blocked with avidin and biotin as described in section 2.7.2.3 but with the exception of TBS being replaced with TBST (Appendix 1.4.3). Slides were blocked with serum free protein block reagent (Dako) for 5 minutes and incubated in the primary antibody, diluted appropriately in

antibody dilution buffer (Dako), for 15 minutes. Three 5 minute TBST washes were used to remove the primary antibody and 100  $\mu$ L of secondary antibody (biotinylated link antibody (Dako) for mouse primary antibodies and biotinylated anti-rabbit antibody (Table 2.5) for rabbit primary antibodies) applied to each slide for 15 minutes. Slides were then washed 3 times in TBST and Streptavidin-biotin complex (Dako), pre-prepared 30 minutes prior to use, added for 15 minutes. Slides were washed three times in TBST and 100  $\mu$ L of amplification reagent (Dako) added to each slide for 15 minutes before being removed by three TBST washes. 100  $\mu$ l of Streptavidin-HRP (Dako) was added to each slide for 15 minutes and removed with three TBST washes and 100  $\mu$ L of DBA reagent (Dako) added to each slide for 10 minutes. Slides were then removed from sequenzas, washed in dH<sub>2</sub>O before being counterstained in Mayers Haematoxylin, dehydrated and mounted as described in section 2.7.2.3.

### **2.7.3 Image capture and analysis**

TissueGnostics software was used to quantify immunolabelling of specific proteins in images of tissue sections or cultured cells. Samples were only comparable if labelled at the same time and if TissueGnostics settings were unaltered after initial optimisation.

#### **2.7.3.1 Image acquisition**

Images of whole tissue sections/cultured cell layers were taken using an Axio Scan.Z1 slide scanner and Zen 2012 (blue edition) software. Images were stored as .czi files and reopened using TissueGnostics HistoQuest (immunoperoxidase) or TissueQuest (immunofluorescence) software.

### **2.7.3.2 Cell identification and immunolabelling assessment**

An initial region of interest (ROI) was selected for software optimisation consisting of less than 200 cells. By altering the nuclear size, remove small objects, remove weakly labelled objects and the automatic background parameters, individual cell nuclei were identified. Immunolabelling intensity was then quantified using the identified cell mask parameter. Dependent on whether the labelled protein was nuclear or cytoplasmic, an outside, inside and outside or inside cell mask was selected. These masks projected from the identified cell nuclei and the scale settings were adjusted until cells boundaries were clearly identified. All labelling within the masks was quantified to produce arbitrary intensity values. Once complete, a larger ROI was selected and the labelling intensity quantified using the optimised settings.

Individual cells in immunoperoxidase labelled images were selected based on haematoxylin staining of cell nuclei by the HistoQuest software. Individual cells in immunofluorescence labelled images were identified based on the Hoechst 33258 labelling of their nuclei by the TissueQuest software.

### **2.7.3.3 Analysis**

DAB/fluorescence intensity values (arbitrary units) were either exported directly into Microsoft excel and statistical analysis conducted or used within TissueGnostics software to generate positive/negative cell labelling ratios. To achieve this, a positive/negative cut-off threshold was established based on visual assessment of labelling and the percentage of cells falling into each group determined.

## **2.7.4 Western Blotting**

### **2.7.4.1 Cell Lysis**

Cultured cells or cells harvested from tissue were washed twice in cold (4 °C) PBS and lysed in 50 µL of 2 % (w/v) SDS lysis buffer (appendix 1.4.5) containing protease inhibitor cocktail (1:500; Sigma Aldrich) and 13 mM dithiothreitol (DTT)

(Sigma Aldrich). To facilitate adherent cell removal into lysis buffer, cells were gently scraped using a cell scraper. Lysed cell solution was collected in a 1.5 mL microcentrifuge tube on ice and sonicated (25 W) for a 10 seconds before being rested for 10 seconds on ice and sonicated for a further 10 seconds. Post-sonication, lysates were rested on ice for 30 minutes before being centrifuged for 30 minutes at 14,000 rpm. The supernatant was collected into a fresh microcentrifuge tube with care being taken not to collect any of the pellet which was discarded.

#### **2.7.4.2 Protein concentration assay**

Coomassie Plus reagent (Thermo Fisher) was used to quantify protein concentrations. Bovine serum albumin (BSA) (Thermo Fisher) standards of 25, 125, 250, 500, 750 and 1000  $\mu\text{g}/\text{mL}$  were generated from a 2 mg/mL stock solution. 10  $\mu\text{L}$  of each standard was pipetted in duplicate onto a 96 well plate (Corning) along with cell lysates which were first diluted 2:25 in dH<sub>2</sub>O. 200  $\mu\text{L}$  of Coomassie Plus reagent at ambient temperature was added to each sample and the absorbance read at wavelengths of 480 and 630 nm on a Multiskan Ascent microplate reader (Thermo Electron Corporation). The protein concentration was calculated from the BSA standard curve taking into account the dilution factor (1:12.5).

#### **2.7.4.3 Protein sample preparation**

Samples containing 20  $\mu\text{g}$  of protein were generated. Samples also contained LDS sample buffer (Invitrogen) in a ratio of 1:4 (v/v) and Reducing agent (Invitrogen) in a ratio of 1:10 (v/v). Samples were made up to a total volume of 35  $\mu\text{L}$  with dH<sub>2</sub>O and heated to 70 °C for 10 minutes before loading.

#### **2.7.4.4 SDS-Polyacrylamide Gel Electrophoresis (PAGE)**

A precast Novex 10 well 4-12% Bis-Tris gel (Invitrogen) was removed from its package and rinsed in dH<sub>2</sub>O. The comb was removed and the gel placed into the running apparatus according to the manufacturers instructions. Approximately 200 mL of running buffer (appendix 1.4.5) was placed into the central well of the apparatus (enough to cover the top of the gel) and 200  $\mu\text{L}$  of antioxidant

(Invitrogen) added. The chamber was checked for leaks before 600 mL of running buffer was then poured into the outer well. Samples were loaded into individual wells. 5  $\mu$ L of precision plus protein™ All Blue prestained protein standard (Bio-Rad) was added to a separate well, the apparatus lid attached and ice packed around the outside. Electrophoresis was carried out at 200 V for 50 minutes.

#### 2.7.4.5 Protein transfer and imaging

PVDF membrane (Millipore) was cut to the approximate size of the gel, dipped into 100 % methanol and rinsed in dH<sub>2</sub>O for 2 minutes. Filter paper was also cut to the approximate size of the gel (2 per gel) and together with blotting pads soaked in transfer buffer (appendix 1.4.5). The gel sandwich was assembled and placed into a transfer apparatus (Novex) according to the manufacturers instructions with care being taken to avoid air bubbles from becoming trapped within the system. The central chamber was filled with transfer buffer and the outer chamber filled with dH<sub>2</sub>O. The apparatus lid was attached, the apparatus surrounded by ice and a voltage of 30 V passed through the system for 2 hour. Upon completion the membrane was removed from the gel sandwich and placed into TBS buffer (appendix 1.4.5). Protein transfer to the membrane was visualised by staining with 42mM Ponceau red in 3 % (v/v) trichloroacetic acid, and washed off in dH<sub>2</sub>O. The membrane was blocked in 10 mL of Odyssey blocking buffer diluted 1:1 (v/v) with TBS on an orbital shaker for 1 hour. The blocking solution was removed and the primary antibody added, diluted in Odyssey blocking buffer / TBST (1:1 v/v) (appendix 1.4.5). The sample was incubated overnight at 4 oC. The membrane was rinsed 4 times for 5 minutes in TBST before the secondary antibody, diluted in Odyssey blocking buffer / TBST (1:1 v/v), was added. The membrane was placed in the dark on an orbital shaker for 1 hour before being rinsed for 5 minutes in TBST and 3 times for 5 minutes in TBS. Epifluorescence imaging at 700 and/or 800 nm using the Odyssey v1.1 software (Li-Cor) was conducted to visualise immunolabelling.

#### **2.7.4.6 Membrane stripping**

Membranes were stripped using the Western Blot recycling kit (Autogen Bioclear) according to the manufactures instructions. The membrane was incubated for 30 minutes in stripping buffer diluted 1:10 (v/v) in dH<sub>2</sub>O. The membrane was rescanned to ensure that stripping had been successful before being rinsed for 5 minutes in TBS. The membrane was then blocked and probed again as described in section 2.7.3.5.

### **2.8 Statistical analysis**

Data was represented graphically using Excel® (Microsoft). Where possible, data was presented as the mean of all replicates with error bars representing  $\pm 1$  standard deviation (SD). Statistical analysis was conducted using instat 3.1 software (Graphpad) when at least three data points were obtained, in which case, the data were confirmed to be drawn from Gaussian distribution. 2-way analysis of variance (ANOVA) tests were used to compare three or more sample means, along with the appropriate post-test. Tukey range test (Tukey test) were used to test which treatments were significantly different from each other. A 2-tailed, paired student T-test was used to compare two sample means generated from the same cell lines. Levels of significance are cited in the test and assumed to be significant where  $p < 0.05$ .

# Chapter 3 - Optimisation of a normal rat urothelial cell culture system

<b>Chapter 3 - Optimisation of a normal rat urothelial cell culture system.....</b>	<b>64</b>
<b>3.1 Chapter Introduction .....</b>	<b>65</b>
3.1.1 The Bladder .....	65
3.1.2 The Urothelium .....	65
3.1.3 Urothelial cell culture models.....	70
<b>3.2 Chapter Aim .....</b>	<b>74</b>
3.2.1 Objectives.....	74
<b>3.3 Experimental approach.....</b>	<b>75</b>
3.3.1 Cell isolation protocol .....	75
3.3.2 Adapting the NRU cell isolation protocol.....	77
3.3.3 Optimising NRU cell culture conditions .....	77
3.3.4 Summary of experimental approach .....	78
3.3.5 Cell lines .....	79
<b>3.4 Results .....</b>	<b>80</b>
3.4.1 Initial comparisons of rat and human urothelium in situ .....	80
3.4.2 NRU cell culture using protocols established for NHU cells. ....	80
3.4.3 Optimisation of the NRU cell isolation protocol.....	83
3.4.4 The effect of fetal bovine serum on primary NRU cell cultures .....	87
3.4.5 NRU cell seeding density.....	95
3.4.6 Optimising surface substrate for NRU cell growth .....	96
<b>3.5 Conclusions and Discussion.....</b>	<b>101</b>
<b>3.6 Key findings.....</b>	<b>102</b>

## 3.1 Chapter Introduction

### 3.1.1 The Bladder

The urinary bladder is the organ responsible for the storage of urine produced by the kidneys, prior to voiding. As such, the bladder has to be highly compliant in order to expand and maintain low pressure as the volume of urine increases and to contract when urine is voided (reviewed by Andersson and Arner, 2004). As an important route of excretion for numerous endogenous and exogenous compounds (discussed by Anzenbacher and Zanger, 2012), urine represents a hostile environment and the bladder must be able to maintain a tight barrier in order to prevent toxin, ion, solute and water flux into the body. The concentrating effect of filtration by the kidneys can result in the lining of the bladder being exposed to higher concentrations of potentially toxic compounds than other organs in the body. The duration of exposure can also exceed that of other organs. Exposure to increased concentrations of toxic compounds for longer durations than other organs increases the risk of damage, and can result in toxicity that is specific to the bladder (Kawanishi et al., 2002; Akagi et al., 2003).

### 3.1.2 The Urothelium

The urothelium is a highly specialised, transitional epithelium that lines much of the urinary tract including the renal pelvis, the ureters and the urinary bladder. It has a stratified structure comprising the three specialised cell zones of the superficial “umbrella” cells, intermediate cells and basal cells. Although superficial cells are regarded as being terminally differentiated (Varley et al., 2004), urothelial cell phenotype has been shown to be plastic, with the cellular localisation or niche determining the differentiation status of urothelial cells (Wezel et al., 2014).

Human urothelial cells normally exist in a quiescent state, undergoing mitosis an estimated 1-2 times per year (Marceau N, 1990). In response to injury or damage, however, the urothelium has been shown to have a high capacity for regeneration

(Baskin et al., 1997; Cohen, 1989; Rebel et al., 1994), which has led to the hypothesis that a urothelial stem cell population exists to regulate this response (Gaisa et al., 2011; discussed by Ho et al., 2012).

In rodent urothelium, cells within the basal cell layer have been shown to be label-retaining *in vivo*, highly proliferative in response to injury and capable of communication with the underlying stroma through sonic Hedgehog/Wnt signalling (Shin et al., 2011; Zhang et al., 2012). This strongly suggests the presence of a stem or progenitor cell population within the basal cell layer (Nguyen et al., 2007; Kurzrock et al., 2008) and that these cells are in close communication with the underlying stromal cells across the basement membrane.

In human urothelium, fewer studies looking for stem cells have been published. By tracking urothelial cells containing non-pathogenic age-related mutations of mitochondrial DNA, Gaisa et al. found that clonal units of cells with the same lineage exist within the urothelium (Gaisa et al., 2011). These units were shown to span all cell layers of the urothelium and all contained a small number of basal cells in contact with the basement membrane. Gaisa et al. proposed that these basal cells could be urothelial stem cells, although they acknowledged that is difficult to confirm without a definitive stem cell marker. A separate study cultured isolated human urothelial cells in the presence of epithelial growth factor (EGF) and basic fibroblast growth factor (bFGF). By doing so they were able to isolate self-renewing CD34+, DC45- urothelial cells that grew into spheroids, which were proposed to be a functional urothelial progenitor/stem cell (Fierabracci et al., 2007).

Alternatively, human urothelial cells have been shown *in vitro* to be capable of self-regulating proliferation and wound response. Urothelial cells from all cell layers of the urothelium are capable of undergoing mitosis (Hicks, 1975) and regulating proliferation and migration in response to wounding through an EGFR mediated autocrine signalling loop (Varley et al., 2005). Furthermore, it has been demonstrated that all normal human urothelial cells have the same capacity for proliferation *in vitro*, independent of their origin *in vivo* (Wezel et al., 2014). These

findings suggest a global urothelial response to injury, thus supporting the concept of cellular localisation or niche determining the differentiation phenotype of urothelial cells.

The urothelium is generally regarded as the tightest epithelial barrier in the human body (reviewed by Anderson and Van Itallie, 2009), allowing it to function as an effective barrier to urine. This is achieved by the expression of asymmetric unit membrane (AUM) plaques on the apical surface of superficial cells, and the presence of tight junctions between urothelial cells. AUM plaques cover between 70-90% of the apical membrane of superficial cells and are divided by hinge areas formed of flexible plasma membrane segments. They are composed of several uroplakins (UPKs), the expression of which has been well characterised (reviewed by Lee, 2011). AUM plaques are found on the apical surface of superficial cells and are reliable markers of differentiation in urothelial cells of all mammalian species, including humans and rats. AUM plaques limit the contact of superficial cells with urine, increasing the durability of cells and their resistance to damage by harmful constituents of urine (Walz et al., 1995; reviewed by Lewis, 2000). Urothelial cell tight junctions are formed from multiple proteins including occludins and claudins, and are regulated during cell differentiation by PPAR $\gamma$  activation (Varley et al., 2006). Peroxisome proliferator-activated receptor  $\gamma$  (PPAR $\gamma$ ) is a member of the nuclear hormone receptor superfamily. When ligand-bound, PPAR $\gamma$  heterodimerises with retinoid X receptor (RXR), forming a transcription factor that binds to specific peroxisome proliferator response elements (PPREs) in the promoter regions of target genes. PPAR $\gamma$  is known to be upstream of several transcription factors, including IRF1, FOXA1, ELF3, KLF5 and GATA3 (Varley et al., 2009; Bock et al., 2014). In urothelial cells, PPAR $\gamma$  activation is known to promote the activation of differentiation-associated genes including uroplakin (UP) 1a, UP2, UP3b, cytokeratin (CK) 13 and CK20 as well as claudins 3, 4 and 5 (Varley et al., 2004; Varley et al., 2006; Varley and Southgate, 2008).

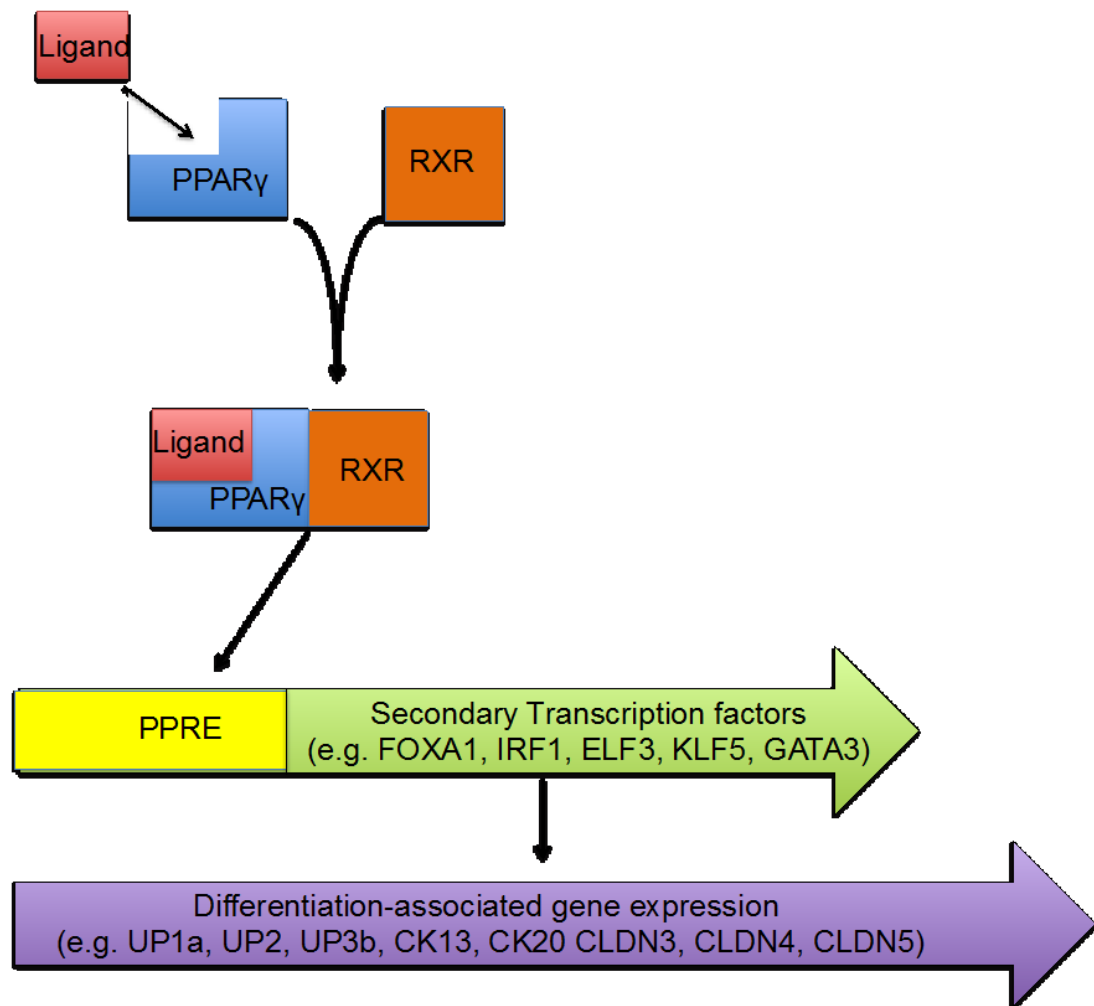


**Figure 3.1 – PPAR $\gamma$  activation of urothelial differentiation-associated gene expression.** Cartoon depicting activation of PPAR $\gamma$  binding through the binding of a PPAR $\gamma$  ligand, initiating heterodimerization with RXR. The PPAR $\gamma$ -RXR transcription factor then binds to peroxisome proliferator response elements (PPRE), resulting in secondary transcription factor expression. These transcription factors subsequently activate differentiation-associated genes.

In particular, the expression of claudin 3, in conjunction with a ZO-1 switch from the ZO-1 $\alpha$  isoform to the ZO-1 $\alpha^+$  isoform, have been shown to be essential for barrier function *in vitro* (Smith et al., 2015). Tight junctions function to prevent paracellular movement of ions and solutes across the urothelium. A glycosaminoglycan (GAG) layer is also present on superficial urothelial cells and may contribute to urothelial barrier function and defence (reviewed by Parsons, 1993).

The urothelium has been reported to have sensory ability, disruption of which may be involved in pathological conditions such as interstitial cystitis (discussed by Apodaca, 2004; Birder et al., 2010). Thus, urothelial cells are able to detect chemical, mechanical and thermal stimuli through the expression of receptors including purinergic, nicotinic and muscarinic receptors and ion channels including TRP channels and epithelial sodium channels (ENaC) (Beckel and Birder, 2012; Birder et al., 1998; Chopra et al., 2008a; Kullmann et al., 2008). Urothelial cells are reported to be capable of responding to stimuli by releasing chemical signalling molecules such as ATP, nitric oxide (NO) and acetylcholine (ACh), allowing for communication within the urothelium and with underlying stromal cells in the lamina propria (reviewed by Birder, 2010). As the urothelium is aneural, chemical communication across the basement membrane allows for urothelial-neuronal interactions and signalling. A useful example of these sensory interactions is in normal and pathological conditions involving bladder voiding. Sensory urgency, a dysfunction condition in which the sufferer continually feels the desire to empty their bladder, is associated with a significant increase in TRPV1 receptors in the urothelium (Daly et al., 2007). Similarly, TRPV4, TRPA1 and TRPM8 antagonists have been shown to have some therapeutic merit in treating lower urinary tract symptoms (Franken et al., 2014). Other prominent TRP channels in the urothelium including TRPV4 are thought to be involved in the sensory regulation of normal bladder voiding (Gevaert et al., 2007; Olsen et al., 2011; Ogawa et al., 2015). In mouse models, TRP1 and TRPV4 knockout animals showed altered voiding characteristics when compared to wild type littermates (Yoshiyama et al., 2015). Although a strong case for the sensory role of urothelium has been presented by some, there are contradictions in the experimental approaches used to support the claims, including the specificity of reagents and the nature of the tissue preparations used (reviewed by Yu & Hill 2011). In cultures of human urothelial cells *in vitro*, a lack of responsiveness to specific TRPV1 and TRPV4 agonists and antagonists has been reported in conjunction with the urothelial expression of functional P2Y<sub>4</sub> receptors (Shabir et al., 2013).

### 3.1.3 Urothelial cell culture models

#### Normal Human Urothelial (NHU) cells

NHU cells can be isolated from surgical biopsies and grown in culture where they switch from a quiescent to a regenerative and migratory phenotype (Hutton et al., 1993; Rebel et al., 1994; Southgate et al., 1994). Cultured in keratinocyte serum free medium under conditions of low calcium and exogenous epithelial growth factor (EGF), Cholera toxin (CT) and bovine pituitary extract (BPE) supplementation (KSFMc medium), isolated NHU cells can be subcultured over several passages (Southgate et al., 1994; Southgate et al., 2002). The proliferative phenotype of NHU cells can be maintained for up to at least 6 passages without changes occurring in cell morphology and NHU cells can be induced to adopt a differentiated phenotype through the addition of adult bovine serum (ABS) and increasing the extracellular calcium concentration to an approximately physiological (2mM) concentration (Cross et al., 2005). When induced to differentiate by this method, NHU cell proliferation is inhibited and the cells express differentiation-associated proteins such as uroplakins and claudins. ABS/Ca<sup>2+</sup> differentiated NHU cells also create a stratified structure *in vitro* that resembles the urothelium *in situ* and acts as a functional barrier, demonstrated by the generation of a transepithelial electrical resistance (TEER) (Rubenwolf and Southgate, 2011; Baker et al., 2014).

#### Normal Rat Urothelial (NRU) cells

Isolation and culture of normal rat urothelial (NRU) cells have been described in the literature by several research groups (detailed in Table 3.1). NRU cells have been reported to grow in “cobblestone-like” colonies which produce a three-dimensional tiered structure in culture and which do not expand to cover all of the available surface area (Zhang et al., 2001). This phenotype is likely to be the result of isolation protocols and/or culture conditions. In particular the use of serum, which is known to induce a differentiated phenotype in NHU cells, would likely result in alterations in NRU cell phenotype and growth characteristics. The culture of NRU cells in KSFMc (low calcium) medium, in which NHU cells adopt a proliferative

phenotype and expand until becoming contact inhibited, has not been reported. Two publications have reported serially sub-culturing NRU cells beyond passage 2 (Zhang et al., 2001; Kurzrock et al., 2005) but this has not been replicated, as all other publications only culture primary NRU cells.

The lack of a standardised NRU cell culture model has resulted in numerous differences between published NRU cell cultures. The strains, ages, weights, gender, isolation protocols and culture conditions that have been published differ greatly (described in Table 3.1). Published NRU cell isolation protocols are different to each other and to the established NHU cell isolation protocol. Varying protocols for isolation and culture could affect NRU cell yield and cell phenotype in culture and result in NRU cell cultures that are contaminated with stromal cells. This would result in NRU cell cultures with different capacities for growth, which is possibly represented by the time that NRU cells were cultured for before being harvested or fixed for analysis. When combined with the differences of strain, age/weight and sex, the various protocols generate NRU cell cultures, which are difficult to compare either with each other or with the NHU cell culture system.

One significant difference between reported culture conditions for NRU cells is the use of serum supplemented cell culture medium, with the most common being fetal bovine serum (FBS). FBS is a common cell culture medium supplement that is required for the growth, proliferation and adhesion of multiple cell lines but is not required for NHU cell proliferation *in vitro* and has an inhibitory effect on NHU cell growth (Southgate et al., 1994; Cross et al., 2005). FBS contains a cocktail of growth factors, antibodies and various other proteins that can have multiple stimulatory effects on cells *in vitro*. (Honn et al., 1975). Despite being used for over 50 years, FBS has never been fully characterised and the most recent studies have shown that it contains in excess of 1,800 protein and 4000 metabolites that can vary significantly between batches (reviewed by Jochems et al., 2002; Gstraunthaler et al., 2013). The exact mechanisms by which FBS stimulates cellular growth are unknown, due to the large number of growth factors it contains, making its use in researching normal

cellular functions and physiology contra-indicated (Gstraunthaler, 2003; discussed by van der Valk et al., 2010). Similarly the use of irradiated fibroblast feeder layers can also distort normal cellular mechanisms by releasing or stimulating the production of a cohort of factors (Eiselleova et al., 2008; Wang et al., 2012).

The lack of consistency in rats sourced, isolation protocols and NRU cell culture conditions poses a problem when attempting to compare NRU cell culture system against both each other and against the normal human urothelial (NHU) cell system. As such, there is a necessity to develop a standardised NRU cell culture system. For the purposes of fulfilling the aims of this project, the standardised system is required to be as similar as possible to the established NHU cell culture system to allow accurate comparisons to be made of the two systems.

Table 3.1 – Details of NRU Isolation Protocols in the Literature

Publication	Strain	Age/Weight	Sex	Primary isolation phase	Secondary disaggregation phase	Experimental time scale
Rozell et al. 1997	Sprague-Dawley	3-6 weeks	Male	Collagenase IV / Trypsin (4 hours at 4 °C)	Collagenase IV / Trypsin (7 mins at 37 °C on a shaker)	24-28 hours
Zhang et al. 2001	Wistar	540-600 g	Male	1 % Collagenase IV (1 hour at 37 °C)	None	13 days
Kurzrock et al. 2005	Sprague-Dawley	200-500 g	-	0.05 % Trypsin (1 hour at 37 °C in 95 % CO <sub>2</sub> )	None	Passage 10
Chopra et al. 2008	Sprague-Dawley	-	-	Dispase (overnight at 4 °C)	Trypsin / EDTA (15 mins at 36 °C)	Confluence
Chopra et al. 2008	Wistar	9 months	Male	0.1 % EDTA (4 hours at 37 °C)	Collagenase IV (30 mins at 37 °C)	Passage 1-3
Kullman et al. 2008	Sprague-Dawley	200-250 g	Female	Dispase (overnight at 4 °C)	Trypsin / EDTA (15 mins at 36 °C)	48-72 hours
Olsen et al. 2010	Sprague-Dawley	-	Female	0.05 % Trypsin (1 hour at 37 °C in 95 % CO <sub>2</sub> )	None	7 days
Beckel et al. 2012	Sprague-Dawley	250-300 g	Female	Dispase (overnight at 4 °C)	Trypsin / EDTA (15 mins at 36 °C)	1-2 days
Juszcack et al. 2012	Wistar	200-250 g	Female	Dispase (overnight at 4 °C)	Trypsin / EDTA (15 mins at 36 °C)	48 hours
O'Mullane et al. 2013	Sprague-Dawley	8-12 weeks	Female	Dispase (3-4 hours at 37 °C)	Trypsin / EDTA (15 mins at 37 °C)	48-72 hours

## **3.2 Chapter Aim**

To develop and optimise a standardised normal rat urothelial (NRU) cell culture system in which cells can be cleanly isolated and cultured in complete keratinocyte serum free medium (KSFMc) for comparison against an existing normal human urothelial (NHU) cell culture system.

### **3.2.1 Objectives**

1. Test the effectiveness of a NHU cell isolation protocol at isolating NRU cells and, if ineffective, develop and optimise an alternative protocol for NRU cell isolation
2. Optimise various cell culture conditions including the presence of serum, the surface substrate and seeding density in order to maximise the lifespan of NRU cells in culture.

## 3.3 Experimental approach

### 3.3.1 Cell isolation protocol

An established NHU cell isolation protocol was initially used and subsequently adapted for NRU cell isolation based on protocols in the literature. The established NHU cell isolation protocol is described below.

#### NHU cell isolation protocol (Illustrated in Figure 3.2)

1. Human bladder/ureter tissue is cut with scissors to expose the urothelium and incubated for 4 hours in an EDTA “stripper” solution at 37°C. The urothelium is then gently removed from the underlying tissue using forceps.
2. Isolated sheets of urothelial cells are incubated for 20 minutes in a collagenase type IV solution at 37°C before being collected by centrifugation and resuspended in KSFMc medium.
3. Urothelial cell number is established by counting cells on a haemocytometer.
4. Urothelial cells are seeded onto N<sub>2</sub> plasma treated tissue culture plastic and cultured in KSFMc medium.

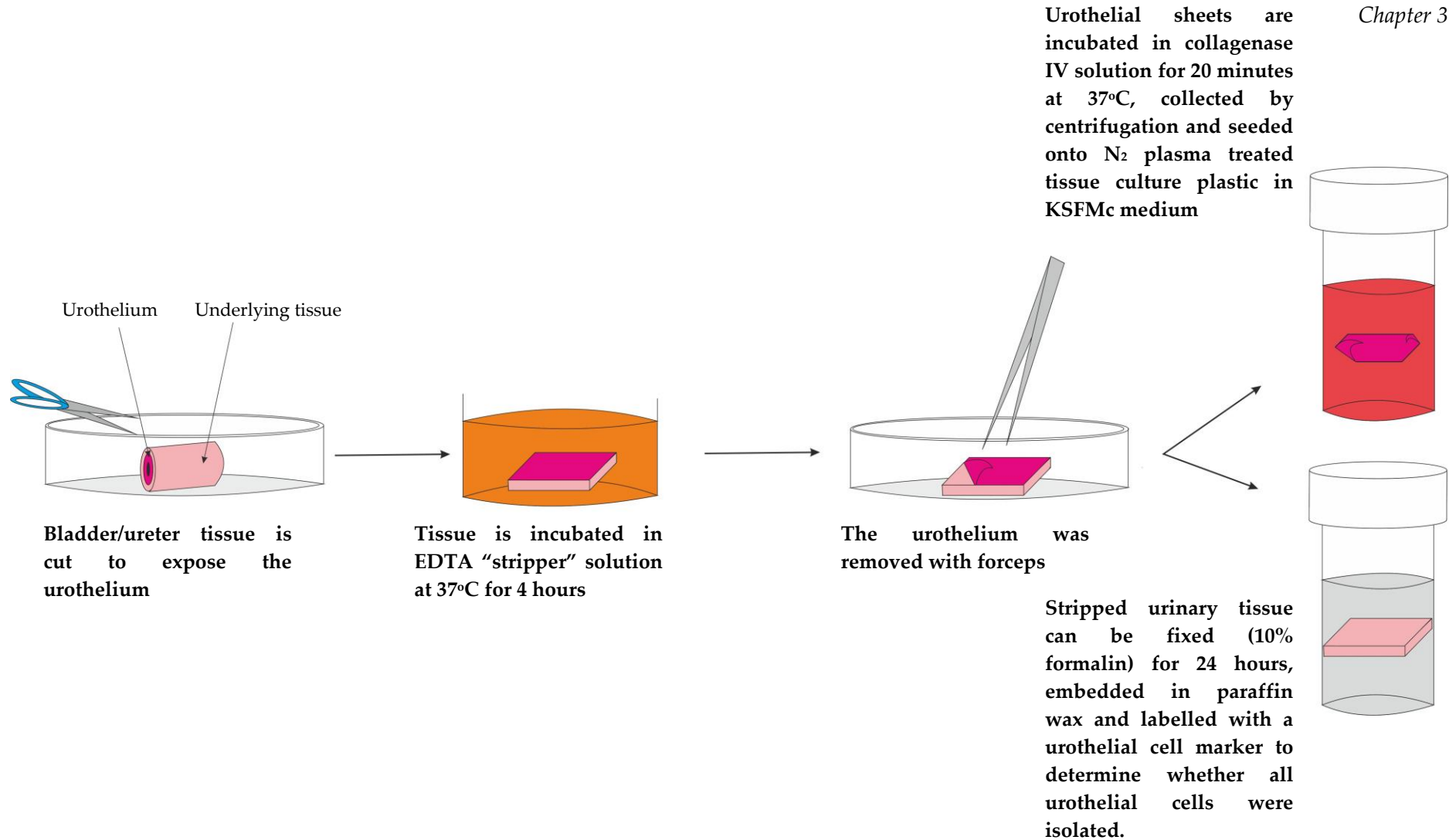


**Figure 3.2 - The isolation of normal human urothelial (NHU) cells.** An annotated cartoon detailing the various stems of the NHU cell isolation protocol including the initial EDTA "stripping" phase, urothelial cell sheet removal and finally the collagenase IV disaggregation of NHU cells prior to cell seeding.

### 3.3.2 Adapting the NRU cell isolation protocol

The NHU cell isolation protocol was adapted based on NRU cell isolation protocols in the literature. The various aspects of the protocols were optimised to generate the greatest possible yield of NRU cells (see Table 3.1). Following testing, the optimised protocol replaced the 4 hour EDTA “stripper” solution incubation with a 3 hour dispase II incubation and the 20 minute collagenase IV incubation with a 10 minute 0.25% trypsin in versene incubation step. Briefly:

1. Rat bladders were cut with scissors to expose the urothelium and incubated for 3 hours in a 0.5% (w/v) dispase II solution at 37°C. The urothelium was then gently removed from the underlying tissue using forceps.
2. Isolated urothelial sheets were incubated for 10 minutes in a 0.25% trypsin in versene solution at 37°C before being collected by centrifugation and resuspended in KSFMc medium.
3. Urothelial cell number was established by counting cells on a haemocytometer and seeded at  $1 \times 10^4$  cells /cm<sup>2</sup>.

### 3.3.3 Optimising NRU cell culture conditions

Having tested the isolation protocol, other aspects of the NRU cell culture system were optimised for maximum NRU cell growth. The presence of bovine serum, the cell seeding density and the tissue culture surface substrate were all optimised for NRU cell culture. To achieve this, NHU cell culture conditions were tested against those reported in the literature to determine which promoted the greatest level of NRU cell growth.

### 3.3.4 Summary of experimental approach

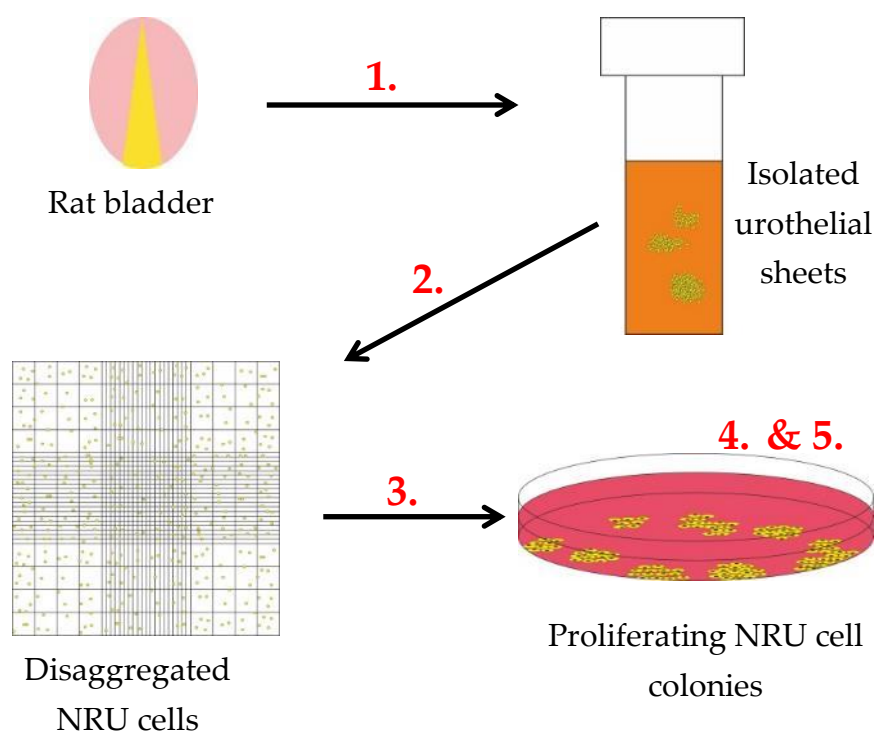


**Figure 3.3 – The NRU cell isolation protocol.** A cartoon illustrating the various processes involved in urothelial cell isolation and culture. The stages (numbered in red) correspond to those in Table 3.2.

**Table 3.2 – The main stages of NRU cell isolation and culture with potential variables**

Number	Stage	Variables
1.	Primary enzyme incubation	<ul style="list-style-type: none"> <li>• EDTA</li> <li>• 0.5% Dispase II</li> </ul>
2.	Secondary enzyme incubation	<ul style="list-style-type: none"> <li>• Collagenase IV</li> <li>• 0.25% Trypsin in versene</li> </ul>
3.	Cell seeding density	<ul style="list-style-type: none"> <li>• <math>1 \times 10^3</math></li> <li>• <math>1 \times 10^4</math></li> <li>• <math>1 \times 10^5</math></li> </ul>
4.	Serum	<ul style="list-style-type: none"> <li>• + 5% fetal bovine serum (FBS)</li> <li>• - 5% fetal bovine serum</li> </ul>
5.	Tissue culture surface substrate	<ul style="list-style-type: none"> <li>• N<sub>2</sub> plasma treated</li> <li>• Collagen I treated</li> </ul>

### 3.3.5 Cell lines

Table 3.3 – NRU cell lines

Code	No. of animals	Sex	Source	Strain	Age/Weight
R006a, b & c	30	M/F	FERA	Homozygous Scottish	5 weeks
R007	5	M	University of York	Sprague Dawley	9 months
R008	20	M	University of Leeds	Wistar	6-9 months
R009	30	M/F	FERA	Homozygous Scottish	3-6 weeks
R010	5	M/F	University of York	Wistar	4 weeks
R012	6	M/F	University of York	Wistar	6 weeks
R013	13	M/F	FERA	Homozygous Scottish	3 weeks
R015	25	M/F	FERA	Homozygous Scottish	2-3 weeks
R016	20	M/F	FERA	Homozygous Scottish	3 weeks
R017	30	M/F	FERA	Homozygous Scottish	3.5 weeks
R020	12	M/F	FERA	Homozygous Scottish	250g
R022	20	M/F	FERA	Homozygous Scottish	3 weeks
R023	4	M/F	FERA	Homozygous Scottish	250g
R024	10	M/F	FERA	Homozygous Scottish	5 weeks
R025	15	M/F	FERA	Homozygous Scottish	3 weeks
R027	9	M/F	FERA	Homozygous Scottish	250g
R028	20	M/F	FERA	Homozygous Scottish	3-4 months

NRU cell lines were generated from donated rat bladder tissue from three strains of rat: Wistar (NRU-W), Sprague Dawley (NRU-SD) and Homozygous Scottish (NRU-HS).

Table 3.4 - NHU cell lines

Code	Tissue of origin	Sex	Age	Age of cells during experiments
Y984	Bladder	M	70	Passage 1-5
Y1052	Renal pelvis	unknown	unknown	Passage 1-5
Y1183	Ureter	M	75	Passage 1-5

## **3.4 Results**

### **3.4.1 Initial comparisons of rat and human urothelium in situ**

The epithelial cell marker cytokeratin 7 (CK7) and the proliferation marker Ki67 were immunolabelled in rat and human bladder sections (Figure 3.4). Native rat urothelium was found to be, on average, 3-4 cells in depth unlike human urothelium, which exceeded 6 cells. Ki67 labelling was present in all but superficial cells in rat urothelium whereas Ki67 positive cells were not seen in human urothelium.

### **3.4.2 NRU cell culture using protocols established for NHU cells.**

NRU cells were isolated using the published protocol for NHU cell isolation, seeded at an approximate concentration of  $1 \times 10^4$  cells/cm<sup>2</sup> onto N<sub>2</sub>-plasma treated tissue culture plastic and cultured in KSFMc medium.

After isolation, NRU-HS cells were difficult to distinguish from cell debris, making seeding inaccurate (Figure 3.5). Growth curves generated over 9 days indicated that NRU-HS cells achieved approximately one cell doubling between 1 and 5 days, after which cell biomass remained approximately the same or reduced (Figure 3.6).

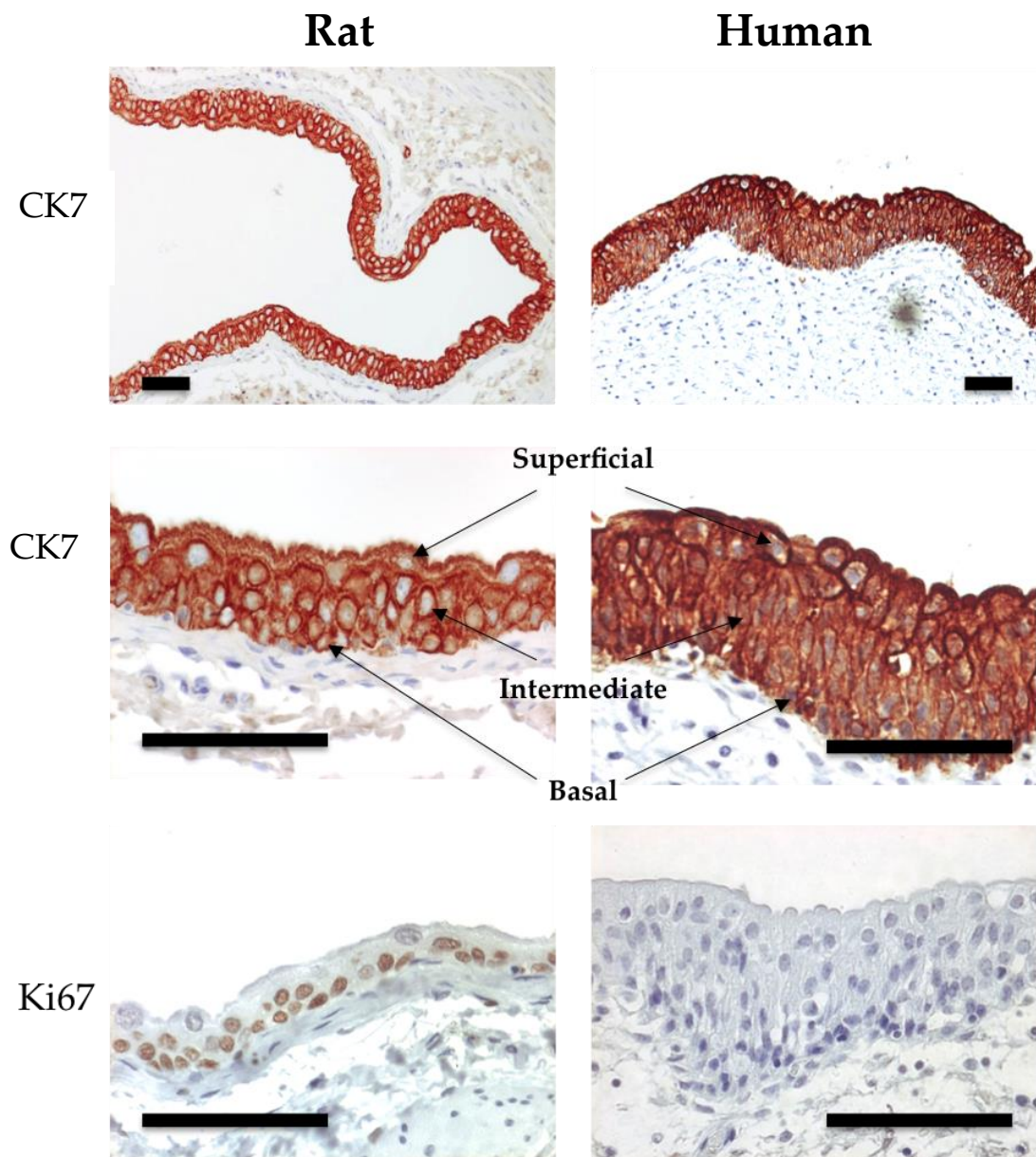


**Figure 3.4 – Differences in the tissue thickness and number of proliferative cells in the native urothelium of humans and rats.** Immunolabelling of the urothelial cell marker cytokeratin 7 (CK7) (top & middle) and the cell proliferation marker Ki67 (bottom) in rat (left) and human (right) bladders. Superficial, intermediate and basal cell zones are labelled. Scale bars = 50  $\mu$ m. Results have been repeated in multiple individual rat bladders ( $n < 5$ ).

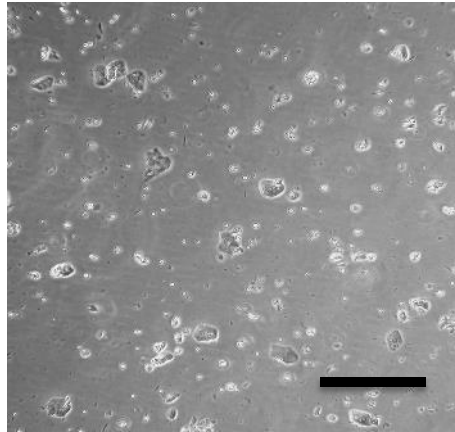


**Figure 3.5 – NRU cells were not cleanly isolated by the NHU cell isolation protocol.** Phase contrast images of NRU-HS cells after isolation using the NHU cell (EDTA/Collagenase) isolation protocol (Section 3.3.1), prior to being seeded. Scale bar = 250  $\mu$ m.

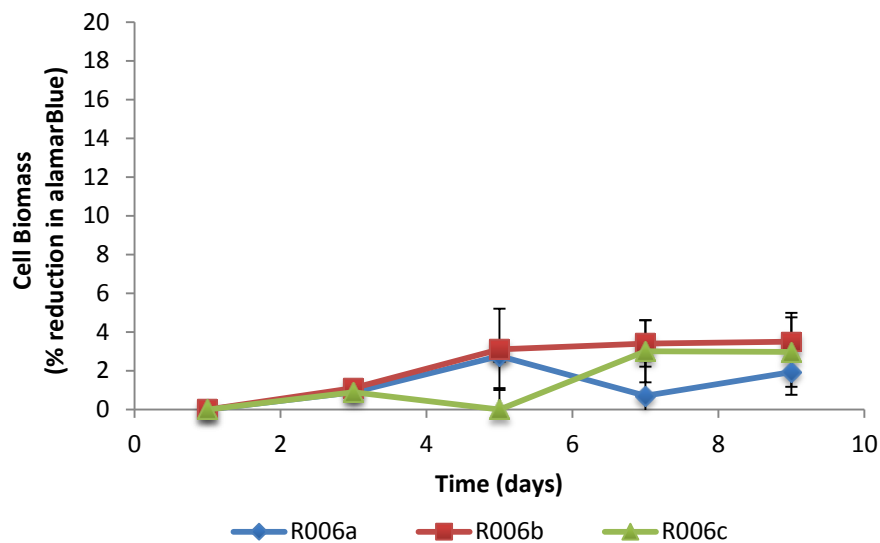


**Figure 3.6 – NRU cells isolated with the NHU cell isolation protocol had limited growth in culture.** Growth curve were generated (Section 2.5.3.1) for NRU-HS cell growth over 9 days cultured in KSFMc after isolation using the NHU cell isolation protocol (Section 3). Data points represent mean  $\pm$  SD. (n=3, R006a, R006b, R006c)

Due to the inability of NRU cells to be cleanly isolated or cultured using the NHU cell isolation protocol, the methods were adapted based on published protocols for NRU cells. Efforts were made to keep the adapted protocol as similar as possible to the NHU cell isolation protocol.

### **3.4.3 Optimisation of the NRU cell isolation protocol**

A Dispase II / Trypsin in versene protocol (NRU cell isolation protocol) was compared against the established EDTA/Collagenase IV protocol for NHU cell isolation (NHU cell isolation protocol) (Southgate et al., 2002). To confirm effective isolation of the urothelium, immunohistochemical labelling of the urothelial cell marker CK7 was conducted on rat bladder tissue after stripping with both protocols (Figure 3.7). With the exception of a small number of labelled cells (which were specially identified and imaged) the majority of tissue was negative for urothelial cells after both protocols. To illustrate the high level of urothelial cell isolation, native rat bladder sections were also labelled as a positive control (Figure 3.7, A&B). Visual assessment of the tissues suggested that more CK7 labelled cells were present after the EDTA stripping protocol compared to dispase II.

Prior to seeding, NRU cells were counted using a haemocytometer and phase contrast images captured. Cell and tissue debris obscured the images after EDTA/collagenase isolation, making it impossible to accurately count individual NRU cells (Figure 3.9). By contrast, NRU cells could be clearly seen and counted on the haemocytometer after isolation using the Dispase II / Trypsin in versene protocol.

To determine the effectiveness of the two protocols in isolating NRU cells, cells isolated using each protocol were cultured for 5 days and colony formation assays performed. The Dispase II / Trypsin in versene isolation protocol achieved the greatest number of NRU-HS cell colonies after 5 days in culture when compared to the EDTA/collagenase protocol (Figure 3.10).

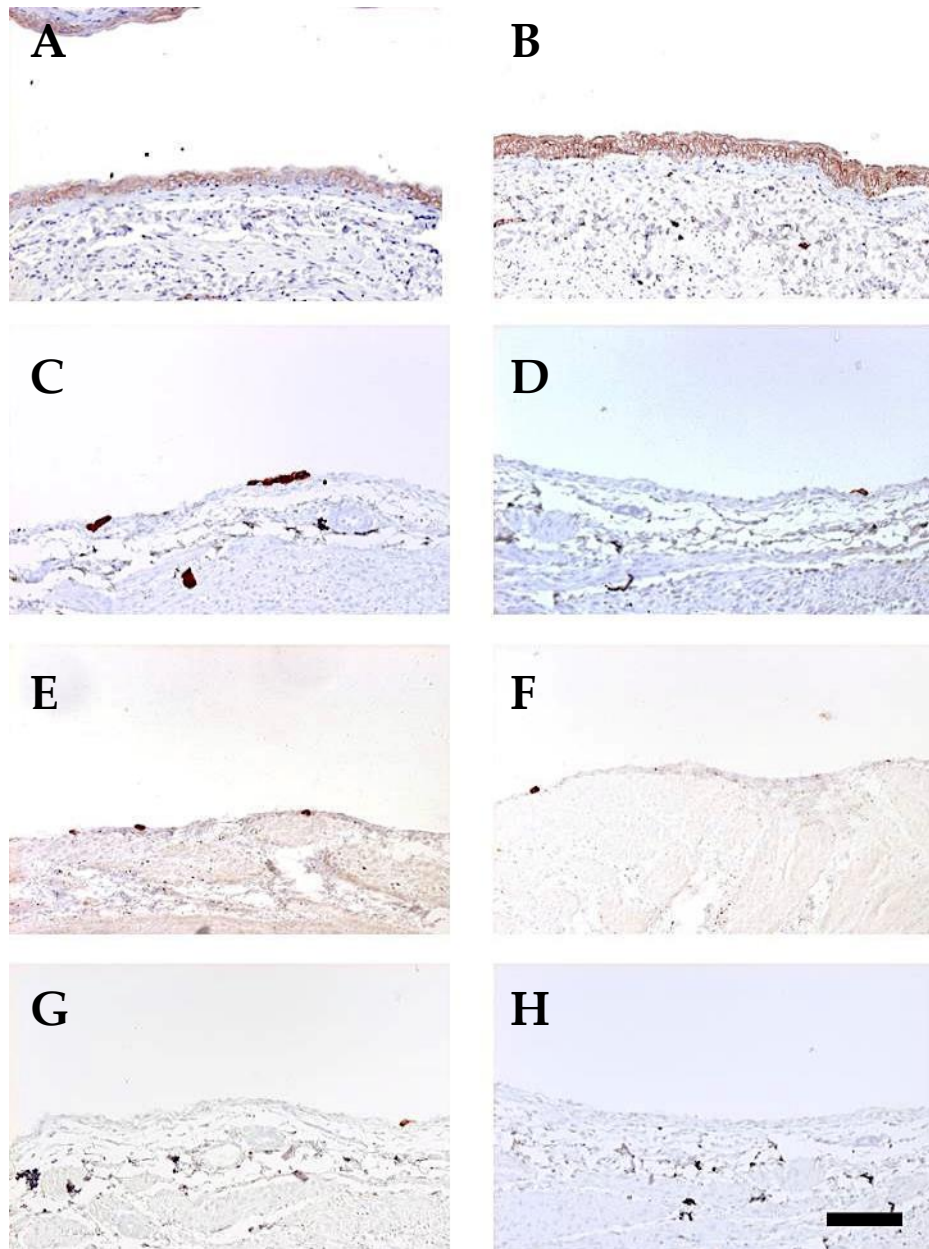


**Figure 3.7 – EDTA/Collagenase and Dispase/trypsin isolation protocols enabled near-complete isolation of urothelial cells.** Urothelial cell marker cytokeratin 7 (CK7) immunolabelling in native rat bladders (A&B) and in rat bladders after urothelial cell isolation using the EDTA protocol (Section 3.3.1; C, E & G) and Dispase/trypsin protocol (Section 3.3.2; D, F & H). Labelled cells were specifically identified and imaged. Scale bar = 50 $\mu$ m. (n=3, R008, R009, R0010).

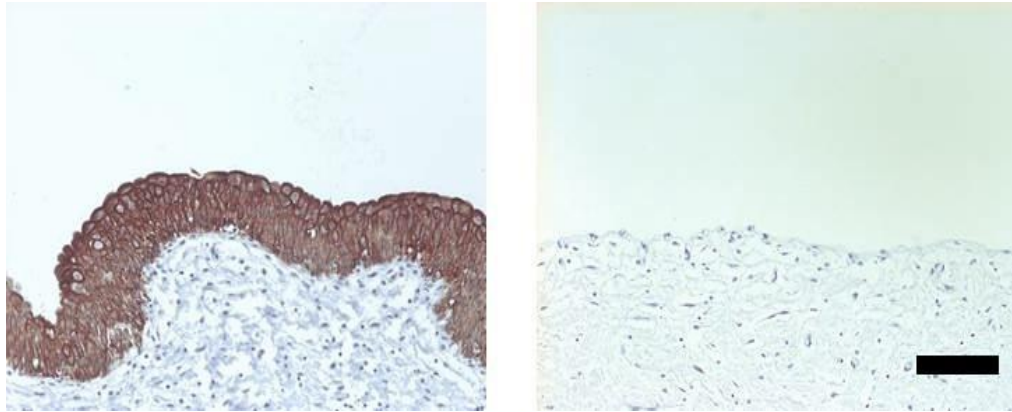


**Figure 3.8 – Complete removal of the urothelium was achieved by stripping human bladder tissue using the EDTA/Collagenase protocol.** Labelling of the urothelial cell marker cytokeratin 7 (CK7) in native human ureter (left) and human bladder tissue after urothelial cell isolation (right) using the EDTA/collagenase protocol (Section 3.3.1). Scale bar = 50 $\mu$ m.

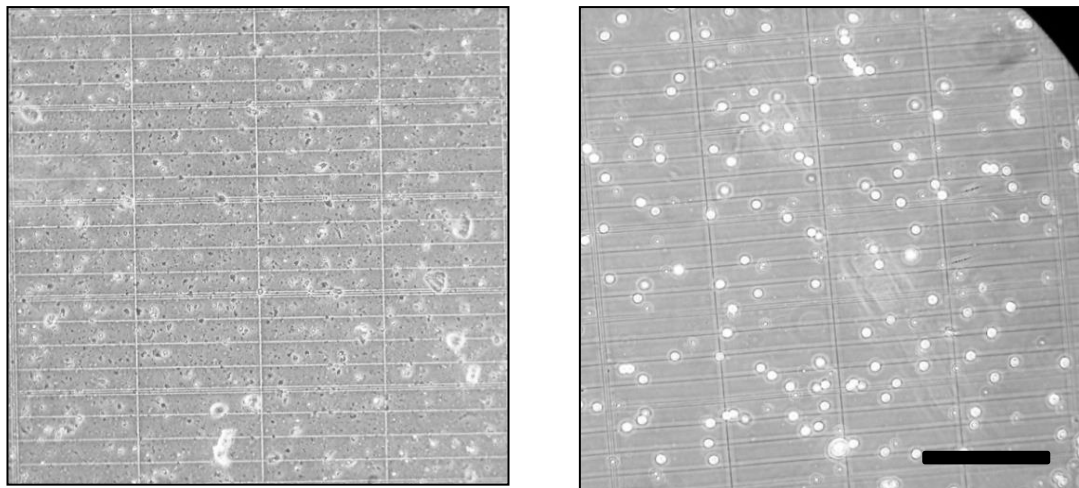


**Figure 3.9 – Clean isolation of NRU cells was achieved using the dispase/trypsin but not the EDTA/collagenase protocols.** Phase contrast images showing primary NRU-HS cells in suspension after isolation with the EDTA/collagenase (Section 3.3.1; left) and Dispase/trypsin (Section 3.3.2; right) protocols on a haemocytometer. Scale bar = 250 $\mu$ m. (n=3, R008, R009, R0010).

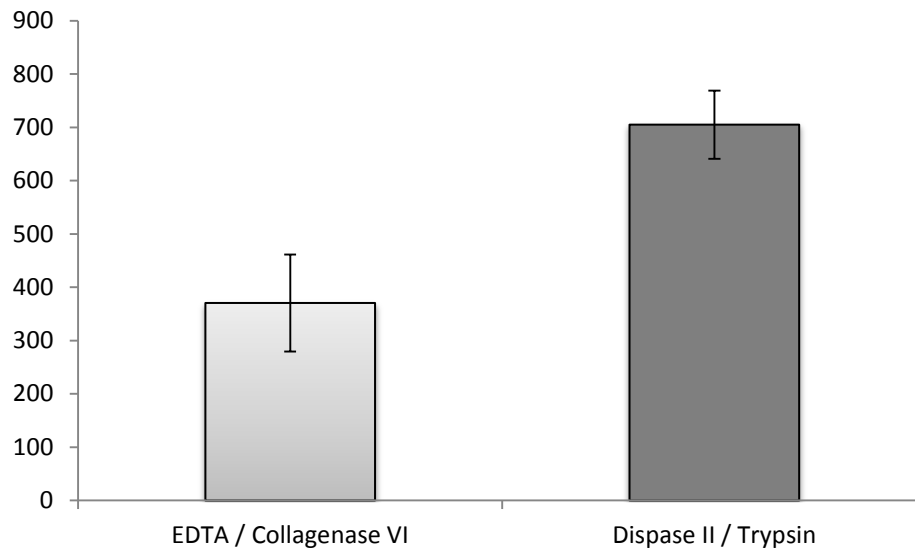


**Figure 3.10 – Primary NRU cells formed more colonies after dispase/trypsin isolation compared to EDTA/collagenase isolation.** Colony formation assay (Section 2.5.3.2) of NRU-HS (adult) cells isolated using both the EDTA/collagenase (Section 3.3.1) and dispase/trypsin (Section 3.3.2) protocols as indicated and cultured on N<sub>2</sub> plasma treated tissue culture plastic. Cells from 2.5 bladders were pooled per well and cultured for 5 days in KSMc +5%FBS. Data points represent the mean  $\pm$  Range (n=2, R009, R0013).

#### **3.4.4 The effect of fetal bovine serum on primary NRU cell cultures**

NRU-W, NRU-SD and NRU-HS cells were cultured on nitrogen plasma treated tissue culture plastic. NHU cells were also cultured for comparison with NRU cells.

Cells were monitored in culture over 7 days by phase contrast microscopy and differences in cell growth rate and morphology observed (Figure 3.11 to Figure 3.14). All NRU cells grew in “cobblestone-like” colonies. NRU-W cell colonies cultured in the absence of serum grew over 5 days whereas the cells grown in the presence of serum did not grow. NRU-HS cell growth only occurred when cells were cultured with 5% FBS whereas NRU-SD cells grew in both the presence and absence of FBS and had no visible effect on phenotype or colony formation. All NRU cell colonies appeared to reach a maximum density and size after approximately 7 days of culture after which colony diameter stopped increasing and appeared to have a three dimensional as opposed to monolayer structure. As a result of this, NRU cell cultures never became fully confluent. This was in contrast to the complete monolayers seen in NHU cell cultures after 5 to 7 days (Figure 3.14). NHU cell growth occurred in the absence of FBS but was inhibited by FBS. The presence of 5% FBS also resulted in an altered NHU cell morphology with cells becoming more elongated in shape and clustering together.

## NRU-HS (Homozygous Scottish)

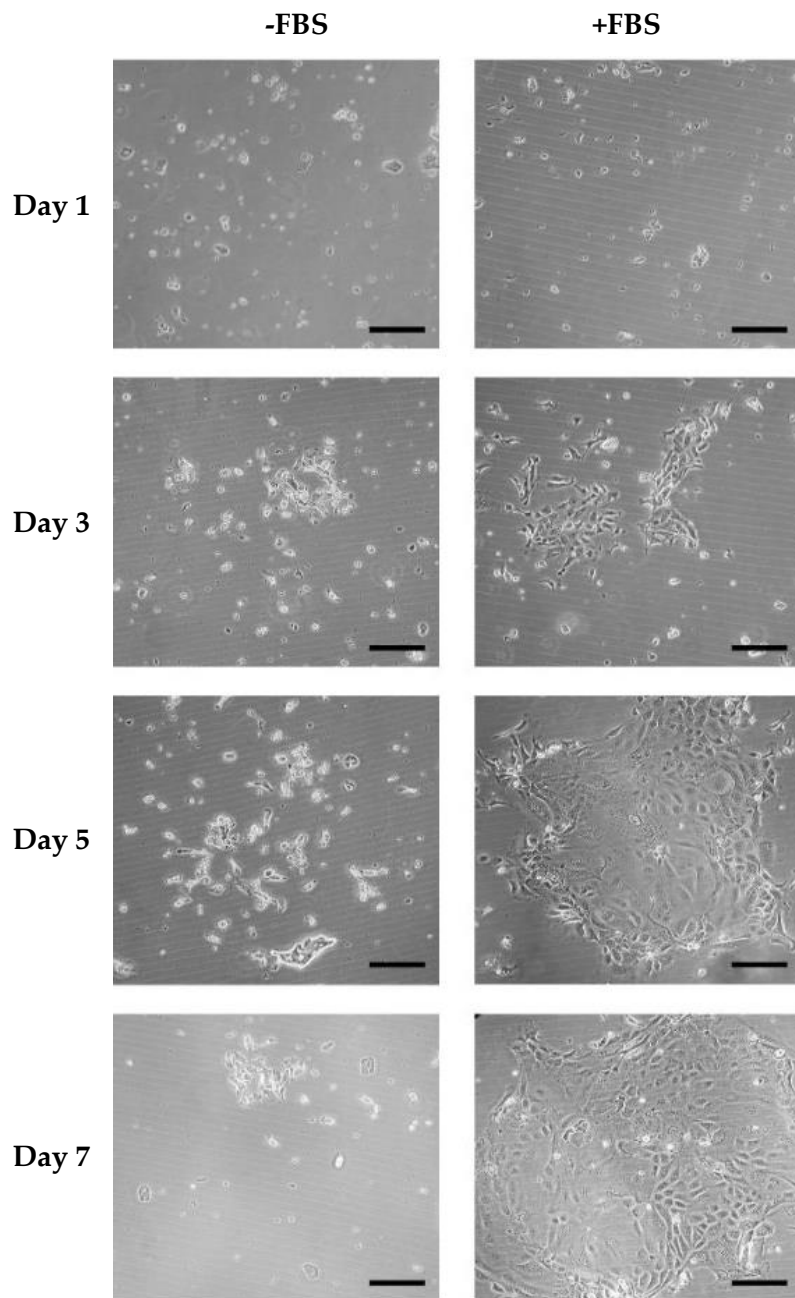


**Figure 3.11 – NRU-HS cells grew in presence but not in the absence of serum.** Representative phase contrast images of NRU-HS cell growth in culture over 7 days in KSFMc medium  $\pm$  5%Fetal Bovine Serum (FBS) (n=3 NRU cell lines, R009, R013, R015). Scale bar = 50  $\mu$ m.

## NRU-SD (Sprague Dawley)

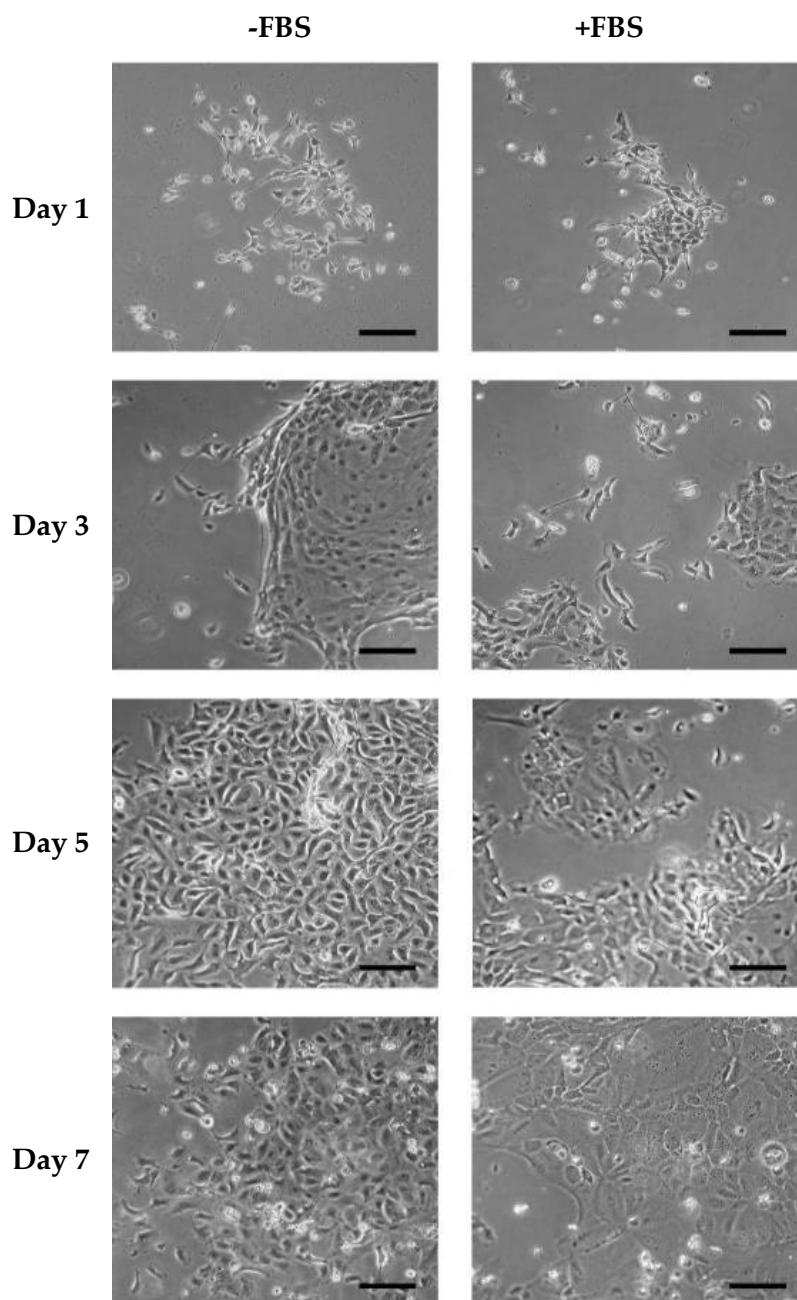


**Figure 3.12 – One NRU-SD cell line grew equally in both serum-free and serum-supplemented medium.** Representative phase contrast images of NRU-SD cell growth in culture over 7 days in KSFMc medium  $\pm$  5%Fetal Bovine Serum (FBS) (n=1 NRU cell line, R007). Scale bar = 50 $\mu$ m.

## NRU-W (Wistar)

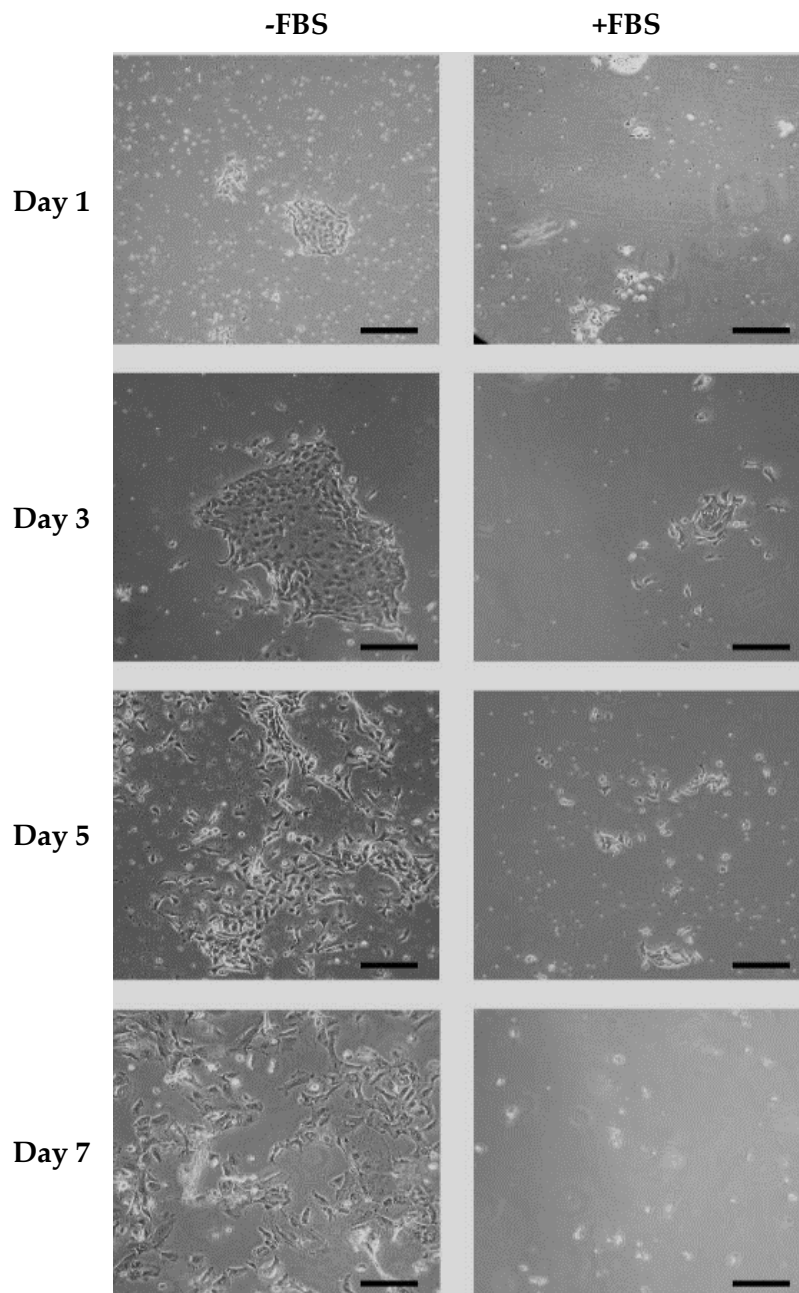


**Figure 3.13 – NRU-W cells grew in the absence but not in the presence of serum.** Representative phase contrast images of NRU-W cell growth in culture over 7 days in KSFMc medium  $\pm$  5%Fetal Bovine Serum (FBS) n=3 NRU cell lines, R008, R010, R012). Scale bar = 50 $\mu$ m.

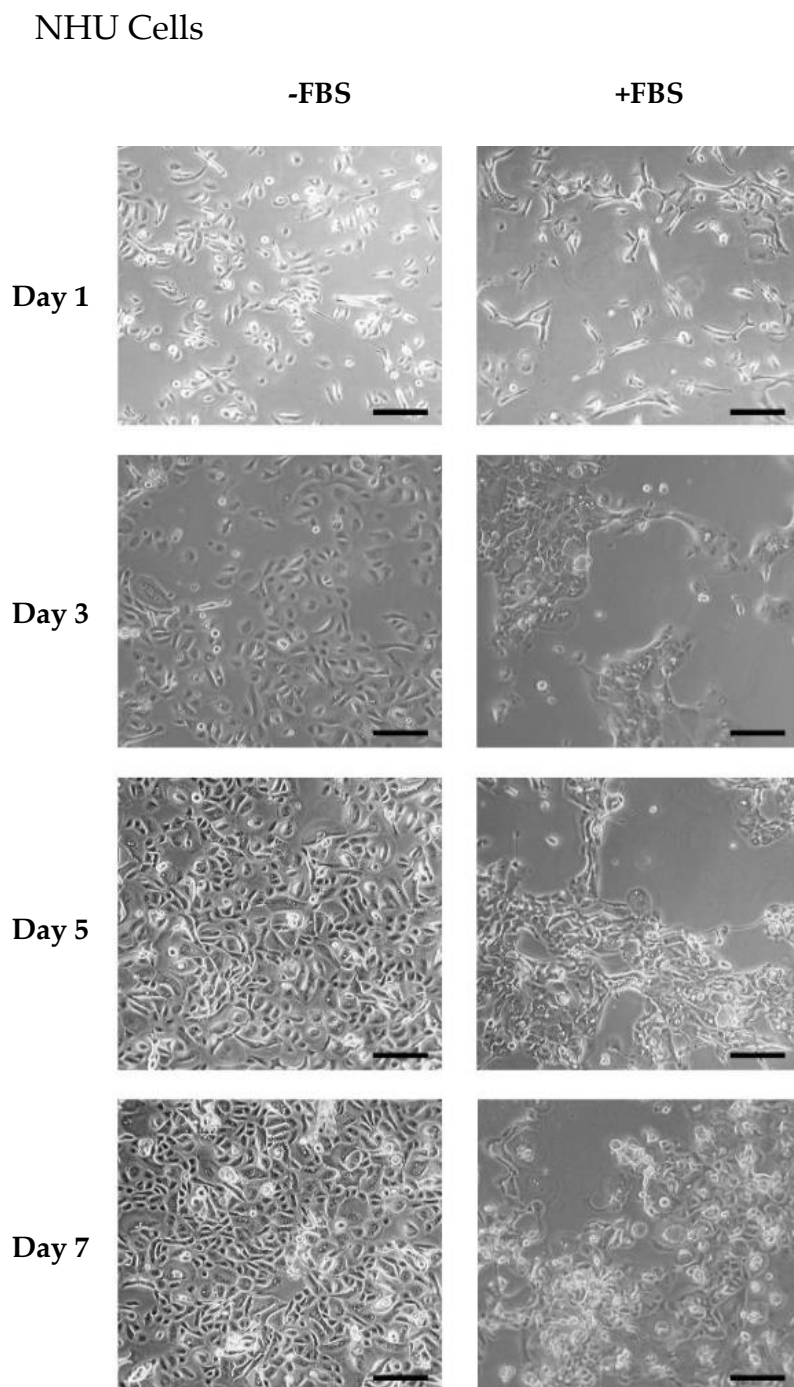


**Figure 3.14 – NHU cells grew normally in serum-free medium but had reduced growth and an altered morphology in serum-supplemented medium.** Representative phase contrast images of NHU cell growth in culture over 7 days in KSFMc medium  $\pm$  5%FBS (n=3 NHU cell lines, Y984, Y1052, Y1183). Scale bar = 50 $\mu$ m.

To further explore the proliferative capability of NRU cells, cell biomass assays were conducted on NRU-W, NRU-HS and NHU cells using the AlamarBlue<sup>®</sup> cell biomass assay (Figure 3.15 & Figure 3.16). Growth curves were generated over 10 days. NRU-W cell growth increased in KSFMc medium but was inhibited by the presence of 5% FBS resulting in cell biomass being significantly reduced by day 6 of culture (Figure 3.17). NRU-HS cells alternatively had the greatest level of growth in the presence of 5% FBS and cell biomass was significantly increased after 6 days by the presence of serum compared to cells cultured in KSFMc alone (Figure 3.18). As a positive method control, growth curves were also generated for three NHU cell lines (detailed in Table 3.4) cultured in KSFMc medium. NHU cells grew rapidly over 5 days before growth plateaued as cells approached confluence.

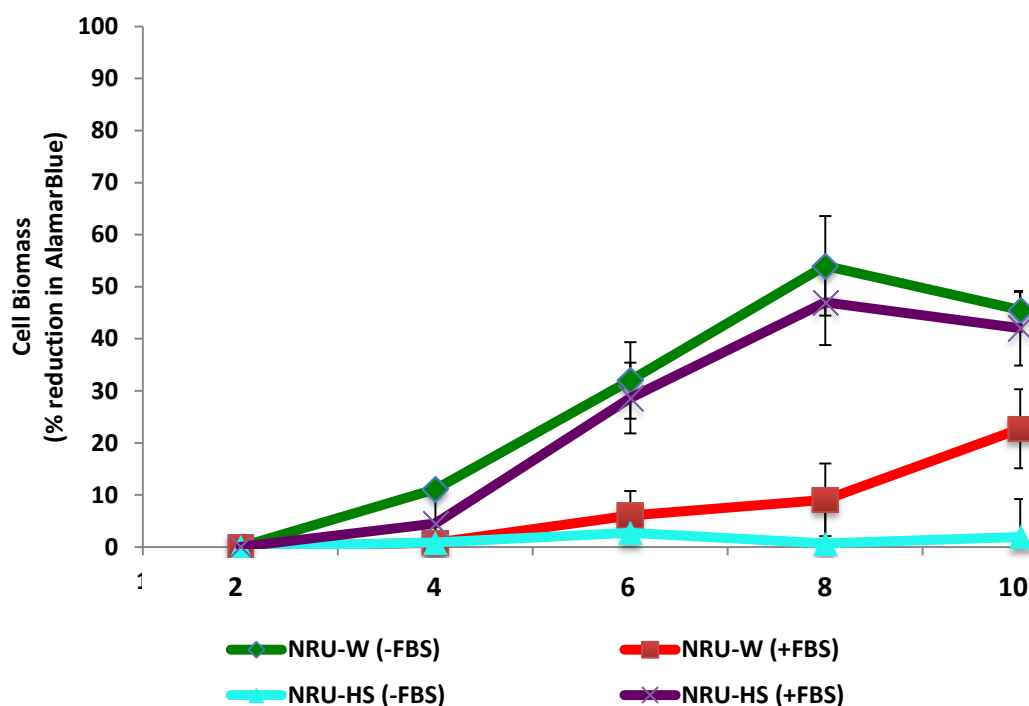


Figure 3.15 – NRU-W cells grew in the absence of serum whereas NRU-HS cells required serum to grow. Growth curves were generated (Section 2.5.3.1) for NRU-W (R008, R010, R012) & NRU-HS (R009, R013, R015) cell cultured over 7 days in KSFMc  $\pm$  5% FBS. Data points represent mean percentage reduction in alamarBlue<sup>®</sup>  $\pm$ SD (n=3).

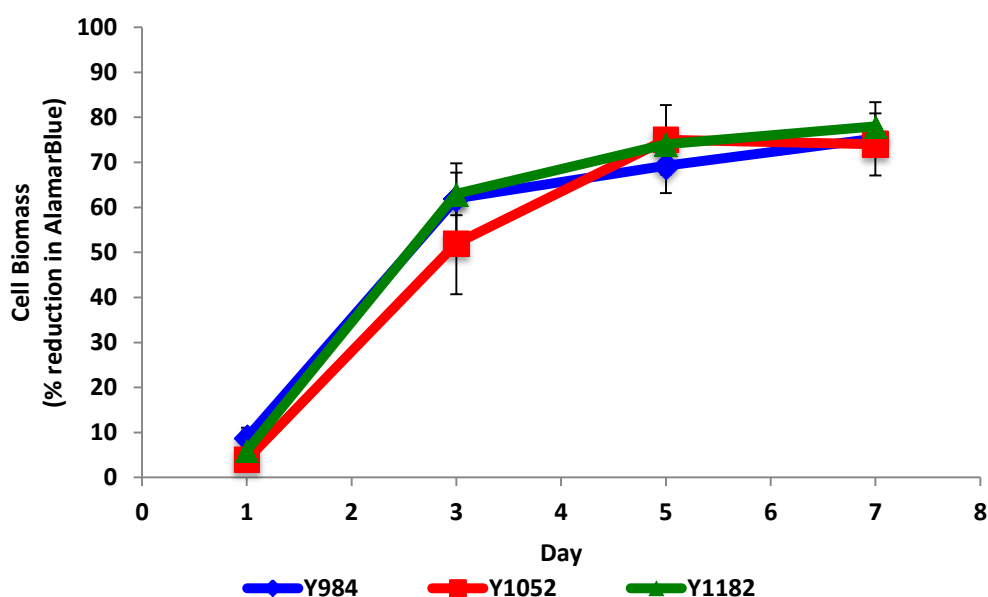


Figure 3.16 – NHU cells show standard expansion and plateau phases of growth when cultured in KSFMc medium. Growth curves were generated (Section 2.5.3.1) for three subcultured (P2) NHU cell lines cultured over 7 days in KSFMc medium. Data points represent mean percentage reduction in alamarBlue<sup>®</sup>  $\pm$ SD (n=3, Y984, Y1052, Y1183).

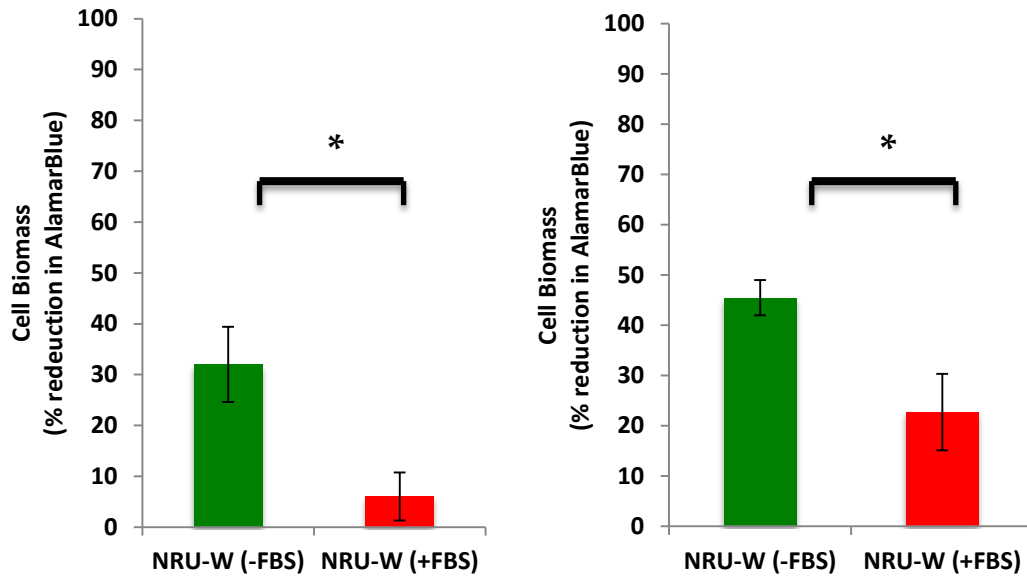


Figure 3.17 – NRU-W cells had significantly greater growth in serum-free medium compared to serum-supplemented medium. Graphs show percentage of alamarBlue® reduction (Section 2.5.3.1) by NRU-W cell cultures on days 6 (left) and 10 (right) of maintenance in KSFMc medium. Data points represent mean  $\pm$ SD (n=3). Student T-Test (paired, 2-tailed) was conducted, \* p < 0.05.

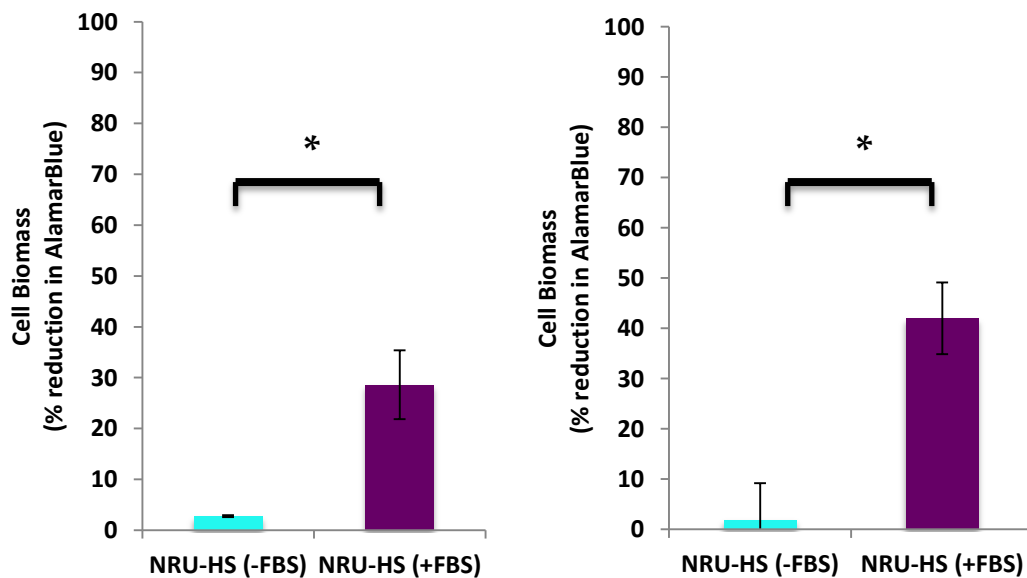
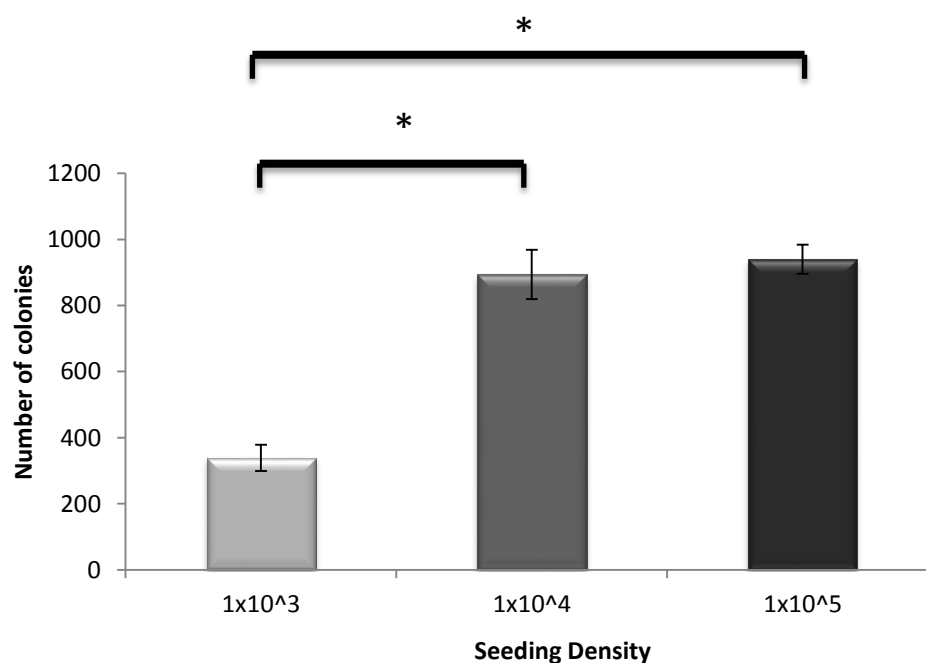


Figure 3.18 – NRU-HS cells had significantly increased growth in serum-supplemented medium compared to serum-free medium. Graphs show the percentage of alamarBlue® reduction (Section 2.5.3.1) by NRU-HS cell cultures on days 6 (left) and 10 (right) of maintenance in KSFMc medium. Data points represent mean  $\pm$ SD (n=3). Student T-Test (paired, 2-tailed) was conducted, \* p < 0.05.

### 3.4.5 NRU cell seeding density

An appropriate NRU cell seeding density was established using colony formation assays, allowing for the minimal amount of NRU cells to be used per experiment. As can be seen (Figure 3.18), seeding NRU cells at  $1 \times 10^4$  cell/cm<sup>2</sup> significantly increased the number of colonies formed compared to cells that had been seeded at  $1 \times 10^3$  cells/cm<sup>2</sup> after 5 days of culture. There was no significant increase in NRU cell colony formation between cultures seeded with  $1 \times 10^4$  cells/cm<sup>2</sup> and  $1 \times 10^5$  cells/cm<sup>2</sup> after 5 days of culture. Based on these results, a seeding density of  $1 \times 10^4$  cells/cm<sup>2</sup> was adopted as the standard NRU cell seeding density for all future experiments.



**Figure 3.19 –  $1 \times 10^4$  cells/cm<sup>2</sup> was the optimal seeding density for NRU-HS cells.** NRU-HS cells were seeded at  $1 \times 10^3$ ,  $1 \times 10^4$  and  $1 \times 10^5$  cells per cm<sup>2</sup>, cultured in KSFMc +5% FBS for 5 days before a colony formation assay (Section 2.5.3.2) was performed. Data points represent mean  $\pm$ SD (n=3, R022, R023, R024). Student T Test (paired, 2-tailed) was conducted, \* = p <0.05.

### 3.4.6 Optimising surface substrate for NRU cell growth

The colony forming ability of NRU-HS cells was assessed on collagen I coated and N<sub>2</sub> plasma treated tissue culture plastic. Supporting earlier observations, NRU-HS cells cultured in the presence of 5% FBS had significantly greater colony numbers than cells cultured in KSFMc alone. Cells cultured on nitrogen plasma treated tissue culture plastic formed significantly more colonies than those cultured on collagen I coated tissue culture plastic after 5 days of culture.

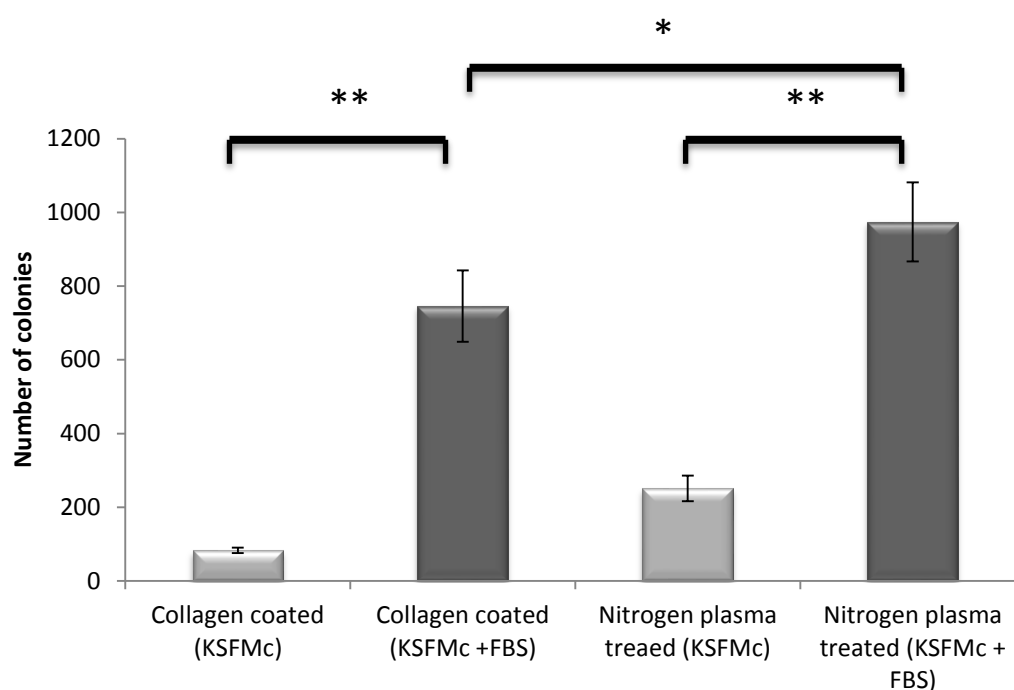


**Figure 3.20 – NRU-HS cells grew best in the presence of serum and on N<sub>2</sub>-plasma treated tissue culture plastic.** Colony formation assays (Section 2.5.3.2) were conducted to examine NRU-HS (P0) cell growth on collagen I and N<sub>2</sub> plasma-treated tissue culture plastic in KSFMc ± 5%FBS. Cells were cultured for 5 days on 6 well plates. Data points represent the mean number of colonies ±SD (n=3, R016, R017, R020). Student T Tests (Paired, 2-tailed) were conducted, \* = p < 0.05, \*\* = p < 0.01.

### 3.4.7 Subculture of NRU cells

NRU-HS cells isolated using both the EDTA/collagenase and dispase II/trypsin protocols were cultured up to day 8 in KSFMc, before sub-culture, involving harvest using EDTA/trypsin in versene and reseeded onto fresh substrates. As shown in Figure 3.21, EDTA/collagenase isolated NRU-HS cell cultures did not recover after passage and the majority of cells had died by day 13. NRU-HS cells isolated using the dispase II/trypsin protocol did grow after subculture. This result was seen in several NRU-HS cell lines.

To quantify this result, growth curves were generated (Figure 3.22 and Figure 3.23). When compared to cells isolated using the EDTA/collagenase protocol, dispase II/trypsin isolated NRU-HS cells had a greater proliferative capacity in primary culture between 3 and 7 days and, when subcultured, continued to proliferate over 5 days. Subcultured NRU-HS cells after dispase II/trypsin isolation did not achieve the same biomass as primary NRU-HS cells but did achieve approximately a 4 fold increase in population size over 5 days. Attempts to subculture dispase II/trypsin isolated NRU cells further were unsuccessful.

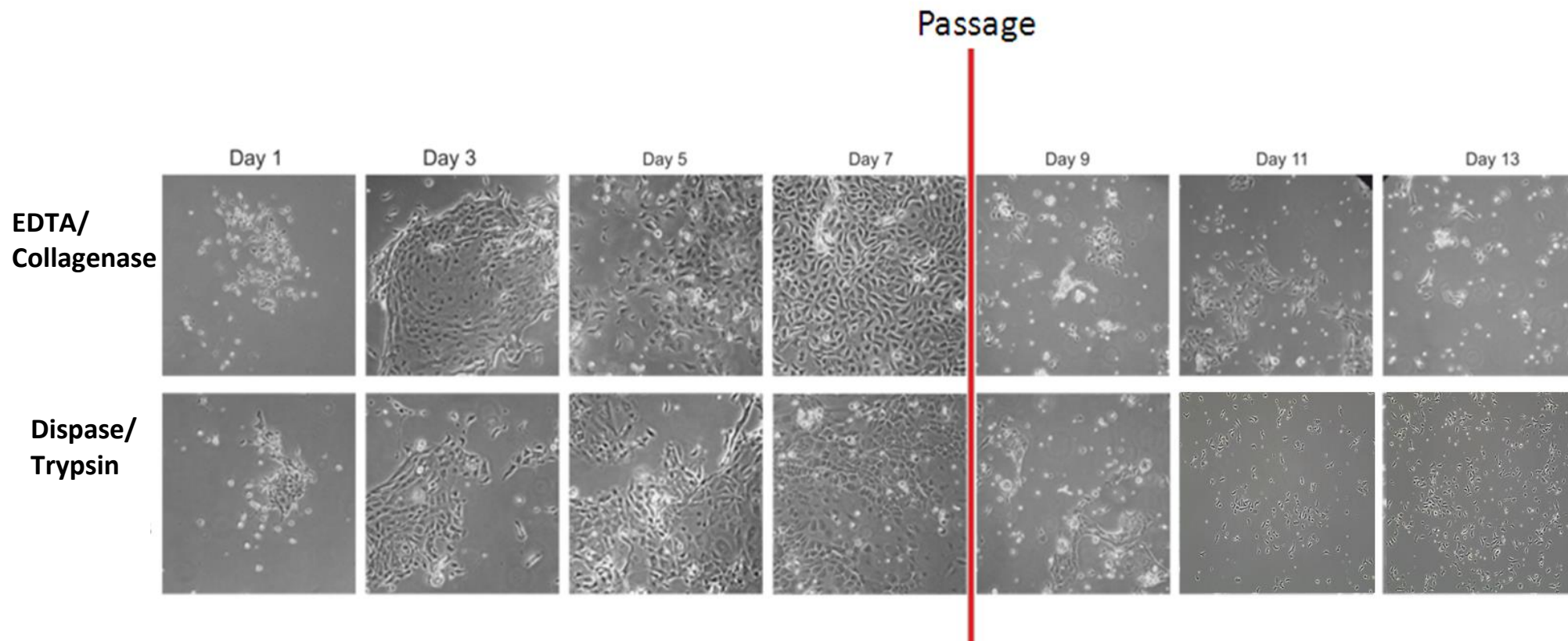


**Figure 3.21** - NRU-HS cells were successfully subcultured after dispase/trypsin isolation but not after EDTA/collagenase isolation. NRU- HS cells growth after EDTA/Collagenase and Dispase/trypsin isolation. On day 8 cells were passaged (Section 2.5.2.4) and split 1:3 before being reseeded at a density of  $1 \times 10^4$  cells/cm<sup>2</sup>. Growth curves were generated for these cells (see

**Figure 3.22 & Figure 3.23;** n=3, R025, R027, R028).

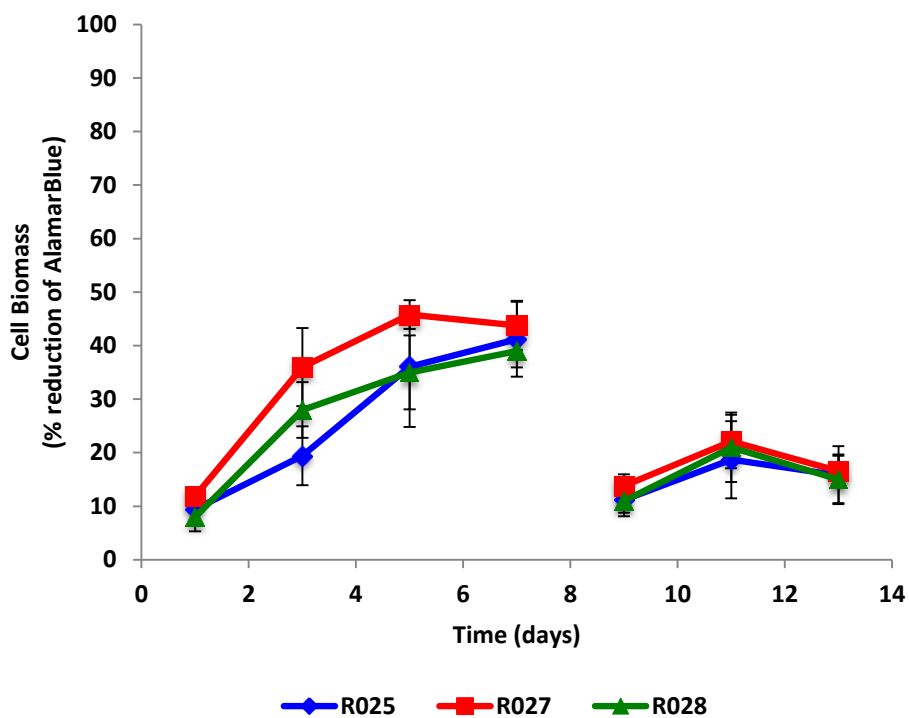


**Figure 3.22 – EDTA/collagenase isolated cells did not grow after being passaged.** Growth curves were generated (Section 2.5.3.1) for three NRU-HS cell lines isolated using the EDTA/collagenase protocol (Section 3.3.1) in primary culture (day 1-7) and after subcultured (day 9-13). Data points represent mean percentage reduction in alamarBlue®  $\pm$ SD (n=3, R025, R027, R028).

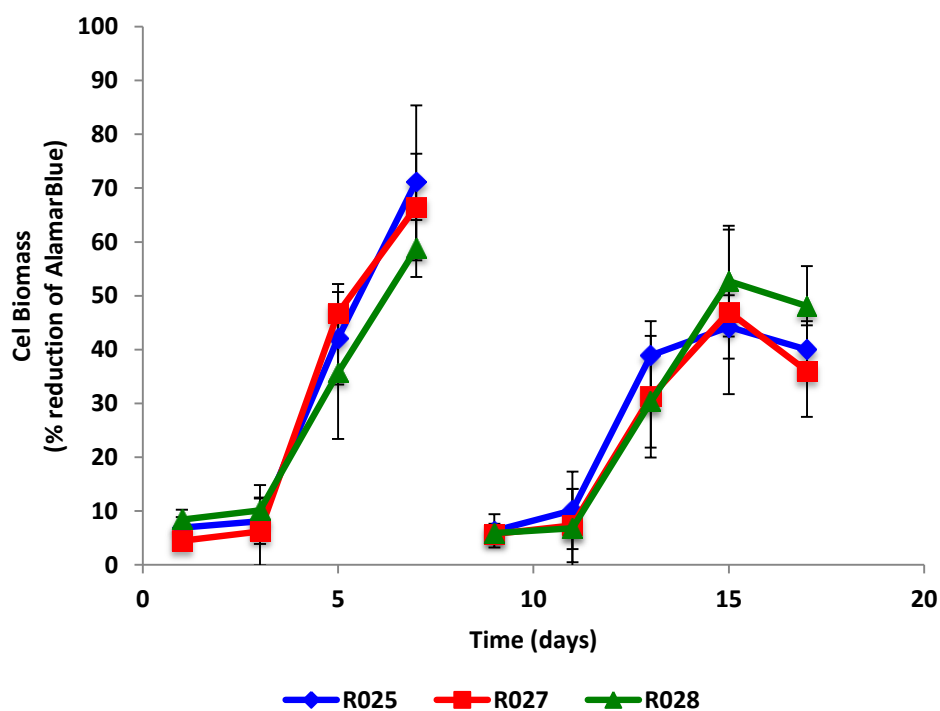


**Figure 3.23 – Dispase/trypsin isolated cells were capable of growth after being passaged.** Growth curves were generated (Section 2.5.3.1) for three NRU-HS cell lines isolated using the dispase/trypsin protocol (Section 3.3.2) in primary culture (day 1-7) and after subcultured (Day 9-13). Data points represent mean percentage reduction in alamarBlue®  $\pm$ SD (n=3, R025, R027, R028).

### 3.5 Conclusions and Discussion

NRU cells are capable of being isolated using multiple isolation protocols but the method of isolation appears to have an effect on the growth capabilities of the cells. The ability to subculture NRU cells also appears to be affected by the method of isolation. NRU cells isolated using the dispase II / trypsin protocol were capable of being subcultured once whereas NRU cells isolated using the EDTA/collagenase IV protocol could not survive a passage. As a result of this finding, the dispase II / trypsin protocol was adopted as standard for all further experiments (Chapters 4, 5 and 6).

Although NRU cells were cultured to passage 1, attempts to subculture cells further were unsuccessful. NHU cells are capable of undergoing several passages before becoming senescent, possibly indicating a difference between the growth/proliferative abilities of normal human and rat urothelial cells. As such the pathways regulating NRU and NHU cell proliferation were further investigated (Chapter 4) to both understand any differences in regulation between rats and humans and to explore whether NRU cell lifespan in culture could be increased through modulation of these pathways.

A strain difference was found to exist between the NRU-W and NRU-HS cells in regard to the requirement of FBS in the culture medium. Such a difference could impact on the results of toxicity tests conducted using different strains. Despite this strain difference being an interesting finding, it was decided to continue exploring interspecies variations between human and rat urothelial cells. As such, subsequent experiments would only utilise cells from the commonly used Wistar rat strain and not cells from the rare inbred Homozygous Scottish rat strain.

Several aspects of NRU cell culture were optimised including seeding density, surface substrate and the presence/absence of FBS in culture medium. These optimised conditions will be adopted as standard for all future NRU cell cultures.

### 3.6 Key findings

- A dispase II / trypsin NRU cell isolation protocol enabled the clean isolation of NRU cells from bladder tissue and produced NRU cultures that could be subcultured up to P1. NRU cell isolation using an EDTA / collagenase protocol optimised for NHU cell isolation produced cultures that were difficult to count and which failed to grow after subculture
- Bovine serum being a prerequisite for NRU-HS cell growth but has inhibitory on NRU-W cell proliferation.
- Seeding NRU cells at a concentration of  $1 \times 10^4$  cells/cm<sup>2</sup> onto nitrogen plasma treated tissue culture plastic after isolation with dispase II / trypsin allowed for the greatest level of cell adhesion and proliferation

# Chapter 4 - The regulation of Normal Rat Urothelial (NRU) and Normal Human Urothelial (NHU) cell proliferation *in vitro*

<b>4.1 Chapter Introduction .....</b>	<b>105</b>
<b>4.2 Chapter Aim .....</b>	<b>107</b>
4.2.1 – Objectives.....	107
<b>4.3 Experimental Approach .....</b>	<b>108</b>
4.3.1 - Proliferation pathways.....	108
4.3.2 Extracellular calcium .....	108
4.3.3 - Cell lines .....	111
<b>4.4. Results – NHU cells .....</b>	<b>112</b>
4.4.1 – Growth Kinetics.....	112
4.4.2 – Proliferation pathways.....	114
4.4.3 – Pharmacological interrogation of proliferation pathways.....	117
4.4.4 – Conclusions .....	118
<b>4.5 Results – NRU cells .....</b>	<b>119</b>
4.5.1 – Growth Kinetics.....	119
4.5.2 –Ki67 expression .....	121
4.5.3 – Phospho-ERK, $\beta$ -catenin and phospho-Akt expression.....	121
4.5.4 – Removal of exogenous EGF.....	128
4.5.5 – PI3K/Akt pathway inhibition .....	129
4.5.6 – Physiological (2mM) extracellular calcium .....	133
4.5.7 – Reduced extracellular calcium .....	136
<b>4.6 Results summary .....</b>	<b>140</b>
<b>4.7 Conclusions and Discussion .....</b>	<b>142</b>
<b>4.8 Key findings.....</b>	<b>143</b>



## 4.1 Chapter Introduction

*In vivo*, human urothelial cells are considered mitotically quiescent, proliferating 1-2 times per year on average. When cultured in keratinocyte serum free medium under conditions of low extracellular calcium (0.09 mM) and supplemented with bovine pituitary extract, epidermal growth factor (EGF) and cholera toxin, NHU cells adopt a proliferative “basal-like” phenotype. Proliferation in NHU cells, due to the absence of the instructive signalling present *in vivo*, is regulated via an autocrine signalling loop in which the epithelial growth factor receptor (EGFR) / Mitogen-activated protein Kinase (MAPK) pathway drives the cell proliferation (Varley et al., 2004; Varley et al., 2005). In addition to exogenous EGF present in KSFMc medium, proliferating NHU cells are known to be capable of secreting EGF, as well as the EGFR ligands epiregulin, TGF- $\alpha$ , and amphiregulin (Varley et al., 2005). As illustrated in Figure 4.1, activation of the EGFR/MAPK pathway also activates the Wnt/  $\beta$ -catenin pathway under conditions of low (0.09 mM) extracellular calcium ion concentrations, by inhibiting GSK3 $\beta$ -mediated destruction of  $\beta$ -catenin, allowing  $\beta$ -catenin to translocate to the cell nucleus and regulate gene expression, facilitating proliferation (Georgopoulos et al., 2014).

NHU cells proliferation can also, in conditions of near physiological extracellular calcium ion concentrations, be regulated by the phosphoinositide 3-kinase (PI3K)/ protein kinase B (Akt) pathway. Under conditions of near physiological extracellular calcium (2 mM Ca<sup>2+</sup>), the EGFR/MAPK pathway is inactive and  $\beta$ -catenin is sequestered to the cell membrane where it is incorporated, with E-cadherin, into adherens junctions. Phenotypically cells assemble into a 3-dimensional, structure but continue to proliferate via PI3K/Akt pathway regulation (Georgopoulos et al., 2010; Georgopoulos et al., 2014). The exact method by which the switch between the EGFR/MAPK and PI3K/Akt pathway is achieved is still under investigation.

In culture, NRU cell lifespan was found to be greatly reduced compared to NHU cells. NRU cells also grew in colonies, which failed to expand across all of the available surface area (Chapter 3). In an attempt to increase NRU cell lifespan in culture, and better understand interspecies differences between NRU and NHU cells, the pathways regulating NRU cell proliferation were investigated.

## 4.2 Chapter Aim

To compare the intracellular signalling pathways regulating NHU and NRU cell proliferation and to explore candidate methods of increasing NRU cell proliferation/longevity in culture through modulating the activity of these pathways either pharmacologically or by varying the extracellular environment.

### 4.2.1 – Objectives

1. Identify and interrogate the signal transduction pathways regulating NHU and NRU cell proliferation
  - Identify which pathways are active in NHU and NRU cells
  - Use pharmacological or recombinant factors to activate/inhibit candidate pathways and assess the effects on proliferation and survival of NRU cells in culture.
2. Explore the effect of modifying extracellular calcium ion concentration on NRU cell proliferation and phenotype
  - Determine the effect of altered exogenous calcium ion concentrations on NRU cell proliferation
  - Determine whether lowering extracellular calcium promotes a more proliferative NRU cell phenotype and investigate the mechanisms involved in regulating this change.

## 4.3 Experimental Approach

### 4.3.1 - Proliferation pathways

Pharmacological agonists and inhibitors of the EGFR/MAPK,  $\beta$ -catenin and PI3K/Akt signal transduction pathways were used to modulate activity (Table 4.1). The effects on cell proliferation were assessed via growth curves and the expression of pathway or proliferation markers.

### 4.3.2 Extracellular calcium

Extracellular calcium ion concentrations are known to evoke urothelial cells to form tight junctions and switch their proliferative regulation from the EGFR/MAPK pathway to the PI3K/Akt pathway (Georgopoulos et al., 2010; Georgopoulos et al., 2014). To investigate the effect of extracellular calcium on NRU cell proliferation the calcium concentration of KSFMc was reduced as follows:

- 0.09mM (control)
- 0.06mM
- 0.03mM
- 0.015mM

Growth curves were generated to assess NRU cell proliferation and the activation of the pathways assessed by quantifying protein marker expression. The ability of cells to form cell-cell junctions was investigated by looking at the localisation and expression of cell-cell junction proteins in NRU cells

Table 4.1 Pharmaceutical agonists/antagonists

Compound	Target	Pathway	Concentration*	IC <sub>50</sub>	Vehicle**
<b>PD153035</b> (PD)	EGFR inhibitor	EGFR/ MAPK	1µM	25pM	DMSO
<b>UO126</b>	MEK1/2 inhibitor	EGFR/ MAPK	5µM	72/58nM	DMSO
<b>SB415286</b> (SB)	GSK3β inhibitor	<b>Wnt/β- catenin</b>	10µM	2.9µM	DMSO
<b>IGF1</b>	IGFR activator	PI3K/Akt	1µM	n/a	PBS
<b>LY294002</b> (LY)	PI3K inhibitor	PI3K/Akt	5µM	1.4uM	DMSO

\* Concentrations previously optimised for NHU cells

\*\* Vehicle concentration did not exceeded 0.01% final volume

All pharmacological agents were administered in KSFMc medium containing bovine pituitary extract (BPE), EGF and cholera toxin.

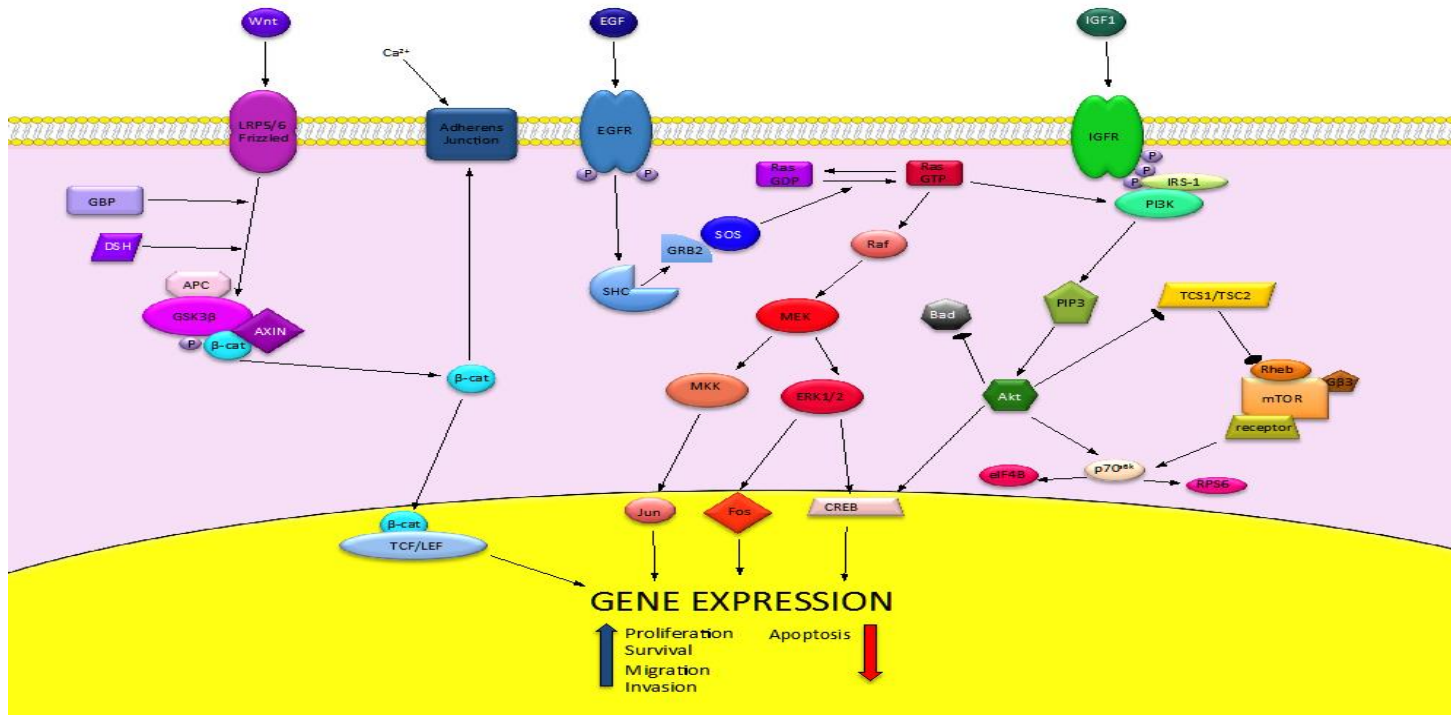


**Figure 4.1 - Summary of the EGF/MAPK, Wnt/ $\beta$ -catenin and PI3K/Akt pathways.** Release of  $\beta$ -catenin (left) from the GSK3 $\beta$  destruction complex enables  $\beta$ -catenin to translocate to either the cell nucleus where it regulates gene expression to promote cell proliferation and survival or, under conditions of high calcium, be incorporated into adherens junctions at the cell membrane. Activation of MEK of EGFR (centre) by EGF activates the MAPK pathway to regulate gene expression to promote cell proliferation, survival and migration while inhibiting apoptosis. Activation of the PI3K/Akt pathway (right), for instance by IGFR activation can activate the mTOR pathway through TCS complex inhibition, inhibits apoptosis through inhibition of Bad and while regulating gene expression to promote cell growth and inhibit apoptosis.

### 4.3.3 - Cell lines

All NHU and NRU cell lines used in this chapter are listed in Tables 4.2 & 4.3. All NRU cells were used in primary (passage 0) culture unless otherwise indicated.

**Table 4.2 NHU Cells**

Code	Tissue of origin	Sex	Age	Age of cells during experiments
Y1430	Ureter	F	71	Passage 2-3
Y1437	Ureter	F	65	Passage 3-4
Y1461	Ureter	M	39	Passage 2-3

**Table 4.3 NRU Cells**

Code	No. of animals	Sex	Source	Strain	Age /Weight
R037	6	M/F	University of York	Wistar	9 month
R038	10	M/F	Covance Inc.	Wistar	1 year
R039	4	F	University of York	Wistar	adult
R040	12	M	University of York	Wistar	250-300g
R041	12	M	University of York	Wistar	250-300g
R042	10	M/F	Covance Inc.	Wistar	300-350g
R046	10	M	University of York	Wistar	300-350g
R047	12	F	University of York	Wistar	250g
R048	40	F	University of Manchester	Hooded Lister	250-280g
R049	2	F	University of York	Wistar	200g
R050	10	M/F	University of Manchester	Hooded Lister	200-300g
R051	20	M/F	University of Manchester	Hooded Lister	200-300g
R052	25	M/F	University of Manchester	Hooded Lister	200-300g
R055	30	M/F	University of Manchester	Wistar	200-300g
R056	5	F	University of York	Wistar	200-300g

## 4.4. Results – NHU cells

### 4.4.1 – Growth Kinetics

Growth curves (Figure 4.2 & Figure 4.3) were generated for NHU cells cultured in KSFMc medium alone and with the pharmacological agents listed in Table 4.1. Results showed that when cultured in low calcium (0.09mM) KSFMc medium (control), NHU cell proliferation increased between 1 and 5 days in culture before plateauing between 5 and 9 days as cultures became confluent.

Activation of the  $\beta$ -catenin pathway, through inhibition of GSK3 $\beta$  (SB415286), and the PI3K/Akt pathway (IGF1) had no significant effect on the growth kinetics of NHU cells over 7 days of culture. Between days 7 and 9, NHU cells cultured with IGF1 showed a reduction of biomass compared to controls but this decrease was not significant ( $p > 0.05$ ).

Inhibition of EGFR (PD153035) or downstream ERK (UO126) appeared to result in an initial increase in proliferation between 1 and 3 days of culture but a significant inhibition of further growth between days 3 and 9 ( $p < 0.05$ ).

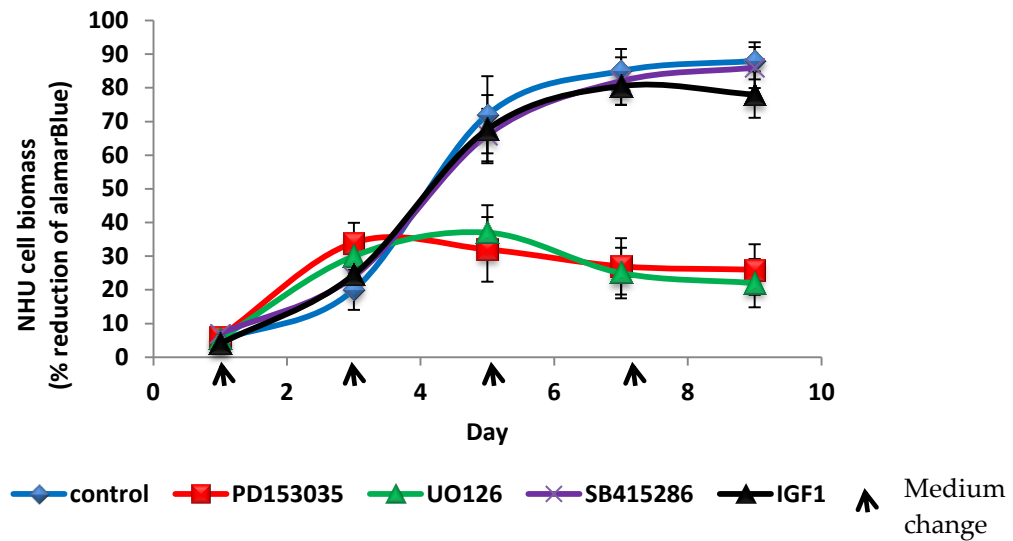


**Figure 4.2 – NHU cell growth was inhibited by EGFR/MAPK inhibition but GSK3 $\beta$  inhibition and PI3K/Akt activation had no effect on growth.** A cell biomass assay (Section 2.5.3.1) was conducted on NHU cells cultured in KSFMc medium  $\pm$  the agonists/inhibitors indicated. Cell culture medium was changed on the days indicated. Data points represent combined means  $\pm$ SD. (n=2, Y1430 & Y1437)

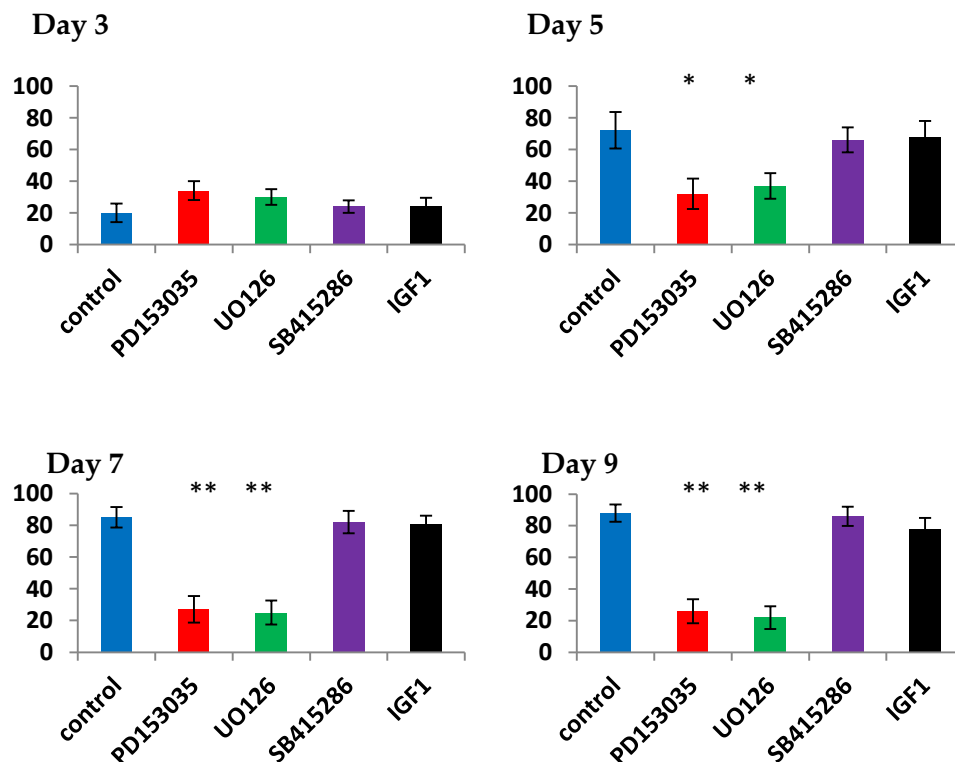


**Figure 4.3 - NHU cell growth was significantly inhibited by EGFR inhibition on Days 5, 7 and 9.** Statistical analysis was conducted on Growth curves presented in Figure 4.2 comparing treatment versus control (n=3; Y1430 & Y1437). An ANOVA test was conducted followed by a Tukey's post hoc test (\* =  $p < 0.05$ , \*\* =  $p < 0.01$ , \*\*\* =  $p < 0.001$ ; n=3).

#### 4.4.2 – Proliferation pathways

NHU cells were fixed (methanol: acetone) on day 5 of culture and immunofluorescence labelling used to investigate the expression of the proliferation marker Ki67 and marker of activation of the EGFR/MAPK pathway (phospho-ERK),  $\beta$ -catenin pathway (active  $\beta$ -catenin) and PI3K/Akt pathway (phospho-Akt). Initial labelling was conducted on proliferating NHU cells (Figure 4.4) and NHU cells differentiated using the published adult bovine serum (ABS)/ calcium protocol (Figure 4.5).

Proliferating NHU cells expressed the proliferation marker Ki67. The nuclear localisation of phospho-ERK and  $\beta$ -catenin in NHU cells suggested that proliferation in these cells was being regulated by the EGFR/MAPK and  $\beta$ -catenin pathways. The lack of phospho-Akt expression in proliferating NHU cells indicated that the PI3K/Akt pathway was not actively involved in regulating proliferation.

When induced to differentiate (Figure 4.5), NHU cells maintained Ki67 expression but active  $\beta$ -catenin can be seen to be sequestered to the cell membranes as well as being present in the nuclei. Phospho-ERK immunolabelling was almost completely absent in differentiated NHU cells but phospho-Akt immunolabelling was increased.

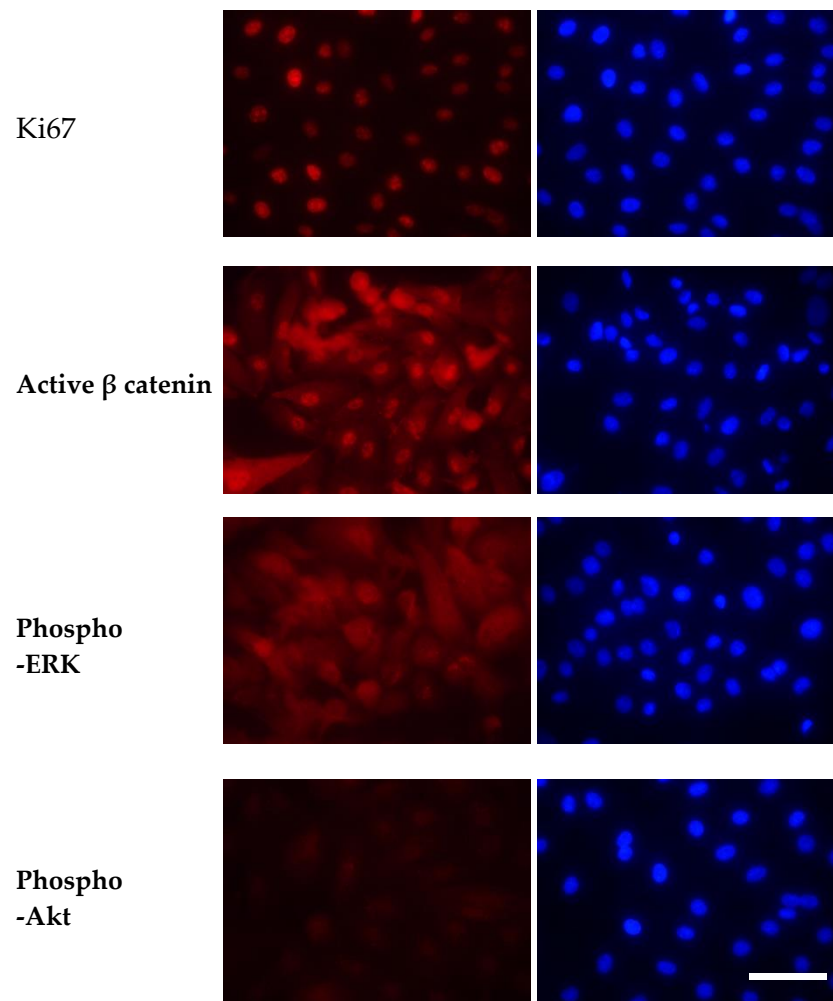


**Figure 4.4 – In undifferentiated NHU cells, Active $\beta$ -catenin and phospho-ERK expression is nuclear and phospho-Akt is not expressed.** Representative immunofluorescence labelling of Ki67, Active $\beta$ -catenin, phospho-ERK and phospho-Akt in NHU cells cultured in KSFMc (0.09mM Ca<sup>2+</sup>) medium. Scale bar = 50 $\mu$ m (n=2; Y1437, Y1461).

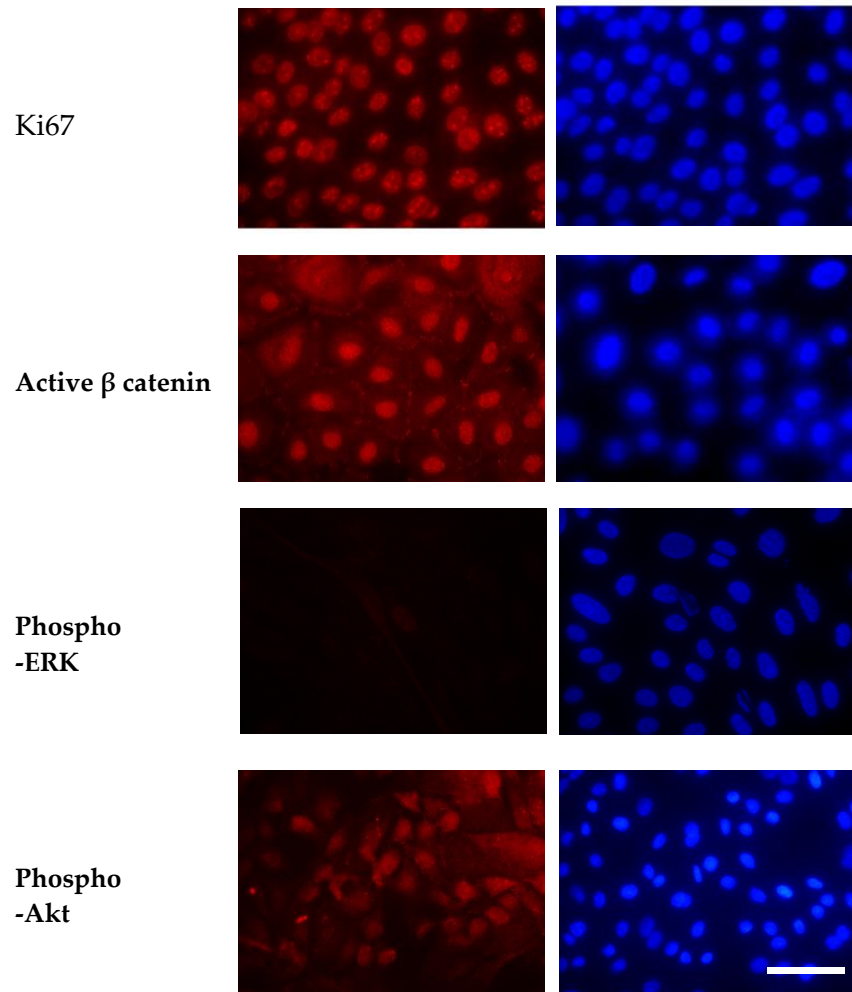


**Figure 4.5 – In differentiated (ABS/Ca<sup>2+</sup>), Active $\beta$ -catenin is both nucleus and membrane localise and a switch in phospho-ERK and Phospho-Akt expression has occurred compared to undifferentiated NHU cells (Figure 4.6). Representative immunofluorescence labelling of Ki67, Active $\beta$ -catenin, phospho-ERK and phospho-Akt in differentiated NHU cells cultured in KSFMc (2mM Ca<sup>2+</sup>) medium supplemented with 5% ABS. Scale bar = 50 $\mu$ m (n=2; Y1437, Y1461).**

#### 4.4.3 – Pharmacological interrogation of proliferation pathways

The effect of pharmacological interrogation of the EGFR/MAPK,  $\beta$ -catenin and PI3K/Akt pathways was investigated on the expression of Ki67, active nuclear  $\beta$ -catenin, phospho-Akt and phospho-ERK in proliferating NHU cells and the results quantified (Figure 4.6). When compared to controls, inhibition of EGFR (PD153035) significantly reduced Ki67 and the three proliferation pathway markers labelled for which agrees with the growth curve data (Figure 4.2). Inhibition of ERK in NHU cells (UO126) over 5 days significantly reduced the expression of phospho-Akt and phospho-ERK when compared against controls but did not have an effect on Ki67 or  $\beta$ -catenin expression.

Activation of the  $\beta$ -catenin pathway through GSK3 $\beta$  inhibition (SB415286) led to a significant increase in  $\beta$ -catenin and phospho-ERK expression in proliferating NHU cells and caused a significant reduction in nuclear phospho-Akt expression. Activation of the PI3K/Akt pathway (IGF1) caused a significant increase in phospho-Akt expression but caused a reduction in Ki67 expression.  $\beta$ -catenin and phospho-ERK were not significantly altered by treatment with IGF1.

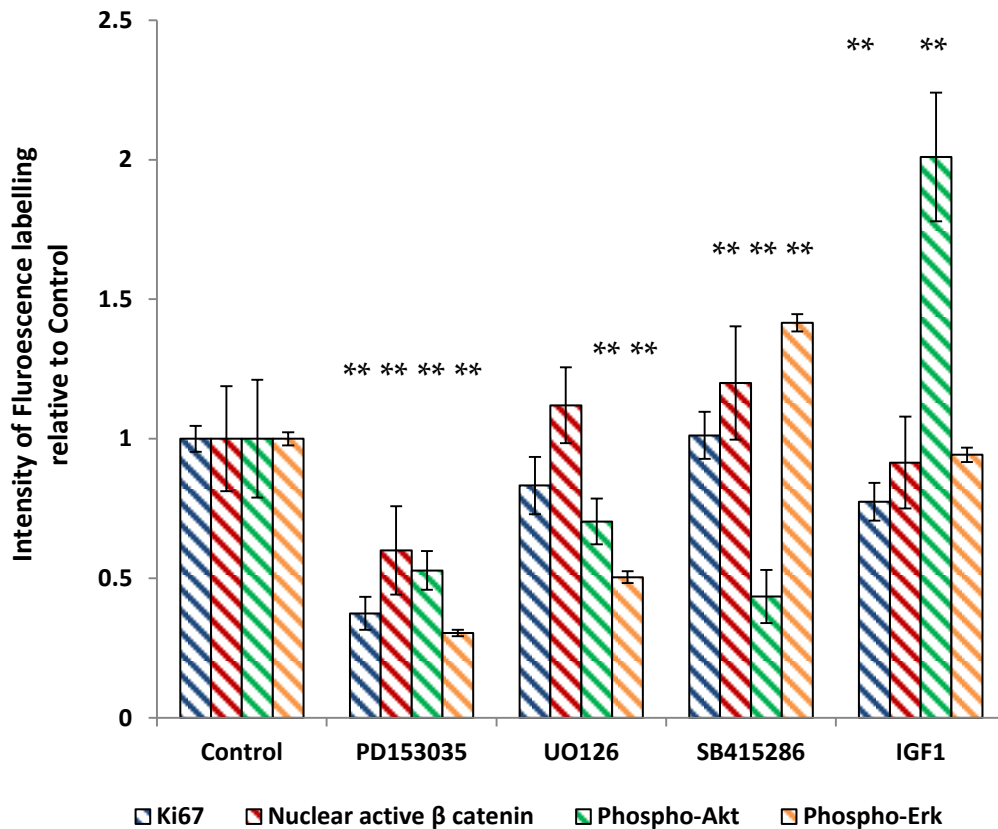


**Figure 4.6 – EGFR/MAPK inhibition significantly reduced expression of proliferation marker Ki67 and proliferation pathway markers Active  $\beta$ -catenin, phospho-ERK and phospho-Akt compared to control cells. Inhibition of GSK3 $\beta$  and activation of the PI3K/Akt pathway (IGF1) did not affect proliferation marker Ki67 expression.** Quantification of fluorescence intensity of Ki67, Nuclear active  $\beta$  catenin, phospho-Akt and phospho-ERK labelling in NHU cells cultured for 5 days in KSFMc medium (control) with the agonists/inhibitors indicated. (n=3 cell lines; Y1430, Y1437, Y1461). Error bars = SD. An ANOVA test was conducted with a Tukeys post hoc test (\*=p<0.05, \*\*=p<0.01, \*\*\*=p<0.1 compared to control)

#### 4.4.4 – Conclusions

Together these results show the specificity of these four pharmacological agents for their targets (Table 10) and show that blocking the active EGFR/MAPK pathway or activating the opposing PI3K/Akt pathway in NHU cells results in a decrease in cell proliferation as indicated by the expression of Ki67. They also demonstrate how increased  $\beta$ -catenin activation, which can be regulated by the MAPK pathway (Figure 4.1; Georgopoulos et al 2014), resulted in an increase in Ki67 expression in NHU cells.

## 4.5 Results – NRU cells

### 4.5.1 – Growth Kinetics

(Figure 4.7 & Figure 4.8)

#### **EGFR/MAPK inhibition**

Inhibition of EGFR or the downstream MAPK pathway molecule ERK by PD153035 and UO126 respectively had a minimal effect on cell growth over 5 days. Between days 5 and 9, inhibition of both targets resulted in a significant reduction in cell biomass when compared to control cells (KSFMc medium + 0.1% DMSO).

#### **GSK3 $\beta$ inhibition**

$\beta$ -catenin activation through GSK3 $\beta$  inhibition did not result in significant differences in NRU cell biomass over 9 days in culture but cell proliferation did appear to be slightly reduced when compared to controls.

#### **PI3K/Akt activation**

Over 9 days in culture, PI3K/Akt activation (IGF1) in NRU cells had no significant effect on cell growth ( $p > 0.05$ ).

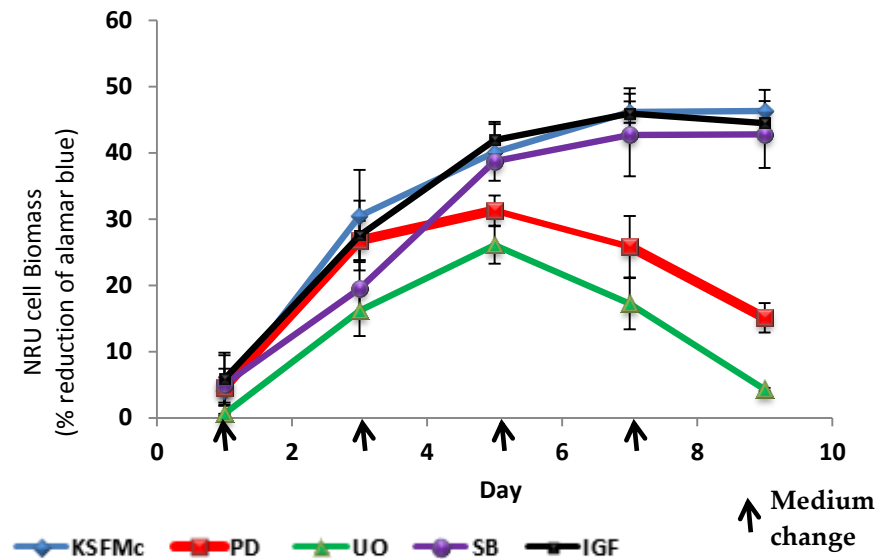


**Figure 4.7 – EGFR/MAPK inhibition reduced NRU cells growth over 9 days of culture.** Cell biomass assay (Section 2.5.3.1) for NRU cells cultured in KSFMc medium  $\pm$  the agonists/antagonists indicated. Cell culture medium was changed on the days indicated. Data points represent combined means  $\pm$ SD. (n=3; R037, R038, R039)

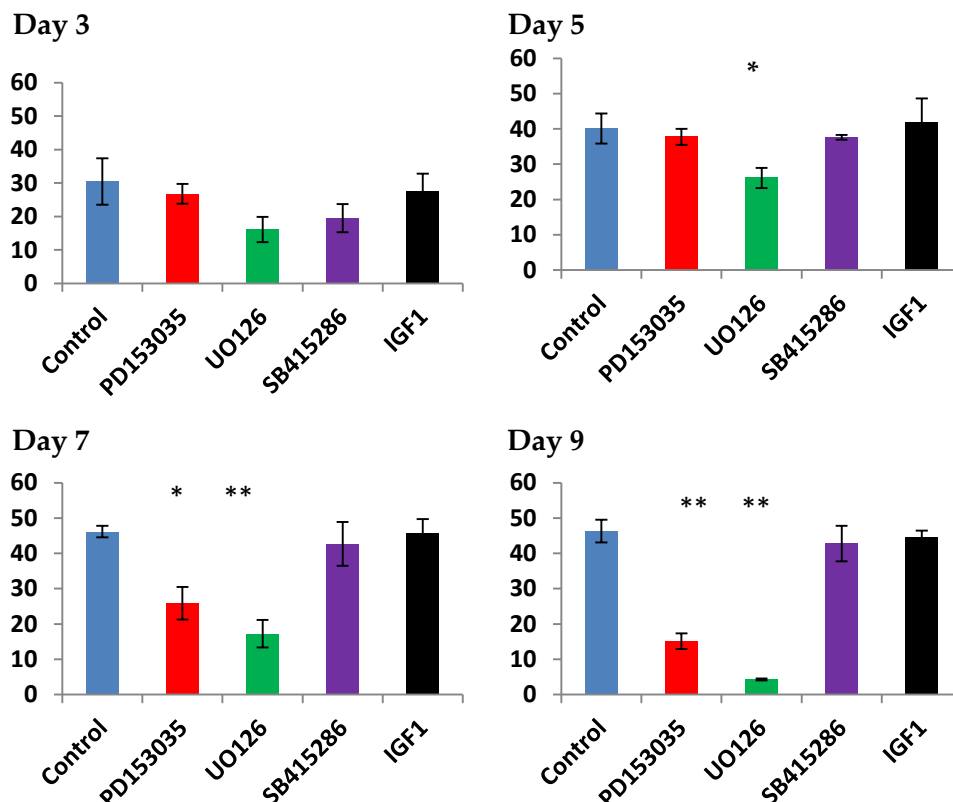


**Figure 4.8 – Quantification of NRU cell growth curves presented in Figure 4.7.** Results represent combined means  $\pm$ SD (n=3; R037, R038, R039). An ANOVA test was conducted with a Tukeys post hoc test (\*= $p < 0.05$ , \*\*= $p < 0.01$  compared to control).

### 4.5.2 –Ki67 expression

After 5 days of culture NRU cells were fixed and labelled for the proliferation marker Ki67 (Figure 4.9). Ki67 is expressed by all proliferating cells but is absent when cells become senescent or quiescent.

Ki67 labelling was positive in three separate primary NRU cell lines and the intensity of labelling quantified (Figure 4.13) In comparison to control NRU cells, EGFR inhibition caused both a visible reduction in Ki67 expression and a significant decrease in labelling intensity in all three cell lines. ERK inhibition did not have an effect on Ki67 expression in NRU cells. Activation of  $\beta$ -catenin, through GSK3 $\beta$  inhibition, had no significant effect on Ki67 expression or intensity but activation of the PI3K/Akt pathway resulted in a significant increase in Ki67 labelling intensities compared to control NRU cells ( $p < 0.01$ ).

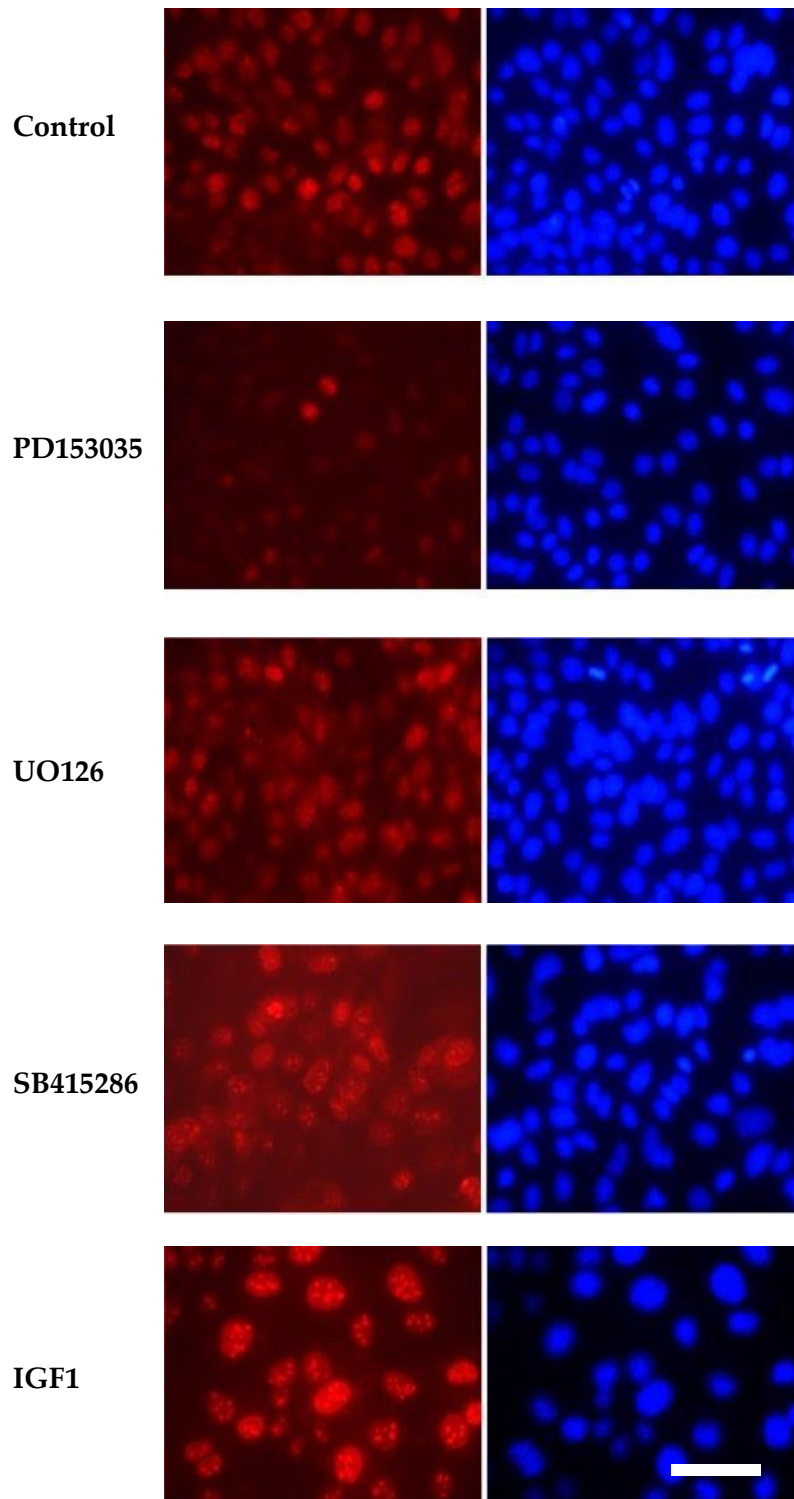
### 4.5.3 – Phospho-ERK, $\beta$ -catenin and phospho-Akt expression

Phospho-ERK expression was used as a measure of EGFR/MAPK activity in NRU cells (Figure 4.10). In control NRU cells and EGFR, ERK and GSK3 $\beta$  inhibited cells Phospho-ERK immunoreactivity was minimal to none. PI3K/Akt activation resulted in a small increase in nuclear phospho-ERK immunoreactivity. These results were too small to quantify but appear to show a lack of EGFR/MAPK activation in proliferating NRU cells.

Labelling of active  $\beta$ -catenin (Figure 4.11) revealed nuclear localisation in control and EGFR/ERK inhibited cells. GSK3 $\beta$  inhibition also resulted in perinuclear localisation of active  $\beta$  catenin but did not produce an increase in nuclear expression when compared against control cells. PI3K/Akt activation resulted in sequestering of  $\beta$ -catenin at the cell membrane, possibly indicating adherens junction formation, and a significant reduction in nuclear  $\beta$ -catenin labelling intensity in two out of three cell lines (Figure 4.13).

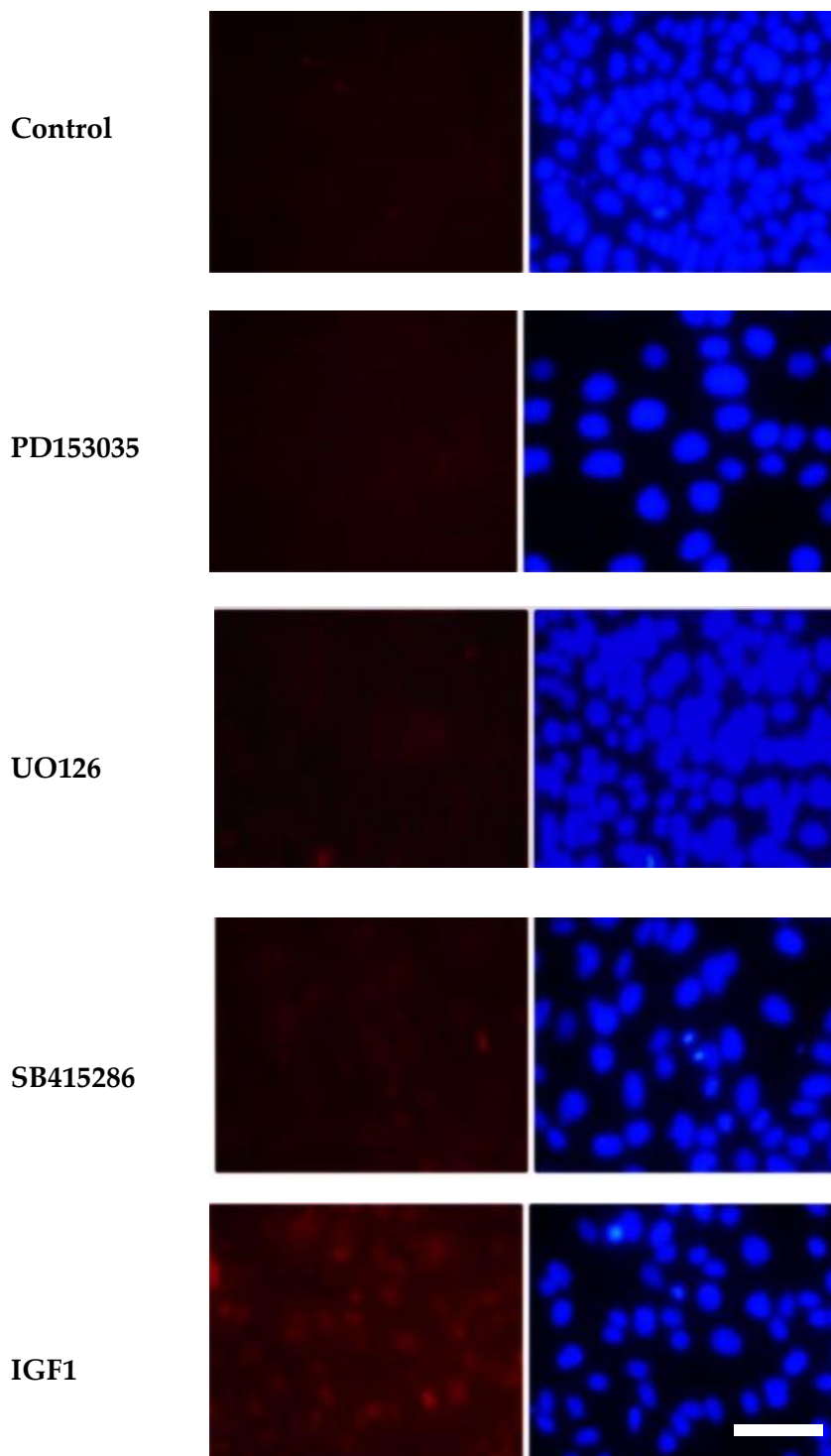
Phospho-Akt was labelled as a marker of PI3K/Akt pathway activation (Figure 4.12). Images are difficult to compare due to expression being both nuclear and cytoplasmic however when nuclear labelling intensity was quantified (Figure 4.13), all treatments significantly increased phospho-Akt expression compared against control cells. After PI3K/Akt activation (IGF1), phospho-Akt appears to be specifically localised to the nuclear membrane where as in control, EGFR/MAPK and GSK3 $\beta$  inhibited cells phospho-Akt is present throughout both cell nuclei and cytoplasm.

## Ki67

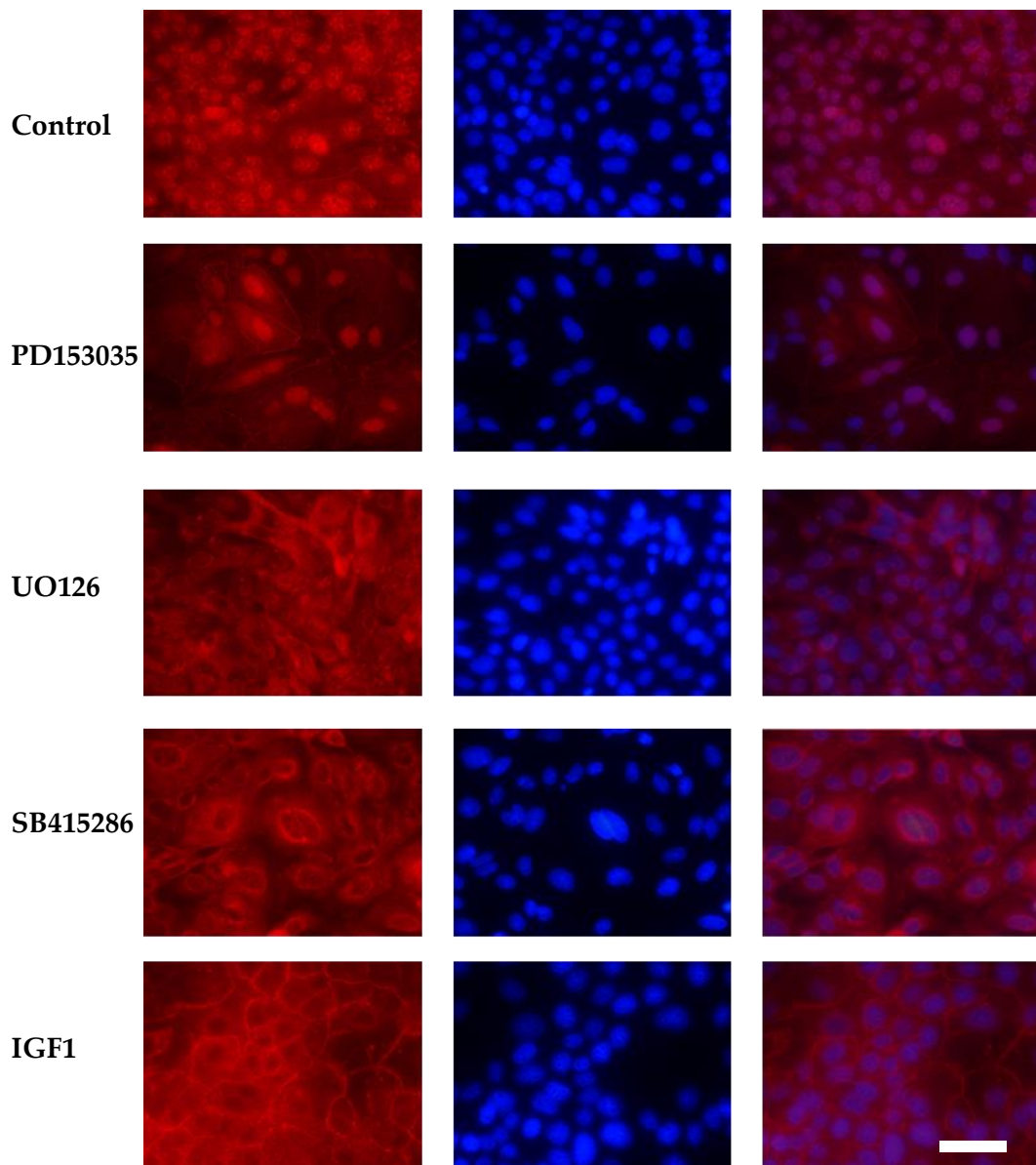


**Figure 4.9 – Ki67 expression appears increased in NRU cells after 5 days of PI3K/Akt expression.** Representative images of Ki67 labelling in NRU cells cultured for 5 days in KSFMc with the agonists/antagonists indicated (n=3; R040, R041, R042). Scale bar = 50 μm.

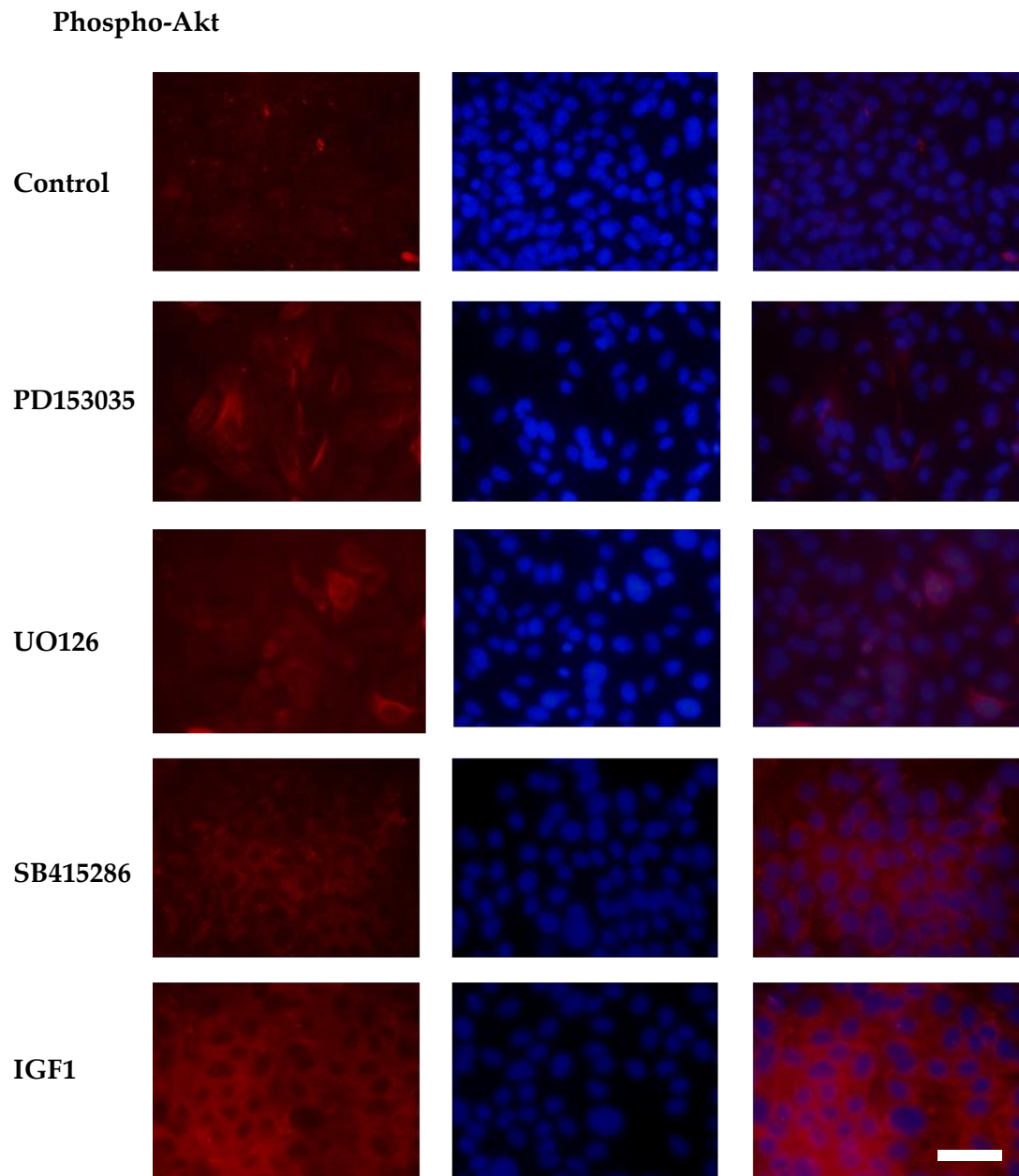
## Phospho-ERK



**Figure 4.10 – Phospho-ERK was not expressed in control, EGFR/MAPK inhibited,  $\beta$ -catenin pathway activated or PI3K/Akt pathway activated NRU cells.** Representative images of Phospho-ERK labelling in NRU cells cultured for 5 days in KSFMc with the agonists/antagonists indicated (n=3; R040, R041, R042). Scale bar = 50 $\mu$ m

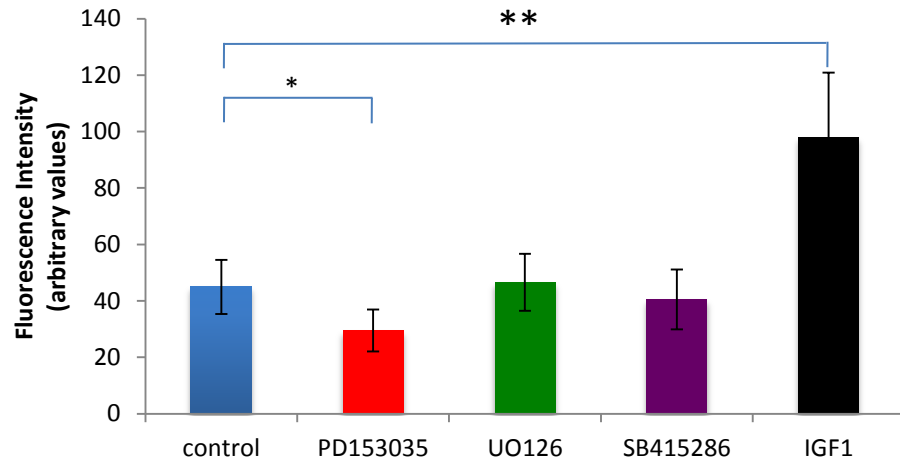
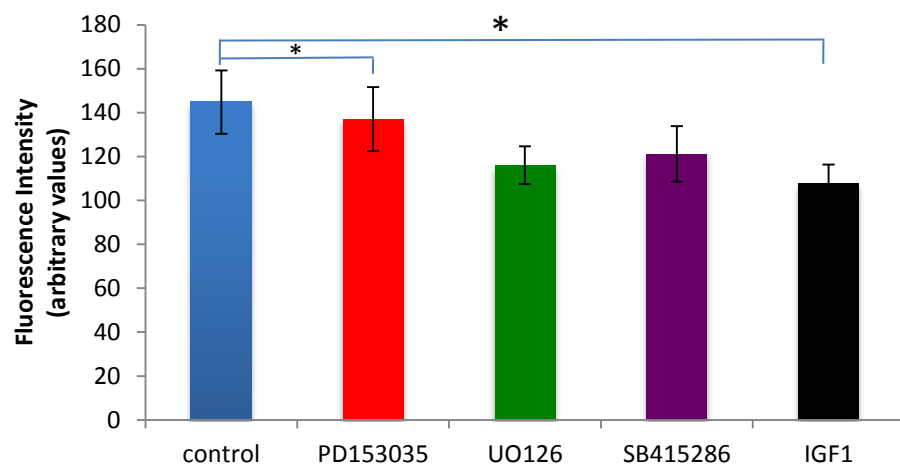
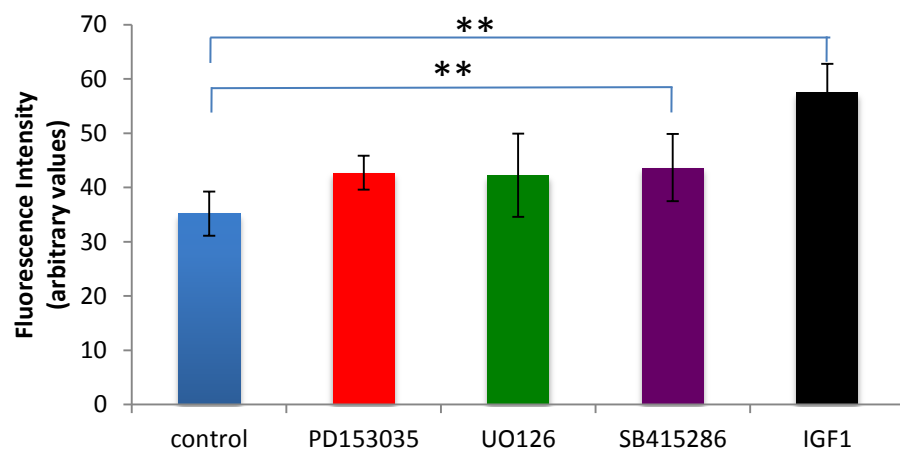
Active  $\beta$  catenin

**Figure 4.11 - Active  $\beta$ -catenin labelling was clearly nuclear in control and MAPK inhibited cells, nuclear/perinuclear in GSK3 $\beta$ -inhibited cells and clearly membrane-localised in PI3K/Akt pathway activated NRU cells. Cells were cultured for 5 days in KSFMc with the agonists/antagonists indicated (n=3; R040, R041, R042). Scale bar = 50 $\mu$ m.**



**Figure 4.12 – Phospho-Akt expression was present in control and in proliferation pathway activated/inhibited NRU cells.** Representative images of phospho-Akt (S47333) labelling in NRU cells cultured for 5 days in KSFMc with the agonists/antagonists indicated (n=3; R040, R041, R042). Scale bar = 50µm.

## Ki67

Active  
β-cateninPhospho-  
Akt

**Figure 4.13 – Ki67 and phospho-Akt expression were significantly increased by IGF1 stimulation but Ki67 was reduced by EGFR/MAPK inhibition.** Mean fluorescence intensity of Ki67, Active β-catenin and phospho-Akt labelling (arbitrary values) for three separate NRU cell lines. Results represent combined means from three separate cell lines ±SD. Quantification was conducted using TissueGnostics TissueQuest software (Section 2.7.3). (\*\*=p<0.01, using a 2-way ANOVA test with a Tukeys post hoc test of comparison).

#### 4.5.4 – Removal of exogenous EGF

Growth assays (Figure 4.14) revealed that the presence of exogenous EGF in the KSFMc medium had no significant effect on the growth of two separate NRU cell lines over 9 days in culture. Cells cultured with and without exogenous EGF showed the same traits in growth, plateauing (reaching confluence) at the same time. The high level of consistency in these data suggests that exogenous EGF is not required for NRU cell growth *in vitro*. The experiment was only conducted in two cell lines, each consisting of cells from several (4-5 individual) animals.

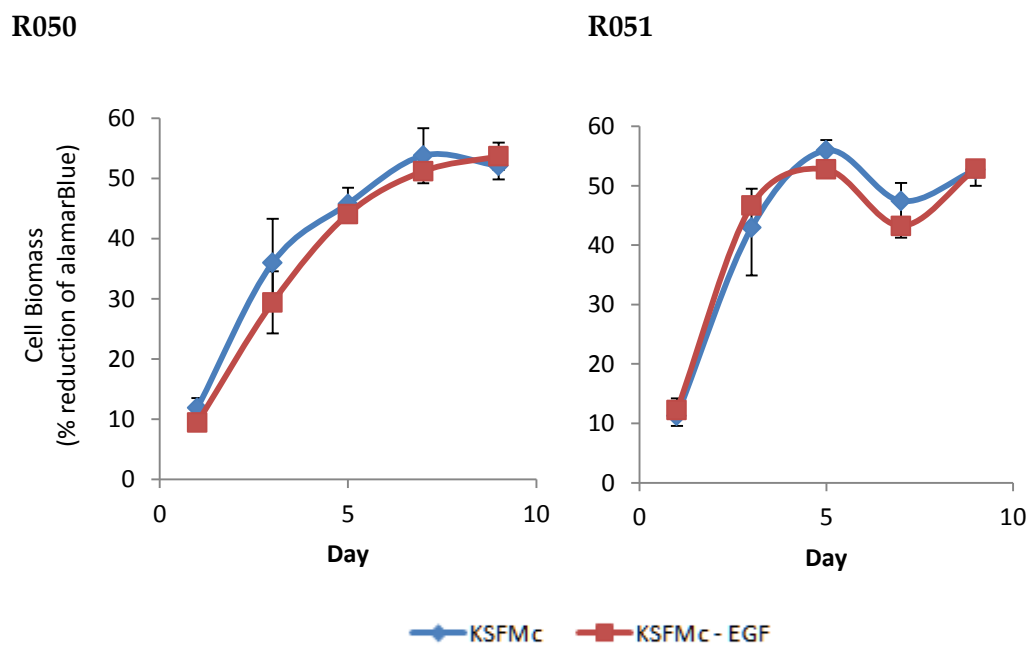


**Figure 4.14 – Removal of EGF had no effect on NRU cells growth in two cell lines (R050 & R051).** NRU cell biomass assays (Section 2.5.3.1) for two NRU cell lines (R050 and R051) cultured in KSFMc medium and KSFMc medium without exogenous EGF. Cell culture medium was changed on days 1, 3, 5 and 7. Data points represent experimental means  $\pm$ SD.

#### 4.5.5 – PI3K/Akt pathway inhibition

The PI3K/Akt pathway was inhibited by itself and in combination with activation of the  $\beta$ -catenin pathway through GSK3 $\beta$  inhibition. PI3K inhibition with and without activation of the  $\beta$ -catenin pathway enabled NRU cells to survive in culture up to passage 2 (Figure 4.15) as opposed to becoming senescent after a single passage (Results chapter 1 – NRU cell optimisation chapter). PI3K inhibition alone did not affect the expression of the proliferation marker Ki67 in NRU cells but in combination with  $\beta$ -catenin activation, Ki67 expression was visibly increased (Figure 4.16).

Active  $\beta$ -catenin was not affected by PI3K inhibition in NRU cells but was increased by GSK3 $\beta$  inhibition. Localisation of active  $\beta$  catenin after combined PI3K and GSK3 $\beta$  inhibition was predominantly nuclear in NRU cells. Use of the PI3K inhibitor LY294002 completely inhibited NRU expression of phospho-Akt.

Inhibition of PI3K with and  $\beta$  –catenin activation did not have an effect on the expression of the tight junction proteins claudin 4 and ZO-1 in NRU cells (Figure 4.17 & Figure 4.18). Quantification of expression showed no significant difference in claudin 4 or ZO-1 between control and treated NRU cells. In control samples the distinct membrane localisation of claudin 4 and ZO-1 is clearly visible however in PI3K inhibited cells this localisation is difficult to see. This could indicate that PI3K-inhibited cells were not forming cell-cell junctions.

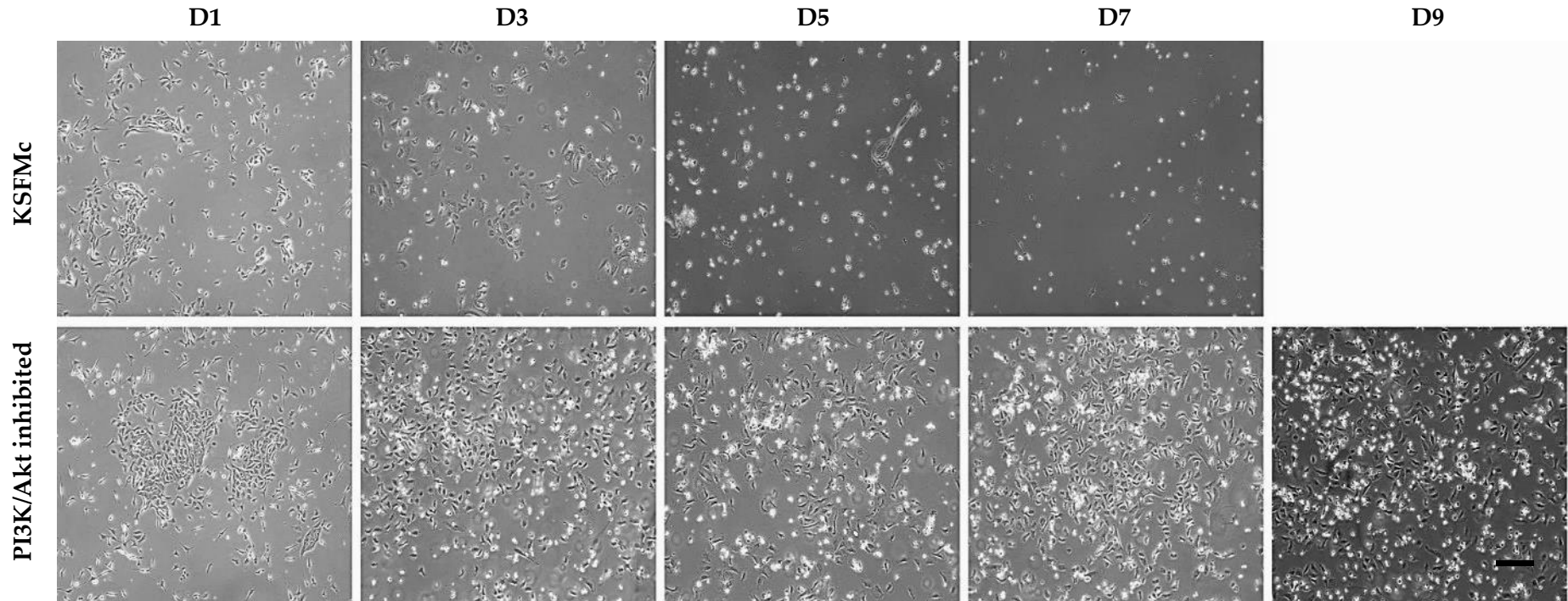


**Figure 4.15 – NRU cells grew being passaged twice when the PI3K/Akt pathway was inhibited whereas NRU cells cultured in KSFMc alone died after passage. 2** Phase contrast images showing NRU cells after passage 2 having been cultured in KSFMc alone or in the presence of the PI3K/Akt inhibitor LY294002. Cells were monitored over 9 days in culture (n=3; R048, R052, R055) Scale bar = 50 $\mu$ m.

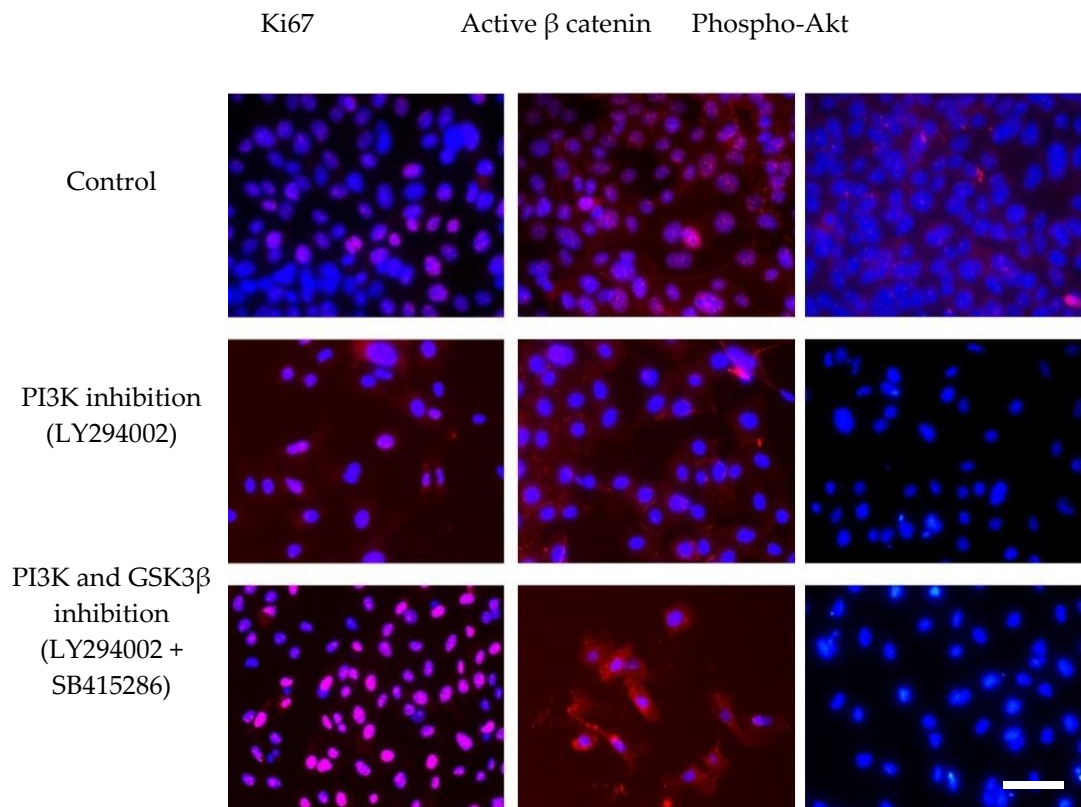


**Figure 4.16 – Phospho-Akt was inhibited in NRU cells by the PI3K/Akt inhibitor LY294002.** Representative Immunofluorescence labelling of Ki67, active  $\beta$  catenin and phospho-Akt (red) in NRU and NHU cells cultured in KSFMc with DMSO (0.01%), LY294002 or LY294002 + SB415286. Nuclei were labelled with Hoechst 33248 (blue). (n=2; R048 & R055). Scale bar = 50 $\mu$ m.

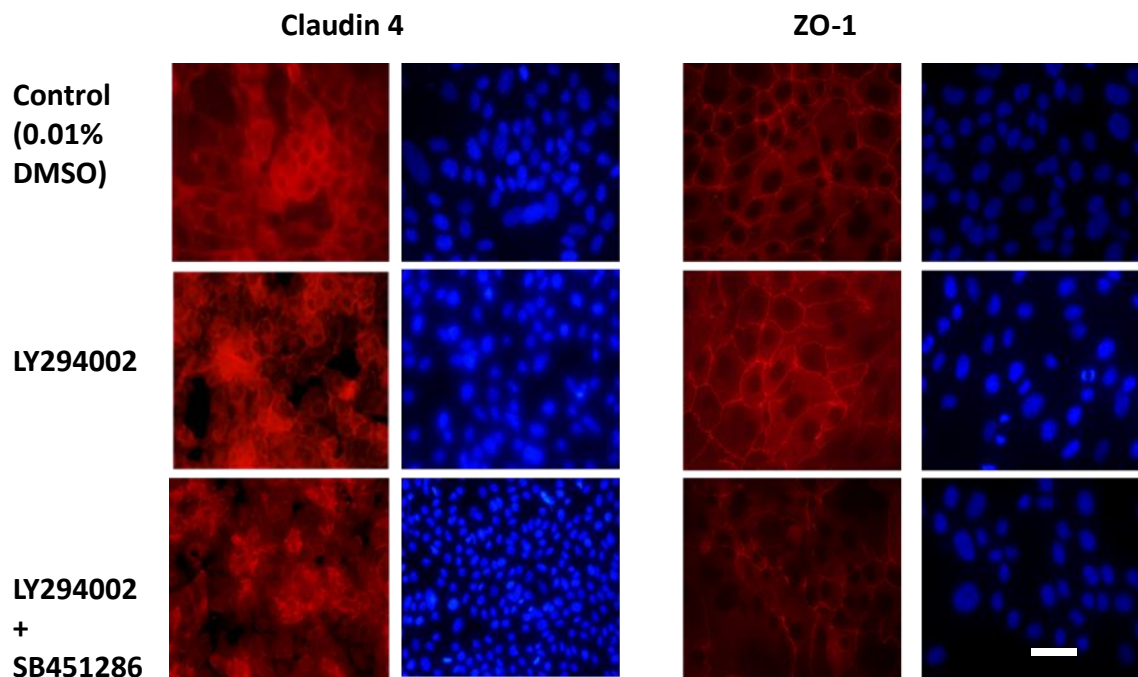


**Figure 4.17– Differentiation-associated markers ZO-1 and Claudin 4 were expressed in control and PI3K/Akt inhibited NRU cells.** Representative immunofluorescence labelling of Claudin 4 and ZO-1 in NRU cells after 5 days of treatment with LY294002 and LY294002 + SB415286. Nuclei were labelled with Hoechst 33258 (blue). (n=2; R048 & R055). Scale bar = 50 $\mu$ m.

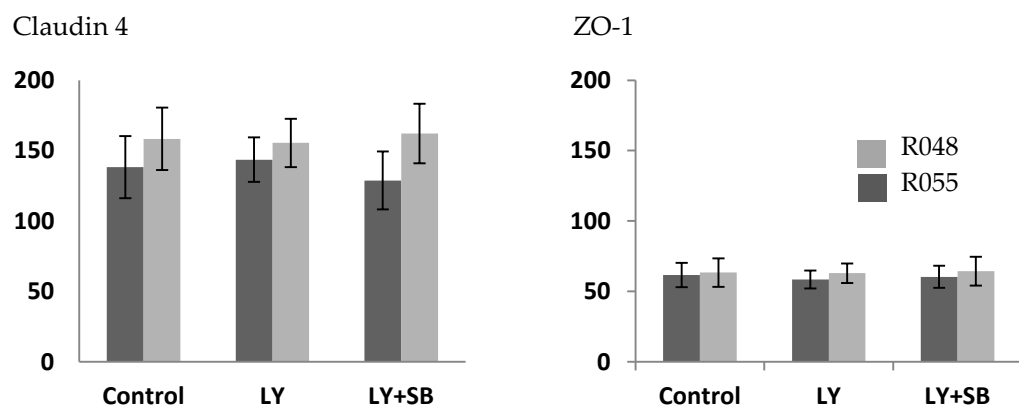


**Figure 4.18 – No difference was seen in the expression of differentiation-associated markers ZO-1 and Claudin 4 in control and PI3K/Akt inhibited NRU cells.** Mean fluorescence intensity of Claudin 4 and ZO-1 labelling (arbitrary values) for two separate NRU cell lines after treatment with LY294002 with and without SB415286. Results represent mean values  $\pm$ SD.

#### 4.5.6 – Physiological (2mM) extracellular calcium

When compared to results conducted in low calcium (0.09mM; Figure 4.21 & Figure 4.22), NRU cell biomass was reduced compared to controls on days 3, 7 and 9. The agonists/inhibitors used all had negative effects on cell biomass in 2mM Ca<sup>2+</sup> however only EGFR and ERK inhibition (PD153035 and UO126) caused a significant reduction when compared to the controls. NRU cells cultured in 2mM Ca<sup>2+</sup> had a reduction in biomass after 5 days in culture, varying from NRU cells cultured in 0.09mM Ca<sup>2+</sup> which plateaued after day 7.

The tight junction proteins ZO-1 and claudin 4 and the differentiation-associated markers uroplakin 3a (late) and aquaporin 4 (early) were labelled for in control NRU cells cultured in low (0.09mM) and physiological (2mM) calcium (Figure 4.23 & Figure 4.24). ZO-1 and claudin 4 expression was not altered by extracellular calcium concentration. UP3a expression was slightly increased in 2mM calcium compared to 0.09mM but the early differentiation-associated marker aquaporin 3 expression did not differ between calcium concentrations.

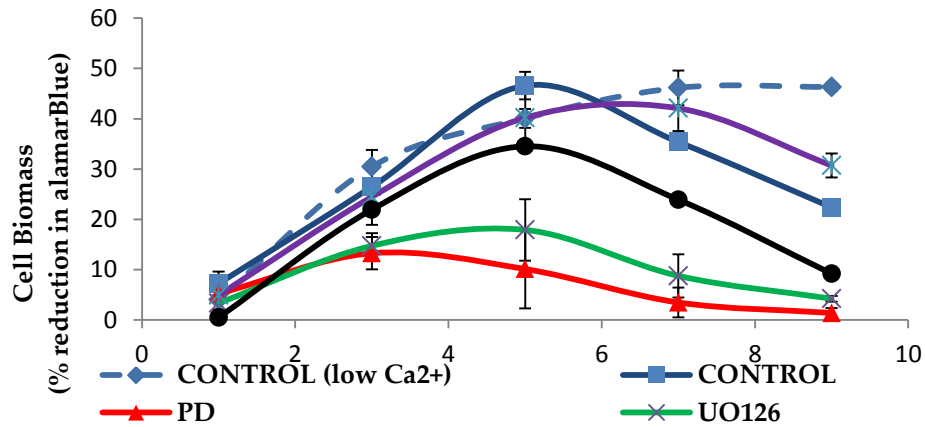


**Figure 4.19** – NRU cells cultured in high extracellular calcium (2 mM) showed the same growth kinetics as those seen in low (0.09 mM  $\text{Ca}^{2+}$ ) up to 5 days in culture. NRU cell biomass assay (Section 2.5.3.1) for cells cultured in KSFMc medium (2mM  $\text{Ca}^{2+}$ )  $\pm$  the agonists/antagonists indicated. Cell culture medium was changed on the days indicated. Data points represent combined means  $\pm$ SD (n=3; R046, R047, R049).

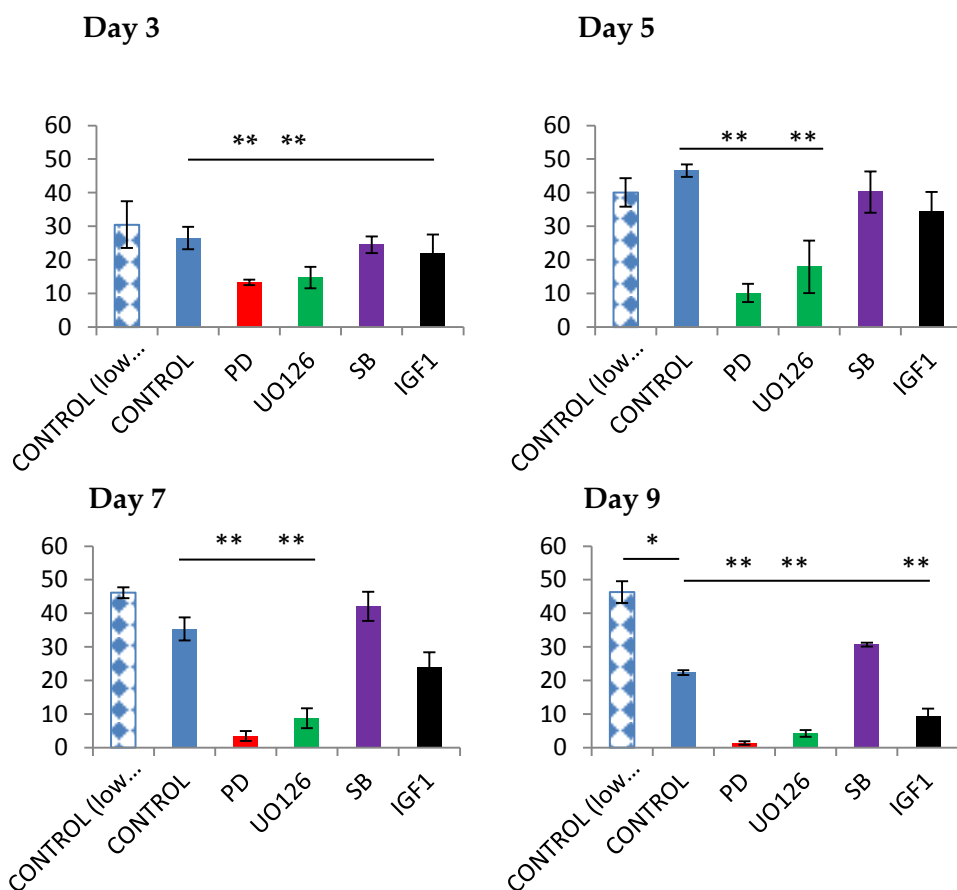


**Figure 4.20** – EGFR/MAPK inhibitors significantly reduced NRU cell growth over 9 days of culture whereas all cells cultured in KSFMc (2 mM  $\text{Ca}^{2+}$ ) had reduced growth at day 9 compared to cells cultured in KSFMc medium (0.09 mM  $\text{Ca}^{2+}$ ). Results represent combined means  $\pm$ SD (n=3; R046, R047, R049). (\*= $p < 0.05$ , \*\*= $p < 0.01$  using a 2-way ANOVA with a Tukeys post hoc test of comparison).

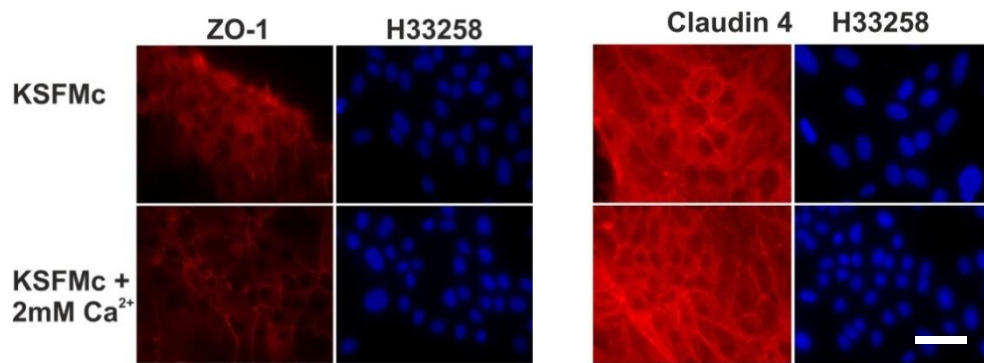


**Figure 4.21 – ZO-1 and Claudin 4 were both expressed in NRU cells cultured in KSFMc medium with 0.09 mM and 2 mM extracellular calcium ion concentrations.** Representative immunofluorescence labelling of ZO-1, and claudin 4 in NRU (P0) cells. Cells were cultured for 5 days in low and physiological (2mM) calcium concentrations before being fixed and labelled. Cell nuclei were labelled with Hoechst 33258 (n=3; R046, R047, R049). Scale bar = 50 $\mu$ m.

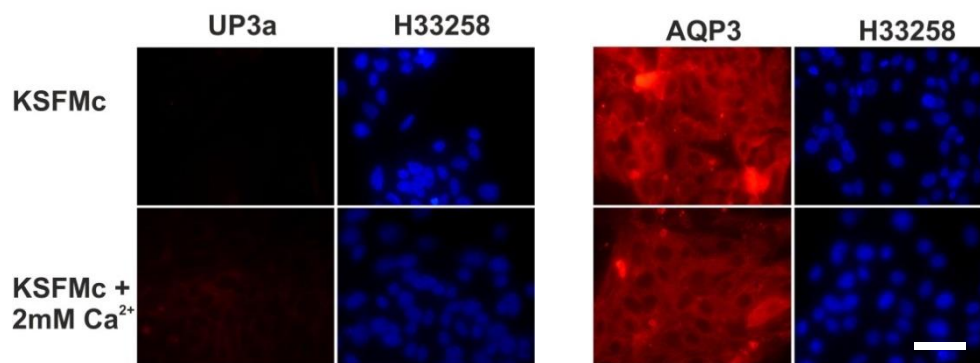


**Figure 4.22 – Uuroplaskin 3a (UP3a) was not expressed by NRU cells but aquaporin 3 (AQP3) was expressed by NRU cells cultured in 0.09 and 2 mM calcium ion concentrations. No visible difference was visible in AQP3 expression between cells cultured in different calcium ion concentrations.** Representative immunofluorescence labelling of the differentiation-associated markers uroplakin 3a (UP3a), and aquaporin 3 (AQP3) in NRU (P0) cells. Cells were cultured for 5 days in low and physiological (2mM) calcium concentrations before being fixed and labelled. Cell nuclei were labelled with Hoechst 33258 (n=3; R046, R047, R049). Scale bar = 50 $\mu$ m.

#### 4.5.7 – Reduced extracellular calcium

Phase contrast imaging revealed that cells cultured in 0.06mM  $\text{Ca}^{2+}$  did not cluster into densely packed colonies, as was the case in 0.09mM (Figure 4.23). Cells cultured in the two lowest calcium ion concentrations also grew in less densely populated colonies however fewer cells were present.

A cell biomass assay (Figure 4.24 and Figure 4.25) was conducted to assess the effect of reduced calcium on NRU cell proliferation. A reduction in  $\text{Ca}^{2+}$  from 0.09mM to 0.06mM had no significant effect on NRU cell proliferation over 9 days in culture. Further reducing extracellular calcium to 0.03 and 0.015mM caused a decrease in cell biomass after 5 days of culture and a significant reduction by day 7. Cell biomass in all concentrations decreased between 7 and 9 days of culture, possibly as a result of cells becoming over-confluent.

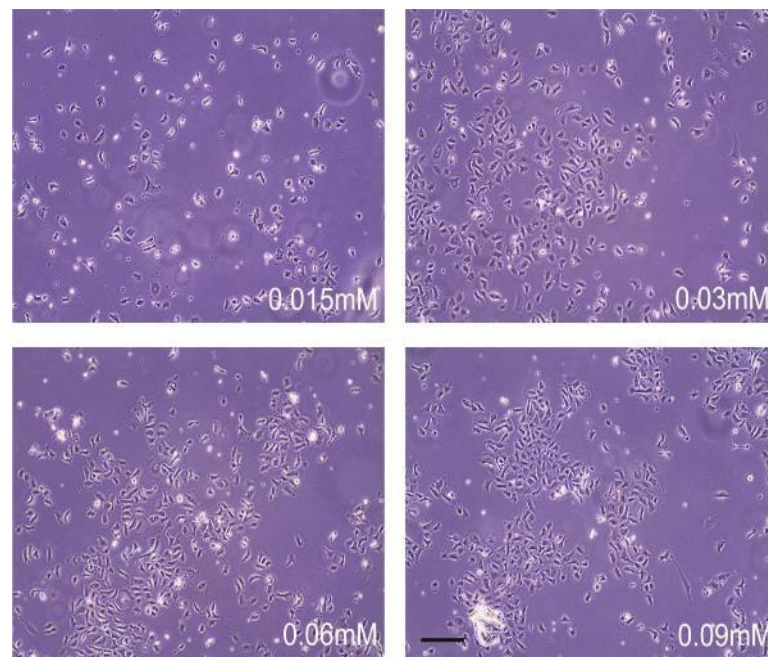


**Figure 4.23 – NRU cell density was visibly reduced at 0.015 mM calcium ion concentrations compared to cells cultured on 0.09 mM  $\text{Ca}^{2+}$ .** Phase contrast images of NRU cells cultured in KSFMc medium containing 0.09, 0.06, 0.03 and 0.015mM calcium as indicated on day 5 of culture. Scale bar = 50 $\mu\text{m}$ .

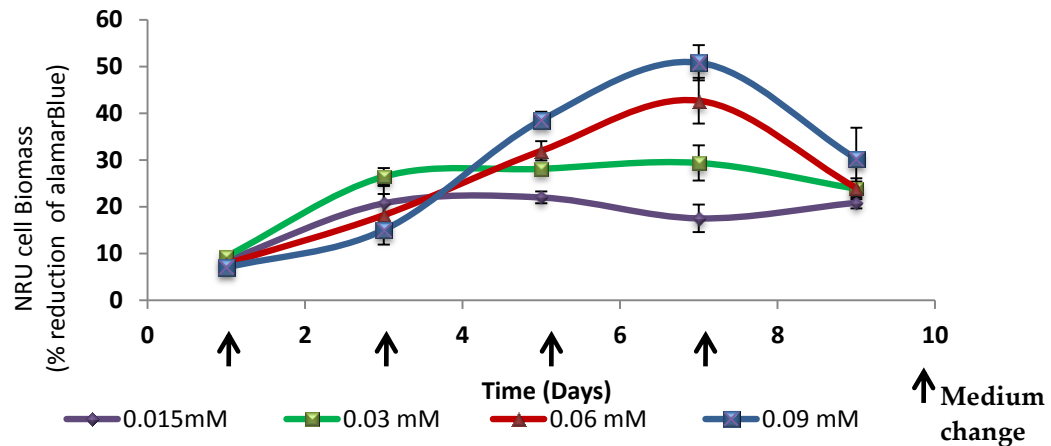


**Figure 4.24 - Extracellular calcium ion concentrations of 0.015 and 0.03 mM reduced NRU cell growth in culture.** NRU cell growth assay (Section 2.5.3.1) in KSFMc medium containing 0.09, 0.06, 0.03 and 0.015mM calcium as indicated. Growth curves were measured using the alamarBlue assay. Data points represent combined means  $\pm$ SD, (n=3; R052, R055, R056).

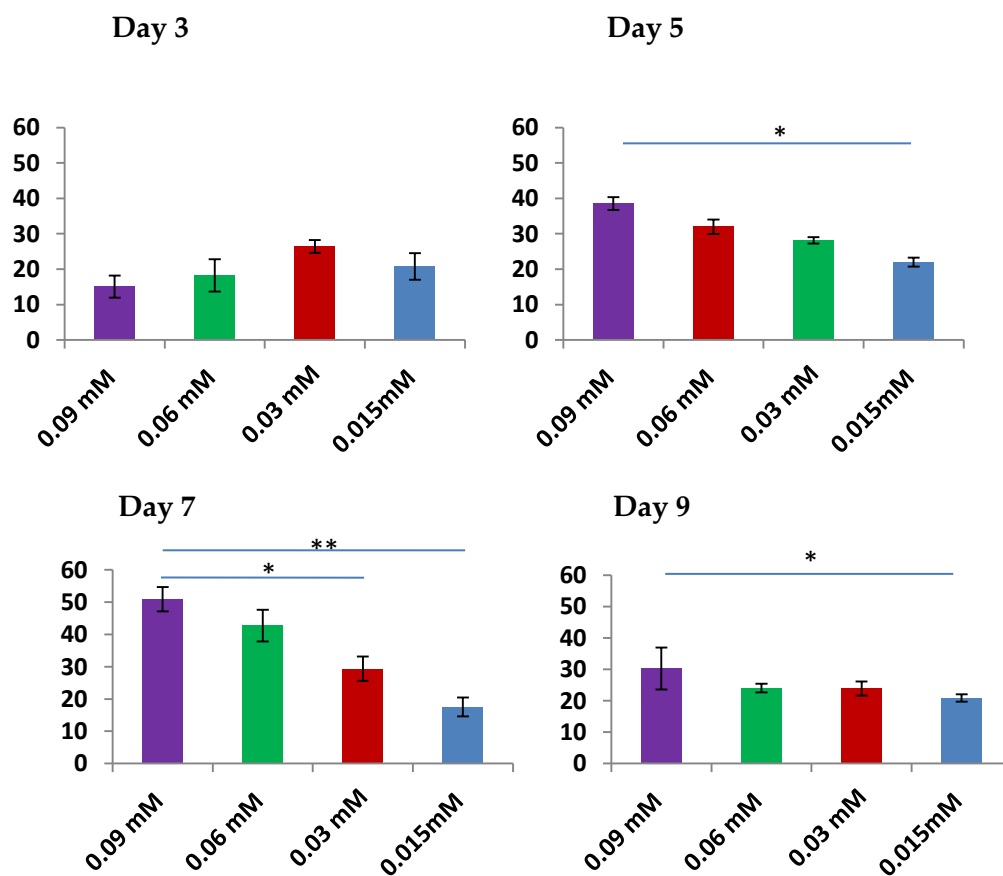


**Figure 4.25 – Extracellular calcium ion concentrations of 0.015 and 0.03 mM significantly reduced NRU cell growth after 5 and 7 days of culture, respectively.** Growth curves (Section 2.5.3.1) of NRU cells cultured KSFMc containing 0.015, 0.03, 0.06 and 0.09mM  $\text{Ca}^{2+}$  ions. Results represent combined means  $\pm$ SD, (n=3; R052, R055, R056). (\*= $p < 0.05$ , \*\*= $p < 0.01$ , using a 2-way ANOVA with a Tukeys post hoc test of comparison).

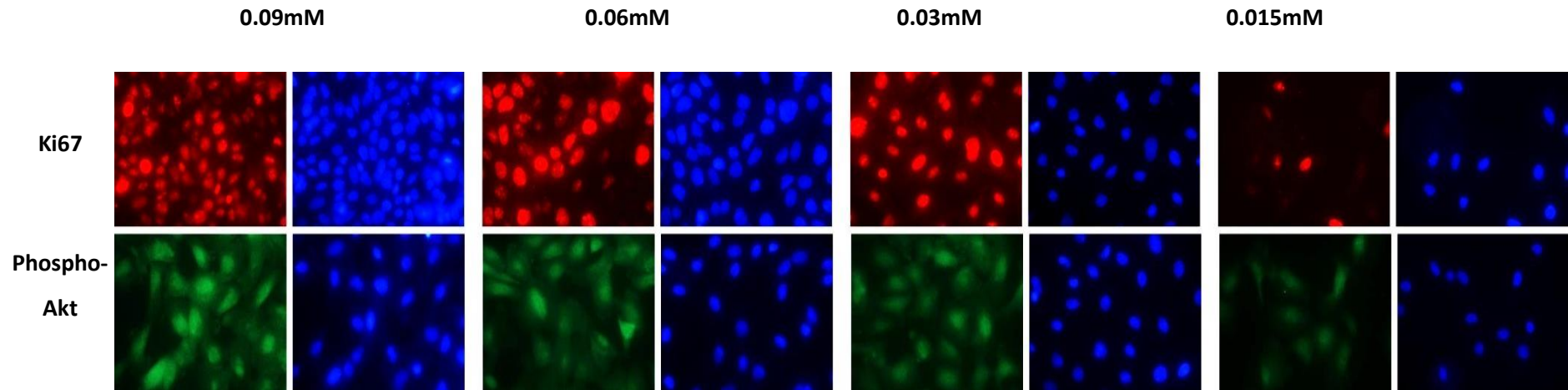


**Figure 4.26** – Phospho-Akt expression appeared to decrease when the extracellular calcium concentration was decreased however the Ki67 expression was unaffected at calcium concentrations of 0.06 and 0.03 mM. Representative immunofluorescence images of Ki67 and phospho-Akt labelling in NRU cells cultured in 0.09, 0.06, 0.03 and 0.015mM Ca<sup>2+</sup> KSFMc for 5 days (n=2; R055, R056). Scale bar = 50µm.

Immunofluorescence labelling of the proliferation marker Ki67 revealed no difference in the expression between control (0.09mM) cells and cells cultured in 0.06 or 0.03mM Ca<sup>2+</sup> (Figure 4.28). A reduction in extracellular calcium to 0.015mM caused a visibly significant reduction in Ki67 expression. Nuclear phospho-Akt expression, which is present in NRU cells culture in all 4 Ca<sup>2+</sup> concentration, was also reduced by the reduction in extracellular calcium.

## 4.6 Results summary

### NRU cell proliferation

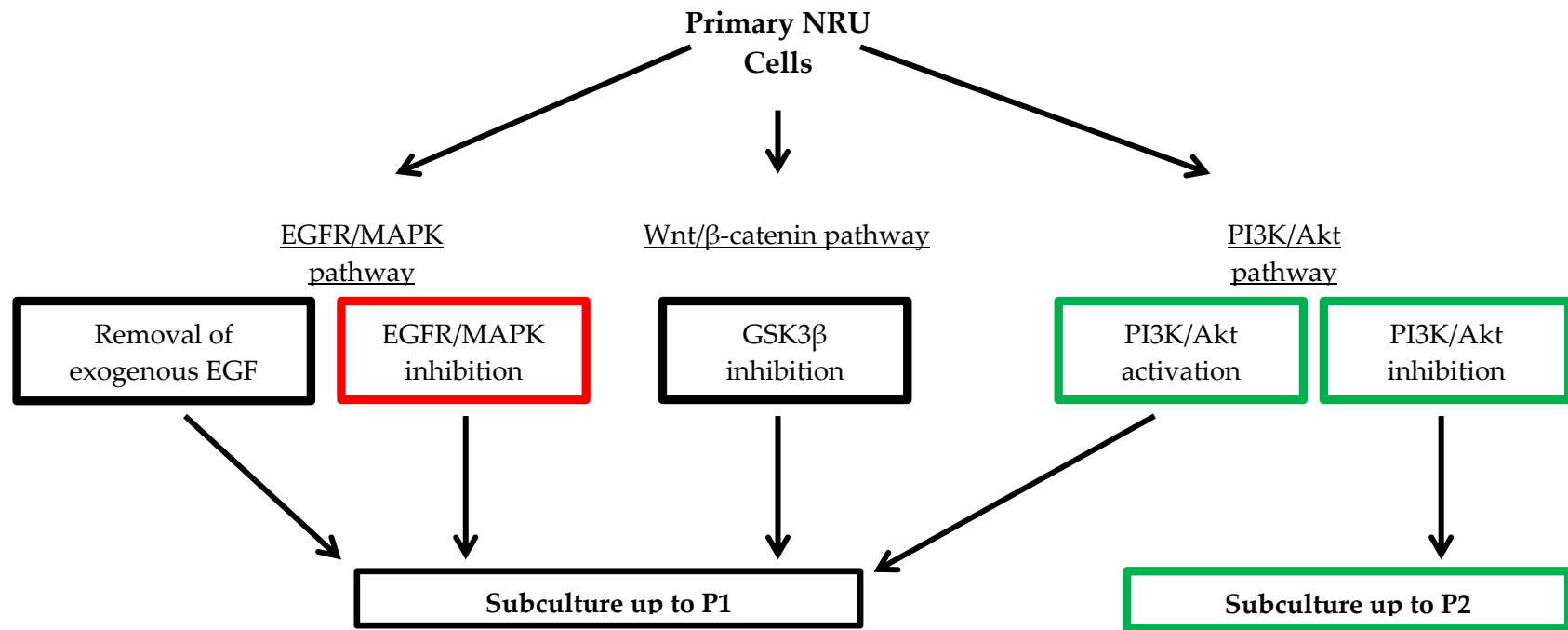
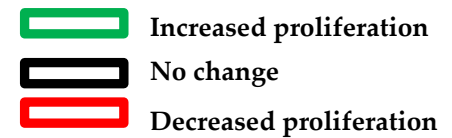


Figure 4.27– Summary of the effects on activating/inhibiting the EGFR/MAPK, PI3K/Akt and  $\beta$ -catenin pathways in NRU cells.



Extracellular calcium

The effect of extracellular calcium ion concentration

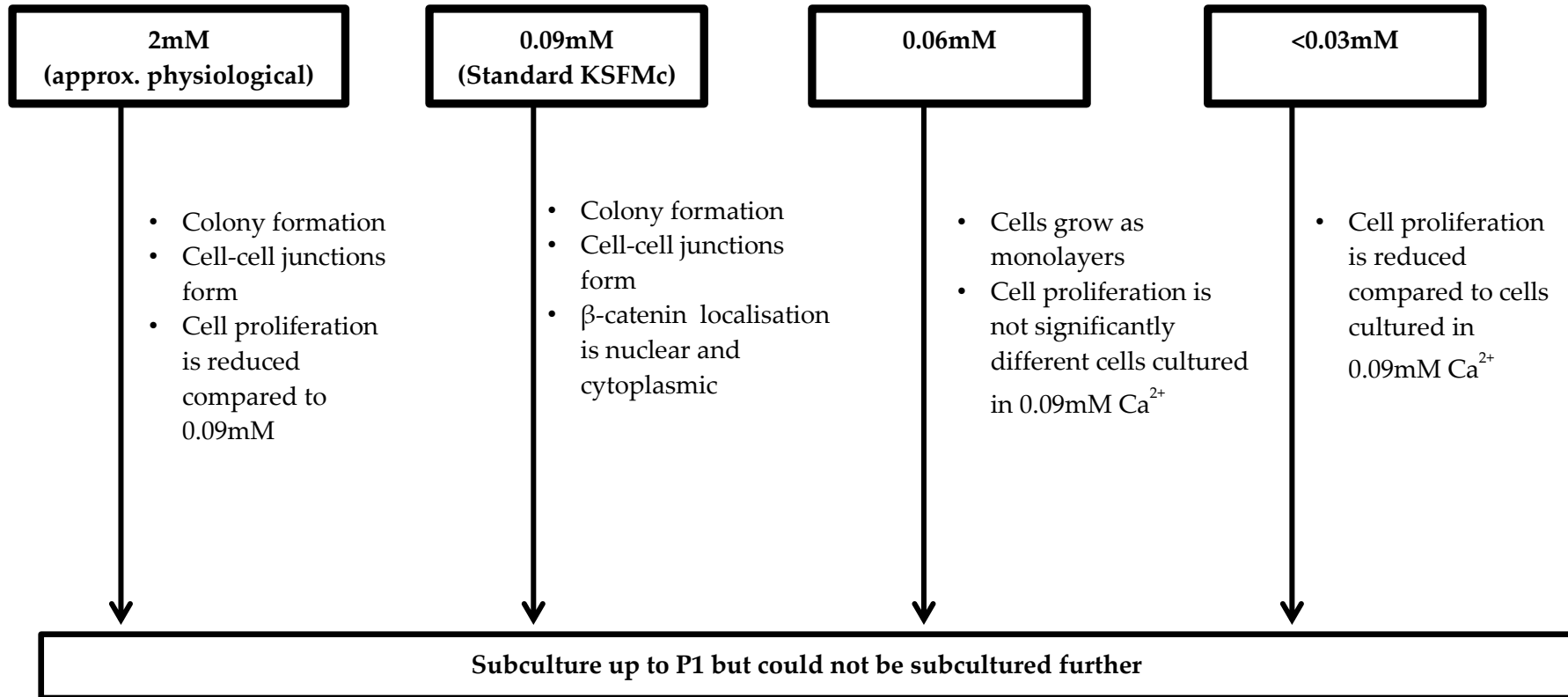


Figure 4.28 – Summary of the effects of modulating the extracellular calcium ion concentration on NRU cell proliferation and growth pathways

## 4.7 Conclusions and Discussion

Through the inhibition of the PI3K/Akt pathway, NRU cells were successfully subcultured up to passage 2. Although it is unknown how PI3K inhibition led to the increase in NRU cell viability, one possibility is that PI3K inhibition enabled activation of the EGFR/MAPK pathway, which is known to regulate proliferating NHU cell proliferation *in vitro* (Varley 2005). This would suggest that NRU cells can adopt a proliferative phenotype equivalent to that of NHU cells, but they require exogenous stimulation to achieve this switch instead of adopting regenerative phenotype through an autocrine EGFR/MAPK signalling loop.

Extracellular calcium concentrations can result in the generation of cell-cell junctions and result in variations in the proliferation pathways driving urothelial cell proliferation. Lowering extracellular calcium did not prevent the expression of tight junction proteins, suggesting that NRU cells remained in a more differentiated state than NHU cells. This could indicate an inability of NRU cells to fully differentiate in the same way as NHU cells or that an aspect of the cell culture system was preventing them from adopting a fully proliferative phenotype. Again this could indicate a basic cellular difference between normal rat and human urothelial cell physiology.

Despite being able to extend their lifespan in culture, NRU cells could only be subcultured to passage 2 before becoming senescent. In an attempt to improve the NRU cell culture system so that it could be used in toxicity testing, and in order to facilitate further comparisons of the NRU and NHU cell culture systems, NRU and NHU cells were immortalised using two separate methods (Chapter 5).

## 4.8 Key findings

- In culture NHU and NRU cells regulate proliferation via different proliferation pathways
- Inhibition of the PI3K/Akt pathway allowed NRU cells to be subcultured up to passage 2.
- Removal of exogenous EGF did not affect NRU cell proliferation but EGFR inhibition caused a reduction in NRU cell proliferation, suggesting an autocrine signalling loop
- When cultured in low calcium (0.09mM) KSFMc medium, proliferating NRU cells express cell-cell junction and differentiation-associated proteins.
- Decreased extracellular calcium (0.06mM) prevented densely populated NRU cell colonies from forming but did not affect cell proliferation, growth in culture or NRU cell's ability to be subcultured.

## Chapter 5 - Overexpression of BMI1 in NRU and NHU cells

<b>5. Overexpression of BMI1 in NRU and NHU cells .....</b>	<b>144</b>
<b>5.1 Chapter Introduction .....</b>	<b>145</b>
5.1.1 Immortalised cell lines .....	145
5.1.2 <i>In vitro</i> immortalisation .....	146
5.1.3 Immortalisation of urothelial cell culture models .....	147
5.1.4 Overexpression of BMI1.....	148
<b>5.2 Aim .....</b>	<b>151</b>
5.2.1 Objectives.....	151
<b>5.3 Experimental approach.....</b>	<b>152</b>
5.3.1 Development of a BMI1 overexpressing retroviral cell line .....	152
5.3.2 Effect of BMI1 or hTERT overexpression on NRU cell growth and lifespan in culture .....	152
5.3.3 Effect of BMI1 and hTERT overexpression on NHU cell growth, lifespan and ability to form a functional barrier in culture .....	153
5.3.4 Cell lines .....	153
<b>5.4 Results .....</b>	<b>154</b>
5.4.1 Development of a BMI1 overexpressing pLXSN retrovirus.....	154
5.4.2 Overexpression of BMI1 and hTERT in NRU cells.....	159
5.4.3 The effect of overexpressing BMI1 and hTERT on NHU cell growth.....	163
5.4.4 Generation of a functional barrier <i>in vitro</i> .....	168
<b>5.5 Conclusions and Discussion .....</b>	<b>173</b>
<b>5.6 Key Findings .....</b>	<b>174</b>

## 5.1 Chapter Introduction

### 5.1.1 Immortalised cell lines

Normal cells undergo a pre-determined and finite number of divisions, beyond which proliferation ceases and cells reach a state of replicative senescence (reviewed by Sherr, 2000). Replicative senescence is the result of telomere erosion that occurs with every cell division. The majority of normal cells do not express telomerase, the enzyme that is able to restore telomeres, and as such have a finite number of cell divisions before reaching senescence, known as the Hayflick limit. *In vitro*, cells are also capable of becoming senescent without the loss of telomeres. Culture stress-induced senescence can occur when the cell culture conditions are not favorable for cell growth. Tissue culture plastic substrate, cell culture medium and cell seeding density are among a number of conditions that can induce cells to become senescent. Urothelial cells in general show a reduction in their proliferative rate *in vitro* before passage 10, resulting in the need to regularly isolate cells from fresh tissue samples and limiting both the number of cells that can be generated from one sample (Puthenveetil et al., 1999). Having to freshly isolate cells also results in multiple isolation protocols and culture systems being developed (described in Chapter 3).

To increase lifespan, normal cells can be immortalised to generate cell lines with extended proliferative capacities. Immortalised cell lines are a useful tool as they can be serially expanded and widely distributed between research groups and industrial companies. They also have the ability to be used in experiments over several months, where finite cell lines would have become senescent, but immortalisation can have the disadvantage of significantly altering the characteristics of cell lines. The techniques required to immortalise cells can reduce cells similarity to their counterparts *in vivo*, reducing their usefulness as predictive models (Stampfer et al., 1997; Castell et al., 2006). If, however, cells can be immortalised without compromising their original characteristics then these cells would provide a valuable tool for use in studies including toxicology testing.

### 5.1.2 *In vitro* immortalisation

Multiple methods exist for establishing immortalised cell lines. The simplest method is to isolate and culture cancer cells from existing tumours. The commonly used HeLa cell line, the first human cell to be cultured, was originally isolated from cervical cancer cells in 1951 (reviewed by Gilgenkrantz, 2014).

In order to immortalise a normal (non-cancerous) cell line, cells can be transfected with either cell-cycle regulatory genes isolated from viruses or through the overexpression of particular human proteins associated with immortalisation. The immortal human embryonic kidney cell line HEK 293 was generated by transfecting human embryonic kidney cells from an aborted fetus with the adenovirus E1 gene (Graham et al., 1977). This caused an insert of a 4.5 kilobase section of viral DNA into human chromosome 19, producing an immortal and highly proliferative cell line that is easily manipulated (Louis et al., 1997). The SV40 large T antigen is another viral gene that acts a proto-oncogene when transfected into mammalian cells, causing immortalisation (Jha et al., 1998). Overexpression of human genes including human telomerase reverse transcriptase (hTERT) is another commonly used method of cell line immortalisation. hTERT overexpression inhibits telomere-controlled senescence by preventing the shortening of telomeres with each mitotic cell division. Osteoblasts, endothelial cells, epithelial cells and fibroblasts are among a few of the cell types that have been immortalised by hTERT overexpression (reviewed by Lee et al. 2004). Combined overexpression of hTERT with cyclin D1 and mutant cyclin dependant kinase 4 (CDK4) isoform have also been used in the successful immortalisation of hepatocytes (Shiomi et al., 2011).

### 5.1.3 Immortalisation of urothelial cell culture models

Immortalisation of NHU cells has previously been achieved by multiple methods including overexpression of hTERT (Petzoldt et al., 1995; Georgopoulos et al., 2011) and transfection with the human papillomavirus 16 (HPV16) E6 gene (Diggle et al., 2000). It was found that human urothelial (HU)-TERT cells had an increased lifespan in culture when compared to NHU cells but their ability to differentiate (ABS/Ca<sup>2+</sup>) and form a functional barrier was severely reduced. It was shown that hTERT immortalisation did not cause gross genomic or karyotypic alterations but P16<sup>INK4a</sup> and proliferator-activated receptor  $\gamma$  (PPAR $\gamma$ ) expression were inhibited. PPAR $\gamma$  is known to be an important regulator of NHU cell differentiation (Varley et al., 2004) and its inhibition in HU-TERT cells would explain cells inability to differentiate *in vitro*. As the production of a barrier between urine and the underlying stromal cells is a key function of the urothelium it is an important aspect to replicate in urothelial cell culture models.

A separate human urothelial cell line was immortalised through transfection with a construct containing the SV40 large T antigen and named the UROtsa cell line (Rossi et al., 2001). UROtsa cells have an undifferentiated cell morphology and have been used, amongst other things, to research heavy metal toxicity in urothelial cells (Somji et al., 2008). A major concern with the use of UROtsa cells in toxicity testing, apart from their dedifferentiated phenotype, is that the cell line appears to have become contaminated with the T24 bladder cancer cell line. A study of multiple UROtsa sources found that all cell lines tested lacked the large T-antigen and short tandem repeat analysis identified as characteristic of the T24 bladder cancer cell line (Johnen et al., 2013). Depending on when the contamination occurred, this has serious implications for all publications using UROtsa cells and reduces the credibility of results published that relate to normal urothelial cell function. Immortalisation of NRU cells using any immortalisation technique has not been published.

### 5.1.4 Overexpression of BMI1

BMI1 is a 37 kDa protein originally identified in lymphoid tumours in mice (Haupt et al., 1991b). It was the first functional polycomb group (PcG) protein to be discovered and shares a high level of homology between humans and rodents (Alkema et al., 1993). In particular the N terminal ring finger domain and central helix-turn-helix-turn (H-T-H-T) motif, the regions essential for inducing telomerase activity, are conserved between species (Li et al., 2006; Cohen et al., 1996). BMI1 is expressed in most tissues but expression is particularly high in the brain, blood, bone marrow and lungs (Huber et al., 2011). As a member of polycomb repression complex 1 (PRC1), it is involved in maintaining specific gene repression through epigenetic silencing (Pirrotta, 1998; Ringrose and Paro, 2004). BMI1 knockout in mouse models is not embryonically lethal, unlike loss of polycomb repression complex 2 (PRC2) members, but the lack of BMI1 does lead to posterior transformation (Alkema et al., 1995), neurological abnormalities and severe hematopoietic defects (van der Lugt et al., 1994).

BMI1 was initially identified as an oncogene which, in combination with c-Myc, caused lymphomagenesis in mice (van Lohuizen et al., 1991; Haupt et al., 1991a). It has now been shown that BMI1 is up-regulated in a number of cancers, including epithelial carcinomas (Raaphorst, 2005; Huber et al., 2011; Kim et al., 2004; Song et al., 2006; Leung et al., 2004; Kang et al., 2006), where it is believed to be involved in cancer stem cell (CSC) maintenance (Valk-Lingbeek et al., 2004; Liu et al., 2006b). BMI1 is highly expressed in CSCs (Lessard and Sauvageau, 2003; Liu et al., 2006c; Song et al., 2006; Liu et al., 2006a) but its up-regulation in cancer is not restricted to CSCs, preventing it from being used as a CSC marker (Oishi N and XW, 2011). BMI1 expression has an inverse relationship with microRNA-218 (miRNA-218), a microRNA on chromosome 4 that is lost in cancers including colon, cervical, lung and bladder (Martinez et al., 2007; Davidson et al., 2010; Tatarano et al., 2011). By inducing expression of miRNA-218 in cancer cells, BMI1 is down-regulated which acts to induce apoptosis and inhibit cell proliferation (He et al., 2012).

Through epigenetic inhibition of gene transcription, BMI1 regulates cell proliferation and prevents cells from becoming senescent (Jacobs et al., 1999). This function has been most commonly reported in stem cells where cell maintenance and self-renewal are dependent on BMI1 expression. This has been documented in normal and progenitor liver stem cells (Lessard and Sauvageau, 2003), hematopoietic stem cells (Hosen et al., 2007) and neural stem cells (Molofsky et al., 2005). In keratinocytes BMI1 is only expressed by basal and suprabasal cells (Balasubramanian et al., 2008).

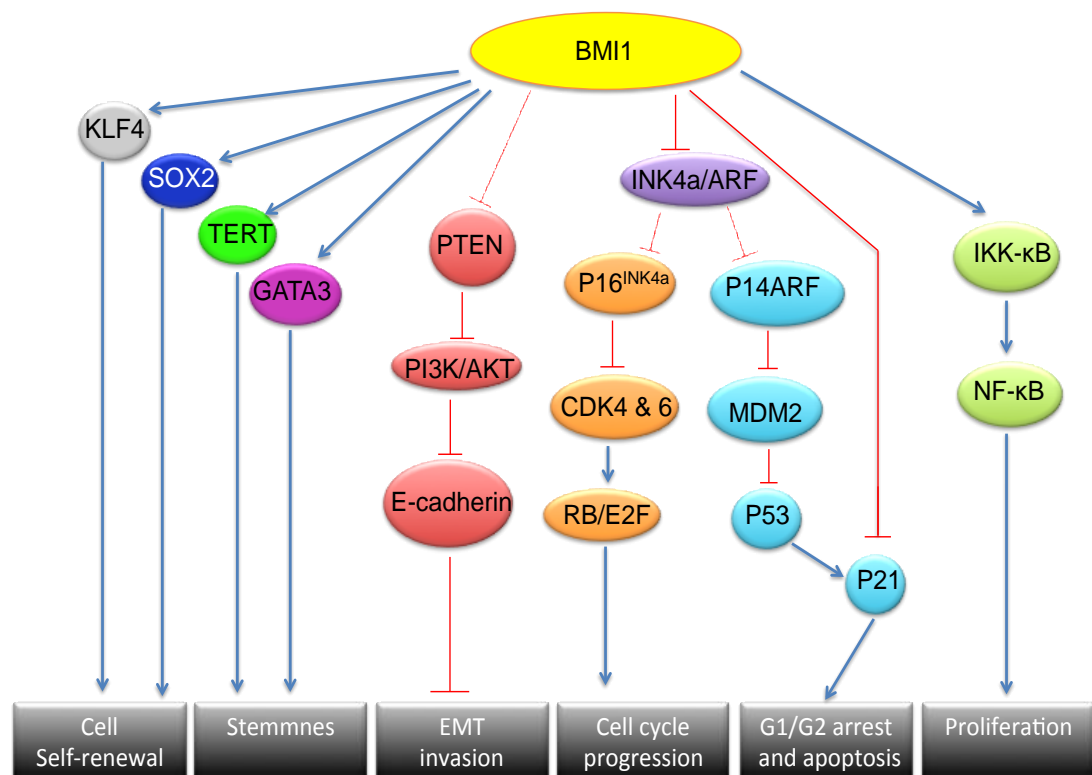


**Figure 5.1 – BMI1 increases cell self-renewal, proliferation and stemness while decreasing apoptosis and senescence.** Cartoon illustrating some of the molecular actions of BMI1 associated with stemness and immortalisation. BMI1 activates transcription factors KLF4, SOX2 and GATA3 as well as the telomerase reverse transcriptase (TERT) to promote self-renewal and stemness. BMI1 activation of the NF- $\kappa$ B and P16<sup>INK4a</sup> pathways result in increased cell proliferation while inhibition of P21 inhibits apoptosis. Downstream inhibition of E-cadherin enables epithelial mesenchymal transition (EMT) and cell invasion (adapted from Siddique & Saleem, 2012).

*In vitro*, down-regulation of BMI1 gene expression occurs when cells become senescent, although expression is unaltered in quiescent cells when compared to proliferating (Itahana et al., 2003). In human stem and cancer cell lines, loss of BMI1 causes cell senescence through signalling events including p16<sup>INK4a</sup> expression and down regulation of SOX-2 and KLF4 (Dong et al., 2011; Molofsky et al., 2005). Due to its ability to inhibit senescence, over-expressing BMI1 has been used as a technique to increase the lifespan of cells in culture (Saito et al., 2005; Fulcher et al., 2009; Dimri et al., 2002).

BMI1 has been overexpressed in epithelial cells, stromal cells and fibroblasts to increase cellular lifespan in culture and is able to do so without altering cell morphology or phenotype (Dimri et al., 2002; Itahana et al., 2003; Takeda et al., 2004; Tátrai et al., 2012). Furthermore overexpression of BMI1 in normal human bronchial epithelial cells increased cell lifespan while preserving the ability of cells to differentiate in culture and generate a functional barrier with a TEER equivalent to that of untransfected cells (Fulcher et al., 2009).

The effects of BMI1 overexpression in NRU or NHU cells have not previously been reported. The generation of immortalised NRU and NHU cell lines that retain the ability to differentiate and generate functional barriers *in vitro* would be beneficial in further comparing NRU and NHU cells, as a means of validating the systems for use in toxicity studies. It would also increase their utility in toxicity studies due to the increased potential for lifespan expansion of immortalised cell lines compared to finite cell lines.

## 5.2 Aim

To investigate the effect of BMI1 overexpression on the lifespan and differentiation potential of NRU and NHU cells *in vitro* and compare results against cells overexpressing human telomerase reverse transcriptase (hTERT).

### 5.2.1 Objectives

1. Generate a BMI1 overexpression retrovirus and transduce NRU and NHU cells
2. Determine the lifespan of NRU cells overexpressing BMI1 or hTERT
3. Investigating the effect BMI1 and hTERT overexpression on NHU cell lifespan
4. Investigate the ability of BMI1 and hTERT overexpressing NHU cells to produce a functional barrier

## 5.3 Experimental approach

### 5.3.1 Development of a BMI1 overexpressing retroviral cell line

Next generation sequencing data was used to demonstrate whether NHU cells express BMI1 transcript. NHU cell cDNA was used to amplify the BMI1 protein-coding sequence, which was cloned into a pLXSN retroviral plasmid. The plasmid was sequenced to ensure the entire cDNA had been amplified and ligated before being transformed and amplified in bacteria. The PT67 mammalian retroviral packaging cell line was transfected with the pLXSN BMI1 plasmid, ready for transduction of urothelial cells. Additional packaging cell lines containing a previously developed pLXSN hTERT plasmid (Georgopoulos et al., 2011) or pLXSN plasmid without an insert (pLXSN Empty) were also generated to act as controls. Successful transfection of packaging cells was confirmed using antibiotic (G418) selection. Untransfected packaging cells acted as antibiotic-selection controls.

### 5.3.2 Effect of BMI1 or hTERT overexpression on NRU cell growth and lifespan in culture

3 NRU cell lines isolated and cultured using the optimised NRU cell isolation (dispase/trypsin) and culture (PI3K inhibition / 0.06 mM Ca<sup>2+</sup>) protocols (see Chapters 3 and 4) were transduced with pLXSN empty, pLXSN BMI1 or pLXSN hTERT and cultured under antibiotic selection (0.025 mM G418). The effects of transduction on cell growth in culture monitored by phase contrast microscopy and by the use of alamarBlue growth curves. Cultures were sub-cultured at just-confluence.

### 5.3.3 Effect of BMI1 and hTERT overexpression on NHU cell growth, lifespan and ability to form a functional barrier in culture

Population doubling graphs were generated using cell counts for NHU cells transduced with pLXSN, pLXSN BMI1 or pLXSN hTERT and cultured under antibiotic selection (0.025 mM G418) to monitor the effect on cell growth. NHU cells were differentiated (ABS/Ca<sup>2+</sup>) and their ability to generate functional barriers *in vitro* examined.

### 5.3.4 Cell lines

Table 5.1 NRU Cells

Code	No. of animals	Sex	Source	Strain	Age/Weight
R041	12	M	University of York	Wistar	250-300g
R042	10	M/F	Covance Inc.	Wistar	300-350g
R046	10	M	University of York	Wistar	300-350g

Table 5.2 NHU Cells

Code	Tissue of origin	Sex	Age
Y1533	Ureter	M	45
Y1570	Ureter	F	51

## 5.4 Results

### 5.4.1 Development of a BMI1 overexpressing pLXSN retrovirus

Next generation sequencing data generated using RNA from freshly isolated (P0), proliferating and differentiated NHU cells was used to confirm that NHU cells expressed BMI1 transcripts. As can be seen in Figure 5.2, all 7 known BMI1 transcript variants, including the full protein-coding BMI1-001 transcript, were expressed in primary, proliferating and differentiated NHU cells.

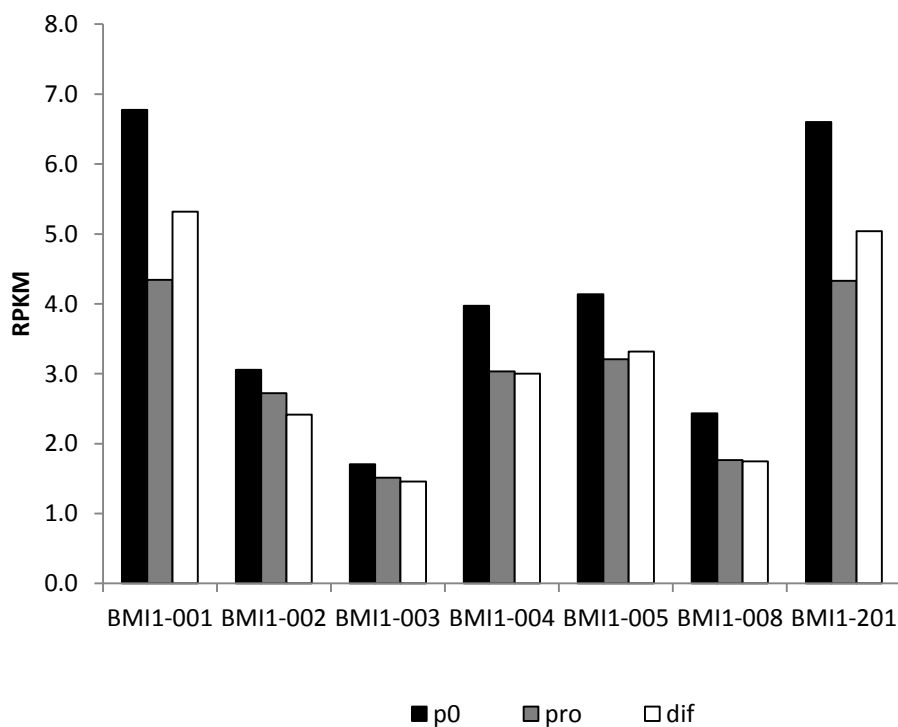


**Figure 5.2 – BMI1 transcripts are expressed by P0, proliferating and differentiated NHU cells.** Next generation sequencing (Section 2.6.3.9) data showing mean reads per kilobase per million mapped reads (RPKM) for BMI1 transcript expression in freshly isolated (P0), proliferating (pro) and differentiated (dif) NHU cells (n=3 individual donors).

RNA was isolated from proliferating NHU cells and primers were designed to amplify the full Bmi-001 protein coding sequence, with restriction enzyme sites for BamH1 incorporated into the forward primer and Hpa1 on the reverse primer and a Kozac sequence before the start codon (appendix 1.6). BMI1 cDNA was amplified using High Fidelity Taq polymerase, which produced a product with TA overhangs for ligation into pGEM T easy vector that was subsequently transformed into bacteria. Ampicillin-selection was initially used to identify successfully transformed bacteria (Figure 5.3). Plasmids from 10 single selected colonies were sequenced to find a colony containing the complete BMI1 cDNA sequence. A single colony was found in which the BMI1 sequence had two single base changes from the reference sequence (Appendix 2.3) (Figure 5.4), neither of which affected the amino acid sequence encoded. This single colony was selected and cultured under continued ampicillin-selection.

BMI1 cDNA was cut from the pGEM T vector using the restriction enzymes BamH1 and Hpa1 (Figure 5.5), purified and ligated into pLXSN retroviral plasmid. Bacteria were transfected with the pLXSN BMI1 vector and a colony RT-PCR conducted to ensure colony had been successfully transfected (Figure 5.6). A colony containing pLXSN BMI1 was chosen, sequenced to ensure the BMI1 sequence was correct and used to generate pLXSN BMI1 for transfection of PT67 packaging cells. After 5 days of G418 selection untransfected PT67 cells had died whereas ones transduced with pLXSN, pLXSN BMI1 and pLXSN hTERT had survived and proliferated (Figure 5.7).

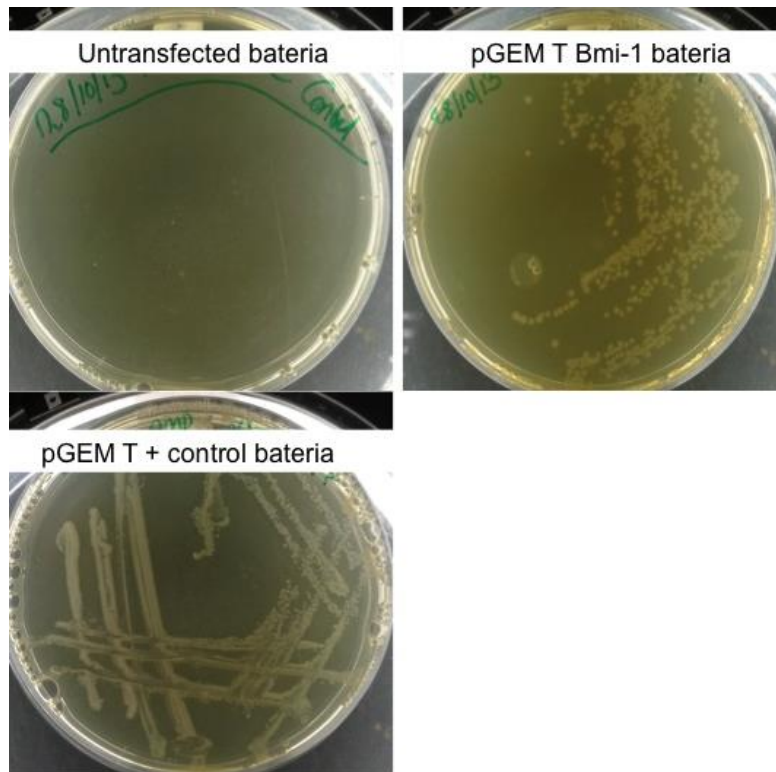


**Figure 5.3 – Successful ligation of BMI1 into pGEM T and subsequent transfection of E.Coli, as confirmed by antibiotic selection.** Ampicillin-selection of XL1-Blue competent E. coli were transformed with pGEM T easy BMI1, pGEM T easy insert DNA (+ control) and negative (untransformed) controls after 24 hours of culture at 37°C (Section 2.6.5).

```

GGATCCACCACCATGCATCGAACAACGAGAATCAAGATCACTGAGCTAAATCCCCACCTGATGTGTGT
GCTTTGTGGAGGGTACTTCATTGATGCCACAACCATAATAGAATGTCTACATTCTTCTGTAAAACGT
GTATTGTTTCGTTACCTGGAGACCAGCAAGTATTGTCTATTTGTGATGTCCAAGTTCACAAGACCAGA
CCACTACTGAATATAAGGTCAGATAAAACTCTCCAAGATATTGTATACAAATAGTTCCAGGGCTTTT
CAAAAATGAAATGAAGAGAAGAAGGGATTTTTATGCAGCTCATCCTTCTGTCTGATGCTGCCAATGGCT
CTAATGAAGATAGAGGAGAGGTTGCAGATGAAGATAAGAGAATTATAACTGATGATGAGATAATAAGC
TTATCCATTGAATTCTTTGACCAGAACAGATTGGATCGGAAAGTAAACAAAGACAAAGAGAAAATCTAA
GGAGGAGGTGAATGATAAAAAGATACTTACGATGCCAGCAGCAATGACTGTGATGCACTTAAGAAAAGT
TTCTCAGAAGTAAAATGGACATACCTAATACTTTCCAGATTGATGTCATGTATGAGGAGGAACCTTTA
AAGGATTATTATACACTAATGGATATTGCCTACATTTATACCTGGAGAAGGAATGGTCCACTTCCATT
GAAATACAGAGTTCGACCTACTTGTAAGAAGATGAAGATCAGTCACCAGAGAGATGGACTGACAAATG
CTGGAGAACTGGAAAGTGACTCTGGGAGTGACAAGGCCAACAGCCCAGCAGGAGGTATTCCTCCACC
TCTTCTTGTTTGCCTAGCCCCAGTACTCCAGTGCAGTCTCCTCATCCACAGTTTCCTCACATTTCCAG
TACTATGAATGGAACCAGCAACAGCCCCAGCGGTAACCACCAATCTTCTTTGCCAATAGACCTCGAA
AATCATCAGTAAATGGGTCATCAGCAACTTCTTCTGGTTGAGTTAAC

```

**Figure 5.4 – BMI1 was accurately amplified from NHU cell RNA with only two, non-amino acid altering mutations.** BMI1 was sequenced (Section 2.6.5.5) after amplification from NHU RNA. Restriction sites are coloured in yellow, the Kozak sequence in green and alternate exons colours in black and grey. Two bases that were changed from the Reference sequence are highlighted in red.

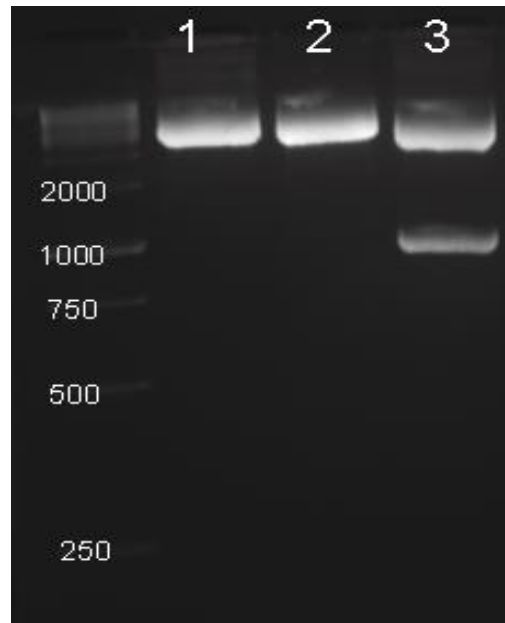


**Figure 5.5 - BMI1 was successfully cut from the pGEMT BMI1 vector.** Gel electrophoresis (section 2.6.5.3) of pGEM T BMI1 isolated from transformed XL1-Blue competent *E. coli* (1), after single BamH1 restriction enzyme digestion (2) and after a double restriction enzyme digestion with BamH1 and Hpa1 (3). The ladder indicates the size of the product in base pairs.

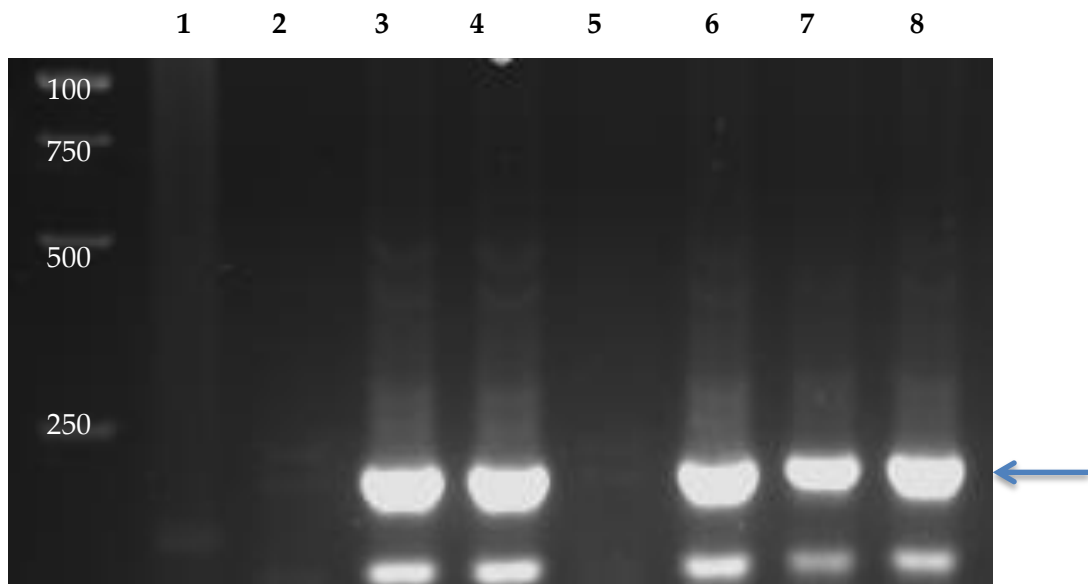


**Figure 5.6 - BMI1 was successfully ligated into pLXSN vector and used to transfect bacteria.** Colony RT-PCR (Section 2.6.3.8) amplifying BMI1 (221bp) from 8 bacterial colonies after transfection with pLXSN BMI1. Base pair ladder indicates the size of the product in base pairs.

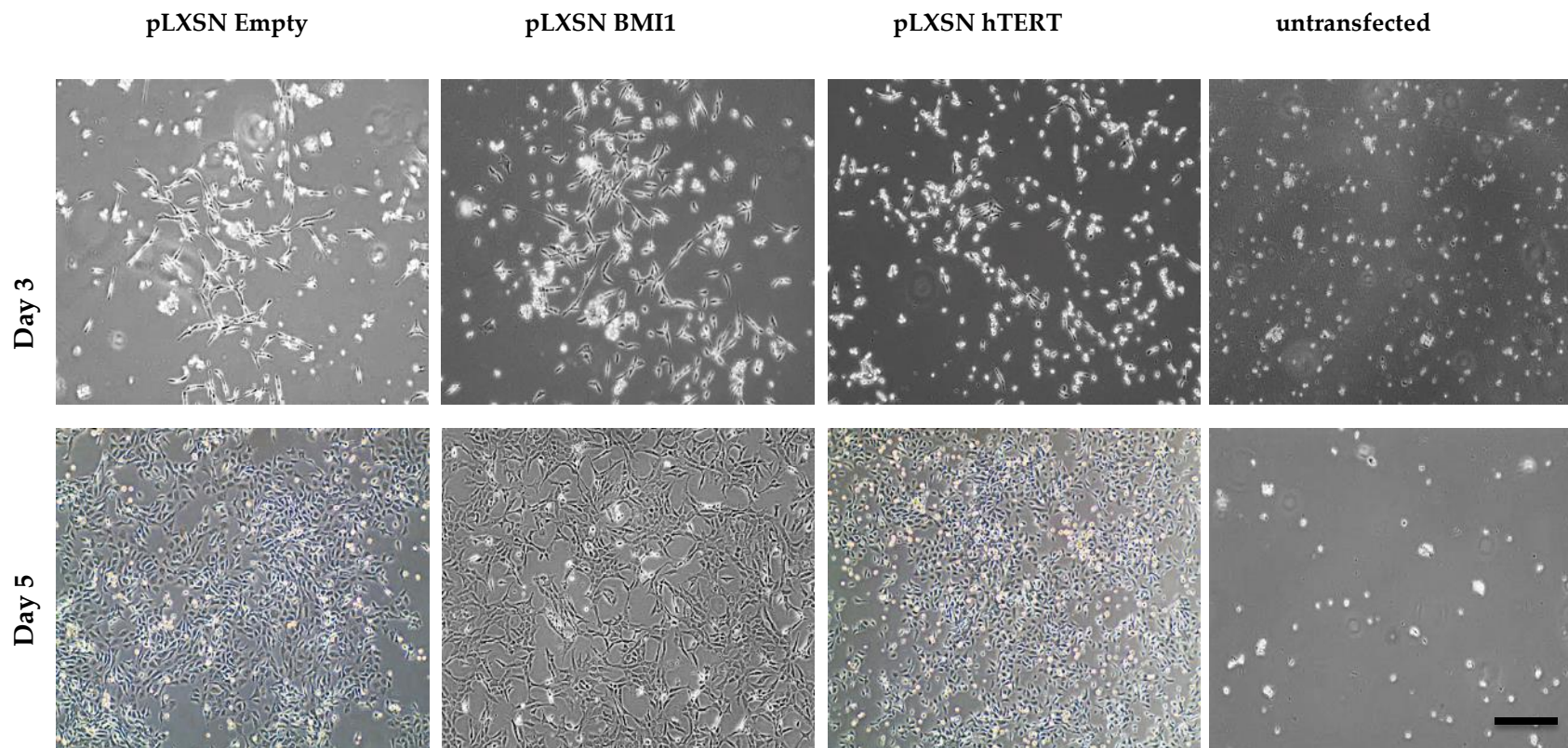


**Figure 5.7 – Packaging cells were successfully transfected with pLXSN BMI1, pLXSN hTERT and pLXSN Empty vectors.** Phase contrast images of PT67 packaging cells transfected with pLXSN empty, pLXSN hTERT & pLXSN BMI1 on days 3 and 5 of G418 selection showing complete death of untransfected cells. Scale bar = 50  $\mu$ m.

### 5.4.2 Overexpression of BMI1 and hTERT in NRU cells

NRU cells transduced with retrovirus during primary culture to overexpress BMI1 or hTERT showed no difference in morphology to cells transduced with empty pLXSN at passage one, following one subculture (Figure 5.8). Population growth was consistent between all transduced cell lines, with 80-90% confluence achieved after 7 days of culture under antibiotic (G418) selection. Non-transduced control NRU cells did not grow in the presence of G418 and approximately 95% of cells died within 7 days of G418 selection and were discontinued.

When passaged a second time (P2), NRU cultures transduced with pLXSN, pLXSN BMI1 or pLXSN hTERT all failed to proliferate and approximately 95% of cells were dead within 7 days (Figure 5.10). NRU cells transduced with BMI1 or hTERT appeared to die at the same rate as cells containing pLXSN empty vector.

The growth of passage 1 and passage 2 NRU cells transduced with pLXSN BMI1 or pLXSN hTERT was quantified (Figure 5.11 & Figure 5.12) and in support of results seen by phase contrast microscopy showed that NRU cells at P1 all shared typical growth kinetics irrespective of BMI1 or hTERT overexpression. No differences were found between NRU cells transduced with pLXSN empty vector and cells transduced with either pLXSN BMI1 or pLXSN hTERT. After an additional passage (P2), all NRU cells showed minimal growth between days 1 and 3 of culture and significant reductions in biomass between days 3 and 5. Overexpression of BMI1 or hTERT did not have a significant effect on NRU (P2) cell growth compared to the empty vector control.

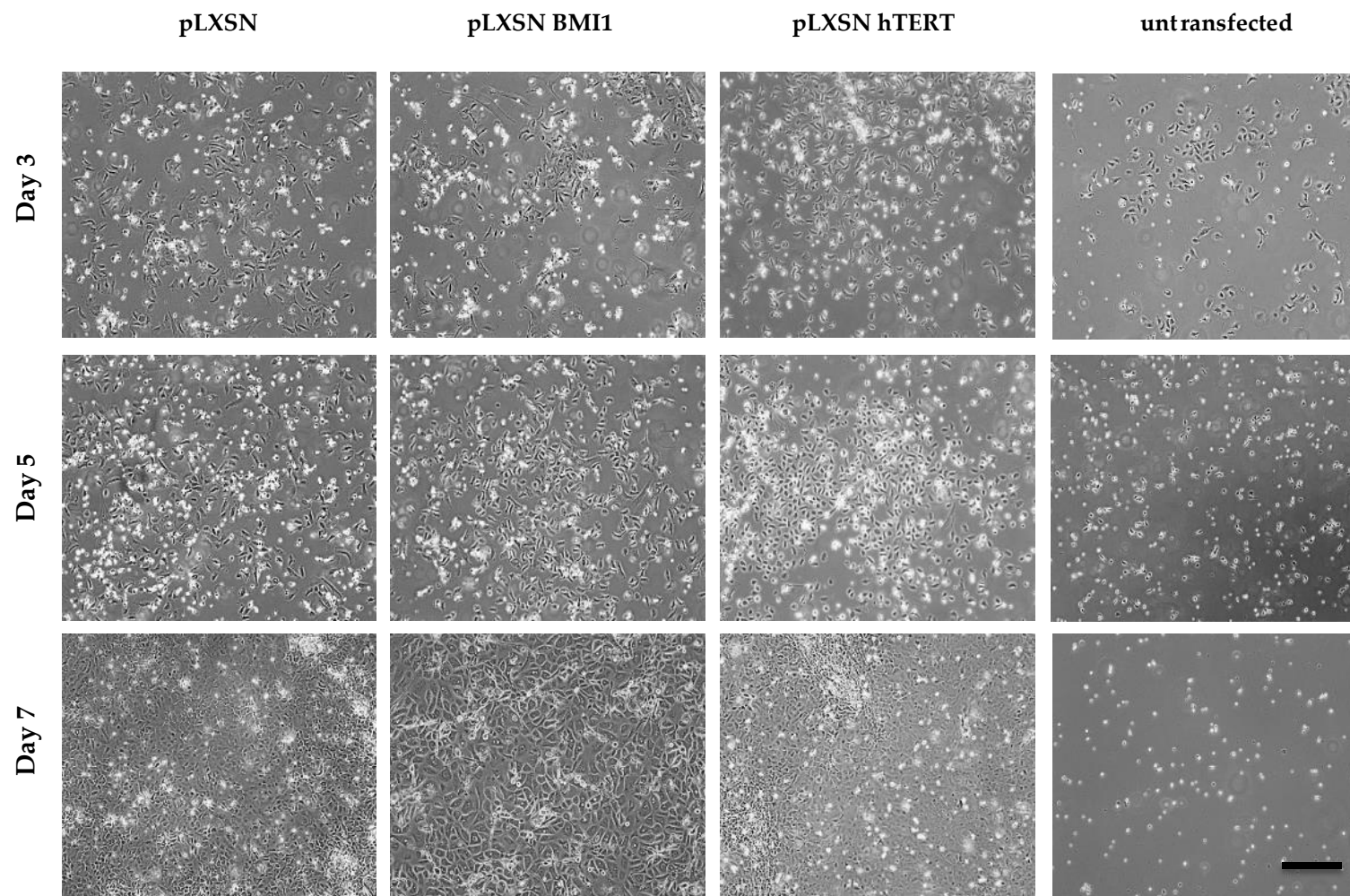


**Figure 5.8** – NRU cells were successfully transfected with pLXSN Empty vector, pLXSN hTERT, pLXSN BMI1 vectors. Phase contrast images of transfected and untransfected NRU cells cultured in KSMc medium (0.06mM Ca<sup>2+</sup>) during the first 7 days after subculture (P1) under G418 selection. Scale bar = 50  $\mu$ m.

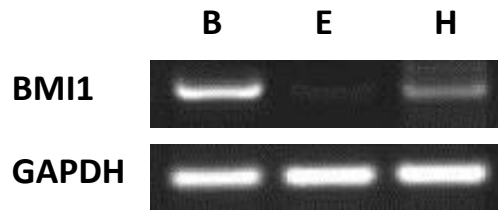


**Figure 5.9** – BMI1 and hTERT were both expressed by NRU cells overexpressing BMI1. RT-PCR (section 2.6.3.8) showing BMI1 expression in NRU cells (P1) transduced with pLXSN BMI1 (B), pLXSN empty vector (E) and pLXSN hTERT (H). GAPDH was included as a loading control.

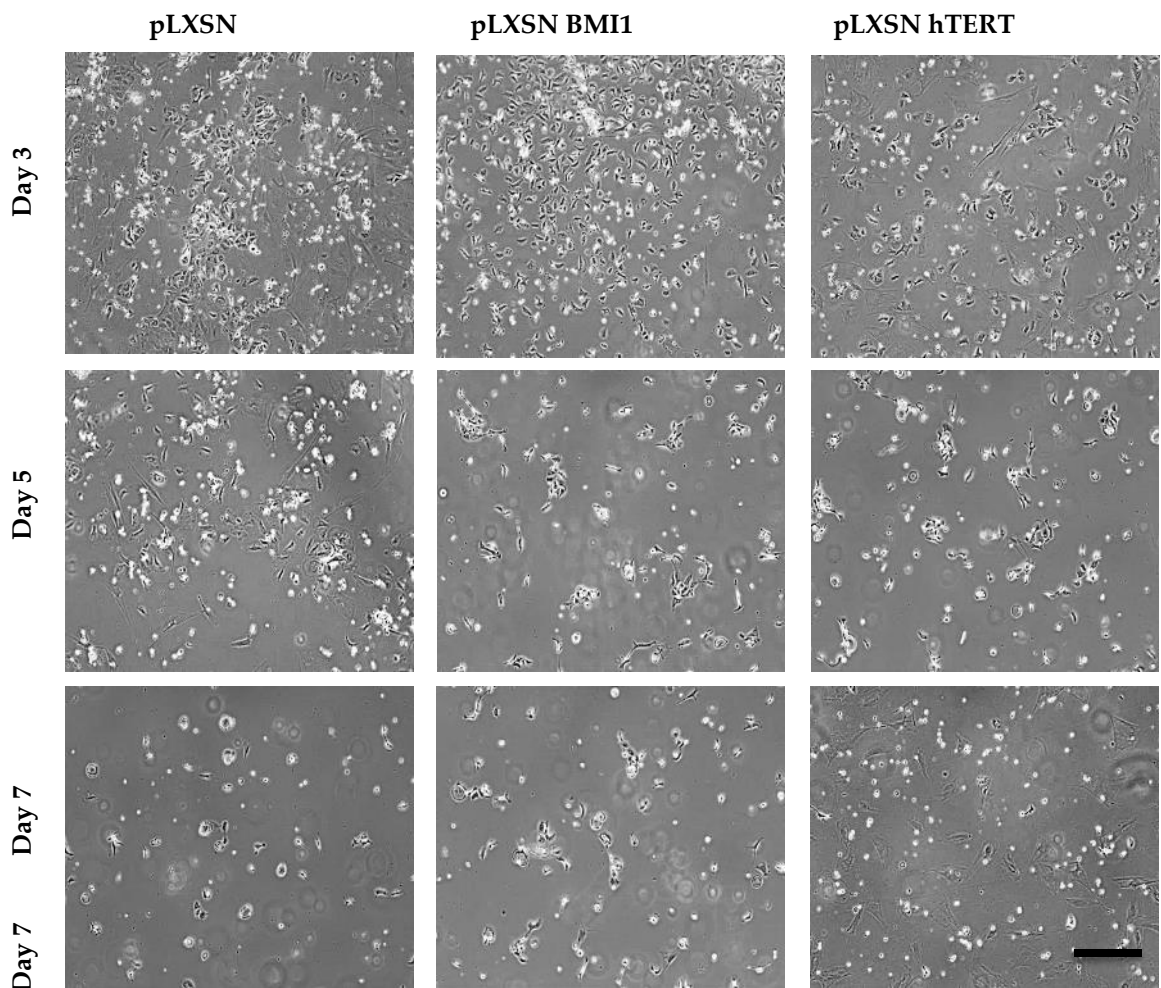


**Figure 5.10** – hTERT and BMI1 overexpressing cells did not survive after passage 2. Phase contrast images of transduced NRU cells cultured in KSFMc medium (0.06 mM  $\text{Ca}^{2+}$ ) on days 3, 5 and 7 after second subculture (P2). Cells remained under G418 selection pressure. Scale bar = 50  $\mu\text{m}$ .

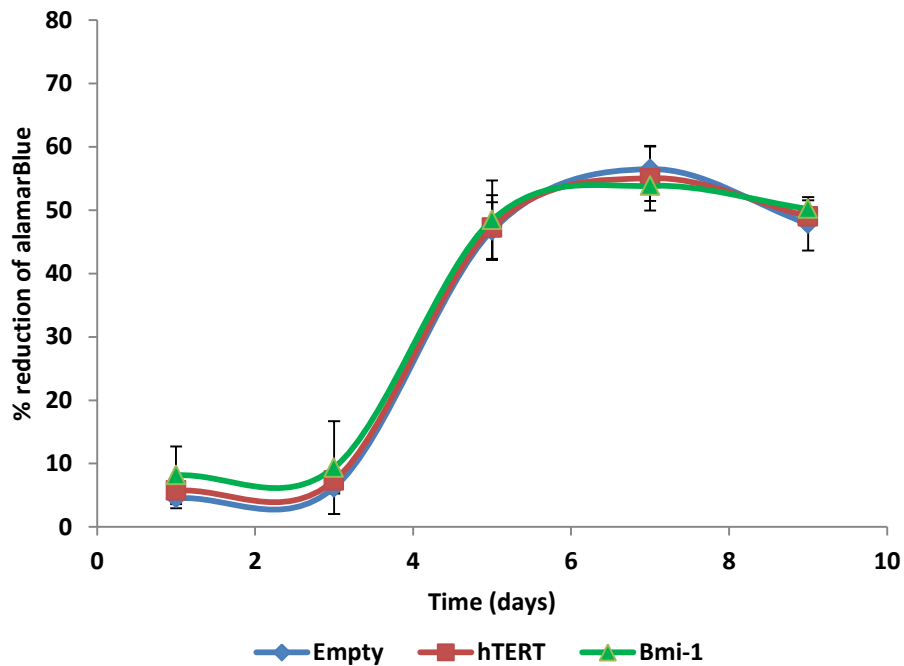


**Figure 5.11 – BMI1 and hTERT overexpressing NRU cells grew at passage 1 equivalent to control cells.** AlamarBlue assay (Section 2.5.3.1) generated growth curves for control, pLXSN BMI1 and pLXSN hTERT transfected NRU cells (P1) cultured in KSFMc medium (0.06 mM  $\text{Ca}^{2+}$ ) containing G418 selection. Error bars represent  $\pm$ SD (n=3, R041, R042, R046).

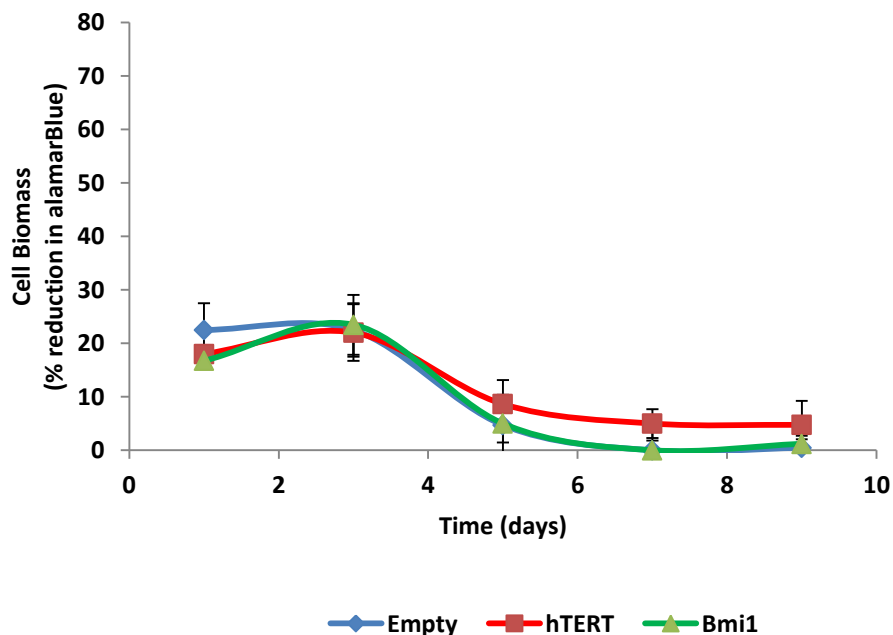


**Figure 5.12 – BMI1 and hTERT overexpressing NRU cells failed to grow at passage 2.** AlamarBlue assay (Section 2.5.3.1) generated growth curves for control, pLXSN BMI1 and pLXSN hTERT transfected NRU cells (P2) cultured in KSFMc medium (0.06 mM  $\text{Ca}^{2+}$ ) containing G418 selection. Error bars represent  $\pm$ SD (n=3, R041, R042, R046).

### **5.4.3 The effect of overexpressing BMI1 and hTERT on NHU cell growth**

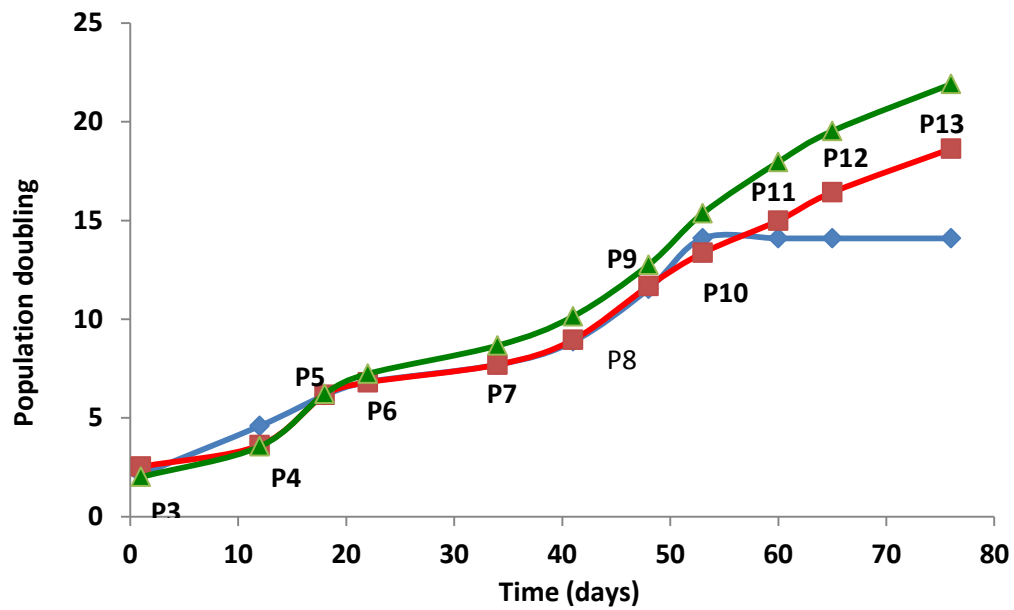
Sublines of NHU cells from two donors (Y1533 & Y1570) transduced with pLXSN BMI1, pLXSN hTERT or pLXSN empty vector at passage 1 were maintained over several months. Cultures were passaged when 80-90% confluent and population doubling curves generated (Figure 5.13 & Figure 5.14). Data from the individual donors is displayed separately to illustrate the donor variations observed.

BMI1 overexpressing NHU cells from both donors showed no difference in growth rate compared to NHU cells overexpressing hTERT or transfected with pLXSN empty vector up to passage 10 (Y1533) and passage 8 (Y1570), at which point NHU cells transduced with empty vector became senescent. BMI1 and hTERT overexpressing cells continued to proliferate beyond the point at which empty vector cells became senescent, with BMI1-transduced cells achieving a greater number of population doublings than hTERT-overexpressing NHU cells at each time point.

One NHU cell line (Y1570) showed a greater population doubling rate than cells from donor Y1533. This variation between donors was mirrored by BMI1 and hTERT-overexpressing cells, indicating that overexpression of either protein did not have any effect on the NHU cell growth rate.

Cells throughout culture were monitored by phase contrast microscopy (Figure 5.14) to allow changes in cell morphology to be monitored. NHU cell lines overexpressing BMI1 or hTERT showed no alterations in cell morphology between passages 6-9. NHU cell cultures transfected with pLXSN empty vector began to contain flattened cells at passage 7 (P7) and had a larger, more rounded cell morphology by passage 9 (P9). Based on the growth curves generated, this coincided with a decrease in cell proliferation and eventual senescence.

Y1533



Y1570

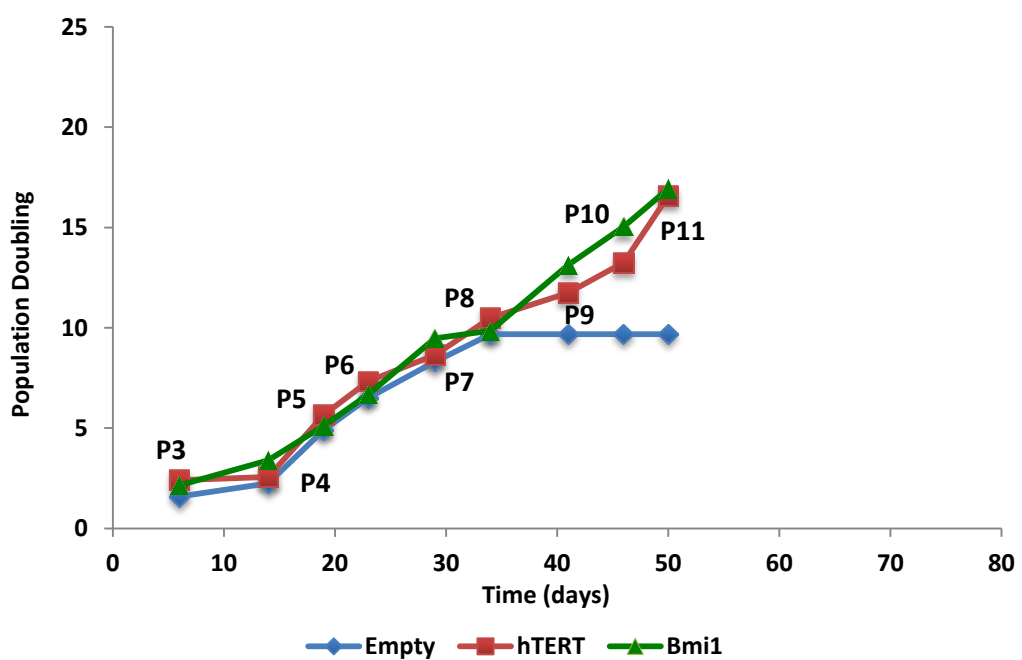


**Figure 5.13 – BMI1 and hTERT overexpression increased NHU cell lifespan in culture compared to control cells.** NHU cell population doubling curves (Section 2.5.4) were generated for two cell lines transduced with pLXSN BMI1, pLXSN hTERT and pLXSN empty vector. Numbers indicate the passage number of the cell line at each time point (n=2, Y1533 and Y1570)

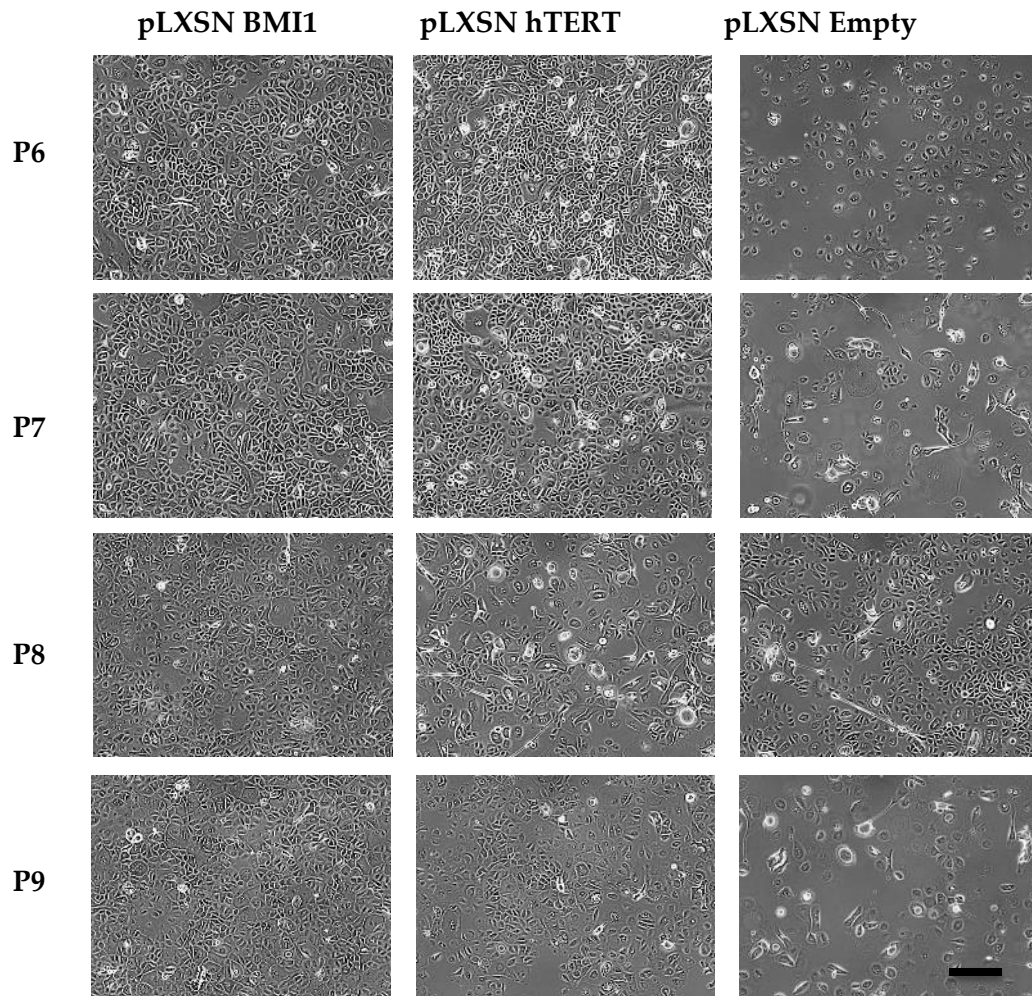


**Figure 5.14 – BMI1 and hTERT overexpressing NHU cells maintained a normal morphology in culture up to passage 9 whereas control (Empty vector) NHU cells became more rounded and were less densely packed in culture. Representative phase contrast images of NHU cells transduced with pLXSN BMI1, pLXSN hTERT and pLXSN empty vector at passages 6-9. (n=1, Y1533). Scale bar = 50  $\mu$ m.**

To confirm the overexpression of BMI1 and hTERT in transduced NHU cells, RT-PCR was conducted on RNA from pLXSN BMI1, pLXSN hTERT and pLXSN empty vector transfected NHU cells at passages 2-12. In pLXSN BMI1 transfected NHU cells, BMI1 was detected at passages 2-12 (Figure 5.15). hTERT was not found to be expressed by BMI1 overexpressing NHU cells.

pLXSN hTERT transfected NHU cells showed both expression of hTERT at passages 2-12 and also expression of BMI1 (Figure 5.16). hTERT expression appeared to increase over the time course. BMI1 expression was visually reduced compared to expression in pLXSN BMI1 transfected NHU cells (Figure 5.16), but was consistently expressed by hTERT overexpressing cells at passages 2-12.

As NHU cells transfected with pLXSN empty vector became senescent, RT-PCR was only conducted on RNA from cells up to passage 8 (Figure 5.17). At no passage did empty vector-transduced NHU cells express BMI1 or hTERT transcript. The lack of BMI1 and hTERT expression in the empty vector cells indicated that the expression seen in the pLXSN BMI1 and pLXSN hTERT transfected cells was a result of the retroviral transduction. As BMI1 was expressed by both pLXSN hTERT transfected NHU cell lines (Y1533 and Y1570), it suggests that the expression of BMI1 in hTERT overexpressing cells was the consequence of hTERT overexpression.

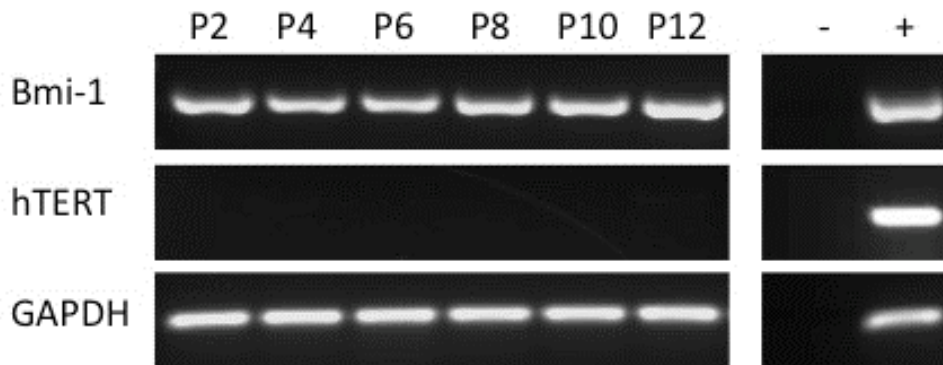


**Figure 5.15 – BMI1 expression was maintained in NHU cells over multiple passages.** RT-PCR (section 2.6.3.8) results showing BMI1 and hTERT expression in BMI1 overexpressing NHU cells at passages 2-12 (Y1533). Water was used as a negative (no-template) control, RNA from BMI1 or hTERT-overexpressing PT67 was used as positive controls; GAPDH was used as a loading control.

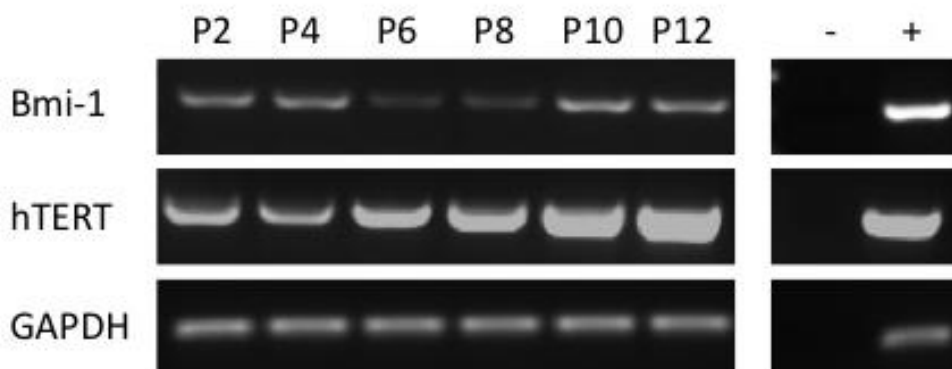


**Figure 5.16 - BMI1 and hTERT were both expressed by hTERT overexpressing NHU cells over several passages.** RT-PCR (Section 2.6.3.8) results showing BMI1 and hTERT expression in hTERT overexpressing NHU cells at passages 2-12 (Y1533). Water was used as a negative control, BMI1 or hTERT overexpressing PT67 cDNA as positive controls and GAPDH as a loading control. (n=2, Y1533, Y1570)

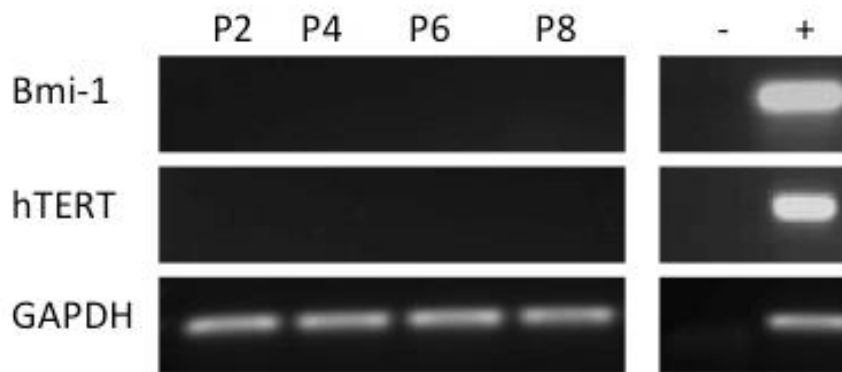
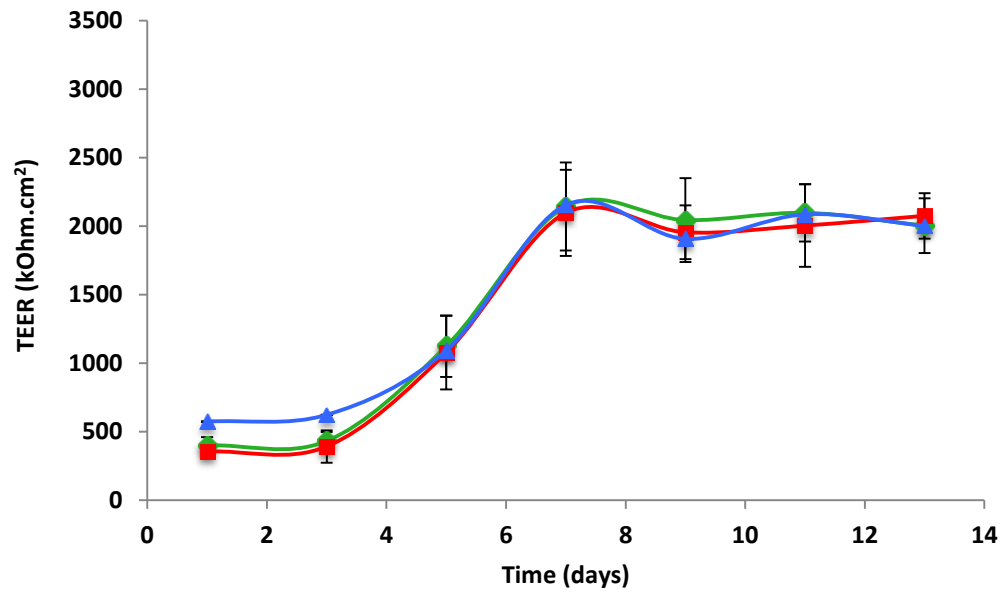


**Figure 5.17 – BMI1 and hTERT were not expressed by Empty vector (control) NHU cells.** RT-PCR (section 2.6.3.8) results showing BMI1 and hTERT expression in pLXSN Empty vector transduced NHU cells at passages 2-8 (Y1533). Water was used as a negative control, BMI1 or hTERT overexpressing PT67 cDNA as positive controls and GAPDH as a loading control. (n=2, Y1533, Y1570)

#### 5.4.4 Generation of a functional barrier *in vitro*

At passage three, NHU cells transduced with pLXSN BMI1, pLXSN hTERT and pLXSN empty vector were subjected to the ABS/[Ca<sup>2+</sup>] differentiation protocol and all were found able to generate a barrier *in vitro*, as measured by TEER. This was conducted in two NHU cell lines and although there were variations between the two donor cell lines, no significant differences in the ability of cells to generate a barrier occurred as a result of overexpressing BMI1 or hTERT compared to empty vector controls (Figure 5.18 to Figure 5.20).



Y1570

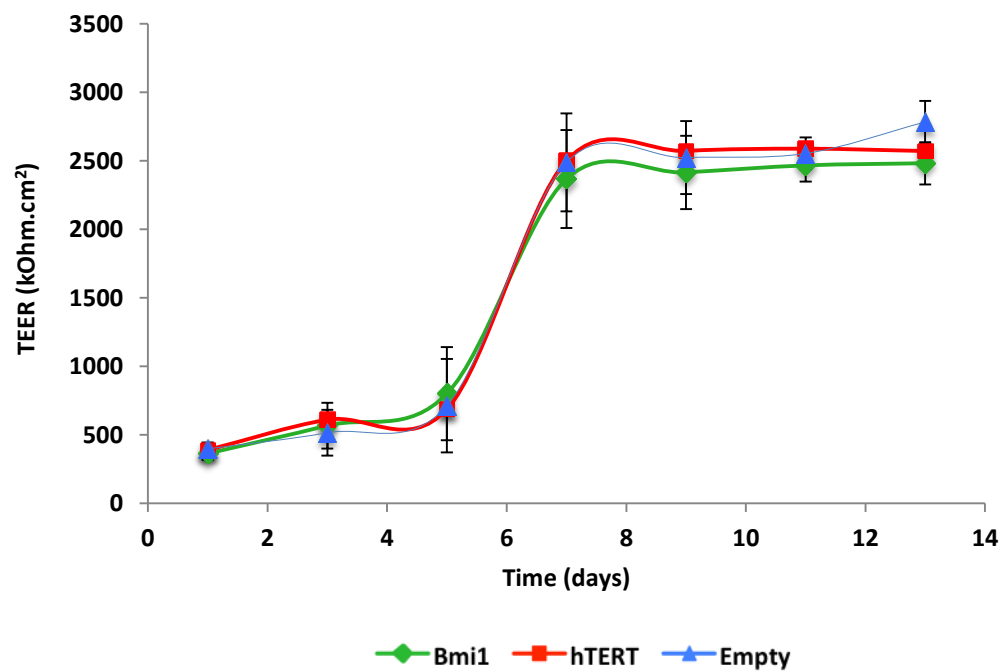
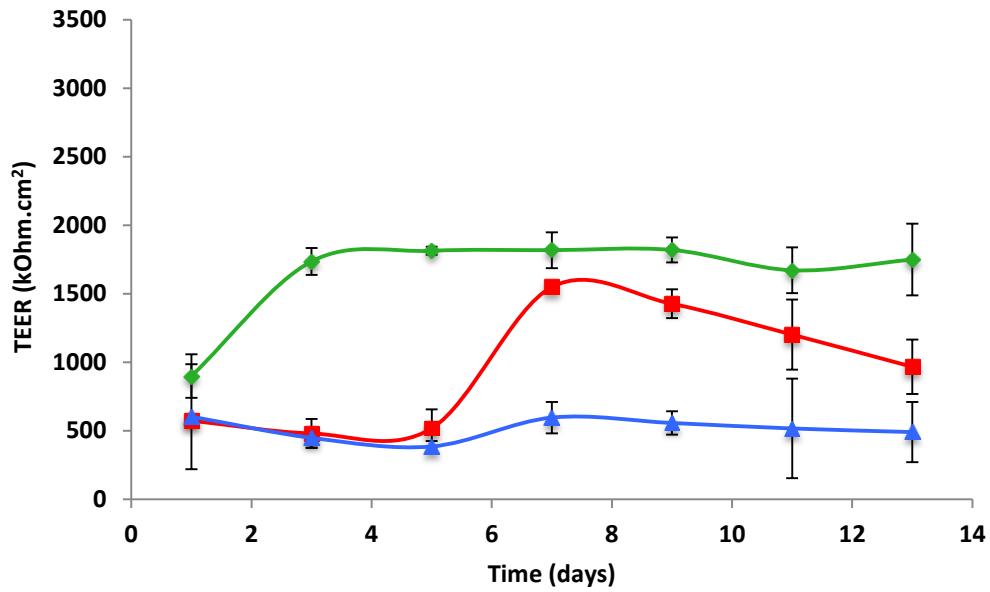


**Figure 5.18** – Functional TEER barriers (>1000 kOhm.cm<sup>2</sup>) were generated by control, BMI1 and hTERT overexpressing NHU cells at passage 3. TEER measurements (Section 2.5.5.2) for two NHU cell lines (P3) transfected with pLXSN BMI1, pLXSN hTERT or pLXSN empty vector. Error bars represent  $\pm$ SD for three replicate cultures.

At passage 6 (Figure 5.19) NHU cells from both NHU cell lines (Y1533 & Y1570) produced a lower TEER than at passage 3 (Figure 5.18). Cells overexpressing BMI1 (green) from both donor cell lines were able to generate a barrier at passage 6 with one donor cell line (Y1533) forming a barrier within three days. NHU cells overexpressing hTERT (red) from one donor cell line (Y1570) showed no significant difference in TEER throughout the time course compared to cells overexpressing BMI1. NHU cells overexpressing hTERT in the other donor cell line (Y1533) took longer to generate a TEER over 1500 kOhms.cm<sup>2</sup> compared to cells overexpressing BMI1 and were not able to maintain the TEER between days 7 and 13. NHU cells transfected with pLXSN empty vector (blue) had reduced TEER values compared to BMI1 and hTERT overexpressing cells. Y1533 empty vector cells at passage 6 failed to produce a barrier whereas Y1570 empty vector cells were able to generate a TEER of over 1500 kOhm.cm<sup>2</sup> however this took longer than in BMI1 and hTERT overexpressing cells and the TEER did not become as high as in the overexpressing cells.

Compared against cells at passage 3 (Figure 5.18) and passage 6 (Figure 5.19), BMI1 and hTERT overexpressing NHU cells at passage 10 (Figure 5.20) did not generate as high TEERs however, unlike NHU cells transfected with empty vector, which had become senescent, BMI1 and hTERT cells were able to produce a barrier. BMI1 overexpressing NHU cells generated barriers of approximately 1500 kOhm.cm<sup>2</sup>. hTERT overexpressing NHU cells produced lower TEERs and took longer to reach a maximum resistance. There was a significant difference between the TEERs generated between BMI1 and hTERT overexpressing NHU cells from the Y1533 donor line (solid bars) at passage 10 whereas NHU cells from the second, Y1570 donor line (dashed lines) produced similar TEER values after 9 days of culture.

Y1533



Y1570

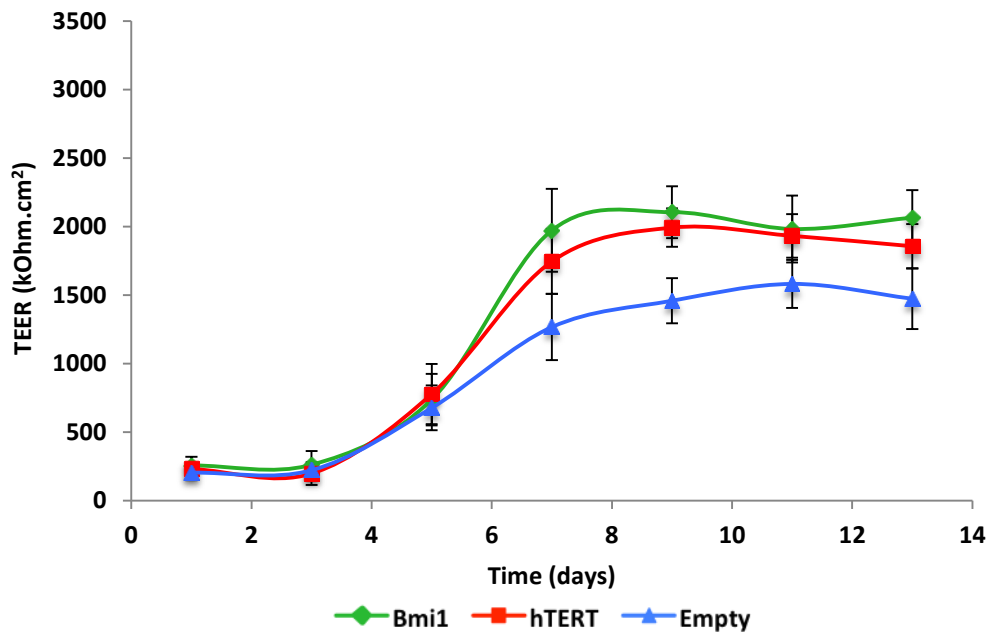
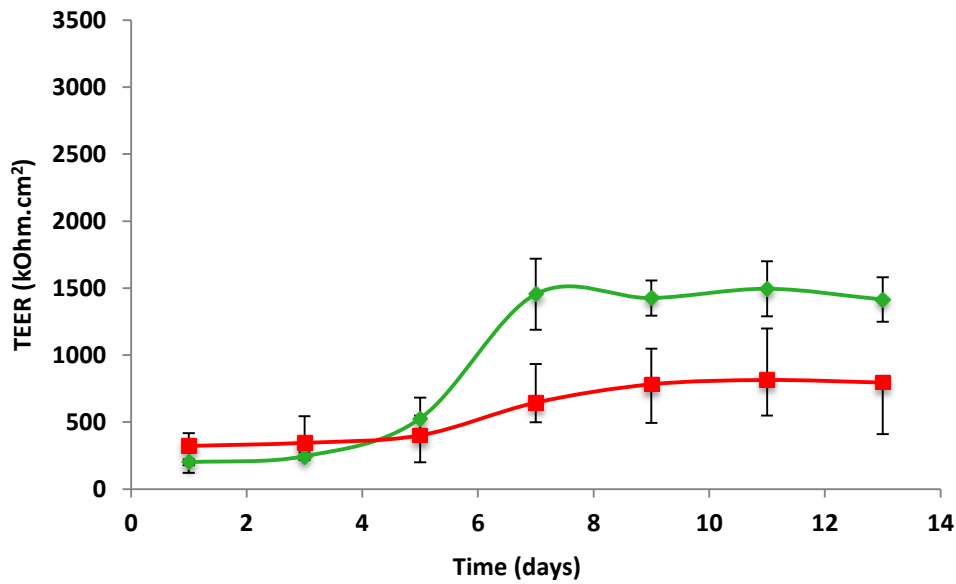


**Figure 5.19 - Functional TEER barriers (>1000 kOhm.cm<sup>2</sup>) were generated by control, BMI1 and hTERT overexpressing NHU cells at passage 6.** TEER measurements (Section 2.5.5.2) for two NHU cell lines (P6) transfected with pLXSN BMI1, pLXSN hTERT or pLXSN empty vector. Error bars represent  $\pm$ SD for three replicate cultures.

Y1533



Y1570

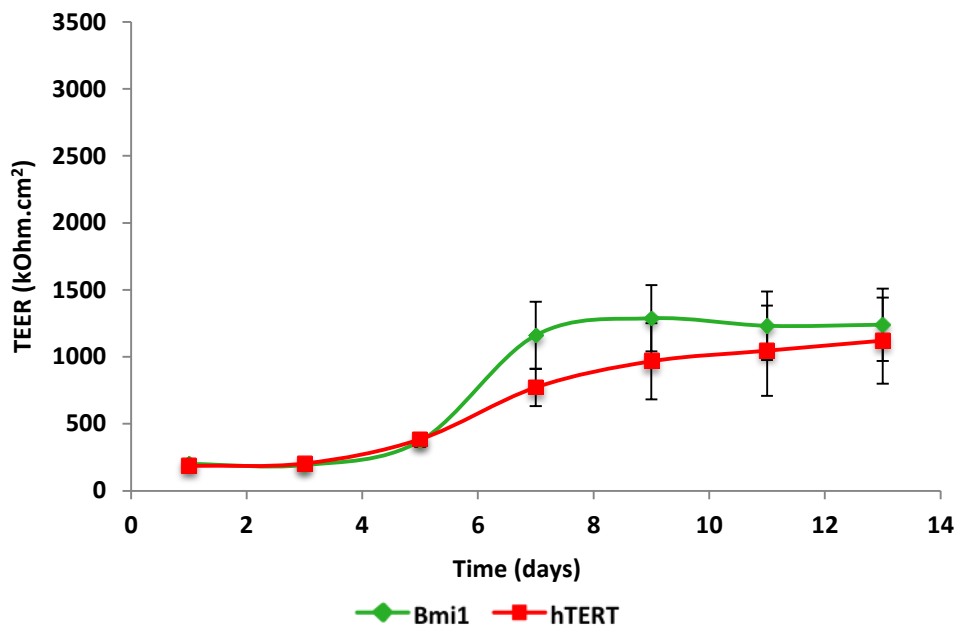


Figure 5.20 – BMI1 overexpressing NHU cells generated a functional TEER barrier (>1000 kOhm.cm<sup>2</sup>) at passage 10 unlike hTERT overexpressing NHU cells. TEER measurements (Section 2.5.5.2) for two NHU cell lines (P6) transfected with pLXSN BMI1, pLXSN hTERT or pLXSN empty vector. Error bars represent  $\pm$ SD for three replicate cultures.

## 5.5 Conclusions and Discussion

A BMI1 overexpressing retroviral plasmid was created and used to generate BMI1-overexpressing NRU and NHU cell lines. hTERT-overexpressing NRU and NHU cell lines were also generated using an existing pLXSN hTERT vector.

In NRU cells, overexpression of either BMI1 or hTERT did not increase cell lifespan in culture or allow cells to be subcultured further than untransduced cells. This is in contrast to BMI1 and hTERT-overexpressing NHU cells which continued to grow in culture for multiple passages after pLXSN empty vector control cells had become senescent.. BMI1 expressing NHU cells did not express hTERT, however, hTERT overexpressing NHU cells did express BMI1. A correlation between BMI1 and hTERT expression in cancerous cells has been established (Zhang et al., 2008) and in combination, BMI1 and hTERT overexpression has been used to immortalise a number of primary cell lines (Saito et al., 2005; Zhang et al., 2006; Haga et al., 2007). In hTERT immortalised oral epithelial cells, BMI1 activation was shown to occur and be crucial for cells retaining their immortalised phenotype and for epithelial-mesenchymal transition (Qiao et al., 2013). The lack immortalisation in NRU cells could be as a result of overexpressing human BMI1 in rats however this would seem unlikely due to the high sequence homology between human and rat BMI1 transcripts (appendix 2.3). The inability of hTERT overexpression to increase NRU cell lifespan could also be due to the difference between human and rat TERT that share approximately 75% identity.

Functionally, BMI1 and hTERT cells were capable of generating functional barriers *in vitro* at passage 6 and 10, when empty vector control cells were not capable of generating a high barrier. Variations between NHU cell lines could be as a result of differences between donors, highlighting the requirement for these results to be replicated in additional NHU cell lines from multiple donors. At passage 10, BMI1-overexpressing NHU cells were capable of generating higher TEERs than hTERT-overexpressing NHU cells but TEERs were reduced compared against those achieved at P3 and P6.

## 5.6 Key Findings

- Retrovirus for overexpression of human BMI1 was successfully generated
- BMI1 and hTERT-overexpression failed to immortalise NHU cell lifespan in culture, despite evidence of successful overexpression.
- BMI1-overexpressing NHU cell proliferation was comparable to that of NHU cells overexpressing hTERT
- BMI1 and hTERT-overexpressing NHU cells were capable of generating functional barriers at P6 and P10.

## Chapter 6 - Induction of Urothelial Cytochrome P450 2B expression *in vivo* and *in vitro*

<b>6.1 Chapter Introduction .....</b>	<b>176</b>
6.1.1 Cellular Metabolism .....	176
6.1.2 Xenobiotic metabolism in humans and rats .....	176
6.1.3 Cytochrome P450 enzymes.....	178
6.1.4 CYPs and the bladder .....	179
6.1.5 Modelling CYPs <i>in vitro</i> .....	181
<b>6.2 Aim .....</b>	<b>183</b>
6.2.1 Objectives.....	183
<b>6.2 Experimental approach.....</b>	<b>184</b>
6.2.1 CYP2B induction <i>in vivo</i> .....	184
6.2.2 CYP2B induction <i>in vitro</i> .....	184
6.2.3 CYP2B induction in <i>ex vivo</i> organ culture models.....	184
6.2.4 Cell lines .....	185
<b>6.3 Results .....</b>	<b>186</b>
6.3.1 CYP2B expression in rat urothelium .....	186
6.3.2 CYP2B homologue expression in rat urothelial cells.....	193
6.3.4 Rat <i>In vivo</i> case study – chemical induction of CYP2B .....	196
6.3.4 Investigation of urothelial CYP2B expression <i>in vitro</i> .....	200
<b>6.4 Conclusions and Discussion .....</b>	<b>208</b>
<b>6.5 Key findings.....</b>	<b>208</b>

## 6.1 Chapter Introduction

### 6.1.1 Cellular Metabolism

Cellular metabolism involves a series of enzyme-catalysed reactions within cells, resulting in the transformation of a compound to its metabolites. Metabolic reactions can be divided into either catabolism or anabolism, both of which are essential for all living cells. Catabolism involves the breakdown of large molecules into their smaller components, with digestion of food being a key example. Anabolism, alternatively, is the addition of reactive groups or molecules to a compound in order to synthesise complex molecules. One important example of anabolism is the metabolism of xenobiotics (discussed by Iyanagi, 2007)

Xenobiotics are compounds foreign to an organism that, if allowed to accumulate, could cause toxicity or other damage. These can include compounds that organisms are inadvertently or advertently exposed to in their environment or by ingestion. Pharmaceutical agents, pesticides and natural poisons are all examples of xenobiotics that humans are routinely exposed to and which have to be cleared from body in order to prevent toxicity (discussed by Omiecinski et al., 2011).

### 6.1.2 Xenobiotic metabolism in humans and rats

Differences in isoform composition, expression, localisation and catalytic activities exist between the metabolic enzymes of humans and rats. Such differences can have significant impacts on the rate and mechanism of xenobiotic metabolism, affecting the activity of a compound and its metabolites (Martignoni et al., 2006).

Cellular metabolism of xenobiotics occurs predominantly in the liver and consists of two distinct phases (illustrated in Figure 6.1). Phase I involves the addition of polar or reactive groups to the target compound and is largely conducted by the cytochrome P450 (CYP) superfamily of enzymes. Phase I metabolism by CYPs accounts for approximately 75% of the total metabolism of pharmaceutical agents. Phase II metabolic enzymes such as UDP-glucuronosyltransferases,

methyltransferases, sulfontransferases and glutathione S-transferases are then able to add complex, water-soluble molecules to the phase I (intermediate) metabolite in conjugation reactions. The conjugated xenobiotic metabolite is then excreted from cells, where it can either be immediately eliminated from the body, for example by glomerular filtration in the kidneys, or undergo further (phase III) metabolism prior to elimination (reviewed by Jancova et al., 2010).

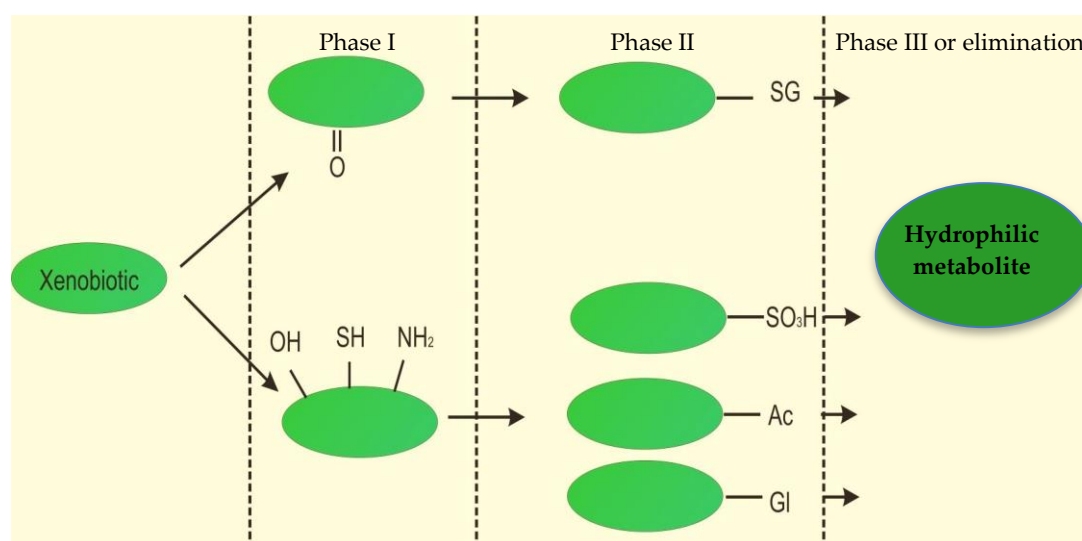


**Figure 6.1 – Illustration of Phase I and Phase II xenobiotic metabolic reactions.** Phase I metabolism, predominantly conducted by CYPs, involving oxidation of electrophilic xenobiotics or reduction of nucleophilic xenobiotics. Phase II conjugation reactions then take place to add glutathione groups (SG) sulfate groups (SO<sub>3</sub>H), acetyl groups (Ac) and glucuronide groups (GI) to the phase I metabolite, rendering the compound inactive. Phase II metabolites are then further metabolised or immediately removed from the body.

Through the addition of polar or reactive groups, phase I metabolism can generate active metabolites or metabolites with increased activity compared to the original compound. This has been exploited in the cases of pharmaceutical prodrugs, including cyclophosphamide (used in the treatment of cancer and autoimmune diseases) and codeine (used as an analgesic), which need to be metabolised into active metabolites in order to have their intended effects. The illicit drug heroin also requires metabolism to its active compounds in order to cause euphoria. Metabolic activation of xenobiotics can result in toxicity if the metabolite is produced in high enough quantities, as is the case when the rate of phase I metabolism exceeds that of

phase II (reviewed by Ekins and Wrighton, 1999; reviewed by Turpeinen et al., 2006).

### 6.1.3 Cytochrome P450 enzymes

The cytochrome P450 (CYP) superfamily of enzymes are primarily responsible for phase I metabolism. CYPs can be constitutively or inducibly expressed in multiple tissues and play an important role in the metabolism of both xenobiotics and endogenous molecules (reviewed by Anzenbacher and Anzenbacherová, 2001). Mammalian CYPs are membrane-associated proteins located in mitochondria or the endoplasmic reticulum. CYPs are terminal oxidase enzymes in electron transfer chains (Meunier et al., 2004). To function, CYP enzymes require additional proteins such as cytochrome P450 reductase (CPR) and NADPH electron donor.

CYPs are most highly expressed in the liver, where their expression profiles and characteristics have been extensively studied, but they are also expressed in other organs including the intestine, kidneys, heart, lungs and bladder (Zhang et al., 1999; Knights et al., 2013; reviewed by Chaudhary et al., 2009; Hukkanen et al., 2002; Brauers et al., 2000; Bieche et al., 2007).

In humans, there are 57 CYP genes and more than 60 CYP pseudogenes, divided into 18 different families that are indicated by a number (e.g. CYP1). Within each family there are multiple subfamilies, indicated by a letter (e.g. CYP1A), and within each subfamily individual enzymes are identified by a number (e.g. CYP1A1). Members of the CYP1, CYP2, and CYP3 families are almost exclusively responsible for pharmaceutical compound metabolism in humans. The other CYP families are involved in the metabolism of endogenous molecules such as vitamin D and retinoic acid (detailed by Sim and Ingelman-Sundberg, 2010). The specific CYPs that conduct the majority of pharmaceutical compound metabolism are illustrated in Figure 6.2, which denotes the percentage of pharmaceutical compounds they metabolise.

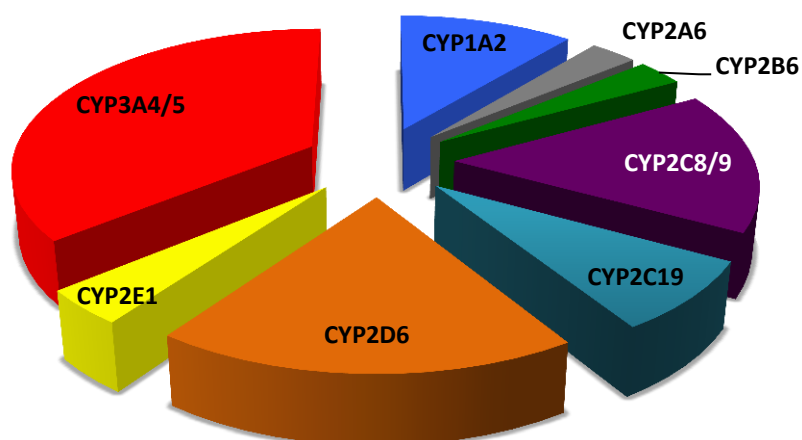


**Figure 6.2 – percentage of total CYP metabolism of pharmaceutical agents by the individual CYP enzymes.** The 8 CYP enzymes responsible for pharmaceutical agent metabolism and the percentage of pharmaceutical agents they metabolise are depicted (adapted from Wrighton and Stevens, 1992).

The expression of CYPs by different tissues can have important ramifications for drug discovery and for predicting xenobiotic toxicity, as expression in the target tissue may modulate the effect or activity of a particular drug.

#### 6.1.4 CYPs and the bladder

Many known bladder toxicants are known to be metabolised to active states by cytochromes including acrylamides, cyclophosphamide and 4-aminobiphenyl (Turpeinen et al., 2006; Ingelman-Sundberg, 2004; Ekhardt et al., 2008). If this metabolism were to occur within the bladder, it would localise the toxicity and subject the urothelium to potentially harmful concentrations of active carcinogens.

Multiple CYPs including CYP1A1, CYP1A2, CYP1B1, CYP2D6 and CYP2E1 have all been shown to be expressed in the bladder, with several other CYPs expressed by urothelial carcinomas (Brauers et al., 2000). The CYP2B family of enzymes responsible for metabolism of xenobiotics including cyclophosphamide, methadone,

tamoxifen and ifofamide have not been investigated in the urothelium (Ekins and Wrighton, 1999; Gervot et al., 1999). CYP2Bs are not constitutively expressed, but instead require induction by xenobiotics such as phenobarbital in order to be present in a tissue and as such are not identified under control conditions (reviewed by Wang and Tompkins, 2008). Regulation of CYP2B induction by phenobarbital is known to involve constitutive androstane receptor (CAR), which translocate to hepatocyte nuclei in response to phenobarbital treatment (Gervot et al., 1999). The phenobarbital-responsive enhancer module (PBREM), which is highly conserved in humans and rats, is a 51 base pair DNA sequence containing two DR4 nuclear receptor response elements, NR1 and NR2. CAR heterodimerises with the retinoid X receptor (RXR) in response to phenobarbital-induced nuclear translocation. The CAR-RXR heterodimer has high affinity for the NR1 site of the PBREM and binding results in the induction of CYP2B genes (Kawamoto et al., 1999; Kodama and Negishi, 2006). A second member of the orphan nuclear receptor family, Pregnane X Receptor (PXR), is also known to bind to the PBREM and the similar xenobiotic response enhancer module (XREM) to activate CYP2B expression (Goodwin et al., 2001).

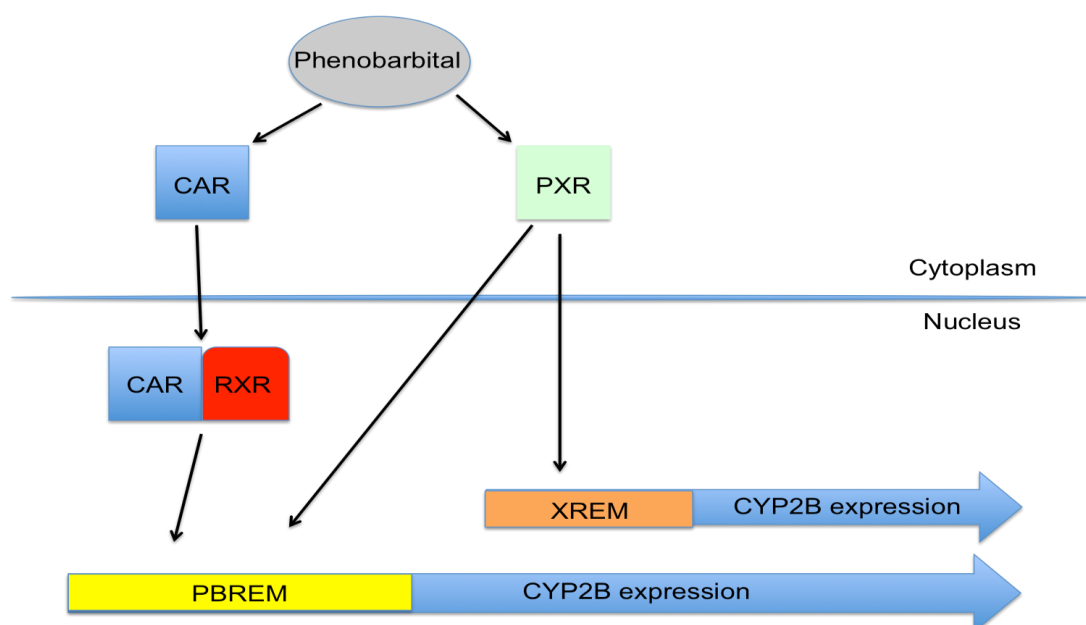


**Figure 6.3 - Phenobarbital induces nuclear translocation of CAR where it heterodimerises with RXR to bind to the PBREM, facilitating CYP2B gene expression. Phenobarbital also induces PXR to bind to either PBREM or XREM, also facilitating CYP2B gene expression.**

CAR-mediated regulation of CYP2B expression is known to be sexually dimorphic in certain rat strains, such as Wistar and the Wistar Kyoto (WKO) rats, in which phenobarbital-induced CAR translocation and PBREM activation only occurred in male rats. Such discrepancies between sexes were not observed in Fisher 344 rats (Yoshinari et al., 2001). Human CYP2B expression varies greatly between males and females and between different ethnic populations. Females have increased CYP2B1 mRNA, protein and enzyme activity compared to males. Hispanic populations were found to have greater CYP2B1 expression and activity than Caucasian or African populations. In females a clear genotype-phenotype association has been demonstrated in which gene expression is a clear indicator of activity, whereas in males such an association could not be established (Lamba et al., 2003).

Humans express two CYP2B homologues, namely CYP2B6 and CYP2B7, with CYP2B6 being the most abundant and important in terms of xenobiotic metabolism (reviewed by Wang and Tompkins, 2008). In rats, six CYP2B homologues are expressed (CYP2B1, CYP2B2, CYP2B3, CYP2B12, CYP2B15 and CYP2B21), with CYP2B1 and CYP2B2 often considered as equivalent to CYP2B6 in humans (Desrochers et al., 1996; Du et al., 2004; Keeney et al., 1998). Along with CYP2B3, CYP2B1 and CYP2B2 are most abundantly expressed by hepatocytes, but have also been found in lung and gastrointestinal tract epithelial cells (Mitschke et al., 2008; Czekaj et al., 2000)

### 6.1.5 Modelling CYPs *in vitro*

Primary hepatocytes are capable of retaining a differentiated phenotype *in vitro* for a limited period, however, they suffer a reduction in CYP expression over time and have a limited lifespan in culture (Abdel-Razzak et al., 1993). Immortalised hepatocyte cell lines have limited or no metabolic functions and hence are not useful tools to study xenobiotic metabolism *in vitro* (Westerink and Schoonen, 2007). As such, *in vivo* models or isolated microsomes from primary cells are used to investigate CYP metabolism.

*In vitro* systems are a desirable platform for studying CYP metabolism. The generation of a metabolically-functional *in vitro* system has thus far proved illusive but, if achieved, would be of significant benefit to investigators of xenobiotic metabolism and toxicity.

## 6.2 Aim

To investigate the potential of urothelial cells to express CYP2B enzymes after treatment with CYP2B- inducing compounds both *in vivo* (rat) and *in vitro* (rat and human).

### 6.2.1 Objectives

1. Determine whether CYP2B induction occurs in rat urothelial cells after *in vivo* exposure to phenobarbital
2. Investigate which CYP2B enzyme is expressed by rat urothelial cells after *in vivo* exposure to phenobarbital
3. Explore the potential of an experimental CYP2B-inducing compound to induce rat urothelial cell CYP2B expression *in vivo*.
4. Assess the ability of urothelium in rat and human cell and organ culture systems to express CYP2B enzymes.

## 6.2 Experimental approach

### 6.2.1 CYP2B induction *in vivo*

Surplus bladder and liver tissue was collected from Syngenta studies where rats had been dosed with phenobarbital or a compound under development that was shown to induce CYP2B activation in the liver. Bladders were collected from untreated control and treated rats upon sacrifice. Tissue was either formalin-fixed and processed into paraffin wax for histology, or the urothelium was harvested for RNA isolation using the dispase protocol (see chapter 3). CYP2B1/2 labelling in urothelium from control and treated rats was quantified using image analysis software (Tissue Gnostics). >1000 urothelial cells were analysed per bladder to provide an arbitrary DAB intensity labelling score. Control and phenobarbital-treated rat liver sections were used as controls.

### 6.2.2 CYP2B induction *in vitro*

NRU and NHU cells were isolated and cultured as previously described (see chapters 2 and 3). Cells were dosed with phenobarbital (500  $\mu\text{M}$ ) at concentrations reported to induce CYP2B expression in the literature (Sidhu and Omiecinski, 1995; Joannard et al., 2006). CYP2B induction was investigated at different time points up to 72 hours by RNA analysis and western blotting. Negative (medium only) controls were included as comparisons.

### 6.2.3 CYP2B induction in *ex vivo* organ culture models

Rat bladders were dissected into quarters and cultured urothelium-side up on PET cell culture inserts (pore size 3  $\mu\text{m}$ ) at a liquid interface. Phenobarbital was added to the medium both above and below the membrane. Tissue was treated for 72 hours before either formalin-fixation and paraffin wax embedding for immunohistochemistry or the urothelium separated using the dispase protocol (see chapter 3) and RNA isolated for analysis.

## 6.2.4 Cell lines

Table 6.1 NRU Cells

Code	No. of animals	Sex	Source	Strain	Age/Weight
R051	20	M/F	University of Manchester	Wistar	200-300 g
R053	6	F	University of York	Wistar	200-250 g
R054	5	F	University of York	Wistar	200-250 g

Table 6.2 NHU Cells

Code	Tissue of Origin	Sex	Age	Age of cells during experiments
Y1533	Ureter	M	45	P1-4
Y1570	Ureter	F	51	P1-4

## 6.3 Results

### 6.3.1 CYP2B expression in rat urothelium

Immunolabelling using antibodies against CYP2B1/2 was conducted on bladder sections from control and phenobarbital-treated (dietary 1200 ppm) rats (male and female) after 3, 7 and 14 days of treatment. After three days (Figure 6.4), urothelial cells from phenobarbital-treated rat bladders showed a high intensity of labelling compared to control animals. The pattern of immunolabelling appeared perinuclear and was present throughout the urothelium in phenobarbital-treated animals. Individual variations were noted within the phenobarbital-treated group, with one bladder having a visibly lower intensity of labelling compared to the others, but still higher than the controls. Urothelium from control rats was very low to completely absent of CYP2B1/2 labelling. At the 7 (Figure 6.5) and 14-day (Figure 6.6) time points, phenobarbital-treated animals also had an obvious increased intensity of CYP2B1/2 labelling than controls. As with the 3-day time point, individual variations in CYP2B1/2 expression existed between phenobarbital-treated animals, but in all cases, labelling was more intense than the controls.

Liver sections from control and phenobarbital-treated rats were included as negative and positive controls, respectively (Figure 6.7). At the different magnifications shown, CYP2B1/2 labelling was apparent surrounding blood vessels in the phenobarbital-treated liver sections but was almost completely absent in the livers of control animals. Negative controls from which primary antibody was omitted were included and showed no labelling (Appendix 2.4).

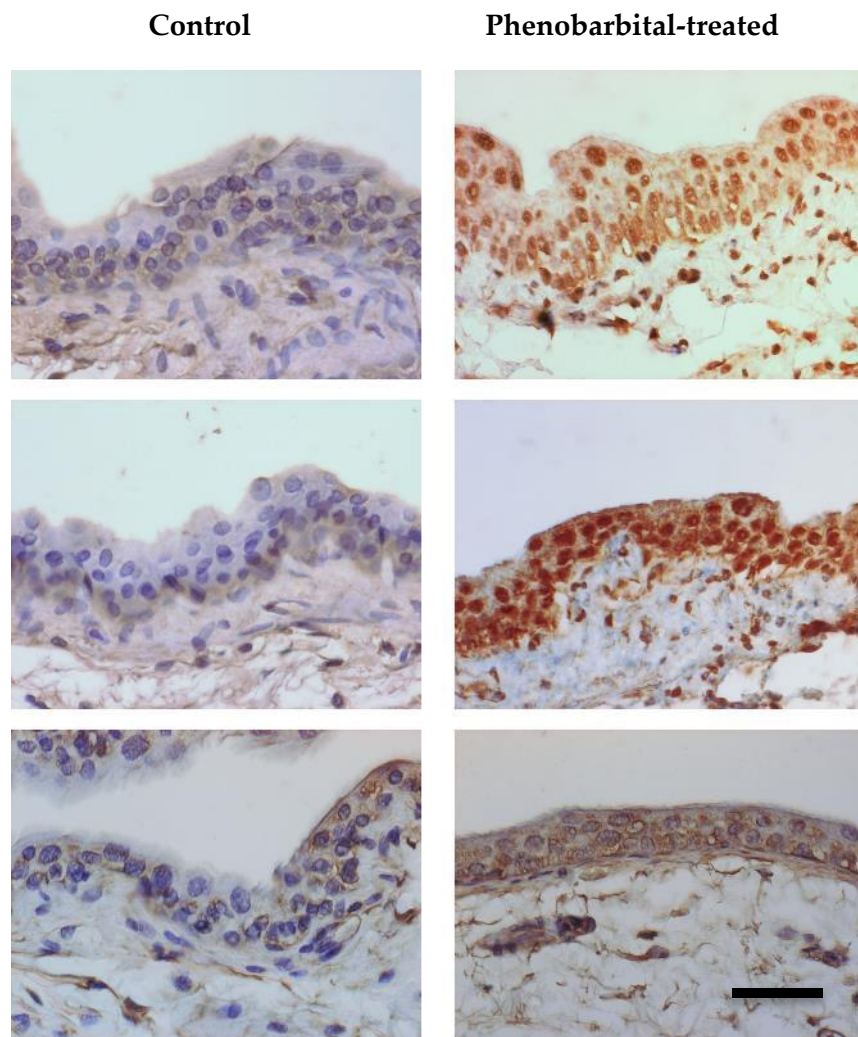


**Figure 6.4** – CYP2B1/2 expression was induced in rat bladders after 3 days of phenobarbital treatment *in vivo*. CYP2B1/2 was immunolabelled (Section 2.7.2) in control and phenobarbital-treated rat urothelium after 3 days of treatment. Scale bars = 50  $\mu\text{m}$  (n=3 individual rats).

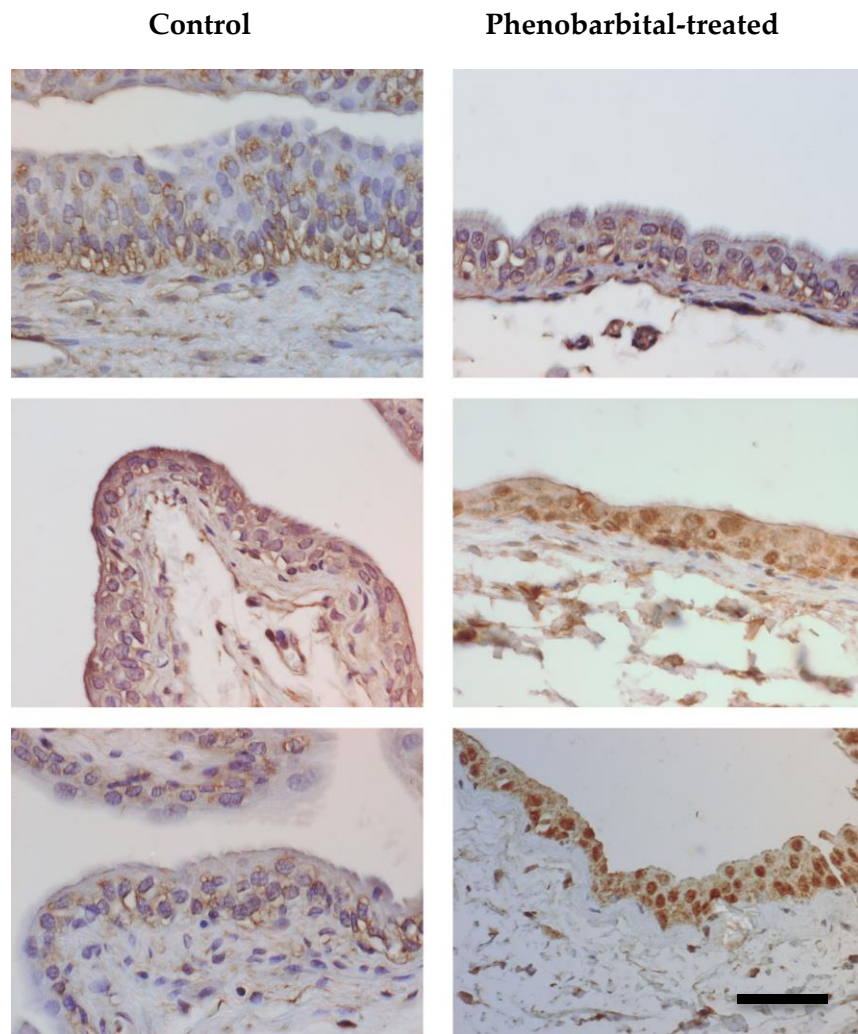


**Figure 6.5** - CYP2B1/2 expression was induced in rat bladders after 7 days of phenobarbital treatment *in vivo*. CYP2B1/2 was immunolabelled (Section 2.7.2) in control and phenobarbital-treated rat urothelium after 7 days of treatment. Scale bars = 50  $\mu\text{m}$  (n=3 individual rats).

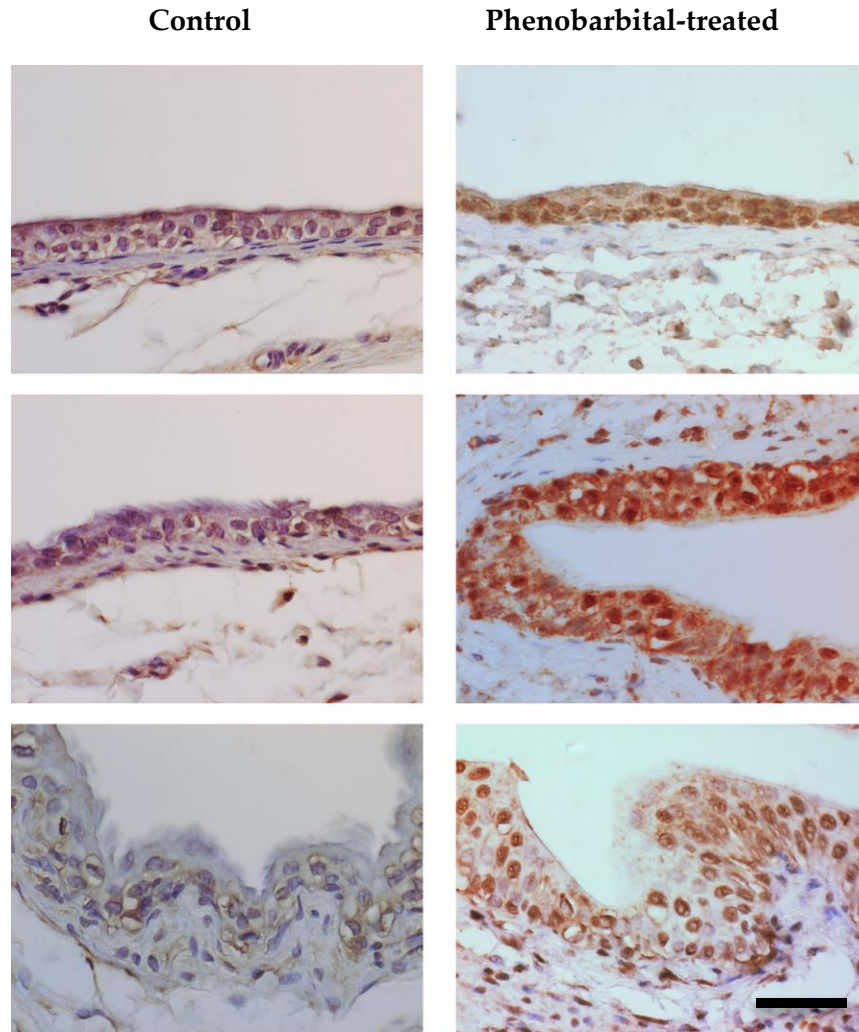


**Figure 6.6** – CYP2B1/2 expression was induced in rat bladders after 14 days of phenobarbital treatment *in vivo*. CYP2B1/2 was immunolabelled (Section 2.7.2) in control and phenobarbital-treated rat urothelium after 14 days of treatment. Scale bars = 50  $\mu\text{m}$  (n=3 individual rats).

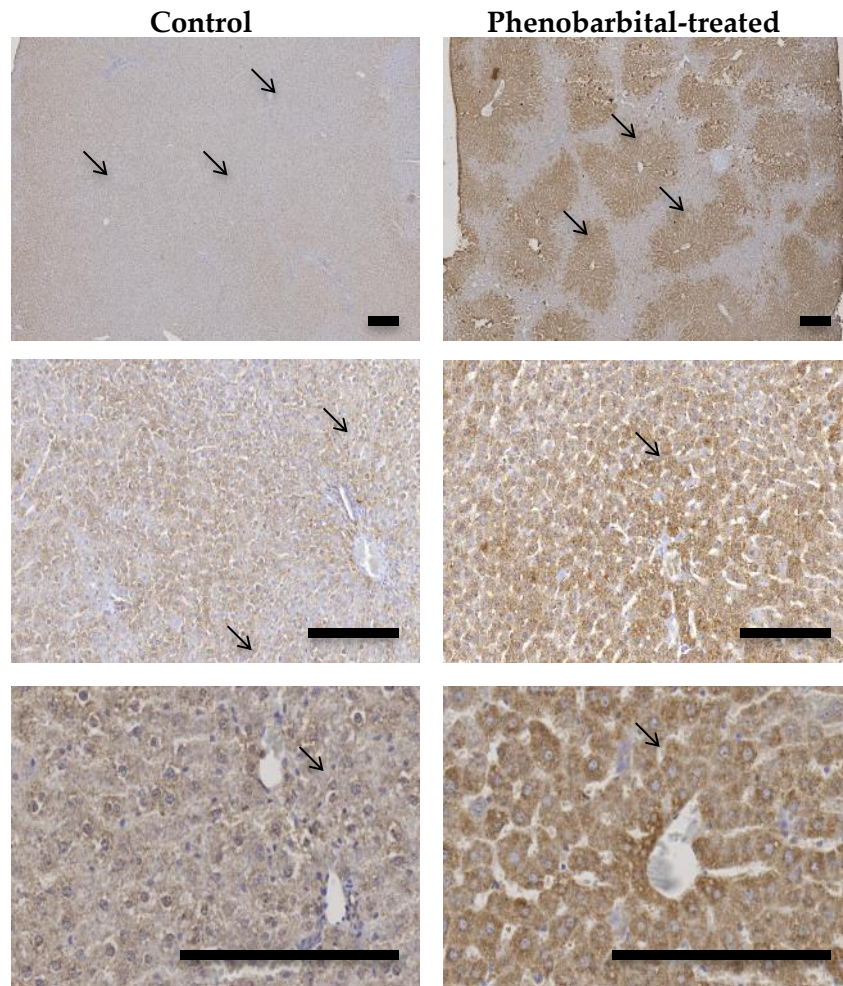


**Figure 6.7** – CYP2B1/2 was expressed by hepatocytes in close proximity to blood vessels in phenobarbital-treated by not control rat livers after 7 days of treatment *in vivo*. CYP2B1/2 was immunolabelled (Section 2.7.2) in control and phenobarbital-treated rat liver sections after 7 days of dietary administration. Sections are shown at multiple magnifications to illustrate the specific labelling pattern around blood vessels (indicated by arrows) in phenobarbital-treated animals. Scale bars = 200  $\mu\text{m}$  (n = 3 individual rats).

Quantification of urothelial CYP2B labelling (Figure 6.8) revealed significant increases in labelling intensity between control and phenobarbital-treated urothelial cells at each time point and also an increase between phenobarbital-treated urothelial cells from days 3 and 14. A significant difference was also shown between control and phenobarbital-treated hepatocytes.

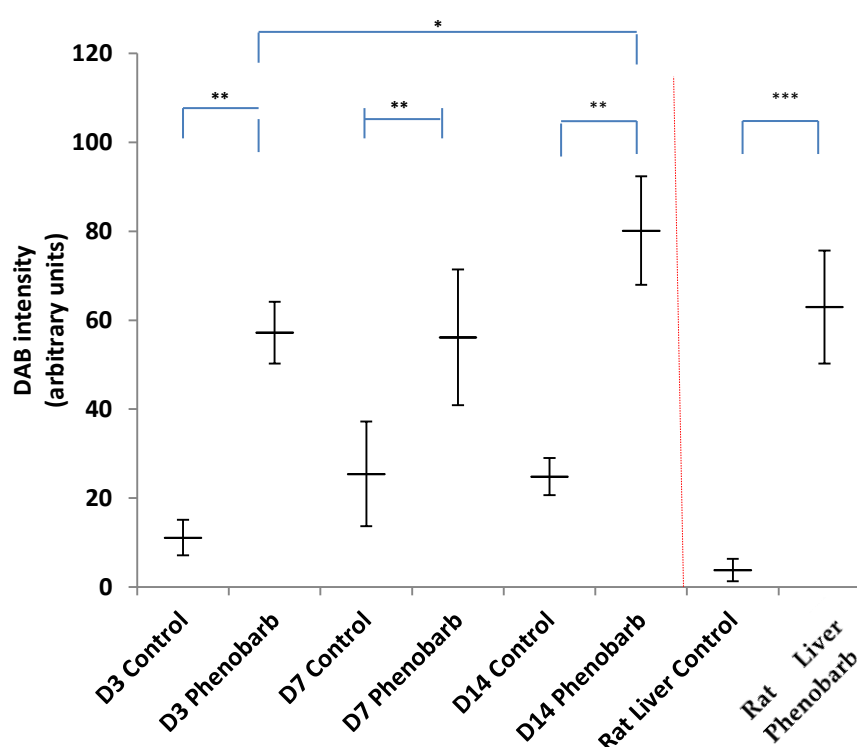


**Figure 6.8 - CYP2B1/2 expression was significantly increased in phenobarbital-treated rat urothelium compared to controls.** Computational quantification (Section 2.7.3) of urothelial CYP2B1/2 immunolabelling in control and phenobarbital-treated rats after 3 (D3), 7 (D7) and 14 (D14) days dietary administration was conducted. Mean DAB intensity in >1000 urothelial cells from three rat bladders per treatment/time group were generated using TissueGnostics software after CYP2B immunolabelling. Error bars  $\pm$  SD (n=3). (\* =  $p < 0.05$ , \*\* =  $p < 0.01$ , \*\*\* =  $p < 0.001$ , using a 2-way ANOVA with a Tukeys post hoc test of comparison).

To support the immunolabelling results, RT-PCR was conducted on urothelial cDNA from 5 control and 5 phenobarbital-treated animals after 7 days of treatment (Figure 6.9) Generic CYP2B primers, designed to amplify all rodent CYP2B homologues, showed clear expression of CYP2B enzymes in the urothelium of 2 control and 5 phenobarbital-treated rats. While showing the ability of rat urothelial cells to express CYP2B in response to phenobarbital, this result also demonstrated a high level of individual variation between animals: a result observed when visually assessing urothelial CYP2B labelling.

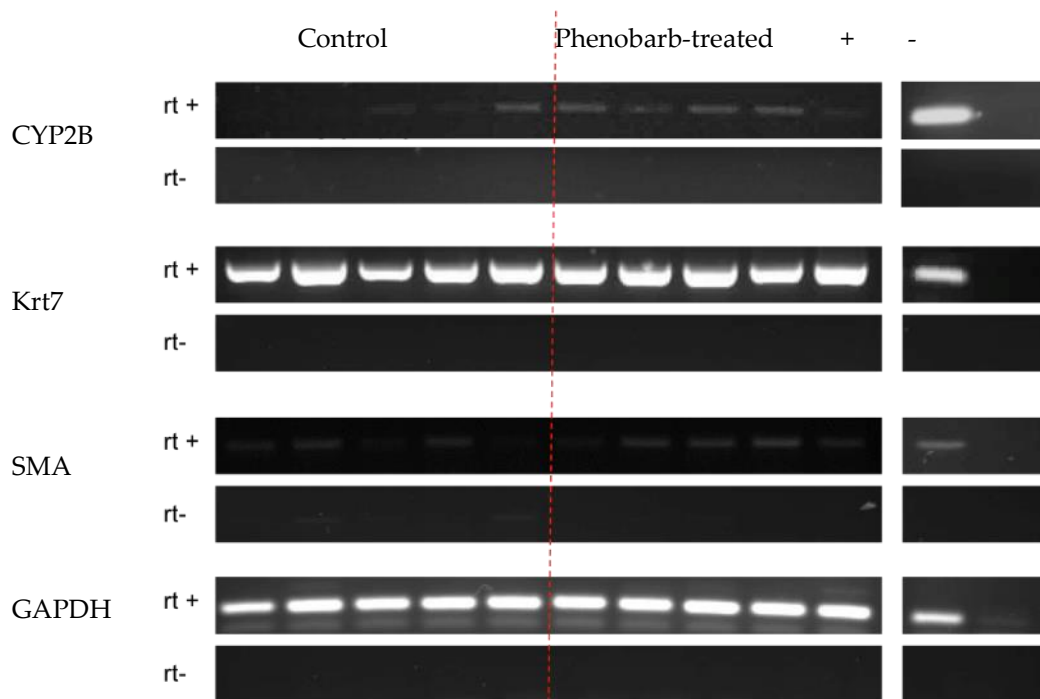


**Figure 6.9 – CYP2B enzymes were expressed in rat urothelial cells after 7 days of dietary phenobarbital treatment.** RT-PCR of CYP2B expression in rat urothelial cDNA after 7 days of treatment with a vehicle control or phenobarbital. Krt7 was included as a control urothelial cell marker, smooth muscle actin (SMA) as a marker of stromal cell contamination and GAPDH as a loading control. Positive (+) and negative (-) primer controls were rat liver cDNA (CYP2B & GAPDH), normal rat urothelial cell cDNA (Krt7) and rat genomic DNA (SMA). Negative (no template) control substituted water for cDNA. Reverse transcriptase negative (RT-) samples were also included alongside reverse transcriptase positive (RT+) samples as controls for genomic DNA contamination.

### 6.3.2 CYP2B homologue expression in rat urothelial cells

Primers were designed to specifically amplify each of the 6 CYP2B homologues present in the rat genome and RT-PCR was conducted on urothelial cDNA from five control and five phenobarbital (day 7) treated rats (Figure 6.10). Primers designed to individually amplify both CYP2B1 (lower band) and CYP2B2 (higher band) produced weak bands in one control and two phenobarbital-treated rat urothelial samples. CYP2B3 amplifying primers also produced weak results in three phenobarbital-treated samples. CYP2B12 and CYP2B15 primers did not generate bands from either control or phenobarbital-treated samples. CYP2B21 primers produced weak bands in two phenobarbital-treated samples.

Together, the RT-PCR results presented a confusing picture of CYP2B expression by the urothelium, with multiple homologues being expressed in some but not all of the individual rats after 7 days of phenobarbital treatment. To further clarify which homologues were expressed, the PCR product amplified from cDNA using generic CYP2B primers (Figure 6.9) from one control and five phenobarbital-treated urothelial samples was TA-cloned into a vector, transformed into bacteria and single clones isolated, cloned and sequenced. Based on specific base pair differences between CYP2B homologues, individual enzymes were identified as expressed (Figure 6.10). Although this approach was not quantitative, it was unequivocal in demonstrating the expression of five out of six CYP2B homologues by phenobarbital-induced rat urothelial cells. CYP2B1, as in the RT-PCR results (Figure 6.9), was found to be absent.

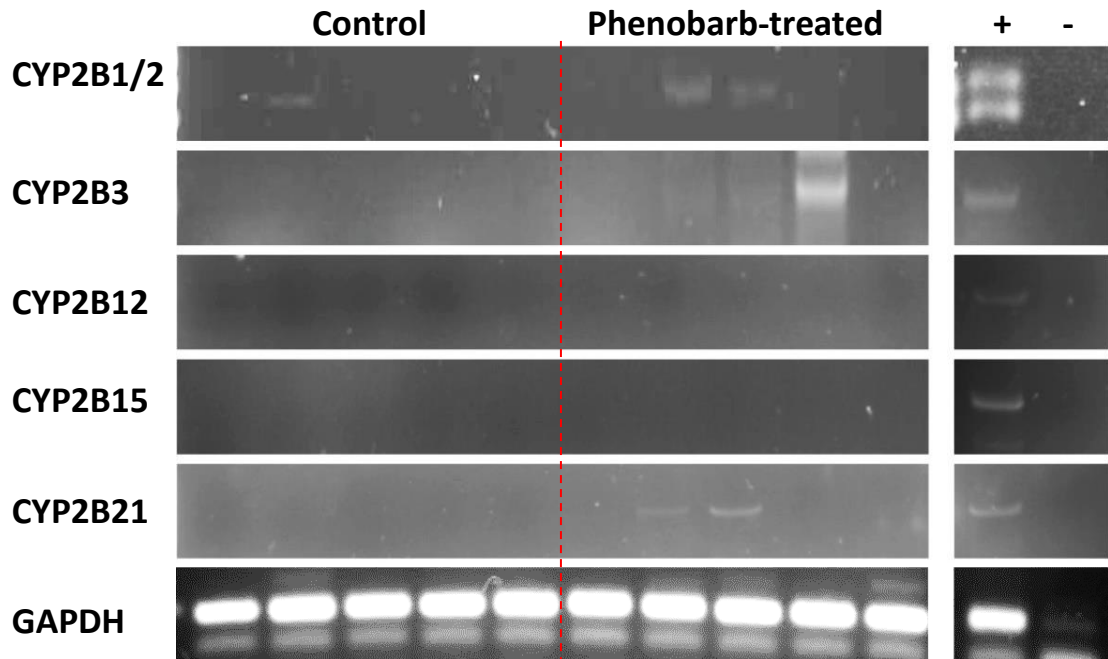


**Figure 6.10** – The specific CYP2B enzyme expressed in rat urothelial cells was not able to be confirmed by RT-PCR. RT-PCR (30 cycles) was conducted on control or 7-day phenobarbital-treated rat urothelial cDNA. Specific primers were designed to amplify each of the 6 CYP2B enzymes found in rat. GAPDH was included as a loading control. Positive (+) control cDNA and negative (-) no template (water) controls were included for each primer set. Rat liver cDNA was used as a control for CYP2B1/2, CYP2B3, CYP2B12, CYP2B15 and for GAPDH primers. Rat skin cDNA was used as positive control for CYP2B21 primers.

```

CONTROL 1 AGGAGATTGATCAGGTGATGGCTCACACCGGCTACCAACCCCTGATGATCGTACCA
CONTROL 1 AGGAGATTGATCAGGTGATCGGCTCACAGCGGGTCCCAACCCCTTGATGACCGCTCCA
PHENOB. 1 AGGAGATTGATCAGGTGATGGCTCCTCACAGGCCACCATCCCTTGATGATCGTACCA
PHENOB. 1 AGGAGATTGATCAGGTGATGGCTCCTCACAGGCCACCATCCCTTGATGATCGTACCA
PHENOB. 2 AGGAGATTGATCAGGTGATGGCTCACACCGGCTACCAACCCCTGATGATCGTACCA
PHENOB. 2 AGGAGATTGATCAGGTGATCAGCTCACACCGGCTACCAACCCCTTGATGATCGTATCA
PHENOB. 3 AGGAGATTGATCAGGTGATGGCTCACACCGGCTACCAACCCCTTGATGATCGTACCA
PHENOB. 3 AGGAGATTGATCAGGTGATCGGCTCACAGCGGGTCCCAACCCCTTGATGACCGCTCCA
PHENOB. 4 AGGAGATTGATCAGGTGATCGGCTCACAGCGGGTCCCAACCCCTTGATGACCGCTCCA
PHENOB. 4 AGGAGATTGATCAGGTGATGGCTCCTCACAGGCCACCATCCCTTGATGATCGTACCA
PHENOB. 5 AGGAGATTGATCAGGTGATGGCTCACACCGGGTCCCAACCCCTTGATGACCGCATCA

```

```

CONTROL 1 AAATGCCATAACTGATGCAGTCATCCACGAGATTCAGAGATTTGCAGATCTGACCCC
CONTROL 1 AAATGCCATACACTGAGGCAGTCATCCATGAGATTCAGAGATTTCTGATGTTTCTCC
PHENOB. 1 AAATGCCATACACTGATGCAGTCATCCACGAGATTCAGAGATTTGCAGATCTTGCCCC
PHENOB. 1 AAATGCCATACACTGATGCAGTCATCCACGAGATTCAGAGATTTGCAGATCTTGCCCC
PHENOB. 2 AAATGCCATAACTGATGCAGTCATCCACGAGATTCAGAGATTTGCAGATCTTGCCCC
PHENOB. 2 AAATGCCATACACTGATGCAGTCATCCACGAGATTCAGAGATTTGCAGATCTTGCCCC
PHENOB. 3 AAATGCCATAACTGATGCAGTCATCCACGAGATTCAGAGATTTGCAGATCTTGCCCC
PHENOB. 3 AAATGCCATACACTGAGGCAGTCATCCATGAGATTCAGAGATTTCTGATGTTTCTCC
PHENOB. 4 AAATGCCATACACTGAGGCAGTCATCCATGAGATTCAGAGATTTCTGATGTTTCTCC
PHENOB. 4 AAATGCCATACACTGATGCAGTCATCCACGAGATTCAGAGATTTGCAGATCTTGCCCC
PHENOB. 5 AAATGCCATACACTGATGCGGTCATCCATGAGATTCAGAGATTTTCAGATCTTGTTCC

```

```

CONTROL 1 AATTGGTCTACCACACAGATCACCAAAGACACCGTGTTCGGAGGGTACCTGCTA
CONTROL 1 AATGGGTTTGCCATGCAGAATCACCAAAGACACATGTTCGGAGGGTACCTGCTA
PHENOB. 1 AATTGGTTTACCACACAGATCACCAAAGACACCATGTTCGGAGGGTACCTGCTA
PHENOB. 1 AATTGGTTTACCACACAGATCACCAAAGACACCATGTTCGGAGGGTACCTGCTA
PHENOB. 2 AATTGGTCTACCACACAGATCACCAAAGACACCATGTTCGGAGGGTACCTGCTA
PHENOB. 2 AATTGGTTTACCACACAGATCACCAAAGACACCATGTTCGGAGGGTACCTGCAA
PHENOB. 3 AATTGGTCTACCACACAGATCACCAAAGACACCATGTTCGGAGGGTACCTGCTA
PHENOB. 3 AATGGGTTTGCCATGCAGAATCACCAAAGCCACATGTTCGGAGGGTACCTGCTA
PHENOB. 4 AATGGGTTTGCCATGCAGAATCACCAAAGACACATGTTCGGAGGGTACCTGCTA
PHENOB. 4 AATTGGTTTACCACACAGATCACCAAAGACACCATGTTCGGAGGGTACCTGCTA
PHENOB. 5 AATTGGTCTGCCACACAGATCACCAAAGACACAAATGTTCGGAGGGTACCTGCTA

```

CYP2B2	CYP2B3	CYP2B12	CYP2B15	CYP2B21

Figure 6.11 – 5 of the 6 CYP2B genes expressed in rats were expressed by rat urothelial cells in response to phenobarbital. Aligned sequencing of cloned CYP2B RT-PCR product from 1 control and 5 phenobarbital-treated urothelial samples using generic CYP2B primers. Individual CYP2B enzymes were identified from small base pair variations within the amplified region. These differences are shaded to indicate specificity of CYP2B product, as indicated by colour in the table. Primer regions are shaded in yellow at either end of the sequence.

### 6.3.4 Rat *In vivo* case study – chemical induction of CYP2B

A compound under development by Syngenta was found to cause urothelial hyperplasia in rats during 28 day toxicity studies. Liver biochemistry assays were conducted by Leatherhead Food Research (LFR) on behalf of Syngenta and the raw data was generously volunteered to assist this study. These data (Figure 6.11 to Figure 6.12) are reproduced here with the full knowledge and permission of Syngenta.

Analysis of liver biochemistry data (Figure 6.12) revealed that the compound significantly increased total hepatic cytochrome P450 content after 28 days at dietary doses exceeding 3000 ppm. A specific marker of CYP2B (7-pentoxoresorufin O-depentyrase) enzyme activity revealed that at dietary doses exceeding 500 ppm, CYP enzyme activity was significantly increased relative to controls. This was further confirmed by immunolabelling of liver sections from control and dosed (3000 ppm for 28 days) rats (Figure 6.13). No labelling was observed in control liver sections, but clearly defined regions of labelling were seen in the livers of treated animals. This pattern of labelling was similar to the CYP2B1/2 labelling seen in liver sections of rats treated with phenobarbital (Figure 6.14).

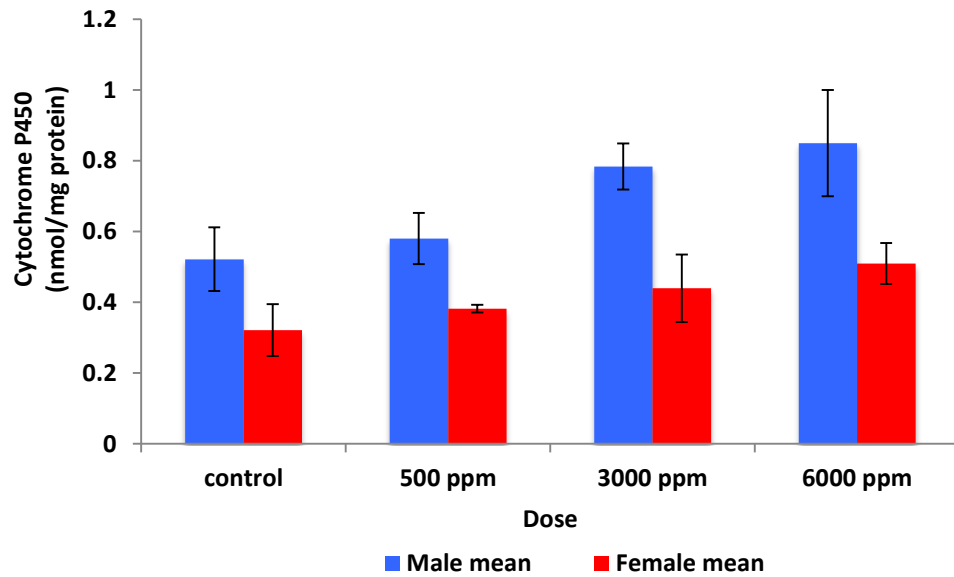


Figure 6.12 – Hepatic CYP content was increased in a dose dependant manner in response to the Syngenta compound. Mean total hepatic Cytochrome P450 content in control and dosed male (Blue) and female (red) rats after 28 days of treatment. Error bars represent  $\pm$ SD (n=5).

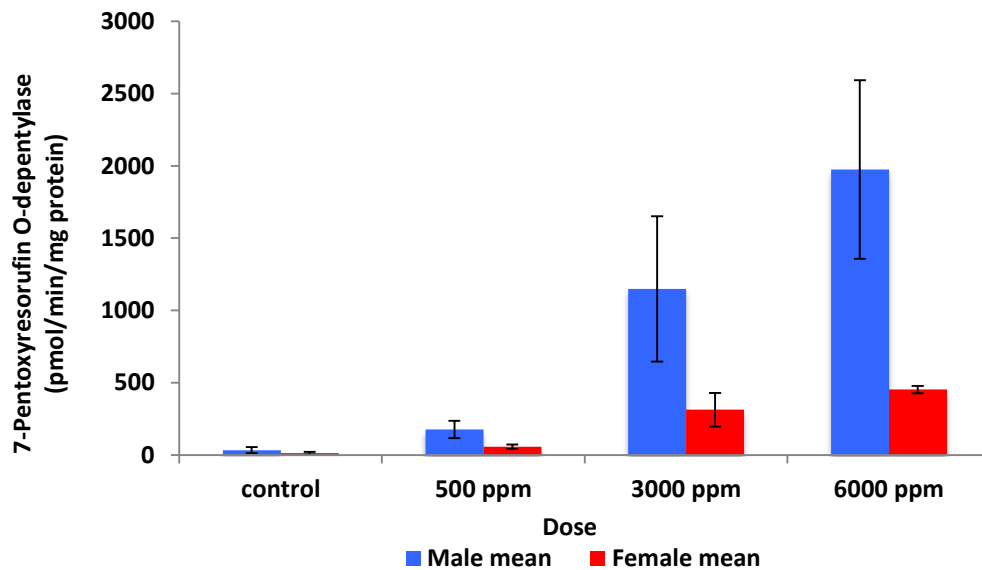
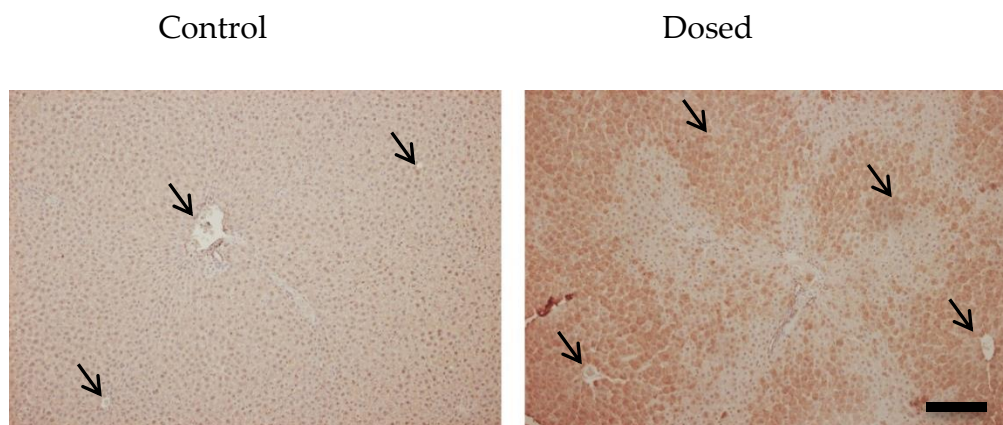
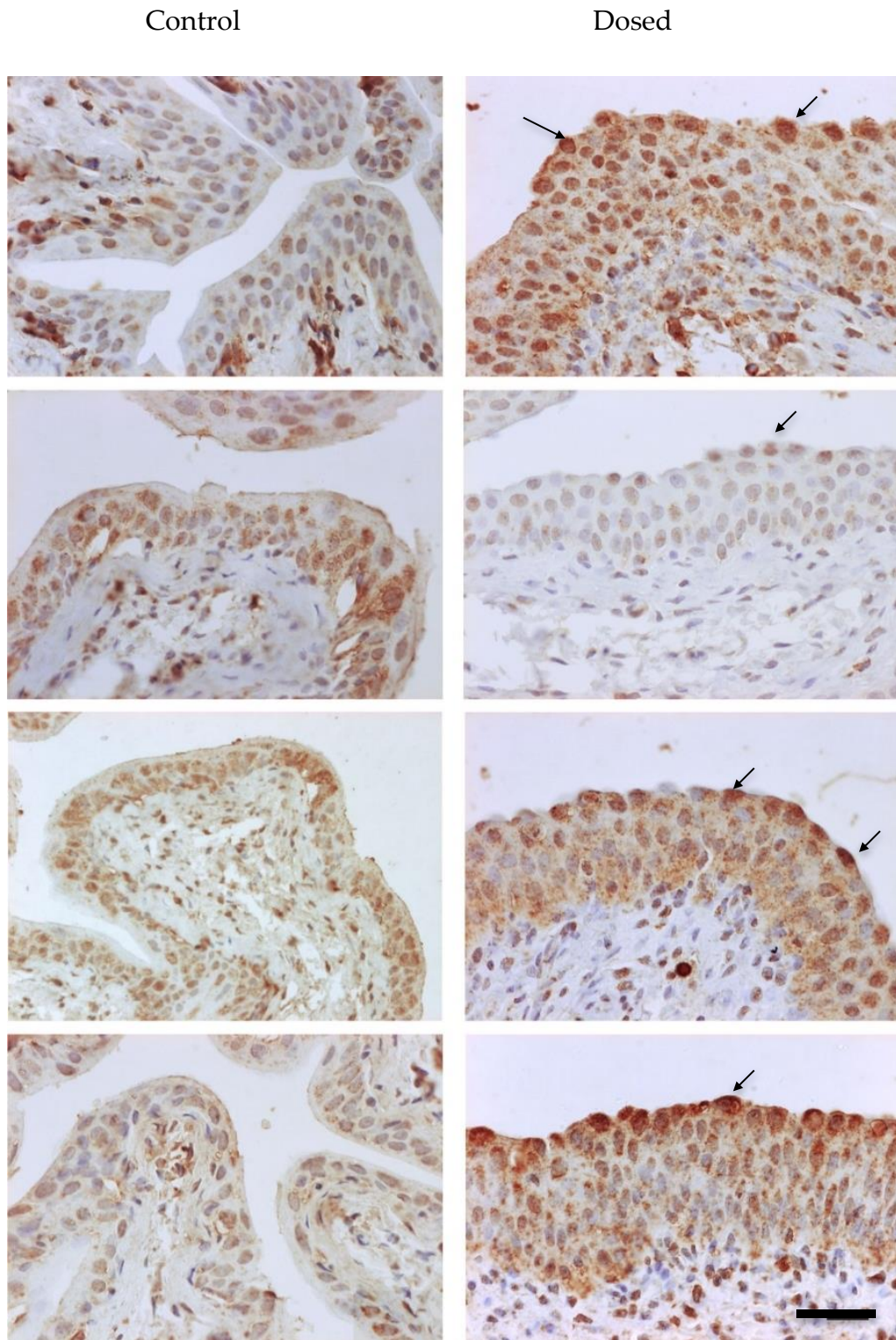


Figure 6.13 – Hepatic CYP2B enzyme expression was increased in response to the Syngenta compound in a dose dependant manner. Hepatic 7-pentoxoresorufin O-depentyllase (CYP2B marker) activity in control and dosed male (blue) and female (red) rats after 28 days of treatment. Error bars represent  $\pm$ SD (n=5).



**Figure 6.14 – CYP2B expression was induced in rat hepatocytes after 28 days of treatment with the Syngenta compound.** Immunohistochemistry labelling of CYP2B1/2 was conducted in liver sections from control rats and rats treated with a developmental compound after 28 days of treatment. Scale bars = 200  $\mu\text{m}$ . Arrows indicate the location of blood vessels. Results were replicated in three individual animals per group (n=3).

Having established the potential of the compound to induce CYP2B expression in the liver, CYP2B1/2 immunolabelling was conducted on bladder tissue from control and dosed (dietary 3000 ppm) rats after 28 days (Figure 6.15). In sections from both control and dosed rats, a small amount of background labelling was present and there were variations between animals within treatment groups. The urothelium of dosed animals appeared thicker than in control animals, supporting the reports of hyperplasia in the treatment group. Superficial cells in particular showed defined, intense CYP2B1/2 labelling (examples indicated). The CYP2B1/2 expression by urothelial cells appeared increased in the 28 day dosed rats. .



**Figure 6.15** – CYP2B1/2 expression was induced by the Syngenta compound *in vivo* after dietary administration for 28 days. Immunohistochemistry labelling of CYP2B1/2 was conducted on control (left) and Syngenta compound-treated (right) rat urothelium after 28 days of treatment. Arrows indicate examples of strong superficial cell labelling. Scale bars = 50  $\mu\text{m}$ . (n=4).

### 6.3.4 Investigation of urothelial CYP2B expression *in vitro*

#### CYP2B induction in NRU cell monolayers

NRU cells were harvested and cultured as previously described (Chapter 3). 80-90% confluent primary and subcultured (P1) NRU cell cultures were treated for 72 hours with a physiologically relevant concentration of phenobarbital (500  $\mu\text{M}$ ) and monitored by phase contrast microscopy (Figure 6.16). Subcultured NRU cells treated with phenobarbital appeared to have a reduced cell density compared to cells cultured in KSFMc alone, but no changes in morphology were observed.

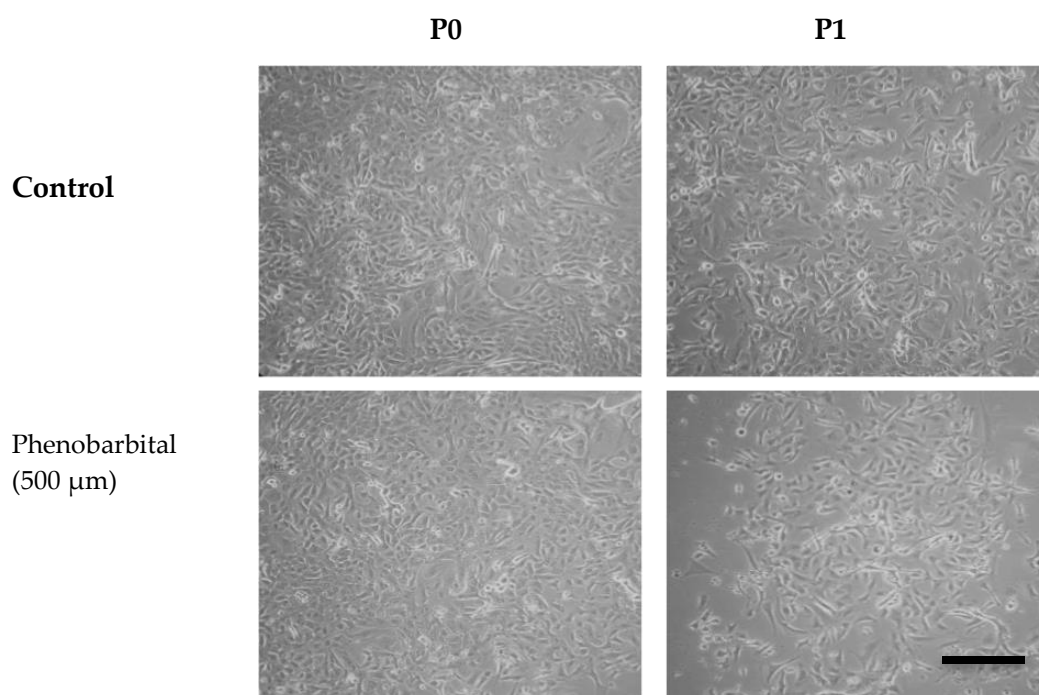


**Figure 6.16 – Phenobarbital had no visible effect on NRU cells in culture after 72 hours of treatment.** Phase contrast images showing primary (P0) and subcultured (P1) NRU cells after 72 hours in control medium (KSFMc) with 500  $\mu\text{M}$  phenobarbital. Scale bar = 50  $\mu\text{m}$  (n=2; R051, R053).

At 72 hours, RNA was harvested from NRU cell cultures and CYP2B expression assessed by RT-PCR (Figure 6.17). Due to limited cell numbers, protein analysis by western blot was not possible. RT-PCR results showed faint bands in primary (P0) control and phenobarbital-treated NRU cells, but no expression in subcultured NRU cells.

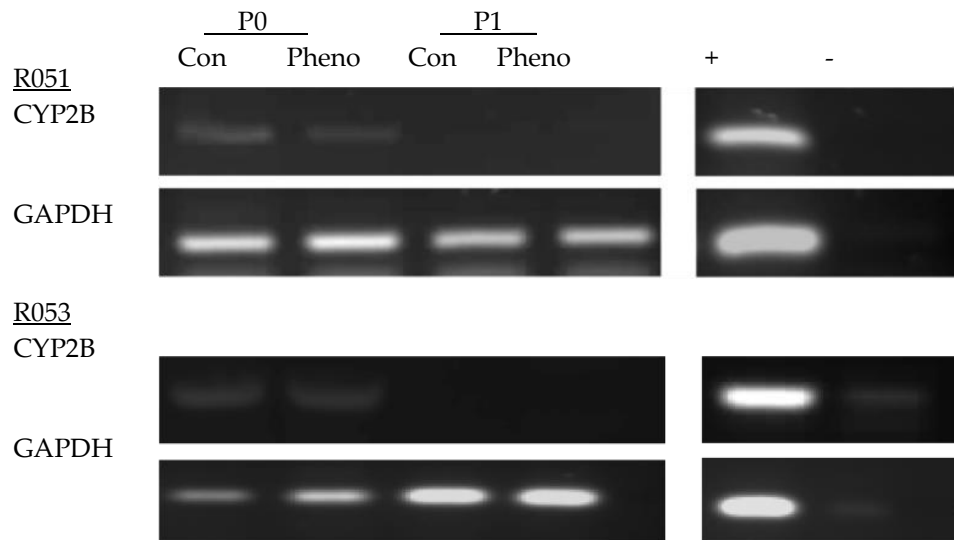


**Figure 6.17 – CYP2B enzyme induction did not occur in NRU cells in response to phenobarbital.** RT-PCR results showing CYP2B expression in primary and subcultured (P1) NRU cells after 72 hours treatment with 500  $\mu$ M phenobarbital (Pheno). Rat liver cDNA was used as positive control, water as a negative control and GAPDH as a loading control (n=2 cell lines; R051 & R053).

### CYP2B induction in an *ex vivo* organ culture system

Isolated NRU cells grown in monolayer culture were not able to replicate the urothelial induction of CYP2B enzymes seen *in vivo*, and so induction in an *ex vivo* organ culture model was investigated as an intermediary between *in vitro* and *in vivo*. Rat bladders were dissected into four approximately 1 cm<sup>2</sup> sections and cultured on a porous membrane, leaving the urothelium attached to the underlying stromal tissue.

Bladder tissue was cultured submerged in medium with and without phenobarbital (500 µM) for 72 hours. To ensure that the organ cultures maintained their *in vivo* urothelial phenotype, cytokeratin 5 (CK5) was immunolabelled as a basal cell marker, cytokeratin 7 (CK7) as a urothelial cell marker, Ki67 as a marker of proliferation and uroplakin 3a (UPK3a) as superficial cell marker in organ cultures and in bladder tissue fixed immediately after being harvested (without culture) (Figure 6.18). Ki67 labelling appeared reduced in organ cultures compared to native tissue, possibly due to a thinning of the urothelium in phenobarbital-treated organ cultures, but organ cultures maintained cytokeratin 5 and 7 expression in similar localisations to native tissue and the presence of UPK3a positive cells demonstrated the retention of the differentiated superficial cell layer.

Immunolabelling of CYP2B1/2 was conducted on control and phenobarbital-treated (72 hours) Wistar rat organ cultures. Organ cultures treated with phenobarbital showed intense CYP2B1/2 labelling (Figure 6.19). At the transcript level (Figure 6.19), urothelial cells from one control and one phenobarbital-treated organ culture showed expression of CYP2B1/2, but expression appeared greatest in urothelial cells from control than phenobarbital-treated organ cultures. No difference in CYP2B expression was obvious between the two concentrations of phenobarbital tested (250 & 500 µM).

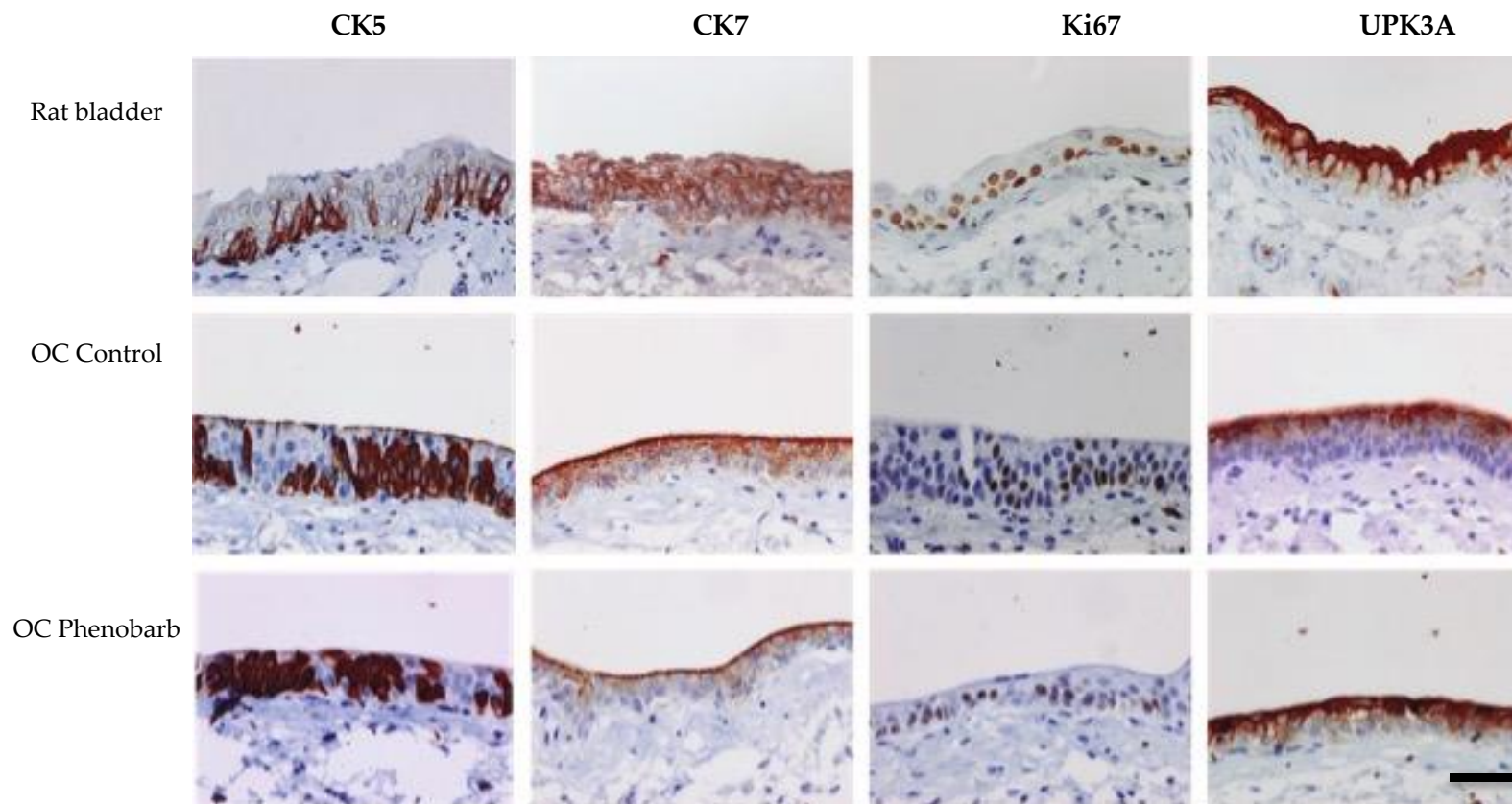


**Figure 6.18 - Confirmation of urothelial cell layer maintenance in control and phenobarbital-treated rat organ cultures.** Immunolabelling of the basal cell marker cytokeratin 5 (CK5), the whole urothelial cell marker cytokeratin 7 (CK7), the proliferation marker Ki67 and the superficial cell maker uroplakin 3a (UPK3A) in native rat bladder and in control and phenobarbital-treated (500  $\mu$ M) rat organ cultures (OC) after 72 hours of culture. Scale bar = 50  $\mu$ m.

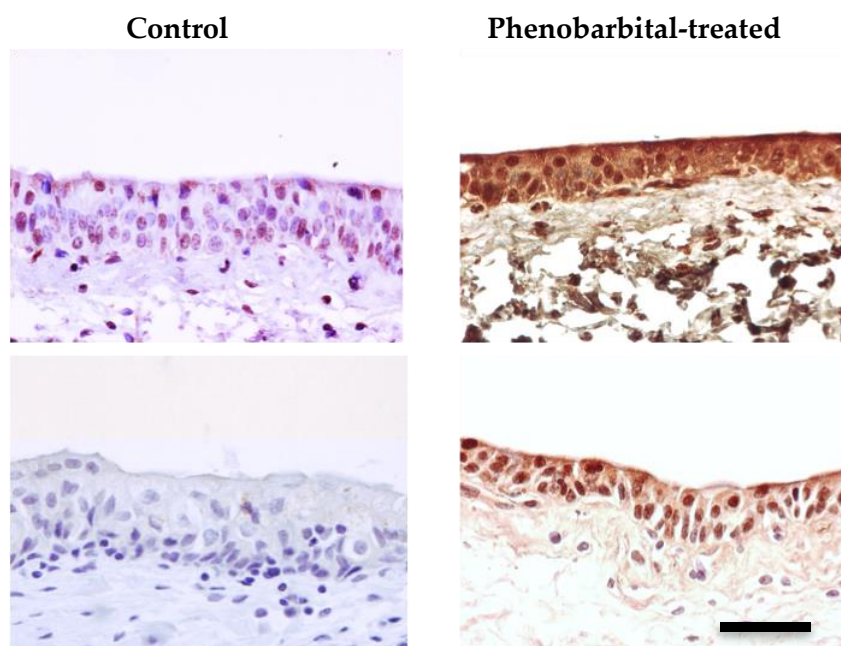


**Figure 6.19 – CYP2B enzyme induction occurred in rat organ cultures after 72 hours of treatment with phenobarbital.** Immunolabelling of CYP2B1/2 was conducted in control and phenobarbital-treated (500  $\mu\text{M}$ ) rat organ cultures generated from two independent Wistar rat bladders after 72 hours treatment. Scale bar = 50  $\mu\text{m}$  (n=2 individual rat bladders).

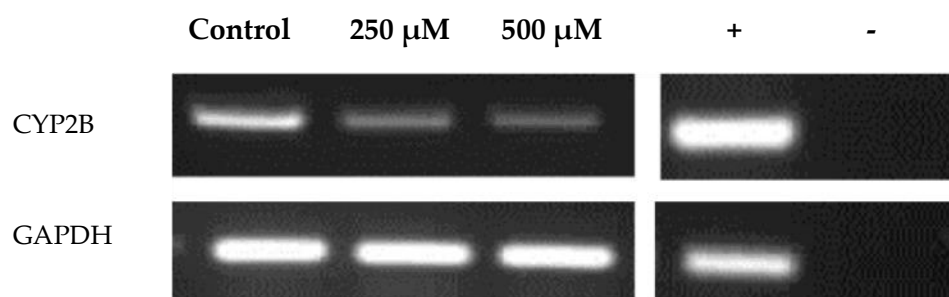


**Figure 6.20 – CYP2B enzyme expression was not induced in rat organ cultures in response to 72 hours of phenobarbital treatment.** RT-PCR results showing CYP2B expression in isolated urothelial cells from organ cultures after 72 hours treatment with phenobarbital at concentrations of 250 and 500  $\mu\text{M}$ . Rat liver cDNA was used as positive control, water as a negative control and GAPDH as a loading control (n=1 NRU cell line).

**CYP2B6 induction in NHU cells**

80-90% confluent NHU cell cultures were induced to adopt a differentiated phenotype using the established ABS/calcium protocol (see chapter 2) over 7 days in culture before being treated with phenobarbital (500  $\mu\text{M}$ ) for 72 hours (Figure 6.21). No visible difference in cell phenotype or density was observable between control and phenobarbital-treated NHU cells at 24 or 72 hours.

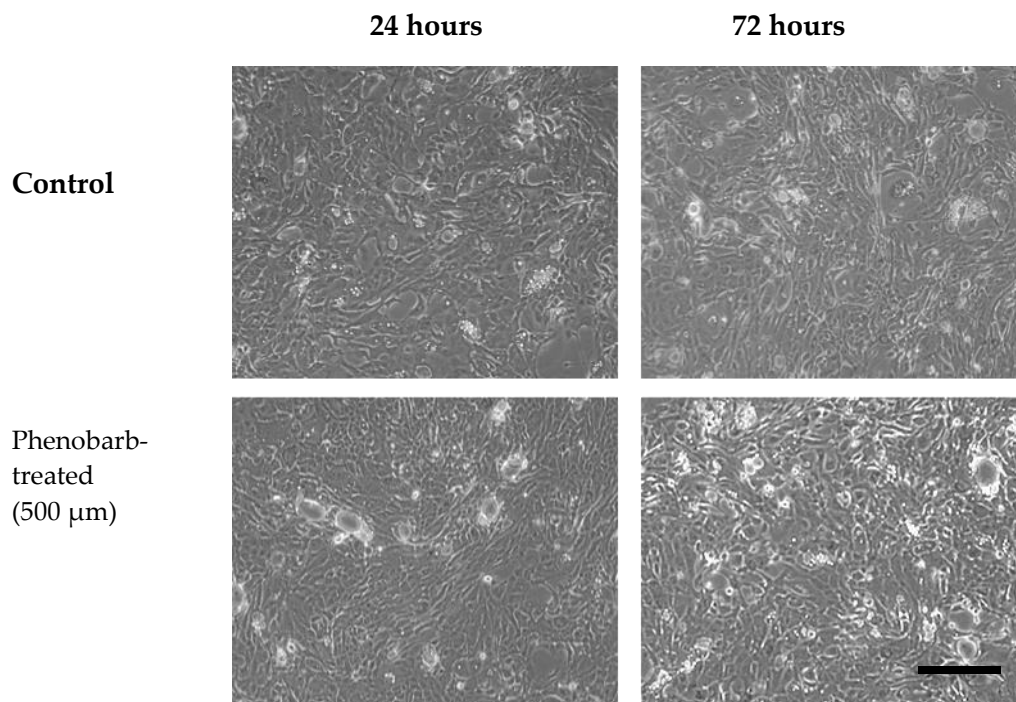


**Figure 6.21 – Differentiated NHU cells were not visible affected by treatment with phenobarbital over 72 hours.** Phase contrast images showing differentiated (ABS/ $\text{Ca}^{2+}$ ) NHU cells after 24 and 72 hours in 500  $\mu\text{M}$  phenobarbital. Scale bar = 50  $\mu\text{m}$ .

After 72 hours, RNA and protein lysates were harvested from control and phenobarbital-treated NHU cells. CYP2B6 transcript was detected in control NHU cells, but not in cells treated with phenobarbital (Figure 6.22). Both control and treated cells showed weak expression of CYP2B and CYP3A4, but there was no increase in expression between control and phenobarbital-treated NHU cells. CYP3A4 is known to metabolise similar xenobiotics to CYP2B enzymes, but is not present in rats.

At the protein level (Figure 6.23), CYP2B6 was weakly expressed in both control and phenobarbital-treated NHU cells. There was no increase in expression in the phenobarbital-treated samples, indicating that CYP2B enzyme expression was not induced in NHU cells. Human liver, which was included as a control, also had minimal CYP2B6 protein expression. By contrast, CYP3A4 was highly expressed in human liver, although no expression was seen in NHU cells. Rat liver samples were included to demonstrate the specificity of the antibodies and as expected showed no expression of CYP2B6 or CYP3A4 protein. Cytochrome P450 reductase (CPR), which is required by all CYPs for catalysis, was included as a loading control and was present in all samples, but reduced in the NHU cell samples compared to the liver samples.

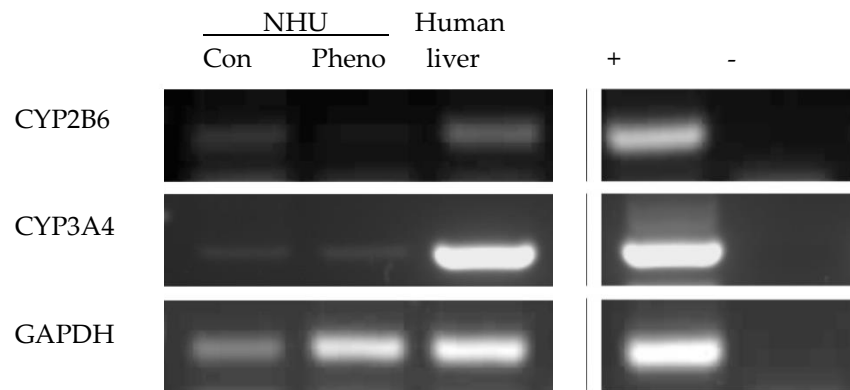


**Figure 6.22 – CYP2B6 and associated CYP3A4 enzyme transcript induction did not occur in NHU cells in response to 72 hours of phenobarbital treatment.** RT-PCR results for CYP2B6 and CYP3A4 expression in human urothelial cells after 72 hours of treatment. Human genomic DNA was included as a positive template control (+). GAPDH was included as a loading control.

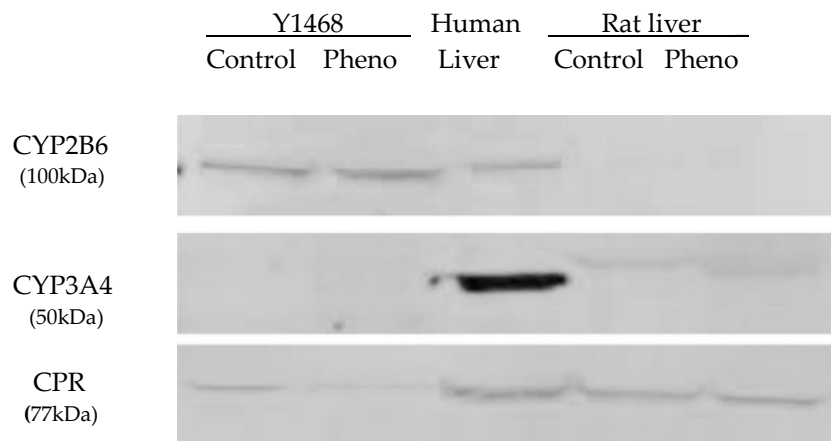


**Figure 6.23 – CYP2B6 and associated CYP3A4 enzyme protein induction did not occur in NHU cells in response to 72 hours of phenobarbital treatment.** Western blot analysis of CYP2B6 and CYP3A4 expression in control and phenobarbital-treated, differentiated (ABS/Ca<sup>2+</sup>) NHU cell microsomes. Differentiated NHU cells were cultured for 72 hours in differentiation medium (KSFMc containing 5%ABS and 2mM Ca<sup>2+</sup>) ± 500µM phenobarbital. Human liver microsomes were included as positive controls, with rat liver microsomes as negative controls for CYP2B6. Cytochrome P450 reductase (CPR) was included as a loading control.

## 6.4 Conclusions and Discussion

CYP2B enzyme expression can be induced in rat urothelial cells *in vivo* by phenobarbital and also by a CYP2B-inducing compound after oral administration for at least 3 days. Attempts to identify the specific CYP2B homologue expressed revealed that transcripts for multiple CYPs are expressed by rat urothelial cells at the 72 hour time point studied after induction. Results also showed that variations in CYP2B induction occur between individuals within a treatment group. *In vitro* urothelial cell models were not able to replicate the CYP2B induction seen *in vivo*. Both human and rat urothelial cell models showed expression, but as it was not inducible at the transcript level or, in NHU cells, at the protein level it is most likely a result of the culture system as opposed to induction by phenobarbital. The success in modelling CYP2B expression in an *ex vivo* organ culture model, however, does suggest that the time points that CYP2B transcript was assessed after phenobarbital treatment (72 hours *in vitro*) was too late. It appears in the *ex vivo* model that transcript is down regulated after induction, suggesting that the peak transcript expression is sooner than 72 hours after induction. This could also have implications of the transcript data seen *in vivo* and suggests that harvesting RNA for analysis at an earlier time point could demonstrate CYP2B induction more clearly. Further work is required to replicate the *in vitro/ex vivo* data, including assessing the expression of CYP2B enzyme transcript at earlier time points.

## 6.5 Key findings

- CYP2B enzyme expression can be induced by xenobiotics in rat urothelial cells, possibly leading to CYP2B metabolism of xenobiotics excreted in urine.
- *In vitro* urothelial cell models are not capable of replicating the CYP2B induction seen *in vivo*, but an *ex vivo* organ culture model could be capable of CYP2B expression.

## Chapter 7 Discussion

<b>7.1 Development of a NRU cell culture system .....</b>	<b>211</b>
<b>7.2 Regulation of urothelial growth pathways.....</b>	<b>214</b>
<b>7.3 Immortalisation of normal urothelial cells.....</b>	<b>219</b>
<b>7.4 Xenobiotic induction of CYP2B enzymes in urothelial cells .....</b>	<b>221</b>
<b>7.5 Practical difficulties experienced during the project.....</b>	<b>222</b>
<b>7.5 Limitations and future work.....</b>	<b>223</b>

The aim of this project was to develop a NRU cell culture system and conduct comparisons between it and an established NHU cell culture system as a means of validating normal urothelial cell culture models for use in toxicity testing. This aim has been partly achieved, as a cell culture system has been developed and optimised to enable the reproducible establishment and maintenance of NRU cell cultures up to passage 2. Investigations into the pathways regulating proliferation in normal urothelial cells *in vitro* uncovered species differences between rats and humans, supporting observations described in the literature (Chopra et al., 2008b). In an attempt to improve the ability of normal urothelial cell culture models to be incorporated into toxicity testing, an immortalised NHU cell line that could be differentiated up to at least passage 10 was successfully generated through the overexpression of BMI1. Finally, a novel mechanism of metabolism within rat bladders was discovered through xenobiotic induction of CYP2B enzymes. CYP2B expression was demonstrated *in vivo* and, although induction did not occur in NRU cell cultures, the *in vivo* results were replicated in an *ex vivo* organ culture model.

#### **Key experimental findings:**

- 1. Optimisation of the isolation and culture of normal rat urothelial cells *in vitro***
- 2. Pathways regulating urothelial cell proliferation *in vitro* differ between NRU and NHU cells, with the PI3K/Akt pathway being active in NRU cells whereas the EGFR/MAPK pathway is known to drive proliferation in (undifferentiated) NHU cells (Varley et al., 2005).**
- 3. Human BMI1 overexpression did not immortalise NRU cells but did enable NHU cells to be passaged and successfully differentiated beyond passage 10.**
- 4. Xenobiotic induction of CYP2B enzymes occurs in rat urothelium and this result was replicated in a rat *ex vivo* organ culture model.**

## 7.1 Development of a NRU cell culture system

A NRU cell culture system was developed, based on an existing NHU cell culture system, and optimised using protocols described in the literature. The NRU cell culture system developed had to be as similar as possible to the established NHU cell culture system, enabling accurate comparisons to be made between the two systems. The lack of consistency between NRU cell culture systems described in the literature (discussed in Chapter 3), in particular the rats used (strains & ages) and the isolation protocols employed, necessitated the creation of an optimised protocol for the clean isolation and subsequent culture of NRU cells.

Aspects of cell isolation protocols described in the literature were compared against the NHU cell isolation protocol, and subsequently adapted and optimised to maximise the yield of NRU cells isolated. NRU cells were cultured in KSFMc medium and grew in “cobblestone-like” colonies, as previously described in the literature (Zhang et al., 2001). The presence of serum (fetal bovine serum) was assessed and an interesting strain variation discovered between the rat strains used. NRU cells isolated from Wistar rats, a commonly used outbred strain, grew in serum-free KSFMc medium but their growth was inhibited by the presence of serum. NRU cells isolated from a rare inbred rat strain (Homozygous Scottish) grew in the presence of serum but their growth was diminished in the absence of serum. NRU cells from a third, outbred, strain of rat (Sprague Dawley) appeared to grow equally in the presence and absence of serum although this result was only performed on one occasion.

Strain differences are not uncommon in rodents *in vivo* and can have a number of implications in relation to pharmacokinetics, metabolism and susceptibility to xenobiotic toxicity (reviewed by Kacew and Festing, 1996). Saccharin-induced toxicity in the urinary bladder, for instance, occurs in Wistar rats, but not in Sprague-Dawley rats (Fukushima et al., 1983). *In vitro*, strain differences have been discovered in hepatocytes (Harbach et al., 1991, Richmond et al., 2010) pancreatic

beta-cells (Reimers et al., 1996) and oocytes (Sterthaus et al., 2009) isolated from different rat strains. Differences included cellular ability to repair DNA after exposure to ultraviolet (UV) radiation, metabolic competency and gene stability. In relation to cellular proliferation, mesenchymal stem cells (MSCs) from different mouse strains have been shown to differ in cell surface epitopes, rates of proliferation and differentiation capabilities (Peister et al., 2004).

Physiological differences between rat strains, such as the variation in serum requirements demonstrated between NRU-W, NRU-HS and NRU-SD cells, are a major disadvantage in toxicity testing as they can complicate the extrapolation of results between rats and humans. The fact that results from two different rat strains can be contradictory makes choosing the most relevant strain difficult and affects the confidence with which results can be used to predict effects in man. Being able to rely on rat *in vivo* results being relevant to humans would be hugely advantageous during compound development, allowing unsuitable candidate compounds to be excluded at an earlier stage, thus reducing the number of *in vivo* studies conducted and the costs associated with them.

No single rat strain would appear to be more reliable at predicting the toxicity of all xenobiotics in humans, as demonstrated by the number of rat strains used in toxicity testing (e.g. Wistar, Sprague Dawley, F344). Based on evidence reviewed by Kacew and Festing (1996), it would appear that choosing the correct rat strain for predicting effects in humans is dependent on the organ/tissue of interest and type of compound being tested. Within the urinary bladder alone there are advantages and disadvantages described for using Wistar, Sprague-Dawley and F344 rats in toxicity testing (Pamukcu et al., 1980, Fukushima et al., 1983, Garland et al., 1989).

The use of outbred rat strains further complicates the extrapolation of results to humans as genetic variations exist within as well as between strains, leading to altered characteristics (Ito et al., 2007). There can be significant genetic variations between outbred rat strains acquired from different breeders, resulting in different

strains sometimes being indistinguishable from each other contrasted by high variation between rats of the same strain (Lovell and Festing, 1982). Additionally, quality control issues have been reported in outbred rat strains, in which outbred rats with reduced lifespan and increased body fat were produced and marketed under the same strain name as animals without these defects (Nohynek et al., 1993).

Such differences within strains are believed to be responsible for the lack of reproducibility of certain results, such as bisphenol A toxicity (reviewed by Sekizawa, 2008). This lack of reproducibility can significantly reduce the effectiveness of toxicity testing and increases the risk of compounds that are not toxic in humans being discarded and compounds that are toxic to humans being developed. These disadvantages in the use of outbred strains have led to calls for inbred strains, such as F344, to be universally used in toxicity testing, replacing the outbred strains (discussed by Festing, 2010).

Based on the single interstrain variation discovered (requirement of serum for cell growth *in vitro*), NRU cells isolated from Wistar rats (NRU-W) would appear to be the most similar to NHU cells. Identifying whether this is the case would require multiple variations to be assessed in a number of rat strains. Although interesting, this observation was not pursued, as it would have detracted from the main aim of the project, to compare rat and human urothelial cells. The obscurity of the inbred (Homozygous Scottish) rat strain and lack of access to tissue from multiple rat strains further discouraged additional investigation into interstrain variations. This variation does act, however, to further demonstrate the difficulties associated with using rats in toxicity testing and highlights the requirement of a more human-relevant system to be developed and incorporated into toxicity studies.

Additional aspects of the culture system, including cell seeding density and tissue culture plastic substrate, were optimised to generate a NRU cell culture system in which cells could be cleanly isolated and grown in culture up to passage 1. Primary NRU cells isolated from both Wistar and Homozygous Scottish rats were able to be

cultured and passaged once but, despite optimisation of several aspects of the cell culture system including seeding density and tissue culture plastic substrate, cell population growth ceased and cultures died at passage 1. This is in contrast to NHU cell cultures, which were able to undergo 6 passages before the onset of senescence as measured by expression of p16<sup>INK4a</sup> (Puthenveetil et al., 1999). There has been a suggestion that regulation of rat urothelial cell proliferation may differ from that of human urothelial cells as a result of differences in cell cycle regulation (observed as differences in Ki67 expression by human and rat urothelium in situ (discussed by Festing, 2010) and that these differences may be responsible for pathologies of the bladder seen in rat (Chopra et al., 2008). As such, the exogenously-regulated signal transduction pathways driving proliferation were investigated, both to identify any interspecies variations in proliferation regulation and as an approach to increase NRU cell lifespan in culture through the use of exogenous factors to promote cell proliferation.

## 7.2 Regulation of urothelial growth pathways

To explore potential species variation in the regulation of urothelial cell proliferation, the pathways regulating proliferation were investigated in NRU cells and compared against those active in NHU cells. In monolayer culture, NHU cell proliferation is known to be regulated by EGFR/MAPK pathway which is activated by both autocrine and exogenous EGF present in KSFMc medium (Varley et al., 2005). It has been shown that EGFR/MAPK pathway activation in low-density NHU cells inhibits GSK3 $\beta$ -mediated destruction of  $\beta$ -catenin, allowing  $\beta$ -catenin to translocate from the cytoplasm to the cell nuclei where it regulates proliferation-associated gene expression (Georgopoulos et al., 2014). In proliferating NRU cells, which were found to have limited proliferative capabilities in culture compared to NHU cells, the PI3K/Akt pathway appeared to be active based on p-Akt immunoreactivity. Subsequent pharmacological stimulation of this pathway did not affect the overall rate of NRU cell proliferation. The lack of difference between PI3K/Akt stimulated and control NRU cells suggests that the PI3K/Akt pathway

was already being stimulated in NRU cells, although the mechanism of activation is unknown. One possible mechanism by which the PI3K/Akt pathway induction in NRU cells was being regulated is through the transforming growth factor  $\beta$  (TGF $\beta$ ) pathway. In mouse urothelium *in vivo*, TGF $\beta$  expression was associated with re-epithelialization and differentiation after injury (de Boer et al., 1994). *In vitro*, exogenous TGF $\beta$  has been shown to have a negative effect on undifferentiated NHU cell proliferation and no effect upon differentiation, but to enhance wound healing in differentiated NHU cells through a TGF $\beta$ /TGFBR/Smad3 autocrine signalling loop (Fleming et al., 2012). Crosstalk between the TGF $\beta$  and PI3K/Akt pathway has been established in normal (Suwanabol et al., 2012) and cancer (Assinder et al., 2009, Zhang et al., 2013) cells from other tissues and offers a potential mechanism by which proliferation of NRU cells was regulated. NRU cells in culture maintained characteristics more closely associated with differentiated than proliferative NHU cells, such as growing in colonies and expressing ZO-1 and claudin 4, supporting the theory that TGF $\beta$  expression was inducing PI3K/Akt pathway-mediated NRU cell proliferation.

Alternatively, E-cadherin has been shown to differentially regulate proliferation pathways in NHU cells with activation of the EGFR/MAPK, PI3K/Akt and  $\beta$ -catenin/LEF pathways being dictated by E-cadherin (Georgopoulos et al., 2010). Loss of E-cadherin resulted in increased NHU cell proliferation through activation of the EGFR/MAPK pathway whereas expression of E-cadherin, achieved through culturing cells in physiological (2 mM) calcium, inhibited the  $\beta$ -catenin pathway through recruitment of  $\beta$ -catenin into adherens junctions. In Figure 7.1, this is represented by  $\beta$ -catenin translation and incorporation into E-cadherin containing adherens junctions in conditions of increased (2 mM) extracellular Ca<sup>2+</sup>. Activation of the PI3K/Akt pathway was shown to occur in NHU cells cultured in physiological calcium when cell-cell contacts were formed. NHU cells cultured in physiological calcium that were not in contact with other cells showed little or no activation of the PI3K/Akt pathway, as indicated by the expression of phospho-Akt.

As NRU cells grew in densely packed colonies in which cells would be in close contact, E-cadherin regulated PI3K/Akt activation would also explain the results seen. Reducing extracellular  $\text{Ca}^{2+}$  concentrations reduced phospho-Akt immunoreactivity in NRU cells, potentially by reducing expression of E-cadherin although this was not confirmed. Reducing extracellular calcium ion concentrations alone, which might be expected to inhibit formation of adherens junctions, was not sufficient to enable NRU cells to be subcultured to P2 or completely inhibit the PI3K/Akt pathway.

Rat and human serum  $\text{Ca}^{2+}$  concentrations have a similar range (approximately 9-10 mg/dl) (Watchorn, 1933, Lester et al., 1982, Pitkin and Gebhardt, 1977) and the calcium binding domains on E-cadherin are highly conserved between all mammalian species (Posy et al., 2008). Therefore if E-cadherin does influence NRU cell proliferation in KSFMc (0.09 mM  $\text{Ca}^{2+}$ ), it would suggest a difference in urothelial cell expression of E-cadherin in adherens junctions between NRU and NHU cells. This theory is further supported by the fact that NRU cells grew in densely packed colonies in KSFMc medium, in which cell-cell contacts would be generated, rather than expanding to form monolayers like NHU cells. The role of E-cadherin in NRU cells is a key area for further developing the cell culture system.

As no increase in proliferation rate was seen between IGF1 stimulated and control NRU cells, it seems likely that control (KSFMc only) NRU cells had reached maximum proliferative rate *in vitro*. Whether this was achieved through an autocrine  $\text{TGF}\beta$  signalling loop, an E-cadherin dependant mechanism or by an alternative, unknown, mechanism of PI3K/Akt activation is unclear, but additional stimulation of the PI3K/Akt pathway with IGF1 had no significant effect on cell growth or lifespan in culture.

Proliferation of PI3K/Akt-inhibited NRU cell cultures was comparable with primary control (KSFMc only) NRU cells, but NRU cells were able to be subcultured to passage 2 (P2). Successful inhibition of the pathway was confirmed by

immunolabelling of phospho-Akt in NRU cells. It is interesting to speculate that the inhibition of the PI3K/Akt pathway may have enabled activation of the EGFR/MAPK pathway, either through an autocrine mechanism or by exogenous EGF present in KSFMc medium. In the literature, crosstalk between the MAPK and PI3K/Akt pathways have been demonstrated (reviewed by Mendoza et al., 2011) with negative feedback loops revealed between the MAPK and PI3K/Akt pathways as illustrated in Figure 7.1 (Zimmermann and Modelling, 1999, Yu et al., 2002, Hoeflich et al., 2009). In response to “strong” IGF1 stimulation, Akt was found to negatively regulate activation of the MAPK pathway (ERK) through the phosphorylation of inhibitory sites in the N-terminus of Raf (Guan et al., 2000, Modelling et al., 2002). Inhibition of the PI3K/Akt pathway prevented Akt inhibition of ERK, enabling activation of the MAPK pathway. As the EGFR/MAPK pathway regulates proliferation of “undifferentiated” NHU cells *in vitro*, it is tempting to speculate that activation of the MAPK pathway in NRU cells was achieved through inhibition of the PI3K/Akt pathway and that this lead to the increased growth capabilities observed.

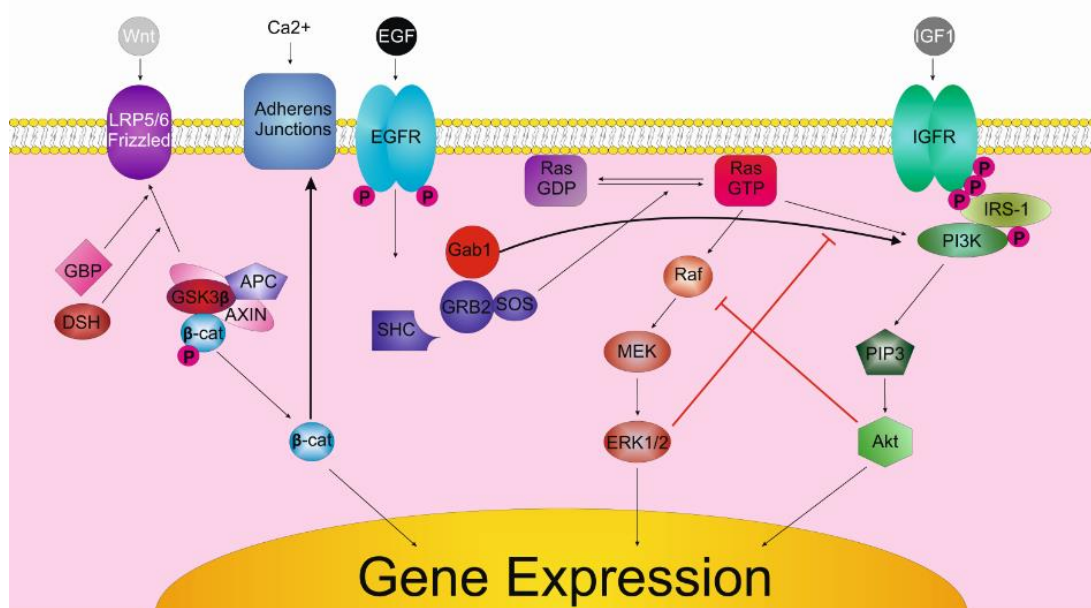


**Figure 7.1 – inhibitory crosstalk can occur between the EGFR/MAPK and the PI3K/Akt pathways but has yet to be investigated in urothelial cells. In conditions of physiological (2 mM) extracellular Ca<sup>2+</sup> ions,  $\beta$ -catenin is sequestered to the cell membrane and does not participate in regulation of gene expression, stimulating proliferation. EGF-stimulated ERK activation results in a decrease in the tyrosine phosphorylation of Gab1 and a decreased association with the PI3K, resulting in reduced activation (Yu et al, 2002). This is possibly achieved through the regulation of SHP2 (not shown), although this has not been confirmed. Akt has been shown to antagonises Raf activity by direct phosphorylation of Ser 259. This modification creates a binding site for 14-3-3 protein (not shown), which is a known negative regulator of Raf (Zimmerman and Moelling, 1999). Under conditions of physiological extracellular calcium ion concentrations,  $\beta$ -cetenin is sequestered to cell membranes and form adherens junctions with E-cadherin (Georgopoulos et al., 2014).**

### 7.3 Immortalisation of normal urothelial cells

The limited growth capabilities of NRU cells *in vitro* made for comparison of NRU and NHU cells difficult and limited the usefulness of the culture system for toxicity testing. The finite nature of NHU cells and their individual donor variability also restricted the development of their use for standardised, reproducible toxicity testing. For use in toxicity testing, NHU cell culture systems would have to be capable of large-scale expansion and be able to be used in long-term (several months) experiments (Evans et al., 2001). In an attempt to address these issues, immortalisation of the two cell culture systems was attempted through the overexpression of BMI1. Comparisons were made to hTERT overexpressing cells and empty vector controls as hTERT overexpression in NHU cells is known to induce immortalisation, but inhibit capacity for differentiation and formation of a functional barrier *in vitro* (Georgopoulos et al. 2011; discussed by Hartung and Daston, 2009).

Overexpression of BMI1 or hTERT in NRU cells did not increase lifespan in culture compared to control empty vector transfected cells. hTERT overexpression has already been shown to increase NHU cell lifespan (Georgopoulos et al., 2011) but it failed to have an effect in NRU cells. One explanation is that a species difference between human and rat telomerase expression exists that caused this result. In post-embryonic mouse cells, telomerase expression is not repressed as it is in humans which prevents telomere degradation from causing in mouse cell senescence and, in turn, prevents telomerase overexpression from acting as a form of cellular immortalisation (Wright and Shay, 2000). If this also occurs in rat cells, it could explain why hTERT overexpression failed generate immortalised NRU cell lines.

BMI1 transcript was shown to be overexpression in NRU cells but cells died at passage 2, leading to the conclusion that BMI1 does not immortalise or increase the lifespan of NRU cells. It is possible that despite the high level of sequence identity

between rat and human BMI1 genes (>75%), the difference in sequence had an affected on the activity of BMI1 in NRU cells.

Alternatively, the molecular mechanism by which BMI1 immortalises human cells may not have the same effects in rat cells. BMI1 interacts with a large number of molecular control pathways within cells as discussed by Siddique and Saleem (2012), including tumour suppressor proteins p16<sup>INK4a</sup>, which regulates the retinoblastoma protein (RB) (Serrano et al., 1993) and ARF which positively regulates p53 (Quelle et al., 1995). A difference in spontaneous transformation (leading to immortalisation) as a result of p16<sup>INK4a</sup> and RB inhibition has been established between mice and humans (discussed by Hahn and Weinberg, 2002) and it is possible that BMI1's effects on these proteins, and others, may differ between species.

Human BMI1 transcript does immortalise rat cells in conjunction with hTERT overexpression as described by Zhang et al. (2009) but neither human nor rat BMI1 transcript have not been overexpressed alone in rat cells as a method of immortalisation. Based on the results generated in this project, it would appear that overexpressing hTERT or BMI1 alone is insufficient to bring about the immortalisation of NRU cells, suggesting an additional level of complexity between the pathways regulating immortalisation in humans and rats. As NRU cells did not survive, the activation of molecules downstream of BMI1, such as p16<sup>INK4a</sup> and ARF, were not able to be assessed in BMI1 overexpressing NRU cells.

In NHU cells, BMI1 overexpressing cells were able to be subcultured further than control empty vector cells, with proliferation matching that of hTERT overexpressing NHU cells. BMI1 overexpressing cells were also capable of generating functional barriers *in vitro* at passages 3, 6 and 10. Further work would be required to investigate whether BMI1 overexpressing NHU cells are capable of maintaining their rate of growth in culture and whether they can generate functional barriers *in vitro* when hTERT-overexpressing NHU cells cannot. hTERT

overexpressing cells in the literature lost the ability to generate a high TEER value at passage 17 (Georgopoulos et al., 2011) so the ability of NHU cells to generate high TEERs beyond passage 17 would represent an achievement in developing a normal human urothelial cell culture system that can be used in toxicity testing.

## 7.4 Xenobiotic induction of CYP2B enzymes in urothelial cells

Xenobiotic metabolism within specific organs can have either protective or toxic effects, both of which are important to understand when investigating xenobiotic toxicity (discussed in Chapter 6). Attempts to model xenobiotic metabolism *in vitro* have had limited success and as such, an *in vitro* system capable of expressing metabolic enzymes would have multiple applications in toxicity testing.

Induction of CYP2B enzymes in urothelial cells has not previously been demonstrated and would represent a method of urothelial defence and possible route of bladder-specific toxicity if active toxic metabolites were generated. In response to phenobarbital and a CYP2B-inducing compound under development by Syngenta, rat urothelial cells were shown, for the first time, to express CYP2B enzymes *in vivo*. CYP2B1/2 expression was demonstrated at the protein level whereas RT-PCR results found that all 6 CYP2B transcripts were present in rat urothelial cells after xenobiotic-induction.

Assessment of CYP2B expression in NRU and NHU cells revealed that neither cell culture system expressed CYP2B in response to xenobiotic (phenobarbital) induction. The failure of the cell culture system to replicate the induction of CYP2B seen *in vivo* is disappointing, particularly given the level of differentiation attained by the NHU cell cultures, as they would have allowed comparisons to be made between rat and human CYP2B enzymes in relation to induction of expression and metabolic abilities. However, it reflects the poor CYP expression seen using

established primary hepatocyte cell culture systems (discussed by Castell et al., 2006).

To examine whether rat urothelial cells had the ability to express CYP2B enzymes in response to xenobiotic-induction when they retained a fully differentiated state and stromal communication, expression in a rat organ culture system was assessed. The urothelium maintained its structure in organ culture, as shown by superficial uroplakin 3a expression and basal cytokeratin 5 expression. 72 hours of phenobarbital treatment appeared to increase CYP2B1/2 protein expression, but CYP2B transcript appeared to be highest in control rather than phenobarbital-treated cells. It is possible that this time point (72 hours) is after the peak in CYP2B transcript expression. An examination of CYP2B expression at earlier time points would determine whether CYP2B transcript is upregulated earlier than 72 hours and would explain the lack of CYP2B transcript seen in phenobarbital-treated cells after 72 hours.

## **7.5 Practical difficulties experienced during the project**

One major difficulty during the project was sourcing a regular supply of rat bladder tissue from a consistent strain of rat. To minimise the number of rats used (3Rs) and limit financial costs, tissue was harvested from control animals from other projects that were being sacrificed. This method of procurement did enable a large amount of bladder tissue to be harvested during the course of the project, but there were inconsistencies regarding the strains available, the time between the death of the animal and the harvesting of the tissue, and the ability to harvest bladders aseptically for culture.

Strains of rat used in this project include Wistar, Homozygous Scottish and Sprague Dawley. Ideally one strain would have been used throughout the project. As already described in section 7.1, there are arguments for and against choosing both inbred and outbred rat strains. As outbred rats, and in particular Wistar rats, are

commonly used in toxicity testing, this strain would most likely have been selected (Gad, 2007).

Wherever possible, bladder tissue was harvested immediately after death of the rat. This is known to be important as in NHU cells, rapid post-mortem changes in the bladder affect the viability of NHU cells isolated (Garthwaite et al., 2014). This, together with the issue of preventing bacterial contamination, was particularly problematic when the projects donating the tissue required the rats to be dissected before the bladders could be harvested.

## 7.5 Limitations and future work

This project was not able to fully validate the use of normal *in vitro* models for use in toxicity testing, but the species variations discovered have important implications when extrapolating results between rats and humans. Results have revealed species differences between rat and human urothelial cells in terms of growth potential, regulation of proliferation and ability of cells to be immortalised through BMI1 and hTERT overexpression. They also demonstrated the ability of rat urothelial cells to express CYP2B enzymes after xenobiotic-induction *in vivo*.

The short lifespan of NRU cells in culture limited the amount of cell characterisation that could be achieved. In particular, the differentiation status of NRU cells in culture needs to be investigated in order to allow a complete comparison of NRU and NHU cell culture systems to be made. Results in this project, such as NRU cells growing in colonies and the expression of a few markers of differentiation, have hinted at the fact that NRU cells may have a different phenotype in culture to NHU cells and this needs to be assessed in order to completely understand the differences discovered. Distinguishing the type of cell death NRU cells were undergoing (e.g. senescence, apoptosis) would also be interesting to investigate as modulation of the mechanism could enable NRU cells to be subcultured further.

In relation to overexpression of BMI1 in NHU cells, time was the limiting factor. Continuing to grow and differentiate BMI1 overexpressing NHU cell lines, in addition to investigating expression of cell senescence associated proteins such as p16<sup>INK4a</sup>, will reveal the full potential of these cells. Repeating the results in at least on more donor cell line is also required. To fully validate normal urothelial cell culture systems for use in toxicity testing additional work is required, in particular to explore the lifespan and differentiation capabilities of BMI1 overexpressing NHU cells. Further investigation of the growth pathways active in NRU cells and would be beneficial for clarifying the differences discovered between NRU and NHU cells.

Induction of all 6 CYP2B transcripts was shown to occur in rat urothelial cells *in vivo* but, based on expression in other tissues (reviewed by Elia, 1996), one of more CYP2B enzymes are likely to be predominantly expressed. To further understand urothelial CYP2B expression and quantify the amount of CYP2B enzymes expressed, quantitative PCR could be conducted on control and phenobarbital-treated rat urothelial RNA. Additionally, microarray analysis would quantify any differential induction of the six rat CYP2B gene transcripts by rat urothelium. Confirming the CYP2B induction seen in the rat *ex vivo* organ culture could also be important in validating the *ex vivo* model for use in metabolism/toxicity testing. Exploring CYP2B induction in a human organ culture could also be interesting and may provide a platform for rat and human CYP2B induction to be compared side by side and would also be interesting in understanding the role of the stroma in regulating urothelial CYP2B expression.

Together, these results demonstrate the potential benefits of *in vitro* systems and highlight the necessity for human relevant models to be included in toxicity testing. The findings reveal species variations in urothelial cells from rats and humans that could have important implications for toxicity testing and demonstrate how these differences can be assessed *in vitro*. Additionally these data reveal a novel metabolic capability of urothelial cells and a possible mechanism for modelling this in an *ex*

*vivo* model. Together this project supports the case for incorporating *in vitro* systems in toxicity testing and provides a platform for the complete validation of normal urothelial cell culture systems for use in toxicity testing.

## Chapter 8 Appendices

### Appendices 1 – Materials and Method

#### Appendix 1.1 – Tissue harvesting and *in vivo* experimentation locations

- Charles River  
Elpinstone Research Centre  
Tranent  
East Lothian  
EH33 2NE
- Food and environment research agency (FERA)  
National Agrifood Innovation Campus  
Sand Hutton  
York  
YO41 1LZ
- Leatherhead Food Research  
Randalls Way  
Leatherhead,  
Surrey  
KT22 7RY
- The University of Leeds  
Worsley Building  
University of Leeds  
Leeds  
LS2 9NL
- The University of Manchester  
Stopford Building  
Oxford Road  
Manchester  
M13 9PL
- The University of York  
BSF  
Department of Biology  
University of York  
Heslington  
York  
YO10 5DD
- Sequani

**Bromyard Road  
Ledbury  
Herefordshire  
HR8 1LH**

## **Appendix 1.2 – List of Suppliers**

- Adgilent Technologies - [www.agilent.com/home](http://www.agilent.com/home)
- Bayer Healthcare Pharmaceuticals - [www.bayerpharma.com](http://www.bayerpharma.com)
- BDH Chemicals - [www.labdepotinc.com/Chemicals](http://www.labdepotinc.com/Chemicals)
- Bioline - [www.bioline.com](http://www.bioline.com)
- Bio-Rad – [www.bio-rad.com](http://www.bio-rad.com)
- CA Hendley – [Oakwood Hill Industrial Estate, Loughton, Essex, UK](http://www.ca-hendley.com)
- Calbiochem - [www.calbiochem.com](http://www.calbiochem.com)
- Cell Signalling Technologies - [www.cellsignal.com](http://www.cellsignal.com)
- CellPath – [www.cellpath.co.uk](http://www.cellpath.co.uk)
- Charles River Laboratories - [www.criver.com](http://www.criver.com)
- Clontech Laboratories – [www.clontech.com](http://www.clontech.com)
- Corning Incorporated – [www.corning.com](http://www.corning.com)
- Dako – [www.dako.com](http://www.dako.com)
- Elga LabWater – [www.elgalabwater.com](http://www.elgalabwater.com)
- Envair – [www.envair.co.uk](http://www.envair.co.uk)
- Eurofins UK – [www.eurofins.co.uk](http://www.eurofins.co.uk)
- Fisher Scientific - [www.fisher.co.uk](http://www.fisher.co.uk)
- Harlan Sera-lab - [www.harlanseralab.co.uk](http://www.harlanseralab.co.uk)
- Hettich Centrifuges UK - [www.hettichcentrifuge.co.uk](http://www.hettichcentrifuge.co.uk)
- Pierce - [www.piercenet.com](http://www.piercenet.com)
- Li-Cor Biosciences – [www.licor.com](http://www.licor.com)
- Life Technologies - [www.lifetechnologies.com](http://www.lifetechnologies.com)
- Millipore – [www.millipore.com](http://www.millipore.com)
- Molecular Probes – [www.lifetechnologies.com](http://www.lifetechnologies.com)
- New England Bioscience Inc. – [www.neb.com](http://www.neb.com)
- Nordic Pharma Group - [www.nordicpharmagroup.com](http://www.nordicpharmagroup.com)

- Novocastra - [www.novocastra.co.uk](http://www.novocastra.co.uk)
- Olympus – [www.olympus.co.uk](http://www.olympus.co.uk)
- Progen Scientific - [www.progensci.co.uk](http://www.progensci.co.uk)
- Promega – [www.promega.com](http://www.promega.com)
- Quiagen – [www.quiagen.com](http://www.quiagen.com)
- Sartorius lab products – [www.sartorius.co.uk](http://www.sartorius.co.uk)
- Sarstedt – [www.sarstedt.com](http://www.sarstedt.com)
- Shimadzu Scientific instruments - [www.ssi.shimadzu.com/](http://www.ssi.shimadzu.com/)
- Sigma Aldrich – [www.sigmaaldrich.com](http://www.sigmaaldrich.com)
- Scientific Lab Supplies (SLS) Ltd. - [www.scientificlabs.co.uk](http://www.scientificlabs.co.uk)
- Starlab UK – [www.Starlab.co.uk](http://www.Starlab.co.uk)
- Statebourne - [www.statebourne.com](http://www.statebourne.com)
- The Binding Site - [www.thebindingsite.com](http://www.thebindingsite.com)
- Thermo Electron Corporation – [www.thermoscientific.com](http://www.thermoscientific.com)
- Thermo Fisher – [www.thermofisher.com](http://www.thermofisher.com)
- Thermo Scientific - [www.thermoscientific.com](http://www.thermoscientific.com)
- Vector Laboratories – [www.vectorlabs.com](http://www.vectorlabs.com)
- VWR chemicals – [www.uk.vwr.com](http://www.uk.vwr.com)
- Zeiss – [www.zeiss.co.uk](http://www.zeiss.co.uk)
- Zymed – [www.lifetechnologies.com](http://www.lifetechnologies.com)

### **Appendix 1.3 Online resources**

- Chromas (v2.4.3) - <http://technelysium.com.au>
- GeneSnap 7.07 software - [www.syngene.co.uk/genesnap](http://www.syngene.co.uk/genesnap)
- HistoQuest - [www.tissuegnostics.com/EN/software/histoquest.php](http://www.tissuegnostics.com/EN/software/histoquest.php)
- Kalign multiple sequence alignment - [www.ebi.ac.uk/Tools/msa/kalign](http://www.ebi.ac.uk/Tools/msa/kalign)
- Primer-Blast - [www.ncbi.nlm.nih.gov/tools/primer-blast](http://www.ncbi.nlm.nih.gov/tools/primer-blast)
- TissueQuest - [www.tissuegnostics.com/EN/software/tissuequest.php](http://www.tissuegnostics.com/EN/software/tissuequest.php)

- Zen (Blue) software -

[http://www.zeiss.co.uk/microscopy/en\\_gb/products/microscope-software/zen-lite.html](http://www.zeiss.co.uk/microscopy/en_gb/products/microscope-software/zen-lite.html)

## **Appendix 1.4 – Solutions**

### **Appendix 1.4.1 General solutions**

#### **Phosphate Buffered Saline (PBS)**

5 x PBS tables (sigma) were dissolved in 1 L of dH<sub>2</sub>O and autoclaved at 121°C (1 bar) for 20 minutes and cooled to room temperature before use.

#### **Tris Buffered Saline (TBS)**

1 L made in dH<sub>2</sub>O consisting of:

0.5M Tris-HCL

0.15M NaCl

The pH adjusted to 7.6

### **Appendix 1.4.2 Tissue Culture**

#### **NHU cell “stripper” solution**

500ml HBSS (-Ca<sup>2+</sup>, Mg<sup>2+</sup>) (Gibco; Life Technologies) was supplemented with 5 mL 1M HEPES (Gibco; Life Technologies), 50 mLs of 1% (w/v) EDTA and 1mL Trasylol (Nordic Pharma) to achieve 100,000 KIU / 100 mLs.

#### **Cholera toxin**

Cholera toxin powder (Sigma Aldrich) was dissolved in 34.3 mL of KSFM medium (without supplements) and stored at 4°C. When diluted in 500 mL KSFMc medium the final concentration of cholera toxin is 30 ng/mL.

#### **Collagenase IV solution**

Collagenase IV powder (Sigma Aldrich) was dissolved in HBSS (+Ca<sup>2+</sup>, +Mg<sup>2+</sup>) + 10mM HEPES (Life Technologies) to a final concentration of 10,000U per 100 mL. The solution was filter sterilized through by a 0.2 µm low protein-binding syringe filter (Gelman; Sigma Aldrich) and stored at -20°C.

#### **0.5% Dispase II solution**

dPBS (-Mg<sup>2+</sup>, -Cl<sup>-</sup>) was heated to 37°C and dispase II added slowly to a concentration of 0.5% (w/v). Samples were vortexed and filtered through Whatman 0 filter paper followed by a 0.2 µm low protein-binding syringe filter (Gelman; Sigma Aldrich). 0.5% Dispase II solution was aliquoted into 5 mL aliquots and stored at -20°C.

#### **0.1% EDTA solution**

1g EDTA (Fisher Scientific) was dissolved in 1000 mL of dPBS and autoclaved at 121°C (1 bar) for 20 minutes and cooled to room temperature before use.

#### **Trypsin in Versene**

20 ml of 10x Trypsin (Sigma Aldrich)  
4 mL 1% (w/v) EDTA  
Made up to 200 mL using HBSS (-Ca<sup>2+</sup>, -Mg<sup>2+</sup>)

#### **Trypsin Inhibitor (Ti)**

100 mg of Trypsin inhibitor (Sigma) was dissolved in 5ml dPBS and filter sterilised with 0.2µm filter (Gelman; Sigma Aldrich). Ti was aliquoted into 100µL aliquots and stored at -20°C.

### **Appendix 1.4.3 Histology**

#### **10% (v/v) Formalin**

100 mL 37% (v/v) Formaldehyde  
900 mL of PBS containing 0.9 mM CaCl<sub>2</sub> and 0.5 mM MgCl<sub>2</sub>

#### **Haematoxylin**

A solution containing 3g Haematoxylin in 20 mL 100% ethanol was added to a solution containing 0.3 g Sodium Iodate, 1 g Citric acid and 50 g Aluminium Potassium Sulphate in 850 mL of dH<sub>2</sub>O were mixed thoroughly together and 120 mL of glycerol added.

#### **Tris Buffered Saline (TBS)**

1 L made in dH<sub>2</sub>O consisting of:  
0.5M Tris-HCL (Sigma Aldrich)  
0.15M NaCl (SLS)  
The pH adjusted to 7.6

#### **Tris Buffered Saline plus Tween®20 (TBST)**

1 L made in dH<sub>2</sub>O consisting of:  
0.5M Tris-HCL

**0.15M NaCl**  
**0.1% Tween®20 (Sigma Aldrich)**  
**The pH adjusted to 7.6**

#### **IF antibody diluent solution**

TBS (pH 7.6) containing 0.1% (w/v) NaN<sub>3</sub> and 0.1% (v/v) BSA. IF antibody diluent was kept at 4°C.

#### **IF anti-fade mounting solution**

0.1% (w/v) p-PhenyldiaminoDihydrochloride in 90% (w/v) glycerol in PBS. The solution was buffered to pH 8.0 using carbonate-bicarbonate buffer (pH 9.6).

### **Appendix 1.4.4 Molecular Biology**

#### **10 x TBE buffer**

0.9 M Tris, 0.9 M Boric acid, 25 mM EDTA in dH<sub>2</sub>O. TBE buffer was diluted 1:10 prior to use.

#### **Luria Broth (LB)**

10 g Tryptone, 10 ng NaCl, 5 g Yeast extract was made up to 1 L in dH<sub>2</sub>O and autoclaved immediately.

#### **LB-Agar**

2 % (w/v) agar was added to LB and the solution autoclaved immediately.

### **Appendix 1.4.5 Western Blotting**

#### **2 x SDS Lysis Buffer**

20% (v/v) glycerol, 2% (w/v) Sodium Dodecyl Sulphate, 125 mM Tris-HCL (pH 6.8), 0.42 g Sodium Fluoride (NaF), 18.4 mg Sodium orthovanadate (Na<sub>3</sub>PO<sub>4</sub>) 0.446 g tetra-Sodium pyrophosphate made up to 50 mL of dH<sub>2</sub>O. 2 x SDS lysis buffer was stored at -20°C.

#### **Protease inhibitor cocktail**

104 mM AEBSF, 80 μM Aprotinin, 4 mM Bestatin, 1.4 mM E-64, 2 mM Leupeptin and 1.5 mM Pepstatin A.

**Transfer Buffer**

12 mM Tris, 96 mM Glycine, 20% (v/v) Methanol made up to 1 L in dH<sub>2</sub>O.

**Western Blot TBS**

10 mM Tris, 140 mM NaCl made up to 1 L in dH<sub>2</sub>O and the pH adjusted to pH 7.4.

**Western Blot TBST**

10 mM Tris, 140 mM NaCl and 0.1% (w/v) Tween<sup>®</sup>20 made up to 1 L in dH<sub>2</sub>O and the pH adjusted to pH 7.4

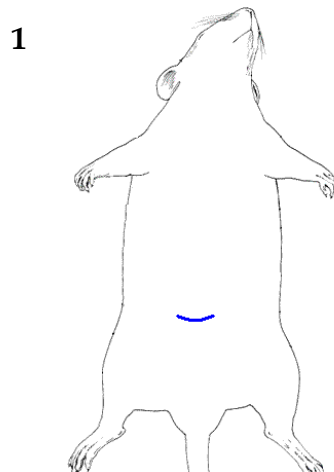
## Appendix 1.6 Primers

Target	Forward/Reverse	Species	Sequence	Product size
BMI1 whole gene	F	Human	AAAAAAGTTAACACCATGCATCGAACAACGAGAATC	999
BMI1 whole gene	R	Human	AAAAAAGGATCCTCAACCAGAAGAAGTTGCTGATG	
BMI1	F	Human	TCATCCTTCTGCTGATGCTG	221
BMI1	R	Human	GCATCACAGTCATTGCTGCT	
CYP2B1/2	F	Rat	GGCCTGTGGTCATGCTATGT	720/740
CYP2B1/2	R	Rat	GCAGGAAACCATAGCGGAGT	
CYP2B3	F	Rat	AGTGCCTCACAGGCAACATA	278
CYP2B3	R	Rat	AAAGTCTCGGGGAGCATTGG	
CYP2B12	F	Rat	CCCAGTGCTCCACGAGATT	701
CYP2B12	R	Rat	CGGGACAGGAAGTTTATCTGGT	
CYP2B15	F	Rat	AGAAGAGGCCTTCTGCGTTC	650
CYP2B15	R	Rat	AAGTCTCGTGGAGTGTTGGG	
CYP2B21	F	Rat	GTACTTTCCTGGCACCACA	628
CYP2B21	R	Rat	ACGCTTTCCTGTGGAGAAGG	
CYP2B generic	F	Rat	CAAAGGAGATTGATCAGGTGA	173
CYP2B generic	R	Rat	AGCAGGTACCCTCGGAAC	
CYP2B6	F	Human	TTGCTACTCCTGGTTCAGCG	84
CYP2B6	R	Human	AAGGTTTCCCAAAGGGGCA	
KRT7	F	Rat	GGCAGAGATTGACACCGTGA	257
KRT7	R	Rat	CAGACAACCTGCTCTCCTCG	
GAPDH	F	Human/Rat	CAAGGTCATCCATGACAACCTTG	90
GAPDH	R	Human/Rat	GGGCCATCCACAGTCTTCTG	
Smooth muscle actin	F	Rat	CGTCCTGGATTCAGGGGATG	155

Smooth muscle actin	<b>R</b>	<b>Rat</b>	<b>TGGTCACAAAGGAATAGCCTCT</b>	
---------------------	----------	------------	-------------------------------	--

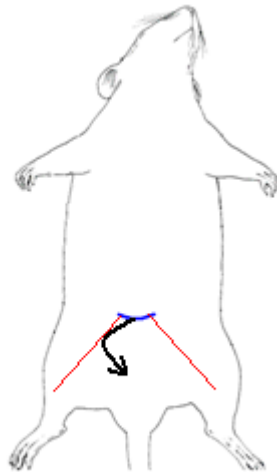
## Appendix 1.7 – Aseptic removal of rat bladder tissue (protocol)

1. Cull rats according to SK1 regulations
2. Lay the animal on its back and spray the abdomen with 70% ethanol.
3. Make incision in approximately the middle of the animal's abdomen equidistant between the bottom of the sternum and the base of the tail. Only penetrate outer layer of skin, do not pierce the abdominal cavity (1).



4. Use a pair of (round nose) scissors to detach the skin from the abdominal wall. To do this lift the skin of the animal using forceps and insert the end of a closed pair of scissors into the incision at approximately a 45° angle pointing down the animal (towards the tail). Open the scissors across the animal between the skin and abdominal wall, separating the two tissues. Use this technique (opening the scissors between the tissues) until the separation extends from the incision to the tail.

2

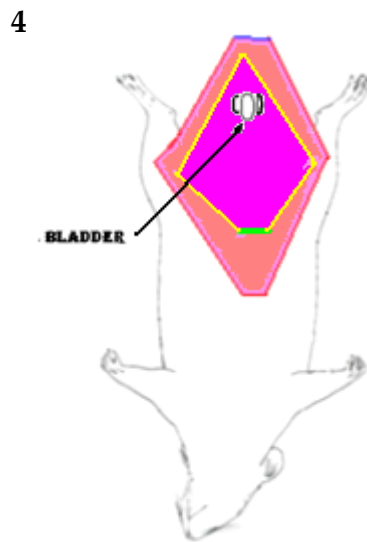


5. Cut the skin diagonally from the central incision to the hips as indicated and pull back the skin to expose the lower abdominal wall (3).
6. Spray the exposed area with 70% ethanol
7. Using fresh instruments lift the abdominal wall at a point just below where the initial incision was made and make an incision in the pleural wall. Cut diagonally outwards to the hips (do not pierce internal organs) (3). This is often easier if the animal is turned around with its head closest to you and its tail furthest away.

3



8. Pull back the external tissue covering the lower organs of the abdomen. When pulled back completely the bladder will be lifted into an erect position, especially when full. Using a fresh set of instruments lift the bladder and cut it at the base. Unlike other tissue in this area, the base of the bladder is visibly vascular. Place the bladder straight into sterile transport medium.

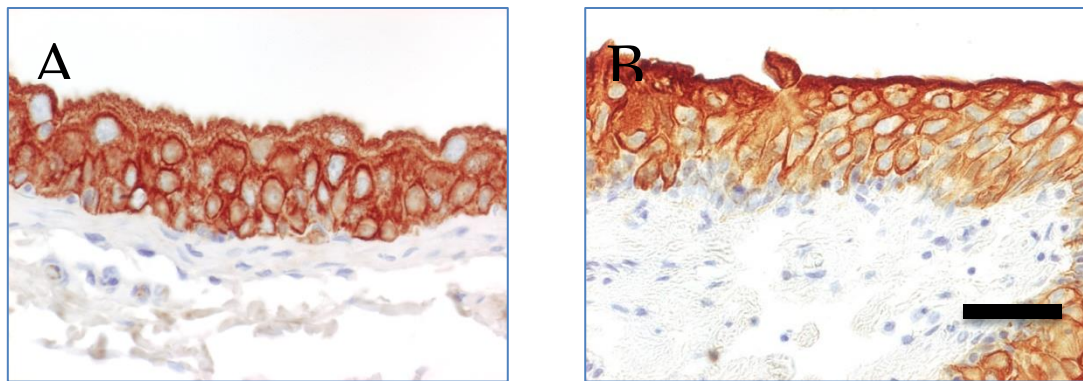


## Appendices 2 – Results

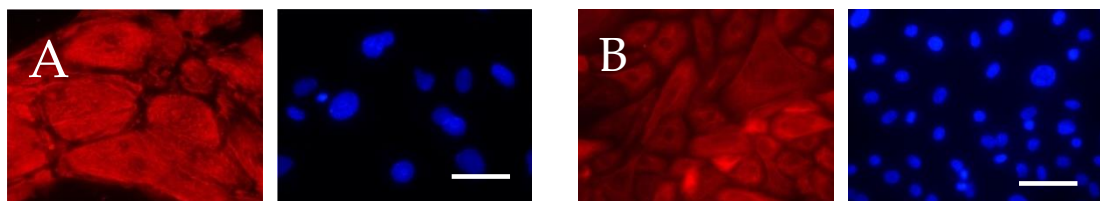
### Appendices 2.1 Antibody specificity

All antibodies were used at optimised concentrations. Appropriate positive and secondary antibody only controls were included in each experiment.

#### Appendix 2.1.1 Cytokeratin 7

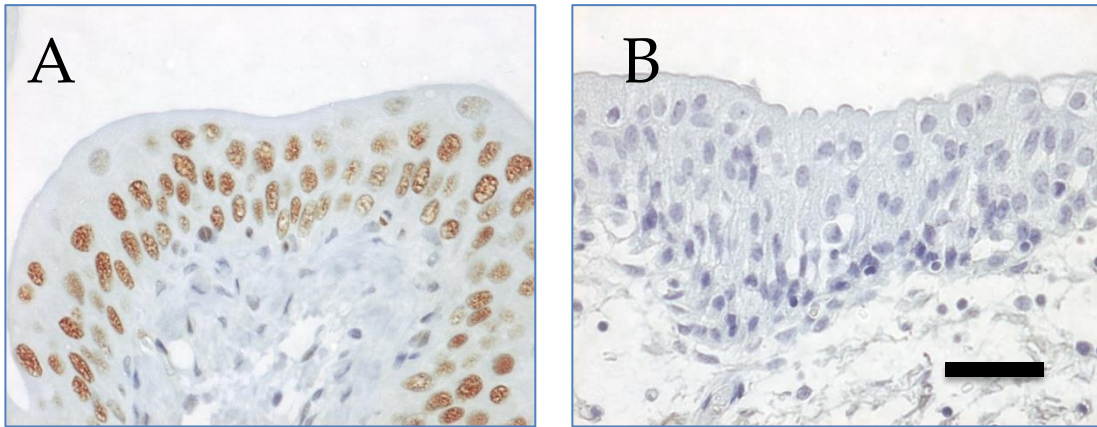


Cytokeratin 7 expression in rat (A) and human (B) bladder sections (FFPE). Scale bars = 50 $\mu$ m.

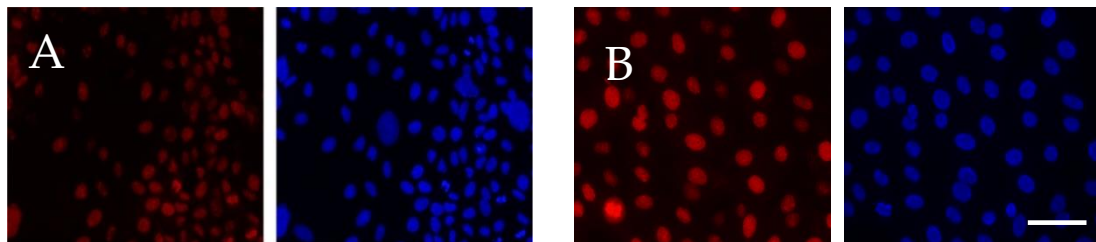


Cytokeratin 7 (CK7) labelling (red) of NRU-W (A) and NHU (B) cells cultured for 5 days in KSFMC medium. Cells were fixed (methanol: acetone) and cell nuclei were stained with Hoechst 33258. Scale bars = 50 $\mu$ m.

Appendix 2.1.2 – Ki67

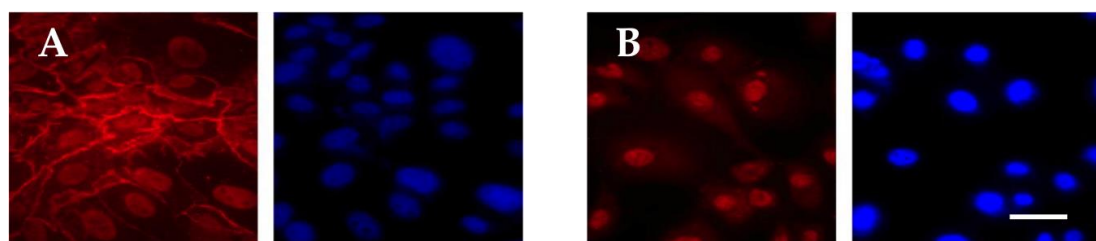


Ki67 labelling of rat (A) and human (B) bladder sections (FFPE). Scale bars = 50µm.



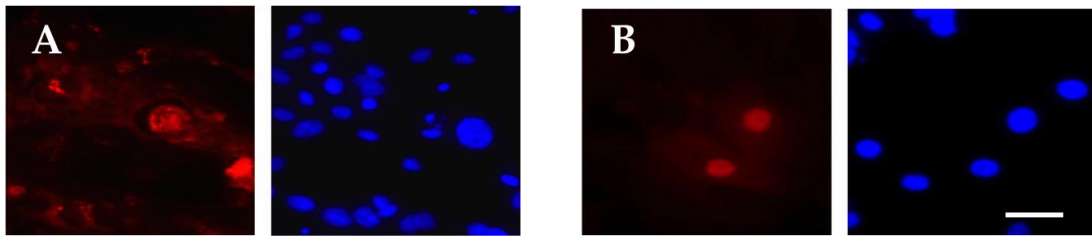
Ki67 labelling (red) of NRU (A) and NHU (B) cells cultured for 5 days in KSFMC medium. Cells were fixed (methanol: acetone) and cell nuclei were stained with Hoechst 33258. Scale bars = 50µm.

Appendix 2.1.3 –  $\beta$ -catenin



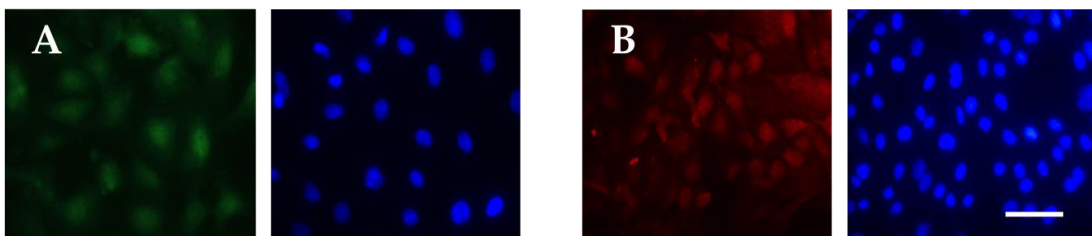
$\beta$ -catenin labelling (red) of NRU (A) and NHU (B) cells cultured for 5 days in KSFMC medium. Cells were fixed (methanol: acetone) and cell nuclei were stained with Hoechst 33258. Scale bars = 50µm.

## Appendix 2.1.4 – phospho-ERK



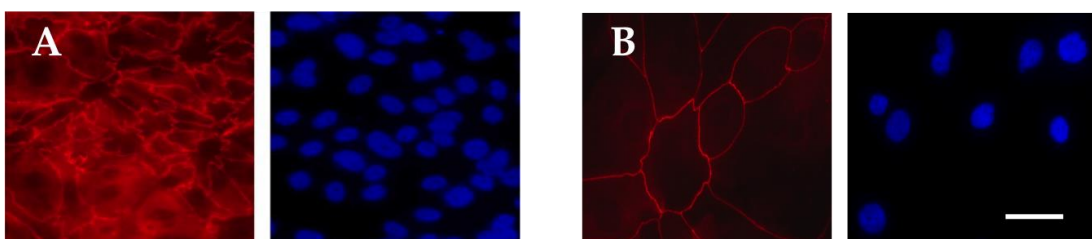
Phospho-ERK labelling (red) of rat stromal cells (A) and NHU (B) cells cultured for 5 days in KSFMC medium. Cells were fixed (methanol: acetone) and cell nuclei were stained with Hoechst 33258. Scale bars = 50 $\mu$ m.

## Appendix 2.1.5 – phospho-Akt

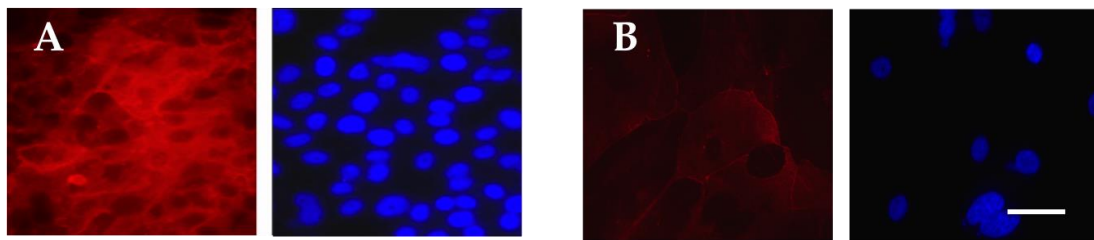


Phospho-Akt labelling (green & red) of control NRU (A) and NHU (2mM Ca<sup>+</sup>) (B) cells cultured for 5 days in KSFMC medium. Cells were fixed (methanol: acetone) and cell nuclei were stained with Hoechst 33258. Scale bars = 50 $\mu$ m.

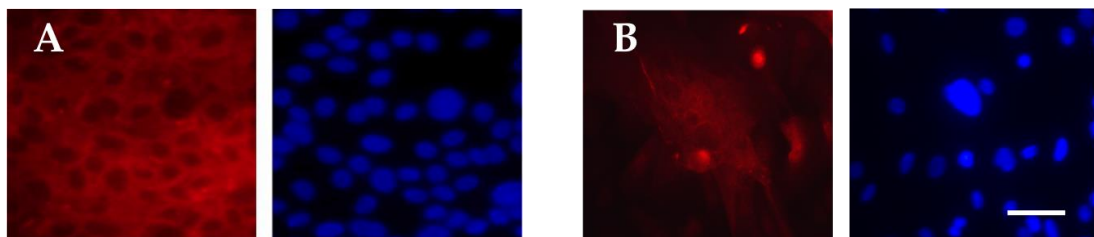
## Appendix 2.1.6 – ZO-1



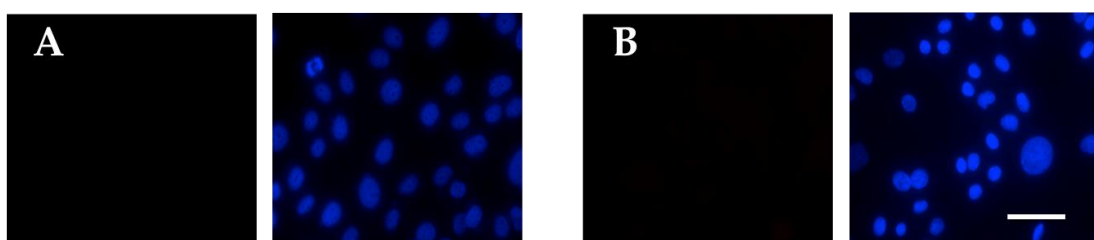
-ZO-1 labelling (red) of control NRU (A) and differentiated (ABS/Ca<sup>2+</sup>) NHU (B) cells cultured for 5 days in KSFMC medium. Cells were fixed (methanol: acetone) and cell nuclei were stained with Hoechst 33258. Scale bars = 50 $\mu$ m.

**Appendix 2.1.7 – Claudin 4 (CL4)**

CL4 labelling (red) of control NRU (A) and differentiated (ABS/Ca<sup>2+</sup>) NHU (B) cells cultured for 5 days in KSFMC medium. Cells were fixed (methanol: acetone) and cell nuclei were stained with Hoechst 33258. Scale bars = 50µm.

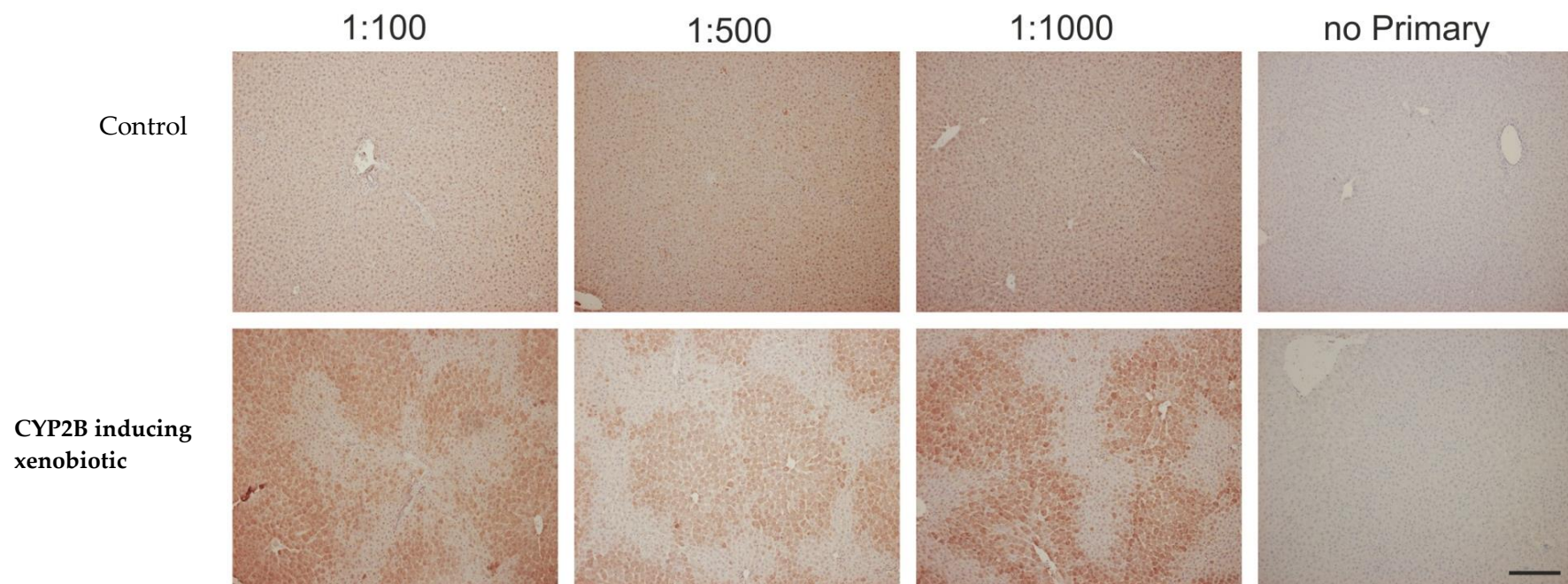
**Appendix 2.1.8 – Aquaporin 4 (AQP4)**

AQP4 labelling (red) of control NRU (A) and differentiated (ABS/Ca<sup>2+</sup>) NHU (B) cells cultured for 5 days in KSFMC medium. Cells were fixed (methanol: acetone) and cell nuclei were stained with Hoechst 33258. Scale bars = 50µm.

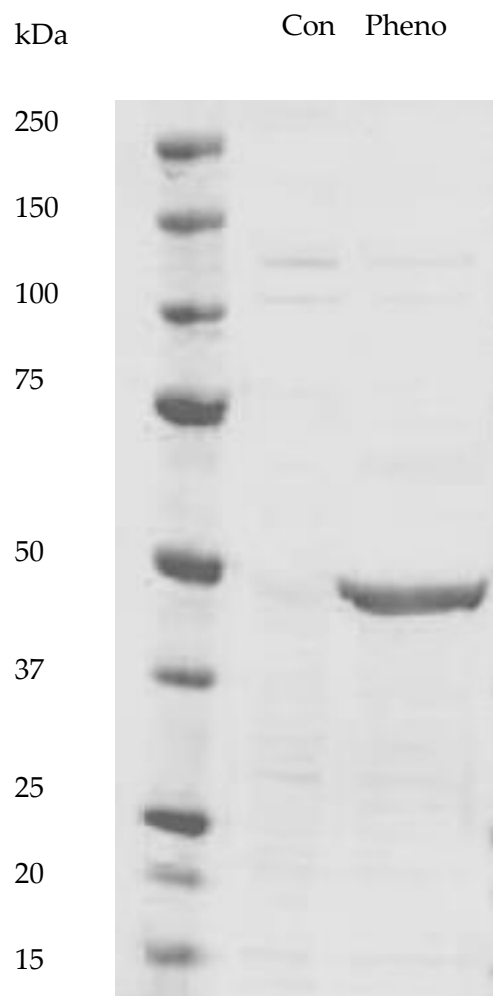
**Appendix 2.1.9 – Secondary Antibody only negative control**

Secondary antibody only negative control labelling (red) of control NRU (A) and differentiated (ABS/Ca<sup>2+</sup>) NHU (B) cells cultured for 5 days in KSFMC medium. Cells were fixed (methanol: acetone) and cell nuclei were stained with Hoechst 33258. Scale bars = 50µm.

## Appendix 5.1.10 Cytochrome P450 2B1/2 labelling



CYP2B1/2 antibody titration on control and CYP2B-inducing xenobiotic treated (7 days) rat liver sections. CYP2B1/2 antibody was tested at dilutions of 1:100, 1:500 and 1:1000 with 1:1000 chosen as the working dilution. A no primary antibody negative control was included. Scale bar = 200  $\mu$ m.

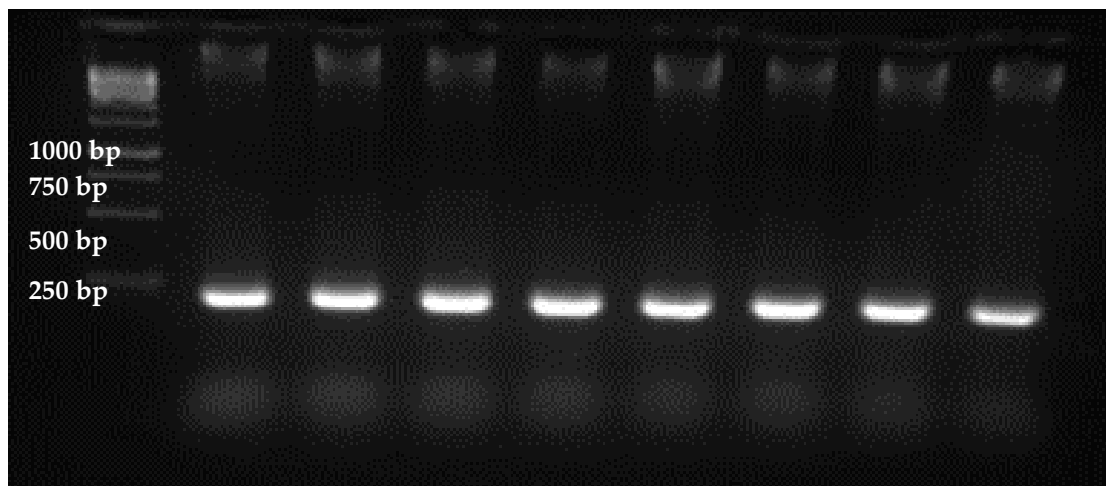


**CYP2B1/2 labelling of control (con) and phenobarbital-treated (Pheno) rat liver microsomes (Xenotech)**

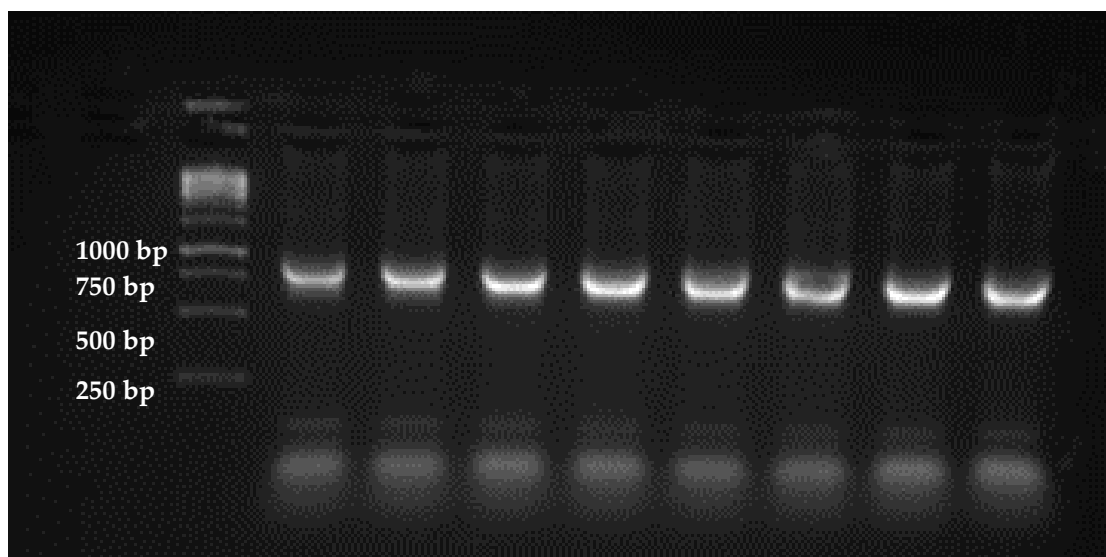
## Appendices 2.2 Primer T<sub>m</sub> optimisation (examples)

Gradient RT-PCR's (30 cycles) were conducted to optimise the annealing temperature (T<sub>m</sub>'s) for each primer set and to confirm the positive controls. T<sub>m</sub>'s ranged from 65°C (left) to 55°C (right). A number of examples are included.

### Appendix 2.2.1 – BMI1

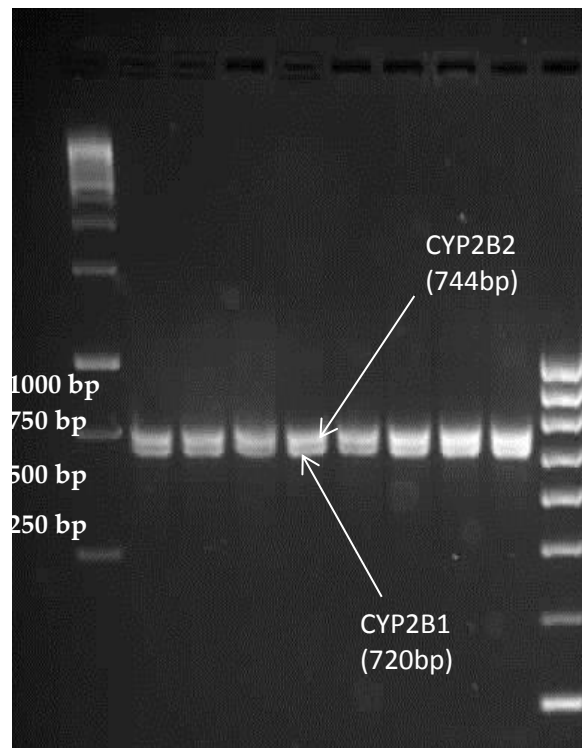


Gradient RT-PCR specifically amplifying a 181 bp section of BMI1 from proliferating NHU cDNA.



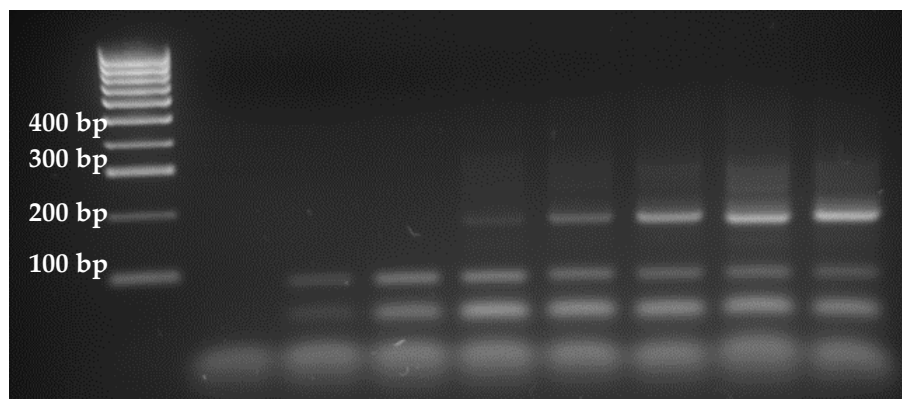
Gradient RT-PCR amplifying the entire BMI1 protein coding sequence from proliferating NHU cell cDNA

Appendix 2.2.2 - Cytochrome P450 2B1/2



Gradient RT-PCR using CYP2B1/CYP2B2 primers using control rat liver cDNA

Appendix 2.2.3 - CYP2B6



Gradient RT-PCR amplifying CYP2B6 from control human liver RNA.

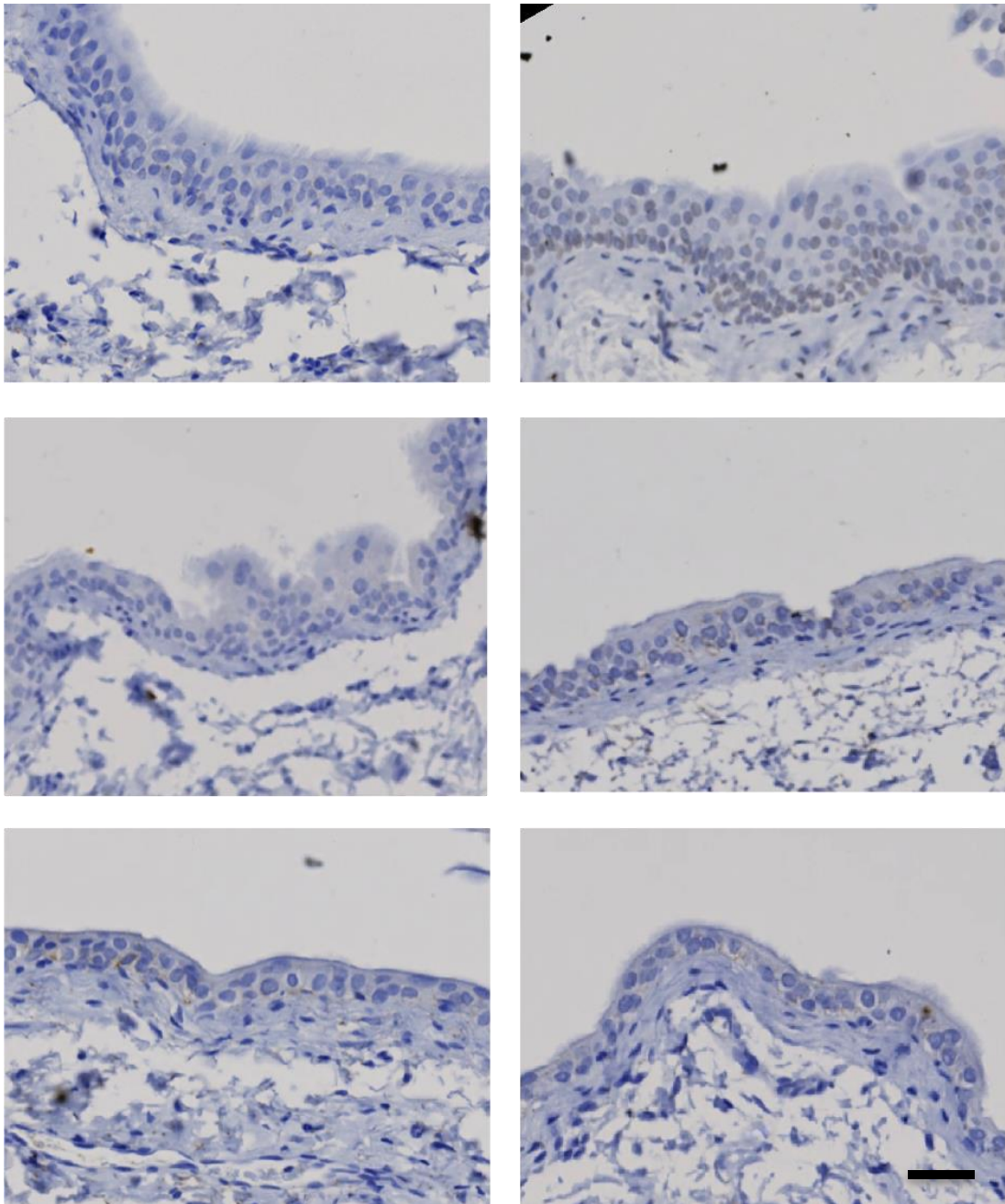
### Appendix 2.3 – BMI1 protein coding sequence

ATGCATCGAACAACGAGAATCAAGATCACTGAGCTAAATCCCCACCTGATGTGT  
GTGCTTTGTGGAGGGTACTTCATTGATGCCACAACCATAATAGAATGTCTACATT  
CCTTCTGTAAAACGTGTATTGTTTCGTTACCTGGAGACCAGCAAGTATTGTCCTAT  
TTGTGATGTCCAAGTTCACAAGACCAGACCACTACTGAATATAAGGTCAGATAA  
AACTCTCCAAGATATTGTATACAAATTAGTTCAGGGCTTTTCAAAAATGAAATG  
AAGAGAAGAAGGGATTTTTATGCAGCTCATCCTTCTGCTGATGCTGCCAATGGC  
TCTAATGAAGATAGAGGAGAGGTTGCAGATGAAGATAAGAGAATTATAACTGA  
TGATGAGATAATAAGCTTATCCATTGAATTCTTTGACCAGAACAGATTGGATCG  
GAAAGTAAACAAAGACAAAGAGAAATCTAAGGAGGAGGTGAATGATAAAAAGA  
TACTTACGATGCCCAGCAGCAATGACTGTGATGCACTTAAGAAAGTTTCTCAGA  
AGTAAAATGGACATACCTAATACTTTCCAGATTGATGTCATGTATGAGGAGGAA  
CCTTTAAAGGATTATTATACACTAATGGATATTGCCTACATTTATACCTGGAGAA  
GGAATGGTCCACTTCCATTGAAATACAGAGTTCGACCTACTTGTAAGAATGA  
AGATCAGTCACCAGAGAGATGGACTGACAAATGCTGGAGAAGTGGAAAAGTGAC  
TCTGGGAGTGACAAGGCCAACAGCCCAGCAGGAGGTATCCCTCCACCTCTTCT  
TGTTTGCCTAGCCCCAGTACTCCAGTGCAGTCTCCTCATCCACAGTTTCTCACAT  
TTCCAGTACTATGAATGGAACCAGCAACAGCCCCAGCGGTAACCACCAATCTTC  
TTTTGCCAATAGACCTCGAAAATCATCAGTAAATGGGTCATCAGCAACTTCTTCT  
GGTTGA

**Appendix 2.4 - CYP2B negative (no primary antibody)**

**controls** Control

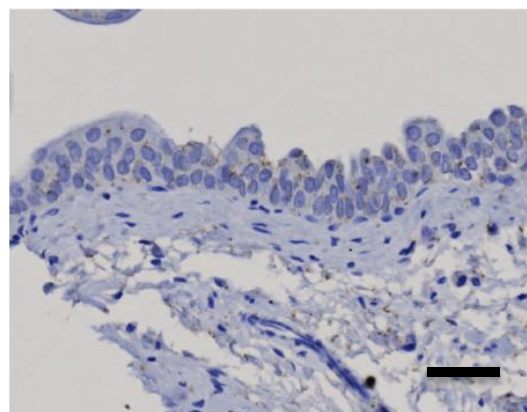
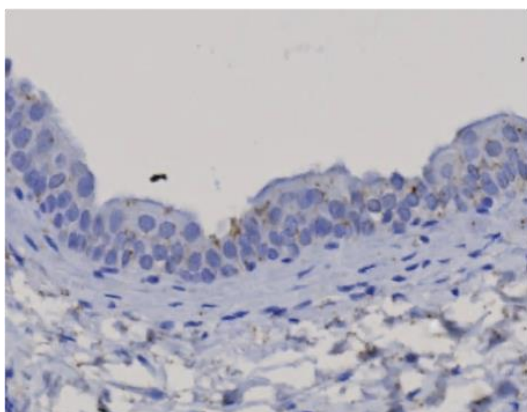
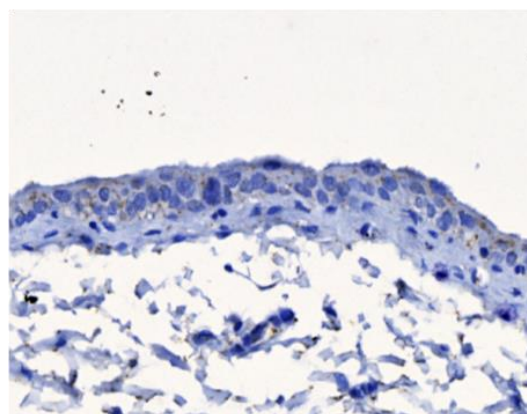
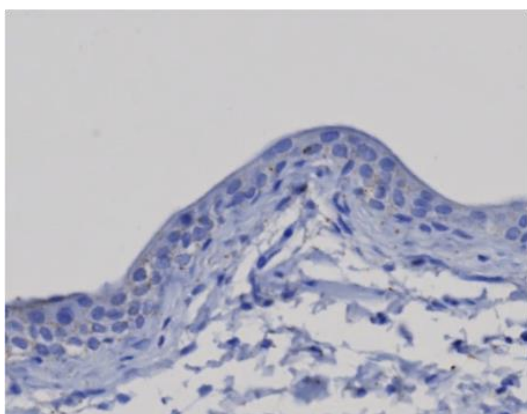
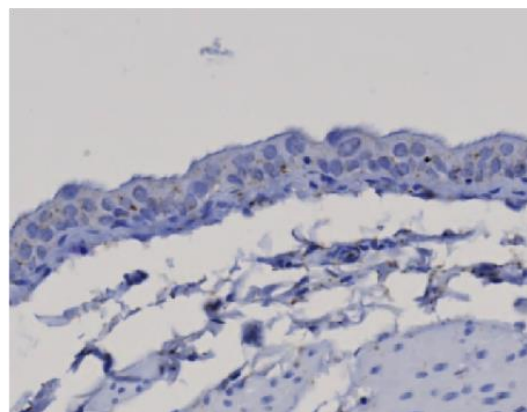
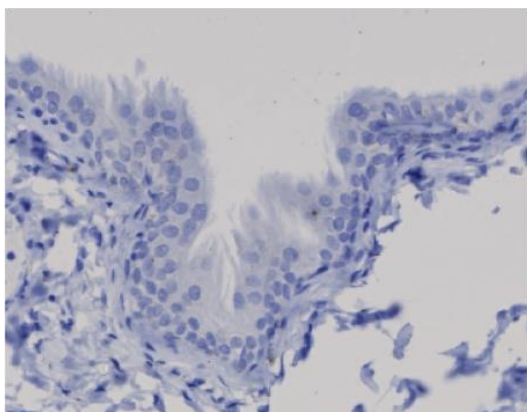
Phenobarbital-treated



Negative (no primary antibody) control immunolabelling images of control and phenobarbital-treated rat bladders after 3 days of treatment. Scale bars = 50  $\mu$ m

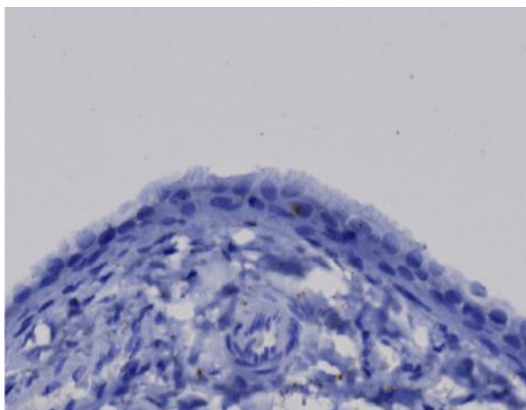
**Control**

**Phenobarbital-treated**

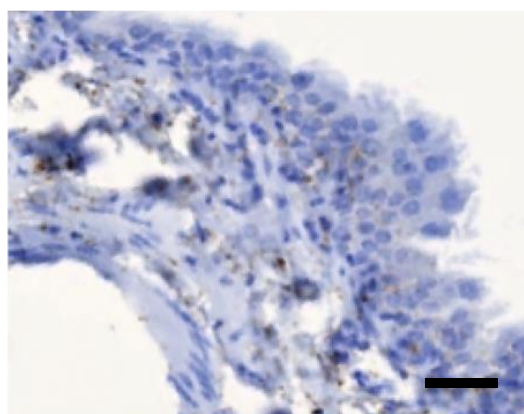
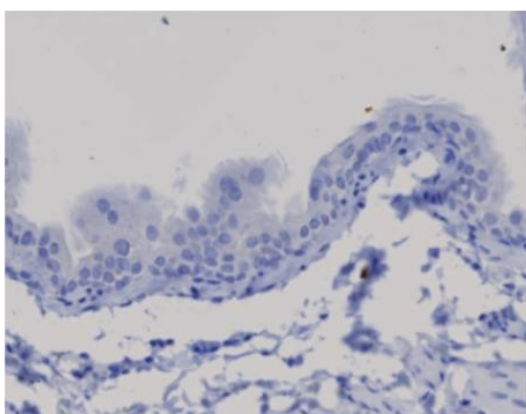
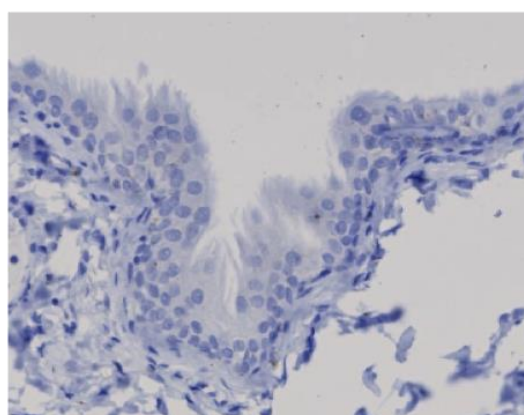
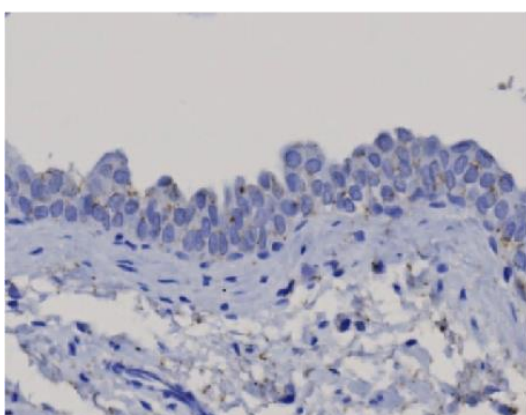
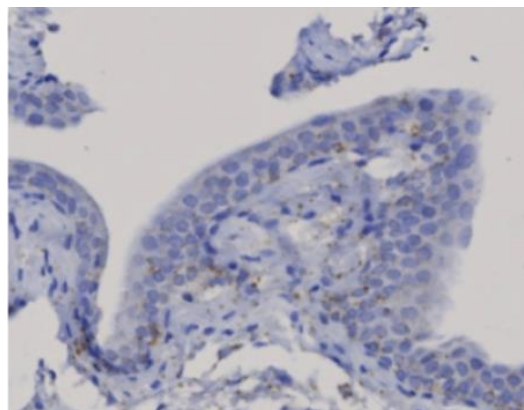


**Negative (no primary antibody) control immunolabelling images of control and phenobarbital-treated rat bladders after 7 days of treatment. Scale bars = 50  $\mu$ m**

Control



Phenobarbital-treated



Negative (no primary antibody) control immunolabelling images of control and phenobarbital-treated rat bladders after 14 days of treatment. Scale bars = 50  $\mu$ m

## Abbreviations

ABS – Adult Bovine Serum  
Akt – protein kinase B  
AQP3 – Aquaporin 3  
AUM – Asymmetric Unit Plaques  
BLAST – Basic Logical Alignment and Search Tool  
bp – base pair  
BPE – Bovine Pituitary Extract  
BMI1 - B cell-specific Moloney murine leukemia virus Integration site 1  
Ca<sup>2+</sup> - Calcium ion  
cDNA – complementary Deoxyribonucleic Acid  
CK - Cytokeratin  
CL4 – claudin 4  
CO<sub>2</sub> – carbon dioxide  
CT – Cholera Toxin  
CYP – Cytochrome P450  
D - Day  
DEPC – Diethyl Pyrocarbonate  
DMEM – Dulbecco's Modified Eagle's Medium  
DMSO - Dimethyl sulfoxide  
DNA - Deoxyribonucleic Acid  
dNTP – Deoxynucleotide triphosphate  
E.coli – Escherichia coli  
EDTA - Ethylenediaminetetraacetic acid  
EGF – Epidermal Growth Factor  
EGFR – Epidermal Growth Factor Receptor  
ERK - Extracellular signal-regulated kinase  
FBS – Fetal Bovine Serum  
FERA – Food and Environment Research Agency  
GAPDH – Glyceraldehyde-3-phosphate dehydrogenase  
GSK3 $\beta$  - Glycogen synthase kinase 3  $\beta$   
hTERT – human telomerase reverse transcriptase  
IC<sub>50</sub> – Half maximum inhibitory concentration  
IGF – Insulin Growth Factor  
JBU – Jack Birch Unit for Molecular Carcinogenesis  
Kb – Kilo-base  
kDa – Kilo Dalton  
KSFM – Keratinocyte Serum Free Medium  
KSFMc – Keratinocyte Serum Free Medium (complete)  
LB – Luria Broth  
M – Molar  
MAPK – Mitogen-Activated Protein Kinase  
MEK - Mitogen-Activated Protein Kinase Kinase  
mg – milligrams  
mL – millilitres  
mM – millimolar  
N<sub>2</sub> – Nitrogen  
ng - nanograms

NHU – Normal Human Urothelial  
nM - nanomolar  
nm – nanometers  
NRU – Normal Rat Urothelial  
O<sub>2</sub> – Oxygen  
°C – degrees centigrade  
P – Passage number  
PBS – Phosphate Buffered Saline  
PCR – Polymerase Chain Reaction  
PD - Population doubling  
Phospho – Phosphorylated  
PI3K - Phosphoinositide 3-kinase  
RNA – Ribonucleic Acid  
rpm – rotations per minute  
RT - Reverse Transcriptase  
SDS-PAGE – Sodium Dodecyl Sulfate - Polyacrylamide Gel Electrophoresis  
TEER – Transepithelial Electrical Resistance  
TGF – Transforming Growth Factor  
UP3a – Uroplakin 3a  
v/v – volume/volume  
w/v – weight/volume  
ZO-1 – Zona occludin 1  
µg - micrograms  
µL – microliters  
µM – micromolar

## Bibliography

- ABDEL-RAZZAK, Z., LOYER, P., FAUTREL, A., GAUTIER, J. C., CORCOS, L., TURLIN, B., BEAUNE, P. & GUILLOUZO, A. 1993. Cytokines down-regulate expression of major cytochrome P-450 enzymes in adult human hepatocytes in primary culture. *Mol Pharmacol*, 44, 707-15.
- AKAGI, K., SANO, M., OGAWA, K., HIROSE, M., GOSHIMA, H. & SHIRAI, T. 2003. Involvement of toxicity as an early event in urinary bladder carcinogenesis induced by phenethyl isothiocyanate, benzyl isothiocyanate, and analogues in F344 rats. *Toxicol Pathol*, 31, 388-96.
- ALKEMA, M., WIEGANT, J., RAAP, A. K., BEMS, A. & VAN LOHUIZEN, M. 1993. Characterization and chromosomal localization of the human proto-oncogene BMI-1. *Human Molecular Genetics*, 2, 1597-1603.
- ALKEMA, M. J., VAN DER LUGT, N. M. T., BOBELDIJK, R. C., BERNS, A. & VAN LOHUIZEN, M. 1995. Transformation of axial skeleton due to overexpression of bmi-1 in transgenic mice. *Nature*, 374, 724-727.
- ANDERSEN, M. E. 2003. Toxicokinetic modeling and its applications in chemical risk assessment. *Toxicology Letters*, 138, 9-27.
- ANDERSEN, M. E. & KREWSKI, D. 2009. Toxicity Testing in the 21st Century: Bringing the Vision to Life. *Toxicological Sciences*, 107, 324-330.
- ANDERSEN, M. E. & KREWSKI, D. 2010. The vision of toxicity testing in the 21st century: moving from discussion to action. *Toxicol Sci*, 117, 17-24.
- ANDERSON, J. M. & VAN ITALLIE, C. M. 2009. Physiology and function of the tight junction. *Cold Spring Harb Perspect Biol*, 1, a002584.
- ANDERSSON, K. E. & ARNER, A. 2004. Urinary bladder contraction and relaxation: physiology and pathophysiology. *Physiol Rev*, 84, 935-86.
- ANZENBACHER, P. & ANZENBACHEROVÁ, E. 2001. Cytochromes P450 and metabolism of xenobiotics. *Cellular and Molecular Life Sciences CMLS*, 58, 737-747.
- ANZENBACHER, P. & ZANGER, U. M. 2012. *Metabolism of drugs and other xenobiotics*, Weinheim, Wiley-VCH.

- APODACA, G. 2004. The Uroepithelium: Not Just a Passive Barrier. *Traffic*, 5, 117-128.
- BAKER, S. C., SHABIR, S. & SOUTHGATE, J. 2014. Biomimetic urothelial tissue models for the in vitro evaluation of barrier physiology and bladder drug efficacy. *Mol Pharm*, 11, 1964-70.
- BALASUBRAMANIAN, S., LEE, K., ADHIKARY, G., GOPALAKRISHNAN, R., RORKE, E. A. & ECKERT, R. L. 2008. The Bmi-1 polycomb group gene in skin cancer: regulation of function by (-)-epigallocatechin-3-gallate. *Nutrition Reviews*, 66, S65-S68.
- BASKIN, L. S., SUTHERLAND, R. S., THOMSON, A. A., NGUYEN, H.-T., MORGAN, D. M., HAYWARD, S. W., HOM, Y. K., DISANDRO, M. & CUNHA, G. R. 1997. Growth Factors in Bladder Wound Healing. *The Journal of Urology*, 157, 2388-2395.
- BECKEL, J. M. & BIRDER, L. A. 2012. Differential expression and function of nicotinic acetylcholine receptors in the urinary bladder epithelium of the rat. *The Journal of Physiology*, 590, 1465-1480.
- BIECHE, I., NARJOZ, C., ASSELAH, T., VACHER, S., MARCELLIN, P., LIDEREAU, R., BEAUNE, P. & DE WAZIERS, I. 2007. Reverse transcriptase-PCR quantification of mRNA levels from cytochrome (CYP)1, CYP2 and CYP3 families in 22 different human tissues. *Pharmacogenet Genomics*, 17, 731-42.
- BIRDER, L. A. 2010. Urothelial signaling. *Auton Neurosci*, 153, 33-40.
- BIRDER, L. A., APODACA, G., DE GROAT, W. C. & KANAI, A. J. 1998. Adrenergic- and capsaicin-evoked nitric oxide release from urothelium and afferent nerves in urinary bladder. *American Journal of Physiology - Renal Physiology*, 275, F226-F229.
- BIRDER, L. A., KANAI, A. J., CRUZ, F., MOORE, K. & FRY, C. H. 2010. Is the urothelium intelligent? *Neurourology and Urodynamics*, 29, 598-602.
- BLAAUBOER, B. J. & ANDERSEN, M. 2007. The need for a new toxicity testing and risk analysis paradigm to implement REACH or any other large scale testing initiative. *Archives of Toxicology*, 81, 385-387.
- BOCK, M., HINLEY, J., SCHMITT, C., WAHLICHT, T., KRAMER, S. & SOUTHGATE, J. 2014. Identification of ELF3 as an early transcriptional regulator of human urothelium. *Dev Biol*, 386, 321-30.

- BRAUERS, A., MANEGOLD, E., BUETTNER, R., BARON, J. M., MERK, H. F. & JAKSE, G. 2000. Cytochrome P450 isoenzyme mRNA expression pattern in human urinary bladder malignancies and normal urothelium. *Cancer Detect Prev*, 24, 356-63.
- BURDEN, N., SEWELL, F., ANDERSEN, M. E., BOOBIS, A., CHIPMAN, J. K., CRONIN, M. T., HUTCHINSON, T. H., KIMBER, I. & WHELAN, M. 2015. Adverse Outcome Pathways can drive non-animal approaches for safety assessment. *J Appl Toxicol*.
- CASTELL, J., JOVER, R., MART, NEZ, J., NEZ, C. P., MEZ, L., N, M. & A, J. 2006. Hepatocyte cell lines: their use, scope and limitations in drug metabolism studies. *Expert Opinion on Drug Metabolism and Toxicology*, 2, 183-212.
- CHAUDHARY, K. R., BATCHU, S. N. & SEUBERT, J. M. 2009. Cytochrome P450 enzymes and the heart. *IUBMB Life*, 61, 954-60.
- CHOPRA, B., GEVER, J., BARRICK, S. R., HANNA-MITCHELL, A. T., BECKEL, J. M., FORD, A. P. D. W. & BIRDER, L. A. 2008a. Expression and function of rat urothelial P2Y receptors. *American Journal of Physiology - Renal Physiology*, 294, F821-F829.
- CHOPRA, B., HINLEY, J., OLEKSIWICZ, M. B. & SOUTHGATE, J. 2008b. Trans-Species Comparison of PPAR and RXR Expression by Rat and Human Urothelial Tissues. *Toxicologic Pathology*, 36, 485-495.
- COHEN, K. J., HANNA, J. S., PRESCOTT, J. E. & DANG, C. V. 1996. Transformation by the Bmi-1 oncoprotein correlates with its subnuclear localization but not its transcriptional suppression activity. *Molecular and Cellular Biology*, 16, 5527-35.
- COHEN, S. M. 1989. Toxic and nontoxic changes induced in the urothelium by xenobiotics. *Toxicology and Applied Pharmacology*, 101, 484-498.
- CROSS, W. R., EARDLEY, I., LEESE, H. J. & SOUTHGATE, J. 2005. A biomimetic tissue from cultured normal human urothelial cells: analysis of physiological function. *American Journal of Physiology - Renal Physiology*, 289, F459-F468.
- CUNNINGHAM, M. L. 2002. A Mouse Is Not a Rat Is Not a Human: Species Differences Exist. *Toxicological Sciences*, 70, 157-158.
- CZEKAJ, P., WIADERKIEWICZ, A., FLOREK, E. & WIADERKIEWICZ, R. 2000. Expression of cytochrome CYP2B1/2 in nonpregnant, pregnant and fetal rats exposed to tobacco smoke. *Acta Biochim Pol*, 47, 1115-27.

- DALY, D., RONG, W., CHESS-WILLIAMS, R., CHAPPLE, C. & GRUNDY, D. 2007. Bladder afferent sensitivity in wild-type and TRPV1 knockout mice. *The Journal of Physiology*, 583, 663-674.
- DAVIDSON, M. R., LARSEN, J. E., YANG, I. A., HAYWARD, N. K., CLARKE, B. E., DUHIG, E. E., PASSMORE, L. H., BOWMAN, R. V. & FONG, K. M. 2010. MicroRNA-218 Is Deleted and Downregulated in Lung Squamous Cell Carcinoma. *PLoS ONE*, 5, e12560.
- DESROCHERS, M., CHRISTOU, M., JEFCOATE, C., BELZIL, A. & ANDERSON, A. 1996. New proteins in the rat CYP2B subfamily: presence in liver microsomes of the constitutive CYP2B3 protein and the phenobarbital-inducible protein product of alternatively spliced CYP2B2 mRNA. *Biochem Pharmacol*, 52, 1311-9.
- DIGGLE, C. P., PITT, E., ROBERTS, P., TREJDOSIEWICZ, L. K. & SOUTHGATE, J. 2000. N;-3 and n;-6 polyunsaturated fatty acids induce cytostasis in human urothelial cells independent of p53 gene function. *J Lipid Res*, 41, 1509-15.
- DIMASI, J. A., HANSEN, R. W. & GRABOWSKI, H. G. 2003. The price of innovation: new estimates of drug development costs. *J Health Econ*, 22, 151-85.
- DIMRI, G. P., MARTINEZ, J.-L., JACOBS, J. J. L., KEBLUSEK, P., ITAHANA, K., VAN LOHUIZEN, M., CAMPISI, J., WAZER, D. E. & BAND, V. 2002. The Bmi-1 Oncogene Induces Telomerase Activity and Immortalizes Human Mammary Epithelial Cells. *Cancer Research*, 62, 4736-4745.
- DONG, P., KANEUCHI, M., WATARI, H., HAMADA, J., SUDO, S., JU, J. & SAKURAGI, N. 2011. MicroRNA-194 inhibits epithelial to mesenchymal transition of endometrial cancer cells by targeting oncogene BMI-1. *Molecular Cancer*, 10, 99.
- DU, L., HOFFMAN, S. M. & KEENEY, D. S. 2004. Epidermal CYP2 family cytochromes P450. *Toxicol Appl Pharmacol*, 195, 278-87.
- EASTWOOD, D., FINDLAY, L., POOLE, S., BIRD, C., WADHWA, M., MOORE, M., BURNS, C., THORPE, R. & STEBBINGS, R. 2010. Monoclonal antibody TGN1412 trial failure explained by species differences in CD28 expression on CD4+ effector memory T-cells. *Br J Pharmacol*, 161, 512-26.
- EISELLEOVA, L., PETERKOVA, I., NERADIL, J., SLANINOVA, I., HAMPL, A. & DVORAK, P. 2008. Comparative study of mouse and human feeder cells for human embryonic stem cells. *Int J Dev Biol*, 52, 353-63.

- EKHART, C., DOODEMAN, V. D., RODENHUIS, S., SMITS, P. H. M., BEIJNEN, J. H. & HUIITEMA, A. D. R. 2008. Influence of polymorphisms of drug metabolizing enzymes (CYP2B6, CYP2C9, CYP2C19, CYP3A4, CYP3A5, GSTA1, GSTP1, ALDH1A1 and ALDH3A1) on the pharmacokinetics of cyclophosphamide and 4-hydroxycyclophosphamide. *Pharmacogenetics and Genomics*, 18, 515-523 10.1097/FPC.0b013e3282fc9766.
- EKINS, S. & WRIGHTON, S. 1999. THE ROLE OF CYP2B6 IN HUMAN XENOBIOTIC METABOLISM<sup>1</sup>\*. *Drug Metabolism Reviews*, 31, 719-754.
- ELIA, A. P. 1996. *Tissue specific regulation of CYP2B gene expression*. [electronic resource] [Online]. University of London.
- EVANS, S. M., CASARTELLI, A., HERREROS, E., MINNICK, D. T., DAY, C., GEORGE, E. & WESTMORELAND, C. 2001. Development of a high throughput in vitro toxicity screen predictive of high acute in vivo toxic potential. *Toxicology in Vitro*, 15, 579-584.
- FIERABRACCI, A., CAIONE, P., GIOVINE, M., ZAVAGLIA, D. & BOTTAZZO, G. 2007. Identification and characterization of adult stem/progenitor cells in the human bladder (bladder spheroids): perspectives of application in pediatric surgery. *Pediatric Surgery International*, 23, 837-839.
- FRANKEN, J., UVIN, P., DE RIDDER, D. & VOETS, T. 2014. TRP channels in lower urinary tract dysfunction. *Br J Pharmacol*, 171, 2537-51.
- FULCHER, M. L., GABRIEL, S. E., OLSEN, J. C., TATREAU, J. R., GENTZSCH, M., LIVANOS, E., SAAVEDRA, M. T., SALMON, P. & RANDELL, S. H. 2009. Novel human bronchial epithelial cell lines for cystic fibrosis research. *American Journal of Physiology - Lung Cellular and Molecular Physiology*, 296, L82-L91.
- GAISA, N. T., GRAHAM, T. A., MCDONALD, S. A. C., CAÑADILLAS-LOPEZ, S., POULSOM, R., HEIDENREICH, A., JAKSE, G., TADROUS, P. J., KNUECHEL, R. & WRIGHT, N. A. 2011. The human urothelium consists of multiple clonal units, each maintained by a stem cell. *The Journal of Pathology*, 225, 163-171.
- GEORGOPOULOS, N. T., KIRKWOOD, L. A. & SOUTHGATE, J. 2014. A novel bidirectional positive-feedback loop between Wnt-beta-catenin and EGFR-ERK plays a role in context-specific modulation of epithelial tissue regeneration. *J Cell Sci*, 127, 2967-82.
- GEORGOPOULOS, N. T., KIRKWOOD, L. A., VARLEY, C. L., MACLAINE, N. J., AZIZ, N. & SOUTHGATE, J. 2011. Immortalisation of Normal Human

- Urothelial Cells Compromises Differentiation Capacity. *European Urology*, 60, 141-149.
- GEORGOPOULOS, N. T., KIRKWOOD, L. A., WALKER, D. C. & SOUTHGATE, J. 2010. Differential Regulation of Growth-Promoting Signalling Pathways by E-Cadherin. *PLoS ONE*, 5, e13621.
- GERVOT, L., ROCHAT, B., GAUTIER, J. C., BOHNENSTENGEL, F., KROEMER, H., DE BERARDINIS, V., MARTIN, H., BEAUNE, P. & DE WAZIERS, I. 1999. Human CYP2B6: expression, inducibility and catalytic activities. *Pharmacogenetics and Genomics*, 9, 295-306.
- GEVAERT, T., JORIS, V., SEGAL, A., EVERAERTS, W., ROSKAMS, T., TALAVERA, K., OWSIANIK, G., LIEDTKE, W., DAELEMANS, D., IDEWACHTER, L., VAN LEUVEN, F., VOETS, T., DE RIDDER, D. & NILIUS, B. 2007. Deletion of the transient receptor potential cation channel TRPV4 impairs murine bladder voiding. *Journal of clinical investigation*, 117, 3453-3462.
- GILGENKRANTZ, S. 2014. [Sixty years of HeLa cell cultures]. *Hist Sci Med*, 48, 139-44.
- GOODWIN, B., MOORE, L. B., STOLTZ, C. M., MCKEE, D. D. & KLIEWER, S. A. 2001. Regulation of the human CYP2B6 gene by the nuclear pregnane X receptor. *Mol Pharmacol*, 60, 427-31.
- GRAHAM, F. L., SMILEY, J., RUSSELL, W. C. & NAIRN, R. 1977. Characteristics of a human cell line transformed by DNA from human adenovirus type 5. *J Gen Virol*, 36, 59-74.
- GSTRAUNTHALER, G. 2003. Alternatives to the use of fetal bovine serum: serum-free cell culture. *ALTEX*, 20, 275-81.
- GSTRAUNTHALER, G., LINDL, T. & VAN DER VALK, J. 2013. A plea to reduce or replace fetal bovine serum in cell culture media. *Cytotechnology*, 65, 791-3.
- GUARINO, R. A. 2009. *New drug approval process*, New York, Informa Healthcare.
- HAGA, K., OHNO, S., YUGAWA, T., NARISAWA-SAITO, M., FUJITA, M., SAKAMOTO, M., GALLOWAY, D. A. & KIYONO, T. 2007. Efficient immortalization of primary human cells by p16INK4a-specific short hairpin RNA or Bmi-1, combined with introduction of hTERT. *Cancer Sci*, 98, 147-54.
- HAHN, W. C. & WEINBERG, R. A. 2002. Modelling the molecular circuitry of cancer. *Nat Rev Cancer*, 2, 331-41.

- HARTUNG, T. & DASTON, G. 2009. Are in vitro tests suitable for regulatory use? *Toxicol Sci*, 111, 233-7.
- HAUPT, Y., ALEXANDER, W. S., BARRI, G., PETER KLINKEN, S. & ADAMS, J. M. 1991a. Novel zinc finger gene implicated as myc collaborator by retrovirally accelerated lymphomagenesis in E<sup>1/4</sup>-myc transgenic mice. *Cell*, 65, 753-763.
- HAUPT, Y., ALEXANDER, W. S., BARRI, G., PETER KLINKEN, S. & ADAMS, J. M. 1991b. Novel zinc finger gene implicated as myc collaborator by retrovirally accelerated lymphomagenesis in E<sub>μ</sub>-myc transgenic mice. *Cell*, 65, 753-763.
- HE, X., DONG, Y., WU, C., ZHAO, Z., NG, S., CHAN, F., SUNG, J. & YU, J. 2012. MicroRNA-218 inhibits cell cycle progression and promotes apoptosis in colon cancer by down regulating oncogene BMI-1. *Molecular Medicine*.
- HICKS, R. M. 1975. THE MAMMALIAN URINARY BLADDERAN ACCOMMODATING ORGAN. *Biological Reviews*, 50, 215-246.
- HO, P. L., KURTOVA, A. & CHAN, K. S. 2012. Normal and neoplastic urothelial stem cells: getting to the root of the problem. *Nature reviews. Urology*, 9, 583-594.
- HOEFLICH, K.P., O'BRIAN, C., BOYD, Z., CAVET, G., GUERRERO, S., JUNG, K., JANUARIO, T., SAVAGE, H., PUNNOOSE, E., TRUONG, T., ZHOU, W., BERRY, L., MURRAY, L., AMLER, L., BELVIN, M., FRIEDMAN, L.S., LACKNER, M.R. 2009. In vivo antitumor activity of MEK and PI3K inhibitors in basal-like breast cancer models. *Clin Cancer Res*, 15, 14, 4649-4664.
- HONN, K. V., SINGLEY, J. A. & CHAVIN, W. 1975. Fetal bovine serum: a multivariate standard. *Proc Soc Exp Biol Med*, 149, 344-7.
- HOSEN, N., YAMANE, T., MUIJTJENS, M., PHAM, K., CLARKE, M. F. & WEISSMAN, I. L. 2007. Bmi-1-Green Fluorescent Protein-Knock-In Mice Reveal the Dynamic Regulation of Bmi-1 Expression in Normal and Leukemic Hematopoietic Cells. *STEM CELLS*, 25, 1635-1644.
- HUBER, G. F., ALBINGER-HEGYI, A., SOLTERMANN, A., ROESSLE, M., GRAF, N., HAERLE, S. K., HOLZMANN, D., MOCH, H. & HEGYI, I. 2011. Expression patterns of Bmi-1 and p16 significantly correlate with overall, disease-specific, and recurrence-free survival in oropharyngeal squamous cell carcinoma. *Cancer*, 117, 4659-4670.

- HUKKANEN, J., PELKONEN, O., HAKKOLA, J. & RAUNIO, H. 2002. Expression and regulation of xenobiotic-metabolizing cytochrome P450 (CYP) enzymes in human lung. *Crit Rev Toxicol*, 32, 391-411.
- HUTTON, K. A., TREJDOSIEWICZ, L. K., THOMAS, D. F. & SOUTHGATE, J. 1993. Urothelial tissue culture for bladder reconstruction: an experimental study. *The Journal of Urology*, 150, 721-725.
- IARC. 1999. *Saccharin and its salts (group 3)* [Online]. <http://www.inchem.org/documents/iarc/vol73/73-19.html>. [Accessed 28th March 2015].
- INGELMAN-SUNDBERG, M. 2004. Human drug metabolising cytochrome P450 enzymes: properties and polymorphisms. *Naunyn-Schmiedeberg's Archives of Pharmacology*, 369, 89-104.
- ITAHANA, K., ZOU, Y., ITAHANA, Y., MARTINEZ, J.-L., BEAUSEJOUR, C., JACOBS, J. J. L., VAN LOHUIZEN, M., BAND, V., CAMPISI, J. & DIMRI, G. P. 2003. Control of the Replicative Life Span of Human Fibroblasts by p16 and the Polycomb Protein Bmi-1. *Molecular and Cellular Biology*, 23, 389-401.
- IYANAGI, T. 2007. Molecular mechanism of phase I and phase II drug-metabolizing enzymes: implications for detoxification. *Int Rev Cytol*, 260, 35-112.
- JACOBS, J. J. L., KIEBOOM, K., MARINO, S., DEPINHO, R. A. & VAN LOHUIZEN, M. 1999. The oncogene and Polycomb-group gene bmi-1 regulates cell proliferation and senescence through the ink4a locus. *Nature*, 397, 164-168.
- JANCOVA, P., ANZENBACHER, P. & ANZENBACHEROVA, E. 2010. Phase II drug metabolizing enzymes. *Biomed Pap Med Fac Univ Palacky Olomouc Czech Repub*, 154, 103-16.
- JOANNARD, F., RISSEL, M., GILOT, D., ANDERSON, A., ORFILA-LEFEUVRE, L., GUILLOUZO, A., ATFI, A. & LAGADIC-GOSSMANN, D. 2006. Role for mitogen-activated protein kinases in phenobarbital-induced expression of cytochrome P450 2B in primary cultures of rat hepatocytes. *Toxicol Lett*, 161, 61-72.
- JOCHEMS, C. E., VAN DER VALK, J. B., STAFLEU, F. R. & BAUMANS, V. 2002. The use of fetal bovine serum: ethical or scientific problem? *Altern Lab Anim*, 30, 219-27.
- JOHNEN, G., ROZYNEK, P., VON DER GATHEN, Y., BRYK, O., ZDRENKA, R., JOHANNES, C., WEBER, D. G., IGWILO-OKUEFUNA, O. B., RAIKO, I.,

- HIPPLER, J., BRUNING, T. & DOPP, E. 2013. Cross-contamination of a UROtsa stock with T24 cells--molecular comparison of different cell lines and stocks. *PLoS One*, 8, e64139.
- KANG, M. K., KIM, R. H., KIM, S. J., YIP, F. K., SHIN, K. H., DIMRI, G. P., CHRISTENSEN, R., HAN, T. & PARK, N. H. 2006. Elevated Bmi-1 expression is associated with dysplastic cell transformation during oral carcinogenesis and is required for cancer cell replication and survival. *Br J Cancer*, 96, 126-133.
- KAWAMOTO, T., SUEYOSHI, T., ZELKO, I., MOORE, R., WASHBURN, K. & NEGISHI, M. 1999. Phenobarbital-responsive nuclear translocation of the receptor CAR in induction of the CYP2B gene. *Mol Cell Biol*, 19, 6318-22.
- KAWANISHI, S., HIRAKU, Y., MURATA, M. & OIKAWA, S. 2002. The role of metals in site-specific DNA damage with reference to carcinogenesis. *Free Radic Biol Med*, 32, 822-32.
- KEENEY, D. S., SKINNER, C., TRAVERS, J. B., CAPDEVILA, J. H., NANNEY, L. B., KING, L. E., JR. & WATERMAN, M. R. 1998. Differentiating keratinocytes express a novel cytochrome P450 enzyme, CYP2B19, having arachidonate monooxygenase activity. *J Biol Chem*, 273, 32071-9.
- KIM, J. H., YOON, S. Y., JEONG, S.-H., KIM, S. Y., MOON, S. K., JOO, J. H., LEE, Y., CHOE, I. S. & KIM, J. W. 2004. Overexpression of Bmi-1 oncoprotein correlates with axillary lymph node metastases in invasive ductal breast cancer. *The Breast*, 13, 383-388.
- KNIGHTS, K. M., ROWLAND, A. & MINERS, J. O. 2013. Renal drug metabolism in humans: the potential for drug-endobiotic interactions involving cytochrome P450 (CYP) and UDP-glucuronosyltransferase (UGT). *Br J Clin Pharmacol*, 76, 587-602.
- KODAMA, S. & NEGISHI, M. 2006. Phenobarbital confers its diverse effects by activating the orphan nuclear receptor car. *Drug Metab Rev*, 38, 75-87.
- KREWSKI, D., WESTPHAL, M., AL-ZOUGHLOO, M., CROTEAU, M. C. & ANDERSEN, M. E. 2011. New directions in toxicity testing. *Annu Rev Public Health*, 32, 161-78.
- KULLMANN, F. A., ARTIM, D., BECKEL, J., BARRICK, S., DE GROAT, W. C. & BIRDER, L. A. 2008. Heterogeneity of muscarinic receptor-mediated Ca<sup>2+</sup> responses in cultured urothelial cells from rat. *American Journal of Physiology - Renal Physiology*, 294, F971-F981.

- KURZROCK, E. A., LIEU, D. K., DEGRAFFENRIED, L. A., CHAN, C. W. & ISSEROFF, R. R. 2008. Label-retaining cells of the bladder: candidate urothelial stem cells. *American Journal of Physiology - Renal Physiology*, 294, F1415-F1421.
- KURZROCK, E. A., LIEU, D. K., DEGRAFFENRIED, L. A. & ISSEROFF, R. R. 2005. Rat Urothelium: improved techniques for serial cultivation, expansion, freezing and reconstitution onto acellular matrix. *The Journal of Urology*, 173, 281-285.
- LAMBA, V., LAMBA, J., YASUDA, K., STROM, S., DAVILA, J., HANCOCK, M. L., FACKENTHAL, J. D., ROGAN, P. K., RING, B., WRIGHTON, S. A. & SCHUETZ, E. G. 2003. Hepatic CYP2B6 expression: gender and ethnic differences and relationship to CYP2B6 genotype and CAR (constitutive androstane receptor) expression. *J Pharmacol Exp Ther*, 307, 906-22.
- LEE, G. 2011. Uroplakins in the lower urinary tract. *Int Neurourol J*, 15, 4-12.
- LESSARD, J. & SAUVAGEAU, G. 2003. Bmi-1 determines the proliferative capacity of normal and leukaemic stem cells. *Nature*, 423, 255-260.
- LEUNG, C., LINGBEEK, M., SHAKHOVA, O., LIU, J., TANGER, E., SAREMASLANI, P., VAN LOHUIZEN, M. & MARINO, S. 2004. Bmi1 is essential for cerebellar development and is overexpressed in human medulloblastomas. *Nature*, 428, 337-341.
- LEWIS, S. A. 2000. Everything you wanted to know about the bladder epithelium but were afraid to ask. *American Journal of Physiology - Renal Physiology*, 278, F867-F874.
- LI, Z., CAO, R., WANG, M., MYERS, M. P., ZHANG, Y. & XU, R.-M. 2006. Structure of a Bmi-1-Ring1B Polycomb Group Ubiquitin Ligase Complex. *Journal of Biological Chemistry*, 281, 20643-20649.
- LIU, G., YUAN, X., ZENG, Z., TUNICI, P., NG, H., ABDULKADIR, I., LU, L., IRVIN, D., BLACK, K. & YU, J. 2006a. Analysis of gene expression and chemoresistance of CD133+ cancer stem cells in glioblastoma. *Molecular Cancer*, 5, 67.
- LIU, L., ANDREWS, L. G. & TOLLEFSBOL, T. O. 2006b. Loss of the human polycomb group protein BMI1 promotes cancer-specific cell death. *Oncogene*, 25, 4370-4375.

- LIU, S., DONTU, G., MANTLE, I. D., PATEL, S., AHN, N.-S., JACKSON, K. W., SURI, P. & WICHA, M. S. 2006c. Hedgehog Signaling and Bmi-1 Regulate Self-renewal of Normal and Malignant Human Mammary Stem Cells. *Cancer Research*, 66, 6063-6071.
- LOUIS, N., EVELEGH, C. & GRAHAM, F. L. 1997. Cloning and sequencing of the cellular-viral junctions from the human adenovirus type 5 transformed 293 cell line. *Virology*, 233, 423-9.
- LOUISSE, J., DE JONG, E., VAN DE SANDT, J. J., BLAAUBOER, B. J., WOUTERSEN, R. A., PIERSMA, A. H., RIETJENS, I. M. & VERWEI, M. 2010. The use of in vitro toxicity data and physiologically based kinetic modeling to predict dose-response curves for in vivo developmental toxicity of glycol ethers in rat and man. *Toxicol Sci*, 118, 470-84.
- MARCEAU N 1990. Cell lineages and differentiation programs in epidermal, urothelial and hepatic tissues and their neoplasms. *Laboratory Investigation*, 63, 4-20.
- MARTIGNONI, M., GROOTHUIS, G. M. & DE KANTER, R. 2006. Species differences between mouse, rat, dog, monkey and human CYP-mediated drug metabolism, inhibition and induction. *Expert Opin Drug Metab Toxicol*, 2, 875-94.
- MARTINEZ, I., GARDINER, A. S., BOARD, K. F., MONZON, F. A., EDWARDS, R. P. & KHAN, S. A. 2007. Human papillomavirus type 16 reduces the expression of microRNA-218 in cervical carcinoma cells. *Oncogene*, 27, 2575-2582.
- MCKIM, J. 2010. Building a tiered approach to in vitro predictive toxicity screening: A focus on assays with in vivo relevance. *Combined Chemistry and High Throughput Screening*, 13, 118-206.
- MEUNIER, B., DE VISSER, S. P. & SHAIK, S. 2004. Mechanism of oxidation reactions catalyzed by cytochrome p450 enzymes. *Chem Rev*, 104, 3947-80.
- MITSCHE, D., REICHEL, A., FRICKER, G. & MOENNING, U. 2008. Characterization of cytochrome P450 protein expression along the entire length of the intestine of male and female rats. *Drug Metab Dispos*, 36, 1039-45.
- MOLOFSKY, A. V., HE, S., BYDON, M., MORRISON, S. J. & PARDAL, R. 2005. Bmi-1 promotes neural stem cell self-renewal and neural development but not mouse growth and survival by repressing the p16Ink4a and p19Arf senescence pathways. *Genes & Development*, 19, 1432-1437.

- NETZER, R., EBNETH, A., BISCHOFF, U. & PONGS, O. 2001. Screening lead compounds for QT interval prolongation. *Drug Discov Today*, 6, 78-84.
- NGUYEN, M. M., LIEU, D. K., DEGRAFFENRIED, L. A., ISSEROFF, R. R. & KURZROCK, E. A. 2007. Urothelial progenitor cells: regional differences in the rat bladder. *Cell Proliferation*, 40, 157-165.
- OGAWA, T., IMAMURA, T., NAKAZAWA, M., HIRAGATA, S., NAGAI, T., MINAGAWA, T., YOKOYAMA, H., ISHIKAWA, M., DOMEN, T. & ISHIZUKA, O. 2015. Transient receptor potential channel superfamily: Role in lower urinary tract function. *Int J Urol*.
- OISHI N & XW, W. 2011. Novel therapeutic strategies for targeting liver cancer stem cells. *international journal of biological science*, 7, 517-535.
- OLSEN, S., STOVER, J. & NAGATOMI, J. 2011. Examining the Role of Mechanosensitive Ion Channels in Pressure Mechanotransduction in Rat Bladder Urothelial Cells. *Annals of Biomedical Engineering*, 39, 688-697.
- OMIECINSKI, C. J., VANDEN HEUVEL, J. P., PERDEW, G. H. & PETERS, J. M. 2011. Xenobiotic metabolism, disposition, and regulation by receptors: from biochemical phenomenon to predictors of major toxicities. *Toxicol Sci*, 120 Suppl 1, S49-75.
- PAMPALONI, F., REYNAUD, E. G. & STELZER, E. H. 2007. The third dimension bridges the gap between cell culture and live tissue. *Nat Rev Mol Cell Biol*, 8, 839-45.
- PARASURAMAN, S. 2011. Toxicological screening. *J Pharmacol Pharmacother*, 2, 74-9.
- PARSONS, C. L. 1993. The role of the glycosaminoglycan layer in bladder defense mechanisms and interstitial cystitis. *International Urogynecology Journal*, 4, 373-379.
- PEREL, P., ROBERTS, I., SENA, E., WHEBLE, P., BRISCOE, C., SANDERCOCK, P., MACLEOD, M., MIGNINI, L. E., JAYARAM, P. & KHAN, K. S. 2007. Comparison of treatment effects between animal experiments and clinical trials: systematic review. *BMJ*, 334, 197.
- PETZOLDT, J. L., LEIGH, I. M., DUFFY, P. G., SEXTON, C. & MASTERS, J. R. W. 1995. Immortalisation of human urothelial cells. *Urological Research*, 23, 377-380.

- PIRROTTA, V. 1998. Polycomb-ing the Genome: PcG, trxG, and Chromatin Silencing. *Cell*, 93, 333-336.
- POSY, S., SHAPIRO, L. & HONIG, B. 2008. Sequence and structural determinants of strand swapping in cadherin domains: do all cadherins bind through the same adhesive interface? *J Mol Biol*, 378, 954-68.
- PRIEBE, P. M. & KAUFFMAN, G. B. 1980. Making governmental policy under conditions of scientific uncertainty: a century of controversy about saccharin in Congress and the laboratory. *Minerva*, 18, 556-74.
- PUTHENVEETIL, J. A., BURGER, M. S. & REZNIKOFF, C. A. 1999. Replicative senescence in human uroepithelial cells. *Adv Exp Med Biol*, 462, 83-91.
- QIAO, B., CHEN, Z., HU, F., TAO, Q. & LAM, A. K. 2013. BMI-1 activation is crucial in hTERT-induced epithelial-mesenchymal transition of oral epithelial cells. *Exp Mol Pathol*, 95, 57-61.
- QUELLE, D. E., ZINDY, F., ASHMUN, R. A. & SHERR, C. J. 1995. Alternative reading frames of the INK4a tumor suppressor gene encode two unrelated proteins capable of inducing cell cycle arrest. *Cell*, 83, 993-1000.
- RAAPHORST, F. M. 2005. Deregulated expression of Polycomb-group oncogenes in human malignant lymphomas and epithelial tumors. *Human Molecular Genetics*, 14, R93-R100.
- REBEL, J. M., DE BOER, W. I., THIJSSSEN, C. D., VERMEY, M., ZWARTHOFF, E. C. & VAN DER KWAST, T. H. 1994. An in vitro model of urothelial regeneration: Effects of growth factors and extracellular matrix proteins. *The Journal of Pathology*, 173, 283-291.
- RINGROSE, L. & PARO, R. 2004. EPIGENETIC REGULATION OF CELLULAR MEMORY BY THE POLYCOMB AND TRITHORAX GROUP PROTEINS. *Annual Review of Genetics*, 38, 413-443.
- ROESEMS, G., HOET, P. H., DEMEDTS, M. & NEMERY, B. 1997. In vitro toxicity of cobalt and hard metal dust in rat and human type II pneumocytes. *Pharmacol Toxicol*, 81, 74-80.
- ROSENKRANZ, H. S. & CUNNINGHAM, A. R. 2005. Lack of predictivity of the rat lethality (LD50) test for ecological and human health effects. *Altern Lab Anim*, 33, 9-19.

- ROSSI, M. R., MASTERS, J. R., PARK, S., TODD, J. H., GARRETT, S. H., SENS, M. A., SOMJI, S., NATH, J. & SENS, D. A. 2001. The immortalized UROtsa cell line as a potential cell culture model of human urothelium. *Environ Health Perspect*, 109, 801-8.
- RUBENWOLF, P. & SOUTHGATE, J. 2011. Permeability of differentiated human urothelium in vitro. *Methods Mol Biol*, 763, 207-22.
- SAITO, M., HANDA, K., KIYONO, T., HATTORI, S., YOKOI, T., TSUBAKIMOTO, T., HARADA, H., NOGUCHI, T., TOYODA, M., SATO, S. & TERANAKA, T. 2005. Immortalization of Cementoblast Progenitor Cells With Bmi-1 and TERT. *Journal of Bone and Mineral Research*, 20, 50-57.
- SERRANO, M., HANNON, G. J. & BEACH, D. 1993. A new regulatory motif in cell-cycle control causing specific inhibition of cyclin D/CDK4. *Nature*, 366, 704-7.
- SHABIR, S., CROSS, W., KIRKWOOD, L. A., PEARSON, J. F., APPLEBY, P. A., WALKER, D., EARDLEY, I. & SOUTHGATE, J. 2013. Functional expression of purinergic P2 receptors and transient receptor potential channels by the human urothelium. *Am J Physiol Renal Physiol*, 305, F396-406.
- SHERR, C. 2000. Cellular senescence: mitotic clock or culture shock? *Cell*, 102, 407-410.
- SHIN, K., LEE, J., GUO, N., KIM, J., LIM, A., QU, L., MYSOREKAR, I. U. & BEACHY, P. A. 2011. Hedgehog/Wnt feedback supports regenerative proliferation of epithelial stem cells in bladder. *Nature*, 472, 110-114.
- SIDDIQUE, H. R. & SALEEM, M. 2012. Role of BMI1, a Stem Cell Factor, in Cancer Recurrence and Chemoresistance: Preclinical and Clinical Evidences. *STEM CELLS*, 30, 372-378.
- SIDHU, J. S. & OMIECINSKI, C. J. 1995. cAMP-associated inhibition of phenobarbital-inducible cytochrome P450 gene expression in primary rat hepatocyte cultures. *J Biol Chem*, 270, 12762-73.
- SIM, S. C. & INGELMAN-SUNDBERG, M. 2010. The Human Cytochrome P450 (CYP) Allele Nomenclature website: a peer-reviewed database of CYP variants and their associated effects. *Hum Genomics*, 4, 278-81.
- SMITH, N. J., HINLEY, J. S., VARLEY, C. L., EARDLEY, I., TREJDOSIEWICZ, L. K. & SOUTHGATE, J. 2015. The human urothelial tight junction: claudin 3 and the ZO-1 $\alpha$ + switch. *Bladder*, 2.

- SOLDATOW, V. Y., LECLUYSE, E. L., GRIFFITH, L. G. & RUSYN, I. 2013. models for liver toxicity testing. *Toxicol Res (Camb)*, 2, 23-39.
- SOMJI, S., BATHULA, C. S., ZHOU, X. D., SENS, M. A., SENS, D. A. & GARRETT, S. H. 2008. Transformation of human urothelial cells (UROtsa) by as and cd induces the expression of keratin 6a. *Environ Health Perspect*, 116, 434-40.
- SONG, L.-B., ZENG, M.-S., LIAO, W.-T., ZHANG, L., MO, H.-Y., LIU, W.-L., SHAO, J.-Y., WU, Q.-L., LI, M.-Z., XIA, Y.-F., FU, L.-W., HUANG, W.-L., DIMRI, G. P., BAND, V. & ZENG, Y.-X. 2006. Bmi-1 Is a Novel Molecular Marker of Nasopharyngeal Carcinoma Progression and Immortalizes Primary Human Nasopharyngeal Epithelial Cells. *Cancer Research*, 66, 6225-6232.
- SOUTHGATE, J., HUTTON, K. A., THOMAS, D. F. & TREJDOSIEWICZ, L. K. 1994. Normal human urothelial cells in vitro: proliferation and induction of stratification. *Laboratory investigation; a journal of technical methods and pathology*, 71, 583-594.
- SOUTHGATE, J., MASTERS, J. & TREJDOSIEWICZ, L. 2002. Culture of Human Urothelium. In: FRESHNEY, I. & FRESHNEY, M. (eds.) *Culture of Epithelial cells*. 2nd ed. Glasgow: Wiley-Liss.
- STAMPFER, M. R., BODNAR, A., GARBE, J., WONG, M., PAN, A., VILLEPONTEAU, B. & YASWEN, P. 1997. Gradual Phenotypic Conversion Associated with Immortalization of Cultured Human Mammary Epithelial Cells. *Molecular Biology of the Cell*, 8, 2391-2405.
- STEBBINGS, R., FINDLAY, L., EDWARDS, C., EASTWOOD, D., BIRD, C., NORTH, D., MISTRY, Y., DILGER, P., LIEFOOGHE, E., CLUDTS, I., FOX, B., TARRANT, G., ROBINSON, J., MEAGER, T., DOLMAN, C., THORPE, S. J., BRISTOW, A., WADHWA, M., THORPE, R. & POOLE, S. 2007. "Cytokine storm" in the phase I trial of monoclonal antibody TGN1412: better understanding the causes to improve preclinical testing of immunotherapeutics. *J Immunol*, 179, 3325-31.
- SUNTHARALINGAM, G., PERRY, M. R., WARD, S., BRETT, S. J., CASTELLO-CORTES, A., BRUNNER, M. D. & PANOSKALTSIS, N. 2006. Cytokine storm in a phase 1 trial of the anti-CD28 monoclonal antibody TGN1412. *N Engl J Med*, 355, 1018-28.
- TAKAYAMA, S., SIEBER, S. M., ADAMSON, R. H., THORGEIRSSON, U. P., DALGARD, D. W., ARNOLD, L. L., CANO, M., EKLUND, S. & COHEN, S. M. 1998. Long-term feeding of sodium saccharin to nonhuman primates: implications for urinary tract cancer. *J Natl Cancer Inst*, 90, 19-25.

- TAKEDA, Y., MORI, T., IMABAYASHI, H., KIYONO, T., GOJO, S., MIYOSHI, S., HIDA, N., ITA, M., SEGAWA, K., OGAWA, S., SAKAMOTO, M., NAKAMURA, S. & UMEZAWA, A. 2004. Can the life span of human marrow stromal cells be prolonged by bmi-1, E6, E7, and/or telomerase without affecting cardiomyogenic differentiation? *The Journal of Gene Medicine*, 6, 833-845.
- TATARANO, S., CHIYOMARU, T., KAWAKAMI, K., ENOKIDA, H., YOSHINO, H., HIDAKA, H., YAMASAKI, T., KAWAHARA, K., NISHIYAMA, K., SEKI, N. & NAKAGAWA, M. 2011. miR-218 on the genomic loss region of chromosome 4p15.31 functions as a tumor suppressor in bladder cancer. *International journal of oncology*, 39, 13-21.
- TÁTRAI, P., SZEPESI, Á., MATULA, Z., SZIGETI, A., BUCHAN, G., MÁDI, A., UHER, F. & NÉMET, K. 2012. Combined introduction of Bmi-1 and hTERT immortalizes human adipose tissue-derived stromal cells with low risk of transformation. *Biochemical and Biophysical Research Communications*, 422, 28-35.
- THOMAS, R. S., BLACK, M. B., LI, L., HEALY, E., CHU, T. M., BAO, W., ANDERSEN, M. E. & WOLFINGER, R. D. 2012. A comprehensive statistical analysis of predicting in vivo hazard using high-throughput in vitro screening. *Toxicol Sci*, 128, 398-417.
- TURPEINEN, M., RAUNIO, H. & PELKONEN, O. 2006. The Functional Role of CYP2B6 in Human Drug Metabolism: Substrates and Inhibitors In Vitro, In Vivo and In Silico. *Current Drug Metabolism*, 7, 705-714.
- VALK-LINGBEEK, M. E., BRUGGEMAN, S. W. M. & VAN LOHUIZEN, M. 2004. Stem Cells and Cancer: The Polycomb Connection. *Cell*, 118, 409-418.
- VAN DER LUGT, N. M., DOMEN, J., LINDERS, K., VAN ROON, M., ROBANUS-MAANDAG, E., TE RIELE, H., VAN DER VALK, M., DESCHAMPS, J., SOFRONIEW, M. & VAN LOHUIZEN, M. 1994. Posterior transformation, neurological abnormalities, and severe hematopoietic defects in mice with a targeted deletion of the bmi-1 proto-oncogene. *Genes & Development*, 8, 757-769.
- VAN DER VALK, J., BRUNNER, D., DE SMET, K., FEX SVENNINGSSEN, A., HONEGGER, P., KNUDSEN, L. E., LINDL, T., NORABERG, J., PRICE, A., SCARINO, M. L. & GSTRANTHALER, G. 2010. Optimization of chemically defined cell culture media--replacing fetal bovine serum in mammalian in vitro methods. *Toxicol In Vitro*, 24, 1053-63.

- VAN LOHUIZEN, M., VERBEEK, S., SCHELJEN, B., WIJNTJENS, E., VAN DER GUIDON, H. & BERNIS, A. 1991. Identification of cooperating oncogenes in E $\mu$ -myc transgenic mice by provirus tagging. *Cell*, 65, 737-752.
- VAN RAVENZWAAY, B. & LEIBOLD, E. 2004. A comparison between in vitro rat and human and in vivo rat skin absorption studies. *Hum Exp Toxicol*, 23, 421-30.
- VARLEY, C., HILL, G., PELLEGRIN, S., SHAW, N. J., SELBY, P. J., TREJDOSIEWICZ, L. K. & SOUTHGATE, J. 2005. Autocrine regulation of human urothelial cell proliferation and migration during regenerative responses in vitro. *Experimental Cell Research*, 306, 216-229.
- VARLEY, C. L., BACON, E. J., HOLDER, J. C. & SOUTHGATE, J. 2009. FOXA1 and IRF-1 intermediary transcriptional regulators of PPAR $\gamma$ -induced urothelial cytodifferentiation. *Cell Death Differ*, 16, 103-14.
- VARLEY, C. L., GARTHWAITE, M. A., CROSS, W., HINLEY, J., TREJDOSIEWICZ, L. K. & SOUTHGATE, J. 2006. PPAR $\gamma$ -regulated tight junction development during human urothelial cytodifferentiation. *J Cell Physiol*, 208, 407-17.
- VARLEY, C. L. & SOUTHGATE, J. 2008. Effects of PPAR agonists on proliferation and differentiation in human urothelium. *Experimental and Toxicologic Pathology*, 60, 435-441.
- VARLEY, C. L., STAHLSCHMIDT, J., LEE, W.-C., HOLDER, J., DIGGLE, C., SELBY, P. J., TREJDOSIEWICZ, L. K. & SOUTHGATE, J. 2004. Role of PPAR  $\gamma$  and EGFR signalling in the urothelial terminal differentiation programme. *Journal of Cell Science*, 117, 2029-2036.
- WALZ, T., HÄNER, M., WU, X.-R., HENN, C., ENGEL, A., SUN, T.-T. & AEBI, U. 1995. Towards the Molecular Architecture of the Asymmetric Unit Membrane of the Mammalian Urinary Bladder Epithelium: A Closed "Twisted Ribbon" Structure. *Journal of Molecular Biology*, 248, 887-900.
- WANG, H. & TOMPKINS, L. 2008. CYP2B6: New Insights into a Historically Overlooked Cytochrome P450 Isozyme. *Curr Drug Metab*, 9, 598-610.
- WANG, Z., WANG, Y., FARHANGFAR, F., ZIMMER, M. & ZHANG, Y. 2012. Enhanced keratinocyte proliferation and migration in co-culture with fibroblasts. *PLoS One*, 7, e40951.

- WESTERINK, W. M. & SCHOONEN, W. G. 2007. Cytochrome P450 enzyme levels in HepG2 cells and cryopreserved primary human hepatocytes and their induction in HepG2 cells. *Toxicol In Vitro*, 21, 1581-91.
- WEXLER, P. 2009. *Information resources in toxicology. edited by Philip Wexler [et al]*, London, Academic.
- WEZEL, F., PEARSON, J. & SOUTHGATE, J. 2014. Plasticity of in vitro-generated urothelial cells for functional tissue formation. *Tissue Eng Part A*, 20, 1358-68.
- WHYSNER, J. & WILLIAMS, G. M. 1996. Saccharin mechanistic data and risk assessment: urine composition, enhanced cell proliferation, and tumor promotion. *Pharmacol Ther*, 71, 225-52.
- WITCHEL, H. J. & HANCOX, J. C. 2000. Familial and acquired long qt syndrome and the cardiac rapid delayed rectifier potassium current. *Clin Exp Pharmacol Physiol*, 27, 753-66.
- WRIGHT, W. E. & SHAY, J. W. 2000. Telomere dynamics in cancer progression and prevention: fundamental differences in human and mouse telomere biology. *Nat Med*, 6, 849-51.
- WRIGHTON, S. A. & STEVENS, J. C. 1992. The human hepatic cytochromes P450 involved in drug metabolism. *Crit Rev Toxicol*, 22, 1-21.
- YOSHINARI, K., SUEYOSHI, T., MOORE, R. & NEGISHI, M. 2001. Nuclear receptor CAR as a regulatory factor for the sexually dimorphic induction of CYB2B1 gene by phenobarbital in rat livers. *Mol Pharmacol*, 59, 278-84.
- YOSHIYAMA, M., MOCHIZUKI, T., NAKAGOMI, H., MIYAMOTO, T., KIRA, S., MIZUMACHI, R., SOKABE, T., TAKAYAMA, Y., TOMINAGA, M. & TAKEDA, M. 2015. Functional roles of TRPV1 and TRPV4 in control of lower urinary tract activity: dual analysis of behavior and reflex during the micturition cycle. *Am J Physiol Renal Physiol*, 308, F1128-34.
- YU, C.F., LIU, Z.X. & CANTLEY, L.G. 2002. ERK negatively regulates the epidermal growth factor-mediated interaction of Gab1 and the PI3K. *J Biol Chem*, 277, 22, 19382-19388
- ZHANG, F. B., SUI, L. H. & XIN, T. 2008. Correlation of Bmi-1 expression and telomerase activity in human ovarian cancer. *Br J Biomed Sci*, 65, 172-7.

- ZHANG, H., LIN, G., QIU, X., NING, H., BANIE, L., LUE, T. F. & LIN, C.-S. 2012. Label Retaining and Stem Cell Marker Expression in the Developing Rat Urinary Bladder. *Urology*, 79, 746.e1-746.e6.
- ZHANG, Q. Y., DUNBAR, D., OSTROWSKA, A., ZEISLOFT, S., YANG, J. & KAMINSKY, L. S. 1999. Characterization of human small intestinal cytochromes P-450. *Drug Metab Dispos*, 27, 804-9.
- ZHANG, X., SODA, Y., TAKAHASHI, K., BAI, Y., MITSURU, A., IGURA, K., SATOH, H., YAMAGUCHI, S., TANI, K., TOJO, A. & TAKAHASHI, T. A. 2006. Successful immortalization of mesenchymal progenitor cells derived from human placenta and the differentiation abilities of immortalized cells. *Biochem Biophys Res Commun*, 351, 853-9.
- ZHANG, Y., LUDWIKOWSKI, B., HURST, R. & FREY, P. 2001. Expansion and long-term culture of differentiated normal rat urothelial cells in vitro. *In Vitro Cellular & Developmental Biology - Animal*, 37, 419-429.
- ZHANG, Y., NUGLOZEH, E., TOURE, F., SCHMIDT, A. M. & VUNJAK-NOVAKOVIC, G. 2009. Controllable expansion of primary cardiomyocytes by reversible immortalization. *Hum Gene Ther*, 20, 1687-96.
- ZIMMERMAN, S. & MOELLING, K. 1999. Phosphorylation and regulation of Raf by Akt (protein kinase B). *Science*, 286, 5445, 1741-1744.